



universität
wien

MASTERARBEIT / MASTER'S THESIS

Titel der Masterarbeit / Title of the Master's Thesis

**„Investigating differences of protein-ligand interactions by
molecular docking comparing human and mouse OCT1“**

verfasst von / submitted by

Mert Basaran, B.Sc.

angestrebter akademischer Grad / in partial fulfilment of the requirements for the degree of

Master of Science (MSc)

Wien, 2022 / Vienna, 2022

Studienkennzahl lt. Studienblatt /
degree programme code as it appears on
the student record sheet:

UA 066 606

Studienrichtung lt. Studienblatt /
degree programme as it appears on
the student record sheet:

Masterstudium Drug Discovery and Development

Betreut von / Supervisor:

Mag. Dr. Barbara Zdrazil, Privatdoz.

Acknowledgments

First and foremost, I would like to express my deepest gratitude to Dr. Barbara Zdrazil for her excellent mentorship, guidance throughout the last year and for providing me with a topic that grew into an exciting story. Beginning with her first lecture in the pharmacoinformatic practical course at the University of Vienna, followed by two internships and the master's thesis in her research group, she expended my interest in large-scale data analyses, *in silico* target prediction, and computational modeling such as molecular docking. I am deeply grateful for our motivating discussions, her support, her patience, and her outstanding supervision of this thesis.

I want to thank all fellow group members – Yordan Yordanov, Stefaniia Vlasova, Mohamed Khalifa, Danilo Dokic, and Ursula Bartuschka for contributing to this atmosphere by sharing your thoughts during our Monday meetings. Special thanks go to our former member Dr. Alzbeta Tuerkova for providing me technical support in the beginning, and Stefaniia for analyzing the remaining docking runs for our publication.

I also want to thank our collaborators Prof. Dr. Mladen Tzvetkov and Dr. Marleen Meyer for this delightful cooperation and for introducing me into the world of the organic cation transporter 1. Given that your remarkable experimental results were the motivation for this thesis and source for our submitted scientific paper.

Last but certainly not least, I want to thank my family and my friends for supporting me in this long journey and staying always by my side. Likewise, I want to highlight the technical support of my friend and roommate, Léon Meka, who made every download possible whenever it seemed impossible.

Summary

The human organic cation transporter 1 (hOCT1), encoded by the SLC22A1 gene, is most abundantly expressed in the liver, mainly in the basolateral membrane of hepatocytes. OCT1 operates by facilitated diffusion mediating the uptake of structurally highly diverse endogenous compounds and xenobiotics. Although polyspecificity is one of its most characteristic features, the mechanisms of drug-binding and transport are not fully uncovered yet, presumably due to unavailability of any crystal structure. To unravel the mechanistic details of this unique feature, the present work focused on the investigation of protein-ligand interactions comparing human and mouse OCT1 using structure-based methods such as molecular docking. The motive for this research study is based on the experimental results generated by Prof. Tzvetkov and Dr. Meyer, our collaborators from the University of Greifswald. By performing mutagenesis analysis, as for instance single-point mutations in human and mouse OCT1, single amino acids in the OCT1 protein that confer the species differences for two approved drugs, fenoterol and trospium, could be identified. Therefore, open-source docking programs such as AutoDock Vina and AutoDock 4, both developed under the AutoDock suite, were used to investigate crucial interactions to get a clearer understanding of the mechanism providing OCT1 polyspecificity, to identify single residues that support experimental data, and to suggest new residues of interest.

Zusammenfassung

Der organische Kationen Transporter Typ 1 des Menschen (hOCT1) mit dem Gensymbol SLC22A1, wird überwiegend in der Leber exprimiert und befindet sich hauptsächlich in der basolateralen Membran von Hepatozyten. OCT1 ermöglicht durch erleichterte Diffusion die Aufnahme von strukturell sehr unterschiedlichen endogenen Verbindungen und Xenobiotika. Obwohl Polyspezifität eines seiner charakteristischsten Merkmale ist, sind die Mechanismen der Substratbindung und des Transports noch nicht vollständig aufgeklärt, was vermutlich darauf zurückzuführen ist, dass keine Kristallstruktur zur Verfügung steht. Um die genauen Ursachen dieser einzigartigen Fähigkeiten zu entschlüsseln, konzentrierte sich die vorliegende Arbeit auf die Untersuchung von Protein-Liganden-Interaktionen, indem OCT1 von Mensch und Maus mit strukturbasierten Methoden wie dem molekularen Docking verglichen wurde. Den Grundstein für diese Forschungsarbeit legten Prof. Tzvetkov und Dr. Meyer, unsere Kollaborationspartner aus der Universität Greifswald, mit ihren vielversprechenden Laborergebnissen. Durch Mutagenese-Analysen, wie z.B. Single-Point-Mutationen in OCT1 von Mensch und Maus, konnten einzelne Aminosäuren im OCT1-Protein identifiziert werden, die die Speziesunterschiede für die beiden zugelassenen Medikamente Fenoterol und Trosipium bewirken. Daher wurden Open-Source-Docking-Programme wie AutoDock Vina und AutoDock 4, die beide im Rahmen der AutoDock-Suite entwickelt wurden, verwendet, um ausschlaggebende Wechselwirkungen zu untersuchen, damit ein besseres Verständnis des Mechanismus hinsichtlich der OCT1-Polyspezifität zu erlangen. Darüber hinaus wird mithilfe von computerbasierten Methoden versucht experimentellen Daten zu belegen, als auch neue entscheidende Aminosäuren zu identifizieren.

Table of Contents

1	Introduction: Membrane Proteins	5
1.1	Structure of membrane proteins	5
1.2	Major classes of membrane proteins	9
1.3	Functions of membrane proteins	12
1.4	Challenges in Studying Membrane Proteins	15
1.4.1	Expression and purification	16
1.4.2	Crystallization	18
1.4.3	Data collection and structure solution	19
1.5	Biophysical techniques	20
1.5.1	X-ray crystallography	21
1.5.2	Electron microscopy	22
1.5.3	Nuclear magnetic resonance	24
1.6	Molecular Modeling	25
1.6.1	Structure-Based Drug Design	27
1.6.2	Homology Modeling	30
1.6.3	Molecular Dynamics	34
1.6.4	Docking	36
1.7	Solute carrier family 22 member 1	46
1.7.1	Human OCT1	53
1.8	Aims and Objectives	56
2	Methods	57
2.1	PyMOL for molecular visualization	57
2.2	Discovery Studio Visualizer	57
2.3	Molecular Docking using AutoDock 4	58
2.4	Molecular Docking using AutoDock Vina	61
3	Results	62
3.1	Transport kinetics of fenoterol and trospium comparing hOCT1 and mOCT1	62
3.2	Molecular docking via AutoDock Vina	66
3.2.1	Rotamer docking of fenoterol into hOCT1 using AutoDock Vina	82
3.2.2	Rotamer docking of fenoterol into mOCT1 using AutoDock Vina	89
3.2.3	Rotamer docking of trospium into hOCT1 using AutoDock Vina	93
3.2.4	Rotamer docking of trospium into mOCT1 using AutoDock Vina	97
3.2.5	Molecular Docking of fenoterol into hOCT1 from AlphaFold DB using AutoDock Vina	104
3.2.6	Molecular Docking of trospium into hOCT1 from AlphaFold DB	108
3.2.7	Flexible Docking of fenoterol into hOCT1 from AlphaFold DB using AutoDock Vina	110
3.2.8	Flexible Docking of fenoterol into mOCT1 from AlphaFold DB using AutoDock Vina	116
3.2.9	Rotamer Docking of fenoterol into hOCT1 from AlphaFold DB using AutoDock Vina	121
3.2.10	Rotamer Docking of trospium into hOCT1 from AlphaFold DB using AutoDock Vina	126
3.3	Molecular Docking via AutoDock4	131
3.3.1	Molecular Docking of fenoterol into hOCT1 from AlphaFold using AutoDock4	131
3.3.2	Molecular Docking of trospium into hOCT1 from AlphaFold DB using AutoDock4	137
3.3.3	Molecular Docking of fenoterol into mOCT1 from AlphaFold DB using AutoDock4	142
3.3.4	Molecular Docking of trospium into mOCT1 from AlphaFold DB using AutoDock4	148

4	<i>Discussion</i>	154
4.1	Experimental findings with AutoDock Vina	156
4.2	Experimental findings with AutoDock 4.....	159
4.3	Concluding remarks	161
5	<i>Appendix</i>	163
5.1	Supplementary Figures	163
5.2	List of figures	183
5.3	List of Schemes	191
5.4	Supplementary Figures	192
5.5	List of Tables	196
6	<i>References</i>	199

1 Introduction: Membrane Proteins

Living organisms have distinct membranes surrounding the compartments. Cellular compartments in cell biology comprise all the closed parts within the cytosol of a eukaryotic cell, such as plasma, nucleus, endoplasmic reticulum (ER), golgi apparatus, lysosome, peroxisome, endosome, mitochondrion, chloroplast, thylakoid, *etc.* [1]

Membrane proteins (MPs) have diverse and important functions in living organisms. They add up to 30% of the known bacterial, archaean, and eukaryotic organisms' genomes. It is known that 50% of all known drug targets in humans are MPs. This already emphasizes the need to comprehensively understand their structure and structure-function relationships. [2]

1.1 Structure of membrane proteins

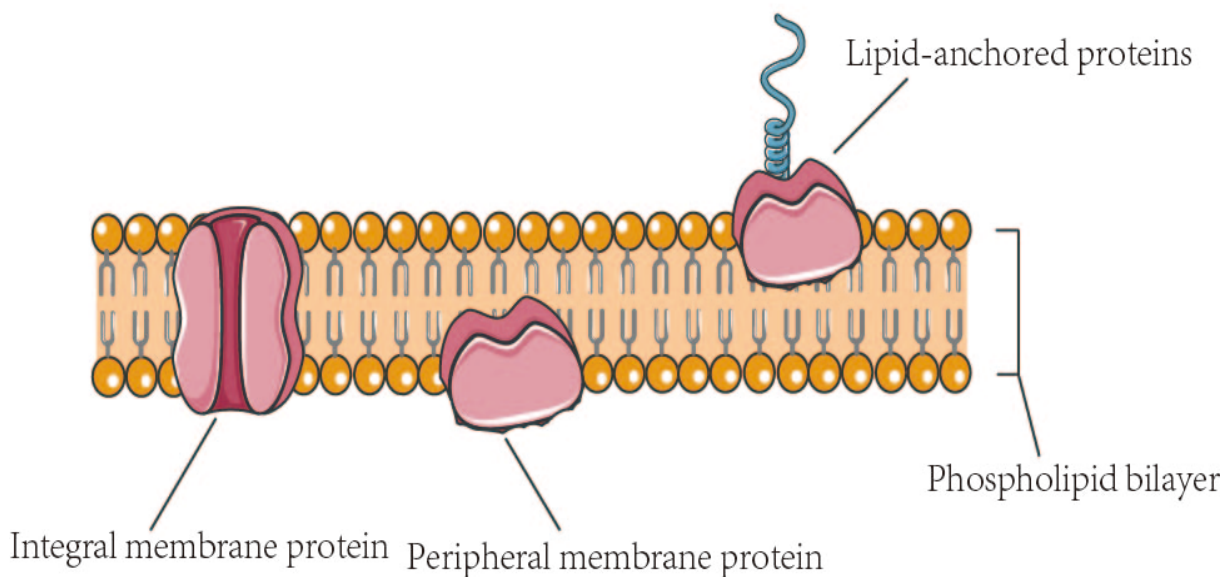


Figure 1: Structural classification of membrane proteins in a simplified way. The phospholipid bilayer is composed of an amphiphilic structure, having a hydrophilic polar head and a hydrophobic tail consisting of two fatty acid chains. Adapted from [3]

Membrane proteins can be distinguished into three main types based on their structure and localization: integral membrane protein, peripheral membrane protein (PMP) and lipid-anchored protein (Fig. 1). Integral membrane proteins are permanently embedded within the cell membrane. According to their relationship with the lipid bilayer, they can be classified into two primary types: integral polytopic and integral monotopic proteins.

Integral polytopic proteins are also known as transmembrane proteins (TMPs), which can span across the membrane due to their amphipathic structure. The hydrophobic part of an integral protein interacts with the hydrophobic core of the lipid bilayer, enabling the protein to travel across the bilayer and form a loop. Figure 2 illustrates three common forms in integral membrane proteins, such as, a single transmembrane α -helix protein (bitopic membrane protein), a polytopic transmembrane α -helical protein and a polytopic transmembrane β -sheet protein (1-3). However, integral monotopic proteins associate to only one side of the membrane and do not span the whole way across (4-7). There are four known types of interaction between integral monotopic membrane protein and cell membranes: Interaction by an amphipathic α -helix parallel to the membrane plane, interaction by a hydrophobic loop, interaction by a covalently bound membrane lipid and electrostatic or ionic interactions with membrane lipids. [3]

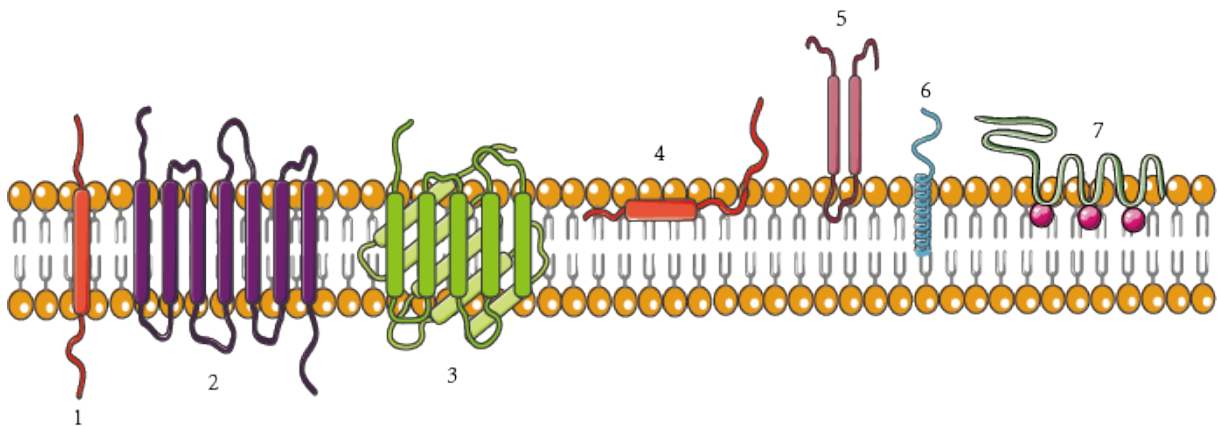
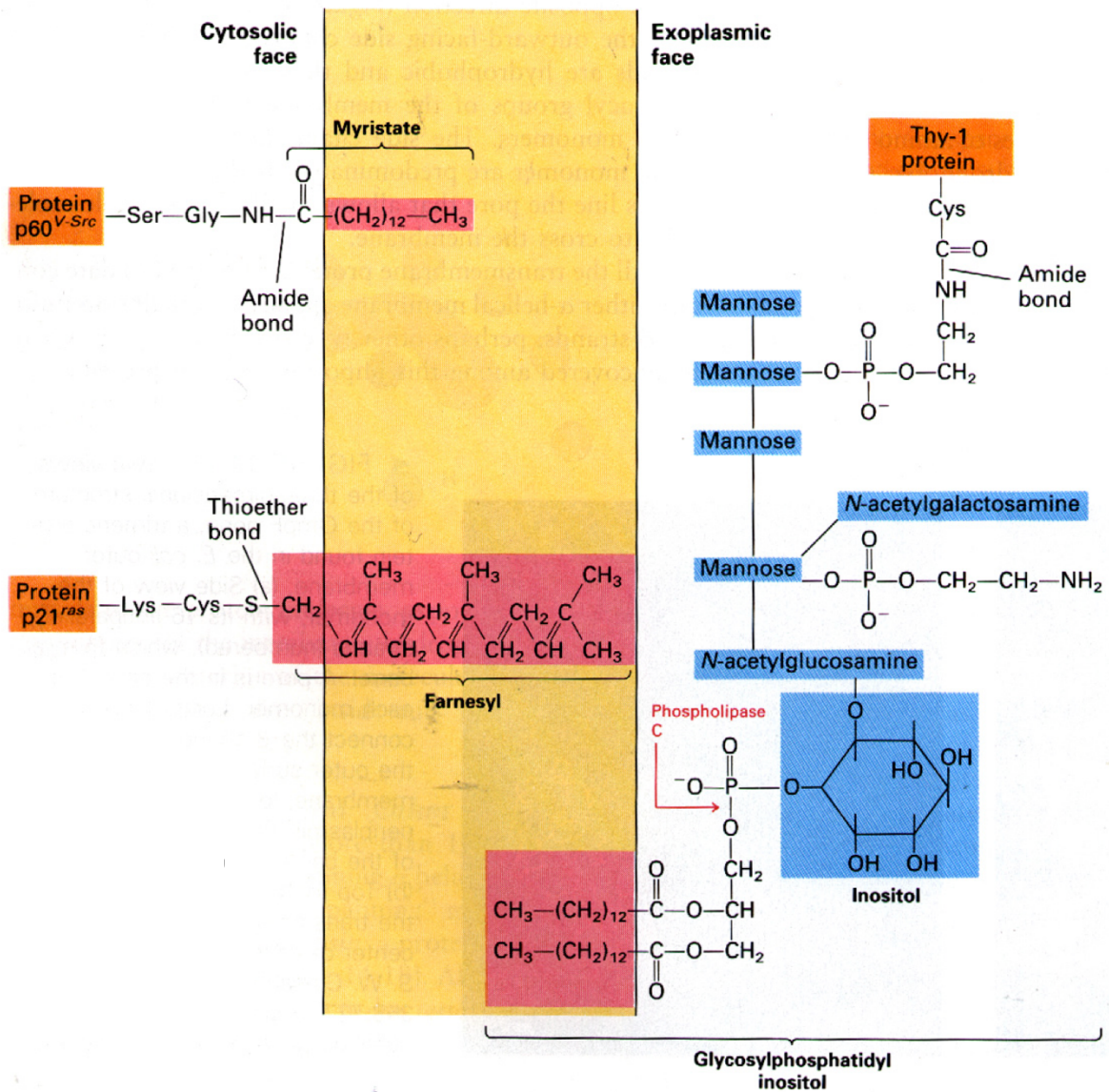


Figure 2: Schematic representation of integral membrane proteins. 1-3 depicts three types of integral polytopic proteins. 4-7 represents four types of integral monotopic membrane protein. The orange circle shows the hydrophilic polar head and the attached fatty acyl tails represent the hydrophobic core. Adapted from [3]

On the other hand, peripheral membrane proteins, also called extrinsic proteins, do not interact with the hydrophobic core of the phospholipid bilayer. They rather are temporarily attached either to the lipid bilayer or to integral proteins by the help of distinct mechanisms. ^[4] There are three major mechanisms underlying the interactions between peripheral membrane proteins and membranes: electrostatic interactions, hydrophobic interactions, and selective fatty acid modification of proteins. Thus, the occasionally transient interaction between a polypeptide and a lipid bilayer is covered by a complex energy landscape. Typically, biological membranes are composed of a combination of zwitterionic and negatively charged phospholipids. Charged membrane surfaces enable long-range electrostatic interactions between peripheral proteins and lipid head groups, attracting a partially positively charged protein to a negatively charged membrane by nonspecific electrostatic interactions. The main drivers in these interactions are the protein's cationic amino acid residues, which fulfill charge complementarity. Whereas hydrophobic interactions are mediated by hydrophobic regions of peripheral membrane proteins. Membrane attachment is enabled either by insertion of a hydrophobic or amphipathic α -helix into the membrane, or by a lipid anchor. Protein-membrane interactions, such as receptor-induced protein unfolding, facilitate a conformational change at the membrane interface, that exposes a buried hydrophobic surface, which then allows insertion of a particular domain into the hydrophobic core of the membrane. As noted earlier, lipid-anchored proteins are anchored to one of the membrane leaflets by being covalently linked to fatty acids. In these proteins, the bound fatty acid is embedded in the membrane, but the polypeptide chain does not enter the phospholipid bilayer. Several common lipid anchors are shown in Scheme 1. Some cell-surface proteins are anchored to the exoplasmic face of the plasma membrane by a complex called glycosylphosphatidylinositol. Upon cleavage of the phosphate-glycerol bond by the enzyme phospholipase C releases glycosylphosphatidylinositol-anchored proteins such as Thy-1 protein from the cell surface. On the other hand, some cytosolic proteins involved in signaling such as Ras are anchored to the cytosolic face of membranes by a hydrocarbon moiety covalently attached to a cysteine near the C-terminus. The most common anchors are farnesyl and palmitoyl groups. Other cytosolic proteins (v-Src, tyrosine-protein kinase transforming protein) are associated with the membrane through myristate, and similar fatty acids attached to an N-terminal glycine residue. ^[5,6]

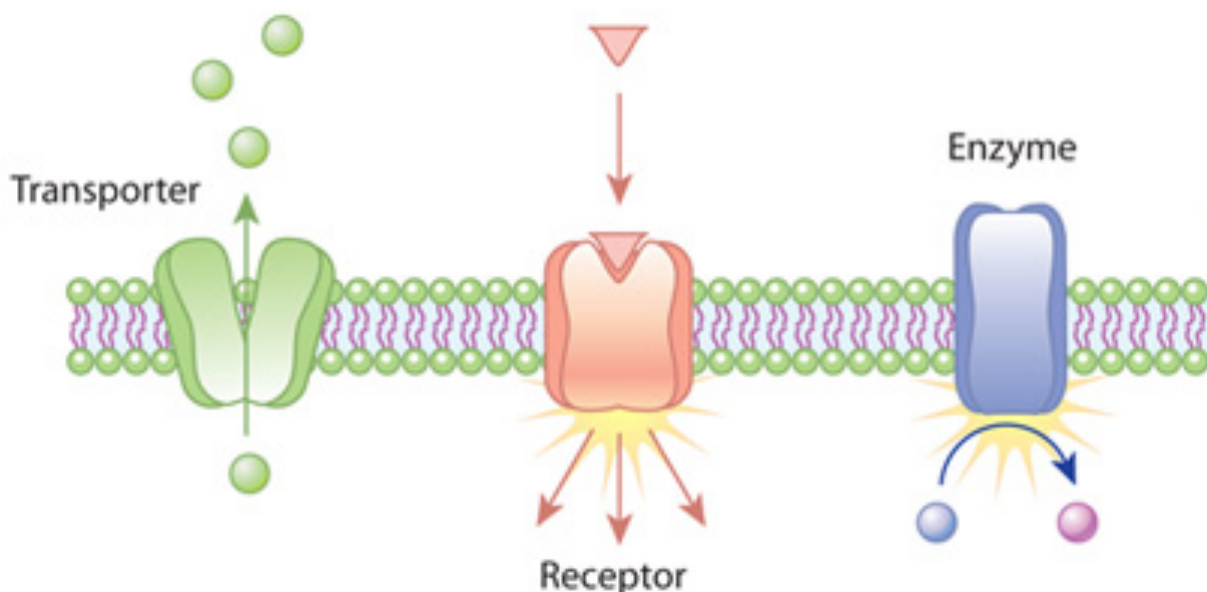


Scheme 1: Overview of common lipid-anchored proteins in the plasma membrane. Protein p60-vSrc and Protein p21-ras are in the cytosolic side, facing the interior of the cell. Thy-1 protein is in the exoplasmic face, facing the outside of the cell. Adapted from [7]

1.2 Major classes of membrane proteins

Membrane proteins encompass a wide variety of functions in the human body required for normal development and physiology. Their disruption can lead to a range of diseases. Also, the identification of membrane proteins with aberrant properties can lead to the discovery of novel therapeutic targets.

The functions of membrane proteins are determined by their subcellular localizations. For instance, proteins at the plasma membrane act as receptors, transferring information from the environment to the cell, thus enabling the cell to alter its behavior in response to external signals. Transduction receptors are a representative group for this type of membrane proteins (Scheme 2). Upon ligand binding, a biochemical cascade occurs, which is a chain of biochemical events known as a signaling pathway. Known examples of membrane transduction receptors include tyrosine kinase receptors, serine/threonine kinase receptors, G protein-coupled receptors and neurotransmitter receptors.



Scheme 2: The different types of membrane proteins and their related functions. Transporters (left) carry ions or molecules in or out of the cell across the membrane, regulating the intracellular composition. Receptors (middle) regulate cell signaling by transmitting a chemical signal from the extracellular environment into the cell. Enzymes (right) serve as catalysts, enabling a biochemical reaction by decreasing the activation energy. Adapted from ^[8]

Likewise, another important class of membrane proteins is the transporter proteins (Scheme 2). In contrast to receptors which are mainly single pass TMPs, membrane transport tends to be multipass TMPs. This group of membrane proteins are divided into two major classes of transport proteins, the carrier and channel proteins. In general, a channel protein is a special arrangement of amino acids which are embedded in the cell membrane, providing a hydrophilic pore for water and small, polar ions. In essence, it enables charged substances to diffuse through the non-polar lipid bilayer into or out of the cell. It can either be open all the time, called the non-gated channel protein or in a closed conformation, called gated channel protein. Both have their distinct features. In the open state the channel proteins enable ions and water to flow through the hydrophobic cell membrane, moving from an area of high concentration to an area with a lower concentration. This process is called facilitated diffusion. Whereas the gated channel protein remains closed, since it has a binding site that is specific for a given molecule or ion. Upon a stimulus, such as a chemical or electrical signal it causes the "gate" to open or shut. ^[9,10] However, not all facilitated diffusion is performed by channel proteins. Carrier proteins are also involved in facilitated diffusion. In contrast, carrier proteins do not form channels, rather interact directly with the molecule of interest due to their binding site. Since large molecules are not able to pass through the narrow pore provided by the channel proteins, they bind to carrier proteins instead. Upon binding they undergo a series of conformational changes to transfer the bound molecule to the other side of the membrane. Thus, carrier proteins work without energy, and move molecules down their concentration gradient such as facilitated diffusion of sugars, amino acids, and nucleosides across cell membranes of most cells. ^[9,10] Conversely, carrier proteins that transport molecules against the concentration gradient are those which use substantial energy. Depending on the energy source, the carrier proteins can be classified as ATP-driven, or electrochemical potential-driven. ATP-driven carrier proteins require ATP coupling to transport molecules, such as the sodium-potassium pump in the plasma membrane. To maintain the appropriate cellular concentrations of sodium and potassium ions it removes three sodium ions from the inside of the cell and replaces them with two potassium ions from the outside into the cell for each ATP molecule used for the transport. This type of active transport wherein chemical energy like ATP drives the process is called primary active transport.

Secondary active transport concludes electrochemical potential-driven carrier proteins which are moved by an electrochemical potential gradient. If the carrier protein carries two molecules in the same direction, it is called a symporter, whereas if two molecules are transported in opposite directions, its name is antiporter. However, there are also single molecules carried by so-called uniporters. ^[11]

Enzymes are another type of protein which can also be membrane proteins (Scheme 2). They mainly act as catalysts, thus catalyzing the biochemical reactions that occur in cells. The mode of action is based on lowering the activation energy of the reaction to make a biochemical reaction more likely to proceed. As a result of that, these reactions run in a much faster way than they would without a catalyst. Enzymes are highly substrate specific and work by binding to one or more substrates. Upon binding the enzyme undergoes a conformational shift that orients or strains the substrates to become more reactive. Enzymes in the membrane, such as oxidoreductase, transferase, or hydrolase, transform a molecule into another form. ^[8]

1.3 Functions of membrane proteins

The proteins in the plasma membrane usually help regulating the cell's response and interaction with its environment. Membrane proteins are responsible for carrying out most of the functions of these membranes. The different subtypes of membrane proteins already give rise to the diverse functions of this class of protein. These include intercellular joining, enzymatic activity, transport, cell-cell recognition, anchorage/attachment, and signal transduction (Fig. 3).^[12]

The transport is an essential function carried out by membrane transport proteins. Generalized, it is the movement of ions, small molecules, and macromolecules, such as another protein, across a biological membrane. Integral transmembrane proteins assist in the movement of substances either by facilitated diffusion or active transport. Facilitated diffusion is performed by hydrophilic channels that are selective for a particular solute. In contrast, other transport proteins require cellular energy for the movement of molecules across a cell membrane from a region of lower concentration to a region of higher concentration against the concentration gradient, so called active transport.

As already explained, all enzymes are a type of protein. An enzyme situated in the membrane, may have its active site facing substances outside of the lipid bilayer. In some cases, several enzymes in a membrane are organized as a team that carries out sequential steps of a metabolic pathway. An example for this would be the absorption of lactose into the cell by galactoside permease, a hydrophobic membrane transport protein for galactosides, followed by the hydrolysis of lactose into the two monosaccharides glucose and galactose by β -Galactosidase.

Signal transduction, also known as cell signaling, is the transmission of a chemical or physical signal through a cell as a series of molecular events, resulting in a cellular response. To ensure an appropriate response cell-surface receptors transmit the signal from a cell's exterior to its interior. Transmission is continued either by a series of biochemical changes within the cell or by modification of the cell membrane potential. Activated receptors stimulate the production of intracellular messengers, also called second messengers, within the cell, which in turn activate other enzymes and so the cascade continues. This transmission is needed when a signaling molecule, such as a hormone or a neurotransmitter cannot pass directly the transmembrane. Since they're hydrophilic and polar, they cannot cross the lipid and non-polar membranes, therefore using signal transduction to transmit their messages.^[13]

Another important function of membrane proteins is the cell-cell recognition. Cell recognition helps the immune system to recognize foreign invaders entering our body. This process is carried out by glycoproteins, a group of complex proteins consisting of a bound carbohydrate molecule located on the exterior surface of cells. Glycoproteins help cells recognize one another by reading unique patterns of oligosaccharides and will bind together. Upon binding, a response for communication, cooperation, transport, defense, and/or growth is triggered. These types of events can be classified into intrinsic recognition and extrinsic recognition. The former describing cells from the same organism associate, whereas extrinsic recognition reports when cells from diverse organism recognize each other. [12]

Neighboring cells have membrane proteins that connect each other through junctions such as gap junctions, tight junctions, or anchoring junctions. This intercellular joining helps the cells communicate and connect. Tight junctions seal adjacent cells together tightly to another, forming a semipermeable diffusion barrier that cannot easily be crossed. The permeability is size- and charge-selective. Cells connected by tight junctions, serve as barriers in the body sealing off cavities and preventing leaks. Anchoring junctions connect neighboring cells in particular spots, but they do not seal the two cells together. In anchoring junctions' internal plaques attached to the cytoskeleton are joined by intercellular filaments. This creates a shade of cells that are strong but also flexible, which is needed in organs where tissues must stretch such as the stomach or bladder. Gap junctions connect adjacent cells with a protein channel that allows for communication and for the transport of small molecules and ions. They are important in heart muscle and smooth muscle because they allow for the flow of ions that let these cells contract as a unit. All these junctions are important for forming strong connections with one another, establishing communication, and preventing the passage of unwanted materials. [14]

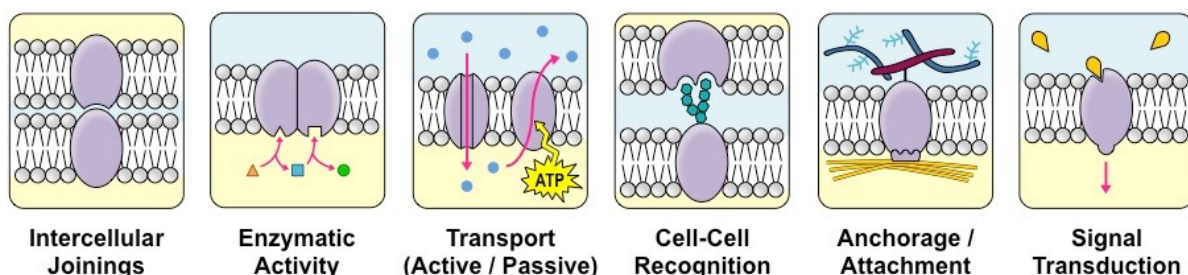


Figure 3: The diverse functions of membrane proteins. Adapted from [15]

In order to achieve cell motility, the plasma membrane and the cell shape are constantly changing. This is enabled by the attachment of microfilaments or other elements of the cytoskeleton to membrane proteins. The network of cytoskeletal fibers connects every corner of a cell and gives the cell its shape. Changes of cell shape rely heavily on one type of cytoskeletal protein, known as actin. Its building block consists of a small globular protein called g-actin which is normally bound to ATP as a monomer. These ATP-bound G-actin monomers polymerize into filaments known as f-actin. Their function is to maintain the shape of the cell and keep the location of membrane proteins stable. [16]

1.4 Challenges in Studying Membrane Proteins

This subset of proteins is represented in 20 to 30% of the proteomes of most organisms. Along with their functions and involvement in various biological processes, it highlights the importance of studying membrane proteins. Not just in view of possible new fundamental roles in biological process but also for finding new drug targets for therapeutics. Anyhow, the area of membrane proteins in structural biology remains challenging and is still a largely unconquered area. To date there are over 177 000 entries in the Protein Data Bank (PDB) repository of protein structures, but only about 1% of these entries represent membrane proteins. ^[17]

This proves that membrane proteins are studied with difficulties for several reasons. The three main reasons are their partially hydrophobic surfaces, flexibility, and lack of stability. This leads to various challenges, starting from expression, solubilization and purification right through to crystallization, data collection and structure solution.

1.4.1 Expression and purification

It is well known that membrane proteins have either been purified from natural sources, produced recombinantly or, in the event of short peptides, synthesized chemically. So far membrane proteins have been successfully expressed in different model organisms such as bacteria, yeasts, insect cells and in mammalian cell lines. Nevertheless, there are a couple of factors, influencing the expression in such organisms. Even though the expression in the bacteria *Escherichia coli* is quick, relatively inexpensive, and easy to use, eukaryotic proteins, in contrast, require mostly the use of eukaryotic systems for expression.

Membrane proteins for example are not just released into the cytosol but must rather be targeted to the host cell membrane before they can fold correctly. Therefore, a specific system such as SRP-Sec61, a translocation pathway for eukaryotic cells, is required in the host cell to insert membrane proteins into the endoplasmic reticulum of eukaryotic cells.

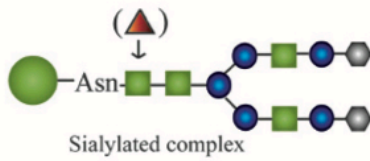
Beyond that, membrane proteins are embedded in lipid, whose composition may differ among the systems, affecting the stability of the protein and consequently its probability of crystallization.

Posttranslational modifications (PTMs) are the last contributing factor that determines the yield, integrity, activity, and stability of synthesized MPs. Common PTMs of eukaryotic MPs are glycosylation, prenylation, phosphorylation, disulfide bond formation and proteolytic processing (Scheme 3).^[18]

These events explain why structures of eukaryotic membrane proteins in the PDB are mostly purified from native sources and only fewer in recombinant methods.

The purification of the protein is another crucial and at the same time challenging process. Using detergents, which cover the hydrophobic surface of the protein, membrane proteins are extracted from the host cell membrane. The choice of detergent depends on extracting the largest quantity of soluble, active, homogeneous, and stable protein, whereby the cost of the detergent is not limiting. The water-soluble lipid-like nonionic detergent dodecyl maltoside (DDM) is most often used for the isolation of hydrophobic membrane proteins from the lipid bilayer as it is inexpensive and preserves protein activity in a stable manner.

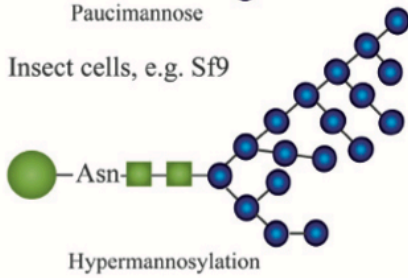
I Glycosylation, e.g. N-linked



Mammalian cells



Insect cells, e.g. Sf9

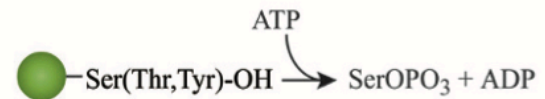


Yeasts, e.g. Pichia

Targeting, stability, activity, folding and conformational changes.

- GlcNAc
- ▲ Fucose
- Mannose
- ⬡ Sialic acid

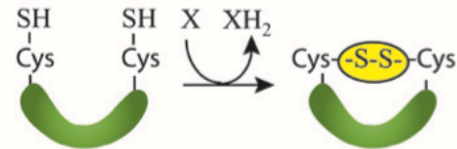
III Phosphorylation



Mammalian cells/ Yeasts/ Insect cells/ *E. coli*

Signal transduction, regulation

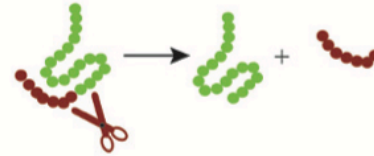
IV Disulfide bond



Mammalian cells/ Yeasts/ Insect cells/ *E. coli*

Folding, stability

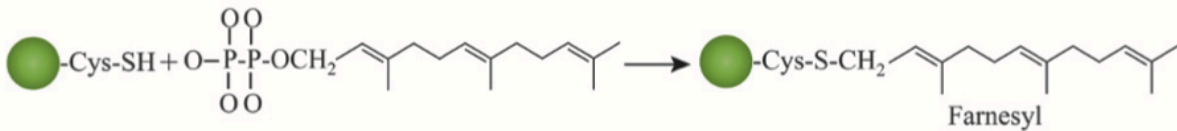
V Proteolytic processing



Mammalian cells/ Yeasts/ Insect cells

Maturation, activation

II Lipidation, e.g. Prenylation



Mammalian cells/ Yeasts/ Insect cells

Membrane anchor, protein-protein interaction

Scheme 3: Posttranslational modification pathways in MP expression systems. Schematic overview of most frequent PTMs and their impact on structure and function of MPs. Adapted from [18]

1.4.2 Crystallization

Comparatively to the detergents in the purification process, the determining step in the crystallization process are the crystallization reagents. Once the ideal crystallization conditions are found, further optimizations are made and the initial screen is followed, using 96-well plates for the crystallization approach. The major challenges are to provide enough protein and to obtain well-ordered 3D crystals. This is mostly achieved through the widely used crystallization technique, the hanging-drop method. Here, crystallization is driven by the increase of precipitant concentration in a, by now, nanoliter drop of protein solution by vapor diffusion. However, proteins with small extramembrane domains are difficult to crystallize since detergents may restrict crystal contacts. In this case, co-crystallization of the protein with structural monoclonal antibody fragments is one strategy which can be used to overcome this problem. ^[19] Since many membrane proteins consist of relatively small hydrophilic domains, this approach increases the probability of obtaining well-ordered crystals by enlarging the polar surface of the protein. Generally, this is enabled by attaching polar domains with specifically binding antibody fragments. ^[20]

1.4.3 Data collection and structure solution

Nowadays, the use of robotics in protein crystallography revolutionized at almost every stage of the pipeline starting from protein cloning, over-expression, purification to crystallization, data collection, structure solution, refinement to validation and data management. The data collection on soluble protein crystals is routinely performed in a high-throughput environment. Crystal mounting robots containing a sample changer, provide automatic sample mounting, orientation, and retrieval with automated data collection and semi-automated structure solution. ^[21]

Due to the high number of detergents forming micelles, which cover the hydrophobic part of the protein, the situation is often more challenging. Thus, the crystals are often unstable, unhandy, diffracted to low resolution and sensitive to radiation during the diffraction experiment. Other than that, crystal quality can vary significantly, even between crystals from the same drop, meaning many crystals must be screened before data can be collected.

Radiation damage impedes to collect data of sufficient quality by single anomalous dispersion (SAD) or multiple anomalous dispersion (MAD) affecting the process of structure solution. Also, non-isomorphism among the crystals can influence structure solution by the isomorphous replacement method. This method is known to be one of the dominant ones in macromolecular crystallography. Hereby, diffraction data sets of two isomorphous crystals, one of the native macromolecules and the second crystal being one of the heavy-atom derivatives of the same macromolecule, are compared with each other reflection by reflection. These differences enable the determination of the substructure. ^[17]

1.5 Biophysical techniques

Transmembrane proteins are important cellular components, performing several indispensable functions for the cell, as already stated. Due to their importance in cell function, they constitute extremely interesting drug targets. It is known for example, that the G protein-coupled receptors (GPCRs) not only comprise the biggest family of membrane receptor proteins but also constitute about 50% of all drug targets. ^[22] Normally, at the large screening scale, drug design is mainly ligand-based and relies mostly on the physico-chemical features of the drug and the mechanism whereby the ligand recognizes the specific binding site. For drug designers targeting TMPs it is advantageous to learn structural properties of the target protein and detect conformational changes of TMP that occur. Nevertheless, even in GPCRs there is a considerable number of genes that have remained unexplored. To understand the function of the remaining genes but also transmembrane proteins in general, structures and dynamic events must be determined.

To date, only a few atomic structures describing TMPs, and their physiological importance have been solved compared with the number of solved water-soluble proteins. However, this illustrates again, that structure determination of TMPs remains a difficult task since their domains are inserted within lipids, which depicts a challenge for their expression and purification. Nevertheless, analysis of conformational changes and functions of TMPs requires high-resolution 3D structures of the different conformations. Following techniques are used to obtain 3D structures: X-ray diffraction, electron microscopy, NMR, and modelling. ^[19]

1.5.1 X-ray crystallography

The most common method to determine high-resolution structures of proteins, such as TMPs, is X-ray crystallography. Thereby, all atomic details of the protein are illustrated showing any bound water, lipid, and detergent molecules. Although protein crystallography is a well-established approach, those intending to solve the structure of TMPs using X-ray crystallography are faced with several challenges. Apart from the already exemplified challenges in crystallization, TMP crystals are often highly sensitive to temperature, difficult to handle and flash-freeze due to the weak interactions and large amounts of amphiphilic molecules.

Once diffraction data from crystal is reasonable, the next step towards 3D reconstruction is the solution of the so-called "phase problem" which, in the case of TMPs, involves the use of heavy-atom derivatives and/or anomalous scattering. Since the structure of a homologous TMP is rarely known, the use of a technique called molecular replacement, where a similar molecule's already-known phases are grafted onto the intensities of the molecule at hand, to solve the phase problem is not usually possible. Other than that, fragility problems occur once the crystals are soaked in a solution of similar composition to the growing medium supplemented with heavy atoms. Another limitation adds up when fixing heavy atoms to specific sites due to a lack of accessibility to these sites and because of non-specific interaction of hydrophobic heavy-atom compounds with the detergent.

It is noteworthy that crystals growing by vapor diffusion often grow larger but have a limited diffraction pattern (typically 3 Å or higher), whereas micro-crystals grown in lipidic cubic phases can easily diffract beyond 2 Å. ^[19]

The next steps are model building and refinement. As soon as diffraction data and phasing information are obtained a first protein model is built from experimental electron-density maps and refined by alternating energy minimization and manual corrections, followed by simulated annealing. Then, water, lipids and detergents tightly bound to the protein are refined. These kinds of molecules can, when resolved in crystal structures, offer unique information respecting lipid-protein interactions and illustrate how such interactions mediate oligomerization of larger complexes.

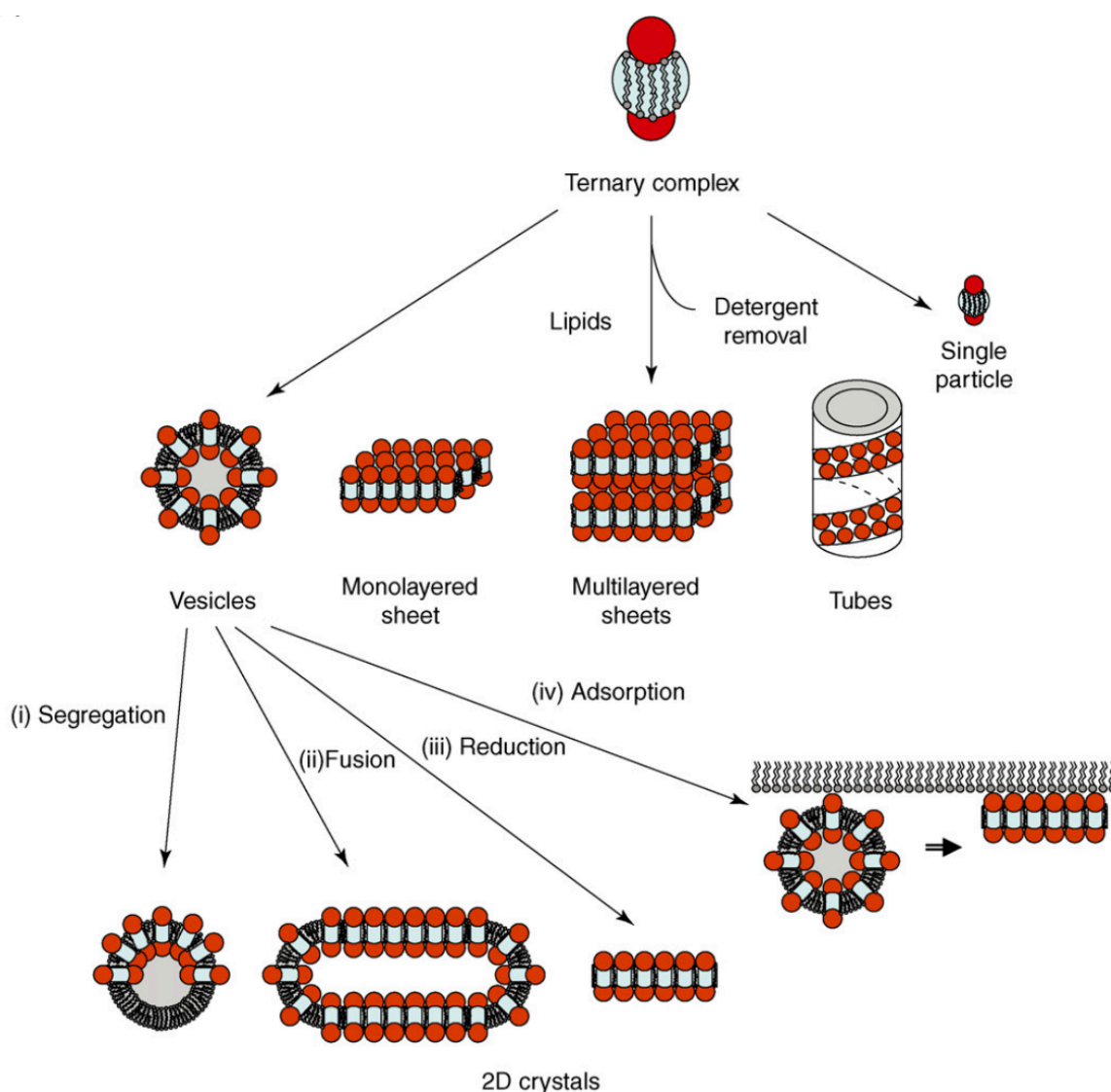
1.5.2 Electron microscopy

Another technique for obtaining high resolution images of biological and non-biological specimens is called electron microscopy (EM). Electron microscopy has been developed to study the structure of biomacromolecules. It enables images at distinct resolutions, ranging from high to medium (1.9 - 4 Å) up to low (10 - 20+ Å) levels. The different resolutions depend on the microscope used, the staining technique and the state of the sample. Highest quality native structures in EM are obtained, when irradiation damage from the electron beam to the sample is reduced. To realize this, the currently well-known technique called cryo-EM was developed. Here, the protein is kept in a very thin layer and frozen. An electron gun shoots electrons at the speed of light, passing through the sample. Then, a high-tech camera captures the electrons to form an image. On the one hand the camera gives you a sharp image in a better condition and on the other hand it can record a movie instead of a steady picture. Furthermore, these images are sorted regarding the protein's orientation. In the end the software builds an accurate, high-resolution, three-dimensional image of the protein. In contrast to X-ray diffraction, which requires 3D crystals, EM imaging is efficient with 2D crystals or single particles for 3D reconstruction. Even though EM crystallography of TMPs embedded in lipid bilayers bypasses the existing "phase problem" in X-ray crystallography, both methods require the difficult step of crystal growth.

Depending on the type of crystal obtained, various 3D-structures can be determined, which also influences the resolution (Scheme 4). To get a 3D reconstruction, different projection maps of the monolayered 2D crystals, being tilted in the electron beam, are merged. Since the sample can only be tilted 70-75° and not fully until 90°, there is a so-called "missing cone" of data in the results, providing spatially inhomogeneous resolution. Other than that, multilayered crystals are not yet useful in obtaining a 3D structure as the analysis of such images is too complex. However, tubular crystals are unique in its analysis because all orientations of a single-bilayer-associated TMP are observed without tilting in a single image of frozen-hydrated tube, meaning that resolution of the reconstructed 3D structures is equal in all directions.

The following techniques enable the formation of 2D crystals from vesicles by forcing protein-protein interactions. It can be induced either by vesicle fusion, protein segregation upon addition of crystallizing agents to proteoliposomes, reduction of lipid-to-protein ratio or adsorption onto functionalized lipid monolayer (Scheme 4). Still the choice of lipids and the lipid-to-protein ratio is crucial for obtaining crystals.

The single-particle EM approach is used to crystallize large complex macromolecules, where particles are either immobilized on a carbon-film surface, also known as negative staining, or within a layer of vitreous ice (cryo-EM). After the imaging process, the individual particles are identified and each of them classified upon its orientation in the micrograph. ^[19]



Scheme 4: Electron microscopy studies can be performed on various material such as ternary complexes observed as single particles or crystals. Adapted from ^[19]

1.5.3 Nuclear magnetic resonance

Nuclear magnetic resonance (NMR) spectroscopy is a technique to observe local magnetic fields around atomic nuclei. It enables the determination of the structure and dynamics of various molecules including peptides and proteins without crystal growth by excitation of the nuclei sample, which is detected with sensitive radio receivers. The idea behind NMR is that all nuclei are electrically charged and many of them have spin, causing them to behave like a magnet. Through an external magnetic field, the base energy is transferred to a higher energy level. If the nucleus has spin at lower energy, it generates a magnetic field in the direction of the external magnetic field and conversely if it has a spin at higher energy. The wavelength of the energy transfer corresponds to radio frequencies, meaning when the spin returns to its base level, energy is emitted at the same frequency and measured.

For the use of TMPs there are different technical approaches, such as solution or solid-state, performed depending on the objects being studied. When using solution NMR, TMPs are usually studied in the presence of deuterated lipids and detergents. Here, the micelle environment is the most-used approach, but recent progress has been made using bicelles made of short-chain and long-chain phospholipids. They represent a promising tool for studying membrane proteins such as TMPs by NMR in a lipid environment. In terms of solid-state NMR, magic-angle spinning, and oriented planar bilayers samples are also used. The latter constitutes the method of choice for determining the orientation and dynamics of TMP helices that are inserted in lipid bilayers in addition to detecting kinks, curvatures, and unwound regions. Whereas magic-angle spinning experiments range from isotopic enrichment (^{13}C block labelling) to structure-determination strategies and provide distance and torsional constraints.

Additionally, NMR techniques can provide dynamic information regarding protein-ligand and protein-protein interactions. By the use of experimental protocols based on labelled (^{13}C and ^{15}N) and unlabeled partners relevant information is gathered by comparing spectra obtained in the absence and presence of partner(s) without the need to solve the structure of the corresponding complex. This is enabled either by chemical-shift mapping, the resonant frequency of a nucleus relative to a standard in a magnetic field or by docking protocols such as high ambiguity driven protein-protein docking (HADDOCK) software, an integrative platform for the modeling of biomolecular complexes. ^[19]

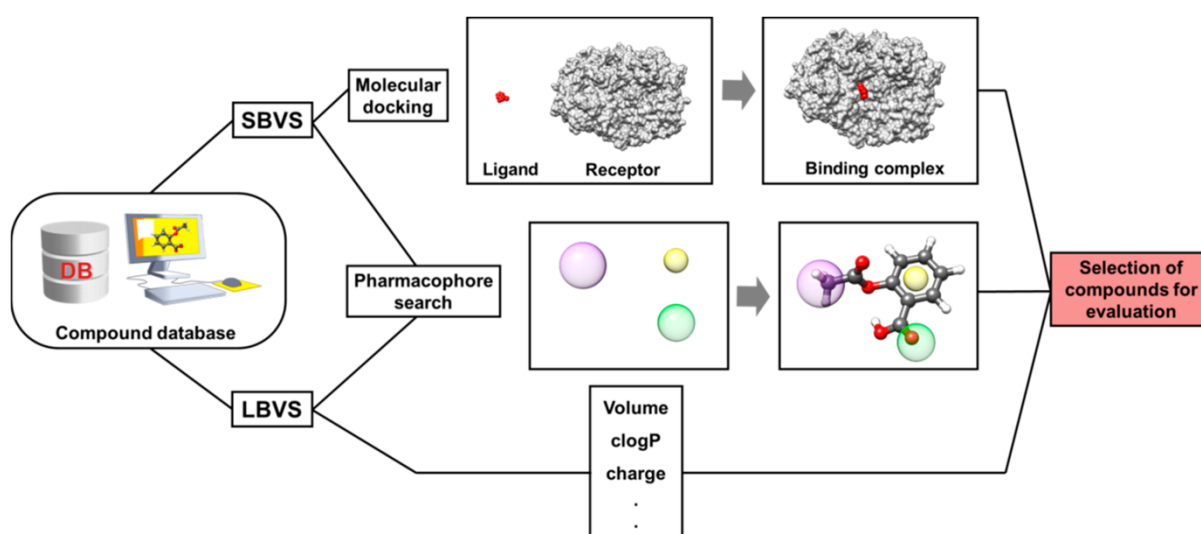
1.6 Molecular Modeling

Molecular modelling comprises all theoretical methods and computational techniques to mimic and study the structures of molecules, starting from small chemical systems up to large biological molecules. Due to the high demand and a lot of open-source software, it has started to become widely used. Using detailed 3D structures various features such as motions, interaction properties and conductance, when dealing with channels, are captured. ^[19] With the help of molecular modeling, potential new drugs can be predicted based on their ability to bind strongly to the target.

Virtual screening (VS) is a collection of several *in silico* techniques in drug discovery to search libraries of small molecules in order to identify chemicals which are actually most likely to bind to a drug target, mostly being protein receptors or enzymes. Virtual screening can be used to select compounds for screening from in-house databases, other than that it can be used to choose compounds which then can be purchased from external suppliers, or it can also be used to decide which compound should be synthesized next. The virtual screening method used is based on the amount of information/data available about a certain disease target. If the 3D structure, which is the protein structure of the target, is known then the preferred strategy is structure based virtual screening (SBVS), performing molecular docking (Scheme 5). The general approach of SBVS is to dock the ligand database into a previously selected target binding site. Then, SBVS provides prediction of the binding mode and a ranking of the docked molecules, which can be applied as the crucial criterion for selecting promising molecules, or it can be merged with other evaluation methods. In the end, the selected compounds are experimentally evaluated to determine their biological activity on the molecular target. The molecular docking approach of SBVS consists of these four steps: (i) molecular target preparation; (ii) compound database selection; (iii) molecular docking; and (iv) post-docking analysis. Each step has to be executed thoroughly to provide reasonable results. ^[23]

Even though this master thesis focuses on structure-based methods, it is worth mentioning that VS strategies include but are not limited to ligand-based virtual screening (LBVS, Scheme 5). The basic principle of LBVS is to investigate molecular descriptors, structural or physicochemical properties of a molecule or part of a molecule, using known active compounds. In this way characteristics of a compound series are identified and subsequently applied as molecular filters to make use of compound selection for experimental evaluation and decrease the chemical space to be explored in further

screening steps. Another significant and valuable LBVS approach is the generation of pharmacophore models, a collection of structural features from known ligands. These ligand-based 3D pharmacophore models are based on structural properties thought to be essential features for one compound's biological activity (Scheme 5). Typical pharmacophore features include hydrophobic centroids, aromatic rings, hydrogen bond acceptors and/or donors, cations, and anions. These four steps have to be followed to generate a 3D pharmacophore model: (i) exploring the conformational space of the compound series; (ii) identifying reciprocal properties; (iii) aligning the molecules according to the identified properties, and (iv) generating the pharmacophore model. Since chemically diverse libraries are used for computational and biological screening, the generated pharmacophores help identifying more molecules which share the same features. Other than that, pharmacophores make use of developing 3D-QSAR models, another useful ligand-based drug design method (LBDD). [23]

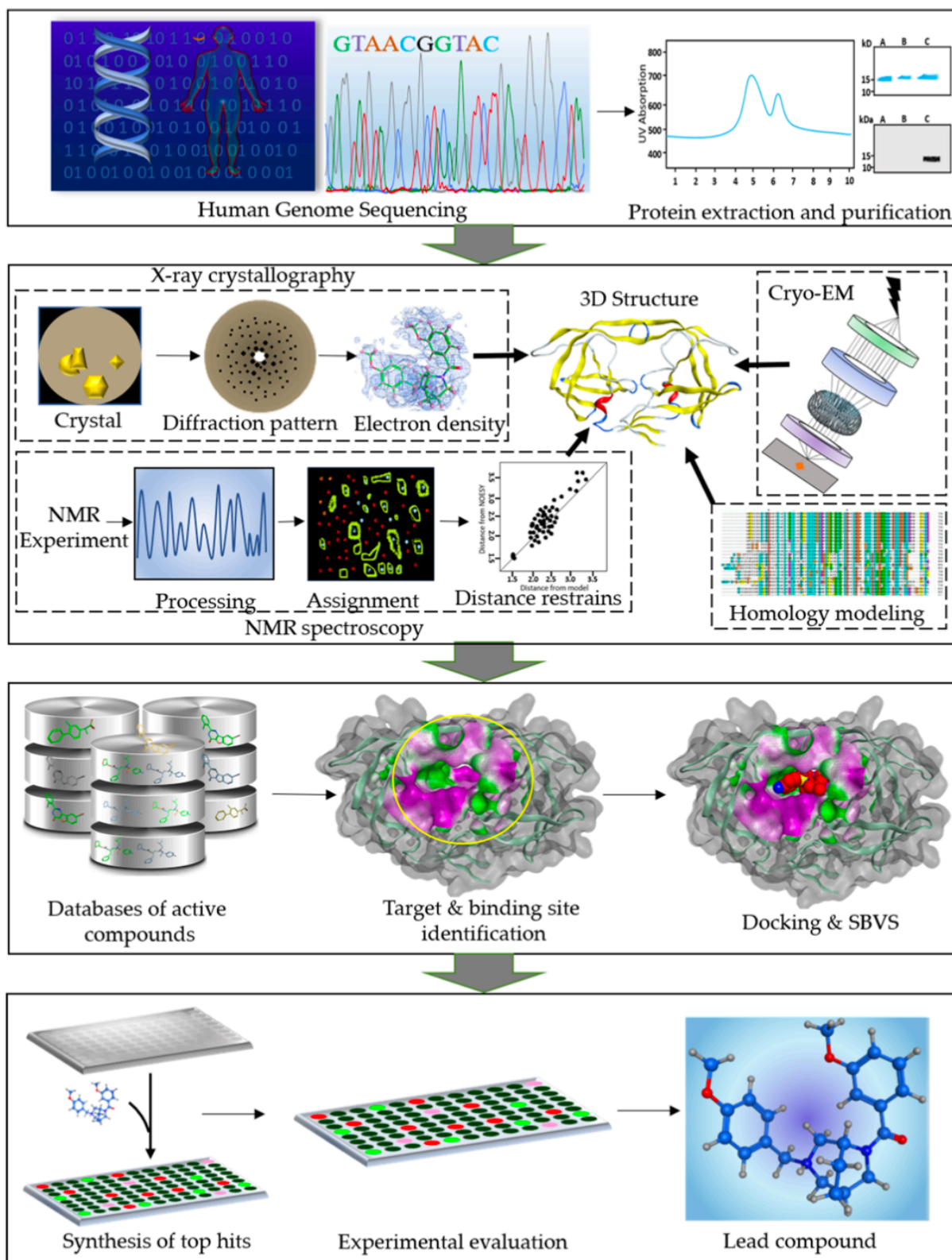


Scheme 5: The outline of SBVS and LBVS approaches. Adapted from [23]

1.6.1 Structure-Based Drug Design

For decades, drug discovery was performed by experimental screening of large libraries of chemicals against a therapeutically relevant target, known today as high-throughput screening (HTS), with the goal of identifying new lead compounds. Thereby, active compounds showing pharmaceutical effects can be observed, which act as a starting point in early-stage drug discovery to understand the role of a particular biochemical process. However, due to its disadvantages such as high costs, being time-consuming and the obscurity of the mode of action of the active molecules the demand of a new revolutionary technique has been created. Now, structure-based drug design (SBDD) methods are widely used in modern medicinal chemistry to understand the principles by which small-molecule ligands recognize and interact with macromolecules. It is known, that SBDD approaches are more efficient to the prior techniques since its goal is not just to identify bioactive compounds but also to understand the ligand-protein binding event on a molecular level. This is enabled by using computational methods and the 3D structural information of the protein target, which is usually obtained experimentally or through homology modeling. The most frequently used SBDD methods are molecular docking, structure-based virtual screening, and molecular dynamics simulation. They provide a broad range in molecular recognition events as for instance binding energetics, molecular interactions and induced conformational changes. The strategy is as follows (Scheme 6): The completion of the Human Genome Project enabled sequencing of the DNA, helping us to discover most human genes and proteins, which could be extracted and purified afterwards. They also serve as a prerequisite of basic research in early drug discovery. A typical SBDD process starts with the biological target protein identification and validation. By the advances in biophysical methods (NMR, X-ray, or cryo-EM) various number of 3D structures were generated or *in silico* methods such as comparative modeling, threading, and *ab initio* modeling are applied to model the protein's 3D structure as it is needed to perform further analyses. Once the 3D structure is predicted, the binding site of the protein needs to be identified, usually a small cavity where ligands bind to the target and elicit their pharmacological effect. As ligands are able to bind either to a proteins orthosteric (active) site as well as to the allosteric site, which is located elsewhere, it is crucial to identify the appropriate site on the target protein. The next step in the SBDD workflow is hit discovery, which is mainly done by docking compound libraries into the binding cavity of the target protein. This is performed by *in silico* methods such as

virtual screening or *de novo* drug design. The former has been previously described being a computationally screening approach of drug-like compound libraries that are already commercially available against targets of well-known structure. Wherefore, *de novo* drug design approach, is utilized to design structurally novel molecules based on the binding site of the 3D structure. In the next stage, top ranked hits showing high affinity towards target protein are synthesized and optimized. Then, biological properties, such as potency, affinity, and efficacy, are evaluated in vitro in biochemical assays. Afterwards, 3D structures of the ligand-receptor complex of all new lead compounds can be solved to analyze various intermolecular interactions enabling the molecular recognition process. In this way, SBDD methods can investigate binding conformations, characterize key intermolecular interactions, unknown binding sites, mechanistic, and clarify ligand-induced conformational changes. Due to the evermore increasing computational power and the improvement of software, methodologies and forcefield parameters, the use of computers in structure-based drug design brings additional advantage of providing new drug candidates in a more time-saving and cost-effective way. This again underlines the important role of computational methods of SBDD and its ever-growing impact in the pharmaceutical research. [23,24,25,26]



Scheme 6: Workflow of the structure-based drug design (SBDD) process. Adapted from [25]

1.6.2 Homology Modeling

3D structure determination is enabled through homology modeling, an accurate computational structure prediction method. Homology modeling, also known as comparative modeling, predicts the 3D structure of a given protein sequence (target) based primarily on its alignment to one or more proteins of known structure (templates). The structure prediction process is composed of multiple steps which are summarized in Scheme 7. [27]

The very first step in homology modeling is to identify and select template structures, which are then used for further procedures. The target (query) sequence is the requirement for searching eligible templates. This is done by different approaches, such as profile-profile alignments, Hidden Markov Models (HMMs) and Basic Local Alignment Search Tool (BLAST). The latter provides pairwise sequence-sequence alignment, being used in databases like National Center for Biotechnology Information (NCBI, <https://www.ncbi.nlm.nih.gov/>) and UniProt (<http://www.uniprot.org/>).

Following features are considered in choosing an eligible template. These include high sequence similarity, phylogenetic similarity, environmental factors such as pH, solvent type, and existence of bound ligand. Also, the resolution of the experimental structure must be considered to ensure the most optimal conditions in building an accurate target structure. [27]

After the identification of the templates, the best structure must be selected with respect to the mentioned factors. Sequence similarity of the template sequence in relative to the target sequence plays an important role to generate 3D structures with high accuracy. Nevertheless, sequence similarity in homology modeling has a minimum value of >25%. [27]

The next step in the workflow is the sequence alignment and alignment correction, if needed. The alignments conclude target-template and template-template in case more than one template is used. Since an error in the alignment of a residue causes shifting of α carbon or single residue gaps in an α helix section triggers rotation of the remaining residues in the helix, alignment of sequences in the right way are essential in homology modeling. Following alignment methods are mostly used: Clustal W (<http://www.genome.jp/tools-bin/clustalw>), T-Coffee (<http://tcoffee.crg.cat/>), 3Dcoffee (<http://phylogeny.lirmm.fr/phylo.cgi/>) and MUSCLE (<https://www.ebi.ac.uk/Tools/msa/muscle/>). [23]

For model building there are various methods used to generate 3D models for the target sequence based on its templates. The model building approach can be

distinguished between rigid body-assembly methods, segment matching methods, spatial restraint methods and artificial evolution methods.

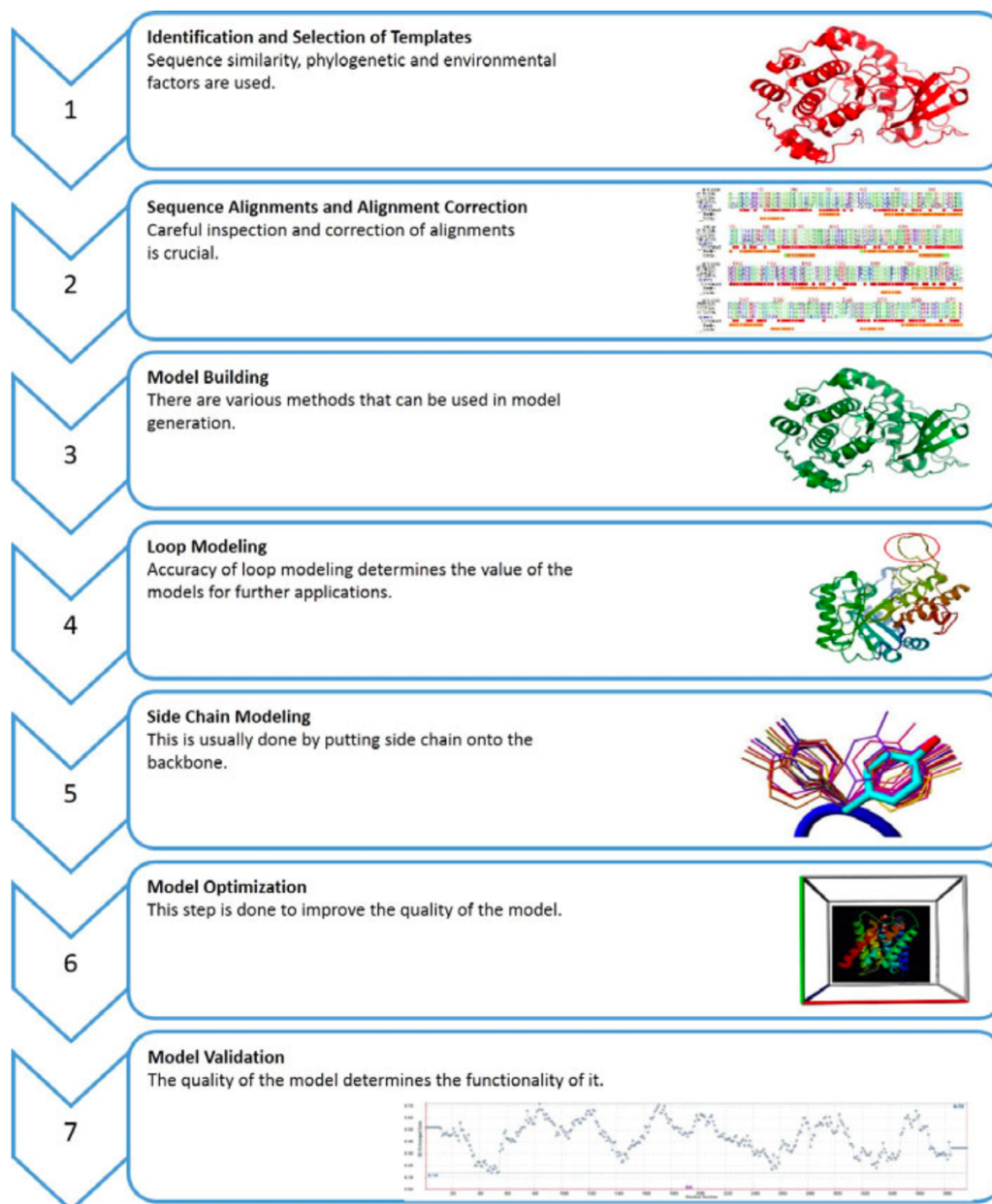
In the first method the protein structure is broken down into basic conserved core regions, loops, and side chains. These rigid parts are picked up from the aligned templates to build a protein 3D structure. This method is used by tools like 3D-JIGSAW, BUILDER and SWISS-MODEL. In the next method a cluster of atomic positions obtained from the template structures are used as leading positions. Based on sequence identity, geometry, and energy selection of segments from known structures is done in databases using SEGMOD/ENCAD. Spatial restraint methods build the model by facing restraints from the template structure. These restraints are defined by stereochemical restraints on bond length, bond angle, dihedral angles and van der Waals contact distances, which is performed by MODELLER. The last method, artificial evolution, uses rigid-body assembly method and stepwise template evolutionary mutations together until the template sequence is the same as the target sequence. This is done by NEST. [27]

The next step in homology modeling is called loop modeling. Homologous proteins contain gaps or insertions which are called loops, whose structures are not conserved during evolution. Loops often define the specificity of the function of a protein structure. That's why the accuracy of loop modeling is a crucial step for the value of the generated models for further applications. However, it is more difficult to predict the structure of a loop compared to strands and helices, since loops show higher structural variability. The development of loops is either done by database search approach or by conformation search approach. The first approach searches for all the known protein structures to detect segments, which provide the critical core regions. The latter depends more on a scoring function optimization. Monte Carlo simulations are *de novo* methods, which are developed for loop conformation predictions by investigating for conformational space. These methods are primarily not limited by the length of the loop, but as the length of the loop increases, possible conformation number increases as well, which makes the modeling very time consuming. Servers used for loop modeling are ArchPRED (<http://www.bioinsilico.org/ARCHPRED/>) and Congen (<http://www.congenomics.com/congen/doc/>). [27]

Side chain modeling follows right after loop modeling. Here, the aim is to put side chains onto the backbone coordinates that are derived from a parent structure. However, the prediction of side chains is facilitated in models with high sequence similarity.

Rotamers are called protein side chains, which are present in few structures with low energy. Then, depending on defined energy functions and search strategies, rotamers are selected corresponding to the preferred protein sequence and the given backbone coordinates. Tools like RAMP (<http://www.ram.org/computing/ramp/>) or SCWRL can be used to predict residues for the hydrophobic core with high accuracy, whereas residues on the surface exposed to water have a lower accuracy. ^[27]

Generated models have to be optimized afterwards. The initial step of model optimization starts with an energy minimization utilizing molecular mechanics force fields. The purpose of this step is to eliminate errors at each energy minimization step. Although few are eliminated, many other small errors arise and start accumulating at the same time. Hence, errors are reduced by restraining the atom positions, introducing energy minimization with a few hundred steps, and applying more precise force fields like quantum force fields and self-parameterizing force fields. If the model needs further optimizations, methods such as molecular dynamics and Monte Carlo can be utilized. Since the generated models have different accuracy due to sequence similarity, environmental parameters and the quality of the templates, its accuracy determines its further use in diverse areas. Therefore, beside model optimization it is also required to verify and validate the constructed model. Starting with stereochemistry of the model, analyzed features are bond length, torsion angle and rotational angle. Common tools to determine stereochemistry of the model are WHATCHECK (<https://swift.cmbi.umcn.nl/gv/whatcheck/>), PROCHECK (<https://www.ebi.ac.uk/thornton-srv/software/PROCHECK/>), Molprobity (<http://molprobity.biochem.duke.edu/>). Spatial features based on 3D conformations and mean force statistical potentials are determined either by SAVES (<https://saves.mbi.ucla.edu>) or by ProSA-web (<https://prosa.services.came.sbg.ac.at/prosa.php>). Environmental parameters are considered by these kinds of tools for model construction appropriate to the expected environmental conditions. ^[27]



Scheme 7: Steps of homology modeling. Adapted from [27]

Homology modeling intends to fill the gap between protein sequences available and protein 3D structures determined experimentally. This is done by generating 3D structures of proteins from their sequences by using templates with an accuracy similar to the experimental methods. As the need for these models has increased in recent years, tools and servers improved the overall model quality and accuracy. Since membrane proteins represent an important therapeutic drug target class, progress in their determination will accelerate the drug discovery process. Therefore, it is believed that homology modeling and its applications in the drug discovery process will also have a huge impact soon. [27]

1.6.3 Molecular Dynamics

In addition to the experimental development, recent technological and computational algorithms advancements along with homology modeling improved *in silico* studies to gather expertise of PMP processes at the atomic level. Since experimental studies have their challenges and limits, computational biology serves as a helpful tool to bridge this gap. They can provide insights into the kinetics and driving forces for protein folding dynamics, conformational changes of transporters, and lipid-lipid, protein-protein, protein-lipid, or protein-ligand interactions. These simulations are performed currently between picoseconds to microseconds. As it is known, protein structures from crystallographic studies are static, but computational tools provide the capabilities to assemble them into a mechanism of motion to observe conformational changes. Computational methods such as molecular dynamics (MD) give an understanding of molecular forces that drive a given process based on the biophysics and biochemistry of a biological system. [28]

MD is a valuable tool providing atomistic details of the interaction and detailed dynamics and energetics of the biological process. Its use is based on Newton's equations of motion and on a forcefield to simulate the flow of atoms with respect to each other. Forcefields are composed of equations and parameters to reproduce stretching, bending and rotations of covalent bonds to maintain planarity and chirality of several groups just as to simulate Van der Waals and electrostatic interactions. [25] These parameters are determined by the basis set used for computations. Large datasets give a deep insight in the molecular understanding of the regarding complex, whereas small datasets are used to get a broad idea of the structure, taking less interactions into account.

Molecular dynamic computations are divided into two classes: *ab initio* and empirical. These can be distinguished by using different starting points for the corresponding computations. Empirical computations, *e.g.*, Hartree-Fock require knowledge of experimental input, while *ab initio* functions without prior knowledge of molecular structures and energies.

Emerged computational power and improved MD software, methodologies and forcefield parameters has made MD as a powerful tool to study lipid and membrane-related questions. Its simulation time, ranging from microsecond to millisecond, can be increased using coarse grained (CG) forcefields, in which groups of atoms are represented by one bead. Following CG forcefields are developed and commonly used:

Klein, MARTINI, or Elba models. MARTINI is a commonly used forcefield not just to simulate proteins but also to study the formation of lipid domains, membrane fusion, self-assembly of surfactant or membrane protein oligomerization. Including but not restricted to CG forcefields, also other forcefields are used in MD software to name but a few *e.g.*, Charmm, Amber, Gromacs, or NAMD. In addition to it, biomolecules are inserted within the membrane by methods like `g_membed` or `inflategro`.^[25]

It is known that molecular dynamics has its use in computing various values of the inserted molecule such as position, orientation, structure, and dynamics. Also, its effect on surrounding lipids that can be correlated with experimental values is studied. In correlation with IR or NMR, molecular dynamics can test the stability of peptide conformation into the membrane by analyzing lipid destabilization induced by the peptide through the lipid order or disorder.^[25]

Nevertheless, like each computational method, MD has also some limitations in its performance. These include the dependency on model parameters for calculations, the requirement to repeat simulations to search for stochastic events, system convergence to equilibrium, and simulation time scales to get an overview of a state transition or particular mechanism.^[28]

1.6.4 Docking

Alongside molecular dynamics, computational docking is widely used to study protein-ligand interactions in drug discovery and development. Due to the ever-increasing number of protein crystal structures publicly available within the PDB the demand of structure-based approaches such as docking is proportional increasing, being also one of the most popular techniques for virtual screening. This computational technique places a small molecule (ligand) in the binding site of its macromolecular target (receptor) and estimates its binding mode and binding affinity. Hereby, biomolecular interactions and mechanisms are studied, based on the complex formed by the constituent molecules with known structures. The purpose of docking is to predict bound conformations and an approximated binding free energy (usually given by a “score”) of small molecules to the target of medicinal interest. Docking can be distinguished between single docking experiments and virtual screening. The former is beneficial to explore the function of the target, whereas the latter may be used to identify new inhibitors of a large in-house or external library for drug development. ^[29]

The following two main components are required to generate a receptor-ligand structure *in silico*: docking and scoring. Docking by itself comprises conformational and orientational sampling of the ligand within the constraints of the receptor binding site. While scoring function selects the best pose in terms of ligand conformation, orientation, and translation for a given molecule and rank orders ligands, if a ligand database is docked or screened. A successful docking run has to predict both: ligand structure (pose prediction) and its binding propensity (affinity prediction). ^[30]

As already introduced in biophysical techniques, the common source of crystallographic structures of receptor for docking is X-ray crystallography, EM, and NMR. Though, due to its known challenges, the gap between sequence and structure availability keeps growing. This leads to the use of protein structure prediction including homology modeling, threading, and *de novo* methods, which then have to be evaluated. Such evaluation has been carried out by Fan *et al.* ^[31] using 38 protein targets from the Database of Useful Decoys (DUD). They showed that comparative models outperform random selection significantly for 27 out of the 38 targets. Also, comparative models are on average no more enriching than the corresponding templates, but a modeled structure based on a paralogous template with at least 25% sequence identity to the target is 2.5 times more enriching than the template. Interestingly, they found that none of the tested sequence or structural attributes, *e.g.*, the overall target-

template sequence identity, the binding site target-template sequence identity, and the predicted accuracy of a model could reliably predict the accuracy of ligand docking. Based on Emil Fischer's Lock-and-Key hypothesis for protein ligand binding, many docking methods follow this theory by treating the ligand flexible but the protein conformation rigid. [32,33] Hence, it is well known that ligand binding is not a static event but a dynamic process, in which both the ligand and protein may undergo conformational changes. These conformational changes extend the potential search space for the system leading not only to an inconvertible approach but also to a computationally more expensive accounting compared to ligand flexibility. [30] That's why second-generation programs evolved a flexible docking approach with the advances in computational power by that time. Unfortunately, all considered optimizations regarding conformation, orientation and translation were based on the ligand, whereas the protein still was kept rigid. Therefore, it is thought that many of these programs were only successful in docking the known ligand back to its co-crystallized protein structure (self-docking), while docking to another protein structure (cross-docking) was followed by a drop in accuracy. This problem reflects once more the need to observe a protein-ligand complex as a complex dynamic system. Next to protein flexibility, displaceable bridging water molecules, metal coordination and local pH do account as well to this assembly. [33]

Since the knowledge within the drug discovery community is steadily increasing and the demand of new lead compounds is high, new docking programs with improved algorithms are required to address the complexity of protein-ligand binding in a more time- and cost-effective manner. The following sections describe programs and methods which were later used in the docking approach.

1.6.4.1 AutoDock Tools

AutoDock is a set of open-source software, which is free to use for the end-user. The set is composed of several complementary tools enabling computational docking and virtual screening of small molecules to macromolecular receptors in research and drug discovery. ^[29] AutoDockTools (ADT) provides an interactive graphical user interface (GUI) used for coordinate preparation, docking and analysis.

It is free-to-use and available in the MGLTools package, at the following webpage: <http://mgltools.scripps.edu/downloads>. ADT takes care of the very first step being the preparation of coordinate files. Since the quality of coordinates will influence the docking results, this step has to be done in detail. Hereby, input molecule files are formatted into suitable coordinate files by going through protonation, adding hydrogen atoms if needed and add charges afterwards. The user must consider that ADT does not provide any charges for metal ions, hence, charges need to be added in the PDBQT file using a text editor by the user himself. The final steps in the preparation of the ligand file would be to define the torsion tree and to choose rotatable bonds if needed. First ADT chooses a root atom, which will stay fixed during molecular docking, with the result that other coordinates can be transformed. The choice is based on the smallest size of the generated branch. Next, AutoDockTools allows the user to assign ligand flexibility. Here, the user can select either the set of torsional degrees of freedom moving the largest number of atoms (torsions near the root) or moving the smallest number of atoms and leaving the core of the molecule rigid by adding torsions gradually from the leaves. When it comes to the receptor the user has to remove water, ligands, cofactors, ions, and unwanted structures that should not be included by a text editor beforehand. Then, ADT will read coordinates, add charges, merge nonpolar hydrogens, add hydrogens even if the coordinate set does not include hydrogen positions and assign proper atom types. In order to perform single docking experiment, a configuration file has to be generated that specifies the PDBQT files for the ligand and receptor and defines the docking parameters. This is enabled by a GridBox, which defines the center and the size of the search space based on the ligand. However, these parameters can also be manually adjusted. Subsequently, the user can perform docking by running AutoDock Vina or AutoDock 4. Both approaches will be explained in detail in the following sections. In the end the user can visualize the docking results in ADT and analyze ranked conformations and energies by clicking through different binding poses. ^[29,34]

1.6.4.2 AutoDock 4

AutoDock 4 is one of the docking engines provided in the AutoDock Suite, which has been released in 2009. It is an updated version from the initial release of AutoDock in 1990. Since then, AutoDock is one of the most used docking simulation programs, showing a solid performance in accurately predicting bound conformations and binding energies of ligands with macromolecules. In silico methodologies have been used for a wide range of biological systems in drug discovery and development. Its development brought not just positive results of binders to wide-spectrum druggable targets, there was also an increase in the number of protein-drug complexes available in the Protein Data Bank. [35] The global search algorithm of AutoDock's first release combines a Monte Carlo (MC) simulated annealing (SA) technique, adapted from the Metropolis method described by Goodsell *et al.* (1990) with rapid energy evaluation using molecular affinity potentials. [36] This search technique requires a predefined binding site of the static protein to perform conformational and positional searching of the ligand. Throughout the simulation the substrate performs a random walk in the predefined region, followed by displacements in each of the degrees of freedom of the trial molecule: translation, rotation, and torsion angle. The method only accepts a new position and conformation if the energy level is lower than the previous step, if not then the result depends on a user defined temperature (T), which is part of the following probability equation:

$$P(\Delta E) = \exp(-\Delta E / \kappa_B T)$$

Here, ΔE represents the difference in energy and κ_B is the Boltzmann's constant. The probability of acceptance of each step is more likely in high temperatures than in lower temperatures. AutoDock relies on a grid-based method for rapid evaluation of the binding energy, where the target is implemented in a 3D grid and a probe atom is placed at each grid point to calculate the interaction energy between both. [34,36]

The release of AutoDock 4 introduced various major advances compared to AutoDock. These include new search methods, such as genetic algorithm (GA), a local search method (LS), and the Lamarckian genetic algorithm (LGA) and the development of an improved semiempirical free energy force field to predict free energies and binding constants of small molecules docked into macromolecules. [37,38]

The first method, genetic algorithm, enables the role of global search in molecular docking following Darwin's theory of evolution which proceeds through natural

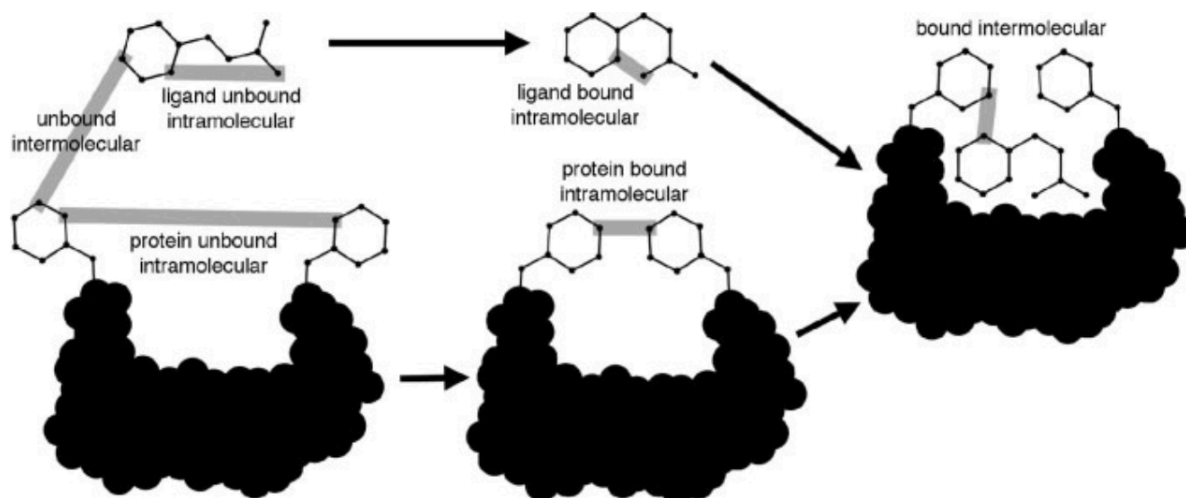
selection. In GA each pose is represented by a vector of genes. The genotype refers to the ligand's state, while the atomic coordinates refer to its phenotype. These genes are defined by state variables such as translation, orientation, and conformation of the ligand with respect to the protein. In this process, genes represent an individual distinct pose, whose collection forms the GA population. During this process, favored poses are passed onto the next generation of an evolving population, whereas unfavorable ones are removed. The addition of the GA-based docking methods advances AutoDock by addressing problems with more degrees of freedom. [33,38,39]

AutoDock 4 withholds the search methods, which were already implemented in AutoDock 3.0. It retains the functionality of earlier simulated annealing versions but adds the options of using a genetic algorithm for global search, a local search method to perform energy minimization, or a combination of both. The LS method is described by Solis and Wets [40] providing two main advantages: First, it does not require gradient information about the local energy landscape, facilitating torsional space search and second, it is adaptive, thus adjusting the step size upon the energies, which have been generated in preceding iterations. [38] The hybrid of both, the GA method with the adaptive LS method build the so-called Lamarckian genetic algorithm, which is used to refine poses identified by GA. LGA generates ligand poses to explore the energy landscape described by the scoring function f . Among these poses, the improved ones are reintroduced into the GA population. This method stops only when either the number of score evaluations or the number of GA generations is reached, which are both defined by the user. In the end, the pose with the best score returns by the LGA. The scoring function f in AutoDock is a semiempirical free-energy force field that quantifies the free energy ΔG of a given binding pose:

$$\begin{aligned} \Delta G = & \Delta H_{vdW} W_{vdW} \sum_{i,j} \left(\frac{A_{ij}}{s(r_{ij})^{12}} - \frac{B_{ij}}{s(r_{ij})^6} \right) \\ & + \Delta H_{hbond} W_{hb} \sum_{i,j} E(t) \left(\frac{C_{ij}}{s(r_{ij})^{12}} - \frac{D_{ij}}{s(r_{ij})^{10}} \right) \\ & + \Delta H_{elec} W_{el} \sum_{i,j} \left(\frac{q_i q_j}{\varepsilon(r_{ij}) r_{ij}} \right) \\ & + \Delta G_{desolv} W_{desolv} \sum_{i,j} (S_i V_j + S_j V_i) e^{\left(-r_{ij}^2 / 2\sigma^2 \right)} \\ & + \Delta S_{tor} W N_{tor} \end{aligned}$$

The force field is defined by four pairwise energetic terms (dispersion/repulsion, ΔH_{vdW} ; hydrogen bonding, ΔH_{hbond} ; electrostatics, ΔH_{elec} ; and desolvation, ΔG_{desolv}), and a term predicting the unfavored entropy of ligand binding due to the restriction of conformational degrees of freedom (ΔS_{tor}).

In AutoDock 4, theoretically the free energy of binding is estimated to be equal to the difference between the energy of the ligand and the protein in a separated unbound state and the energy of the protein-ligand complex. The evaluation is performed in two steps (Scheme 8). First, the intramolecular energetics of the ligand and protein in an unbound state are evaluated separately. After the complex is formed, the semiempirical force field takes the intermolecular energetics into account. The difference to a traditional molecular mechanics' force field is, that the surrounding water is considered, to capture the complex enthalpic and entropic contributions. After the job is performed successfully, the best poses (lowest score) are returned and clustered using the root-mean-square deviation (RMSD) as distance metric. [37,39]



Scheme 8: The evaluation of the force field in AutoDock 4. Adapted from [37]

If wanted, the user has the option to perform flexible docking in AutoDock4. When preparing the protein in AutoDockTools, an easy-to-use graphical user interface of AutoDock, specific sidechains of the protein can be chosen to stay flexible. As a result, these are separated from the protein and treated explicitly, allowing rotation around torsional degrees of freedom. ^[34] In addition to the progress in receptor flexibility, developers of AutoDock 4 have introduced two methods for covalent docking of protein-ligand complexes: a grid-based approach and a modification of the flexible sidechain approach. The former method calculates a special map for the site of attachment of the covalent ligand by the help of a Gaussian function. The flexible sidechain method enables to treat the ligand attached to the sidechain in the protein as flexible during the docking simulation, thus torsional degrees of freedom are searched to improve the interaction with the rest of the protein. ^[30,34]

1.6.4.3 AutoDock Vina

In the same year of AutoDock 4's release, Oleg Trott has rewritten a new program for molecular docking and virtual screening, called AutoDock Vina. As already introduced in AutoDock 4, the main goal is to predict the bound conformations and the binding affinity here, too. The motivation of this approach is to maximize the accuracy of the predictions while the computer time should be minimized. The results of AutoDock Vina are based on a hybrid scoring function. Since it combines a knowledge-based method with an empirical approach, it is viewed more as a machine learning than a superficially physics-based approach. Trott clarifies that the scoring function is mainly inspired by X-Score with some minor differences. X-Score only counts intermolecular contributions, whereas AutoDock vina considers a sum of both intermolecular and intramolecular interactions by following equation:

$$c = c_{inter} + c_{intra}$$

Autodock Vina ranks the conformations according to this equation, but it derives from the general functional form of the conformation-dependent part of the scoring function which is defined as follows:

$$c = \sum_{i < j} f_{t_i t_j}(r_{ij})$$

Like AutoDock 4, AutoDock Vina has introduced new search methods including genetic algorithms, particle swarm optimization, simulated annealing, which are combined with various local optimization procedures to speed up the optimization. Nevertheless, the algorithm was set on the Iterated Local Search global optimizer, combining genetic algorithm with local gradient optimization. The local optimization is based on the Broyden-Fletcher-Goldfarb-Shanno (BFGS) method, which is an efficient quasi-Newton method. The advantage of BFGS and all other quasi-Newton optimization methods is, that they use not only the value of scoring function, but also its gradient, meaning the derivatives of the scoring function with respect to its arguments. These are the position and orientation of the ligand, as well as the values of the torsions for the active rotatable bonds in the ligand. In this way the optimization algorithm receives a certain direction from a single evaluation. Depending on the complexity of the problem, the number of steps can be adapted, and runs can be performed starting from random conformations. AutoDock Vina enables to perform these runs simultaneously, by using multithreading. This approach speeds up the execution by taking advantage of multiple central processing units (CPUs) or CPU cores. [41]

1.6.4.4 Comparison of AutoDock 4 and AutoDock Vina

Among all publicly available molecular docking software AutoDock 4 and AutoDock Vina belong to the few programs that are free-to-use in academia and industry. Both AutoDock software are maintained by the Scripps Research Institute (Center for Computational Structural Biology) and released under open-source licenses as GNU General Public License (AutoDock 4) and Apache License (AutoDock Vina).

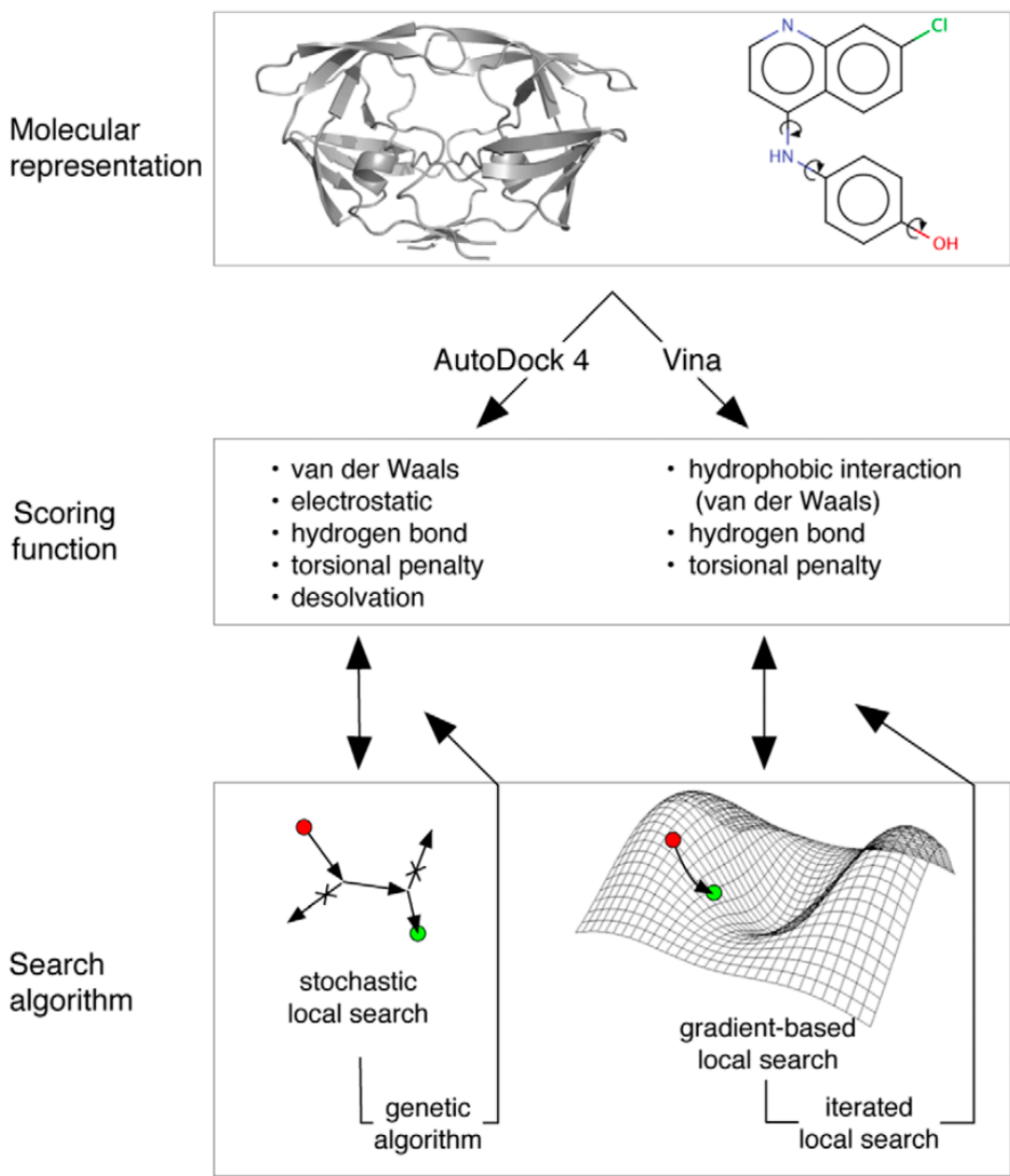
As depicted earlier, both software perform in a nearly similar manner by pairing an empirically weighted scoring function with a global optimization algorithm. The major differences are the local search function and the distribution of the scoring function illustrated in Scheme 9.

In general, the performance of docking programs can vary due to the following three components: molecular representation, scoring function, and search algorithm. Both programs use the same type of input files describing the receptor rigid and the ligand flexible. However, the remaining two other components share similarities in principle, but have clear differences. Regarding the scoring functions, both are empirically weighted and share values such as hydrogen bonding and rotatable bonds. Nevertheless, AutoDock Vina does not cover parameters like desolvation and electrostatic interactions, which play a crucial role in a protein-ligand complex.

As to search algorithm, both software apply a hybrid global-local search, but the essential difference is in the local optimization. AutoDock 4 uses a stochastic search method by making use of small random steps to generate more favorable conformations. Contrary to AutoDock 4, AutoDock Vina calculates derivatives to generate a gradient, performing its optimization accordingly. ^[41,42]

These differences were observed in the overall performance of various docking studies. Chang *et al.* report that AutoDock 4 and AutoDock Vina displayed the binding affinity of small molecules with a low number of rotatable bonds in a similar manner. In contrast, AutoDock Vina showed clear superiority over AutoDock 4 in docking larger and more flexible compounds containing more rotatable bonds. Other than that, AutoDock Vina has a much faster docking performance compared to AutoDock 4. ^[42]

The authors of AutoDock have shown in another study that the accuracy of AutoDock Vina is greater than AutoDock 4. Redocking of 190 protein-ligand complexes was performed by AutoDock Vina with an accuracy of 78% within 2 Å RMSD, while AutoDock 4 achieved only 49%. ^[41]



Scheme 9: Methodology comparison of AutoDock 4 and AutoDock Vina. Adapted from ^[41]

Nevertheless, both docking programs face their limits in their performances. Known challenges occur either if the modeled structure has poor quality, is too flexible, or when the ligand contains too many torsions. Adding flexibility to the docking approach causes several problems: The whole run is more time-consuming, since the calculation of the receptor energy exponentially expands the potential search space, hence being computationally more expensive. Other than that, the conformational space is larger, which increases the risk for potentially false positives. ^[30,34] Corbeil *et al.* ^[33] clarifies that among all challenges, the most crucial one is to identify the correct pose among the ones generated in the molecular docking approach.

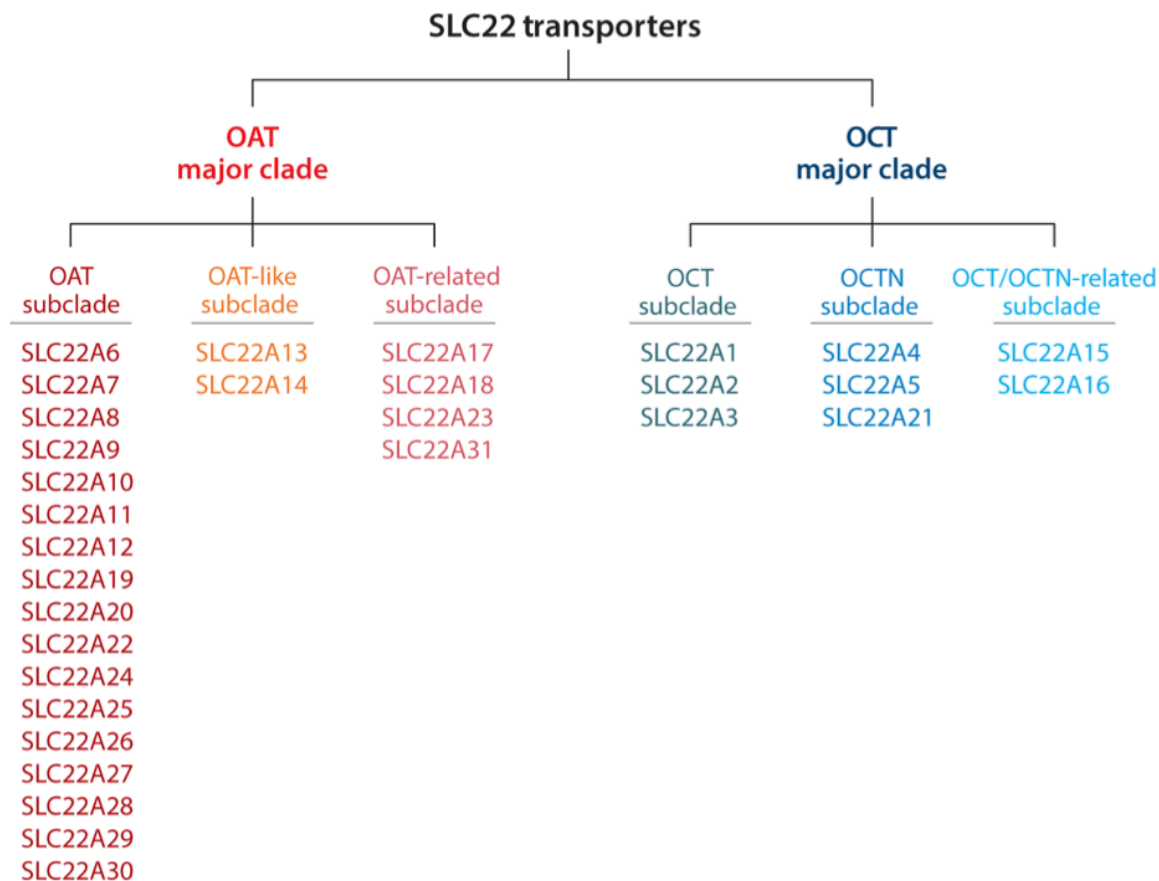
1.7 Solute carrier family 22 member 1

By now, there are approximately 2000 genes in the human genome that encode for transporters or transport-related proteins.^[43] Membrane transporters are distributed into two major superfamilies: the ATP binding cassette (ABC) family and the solute carrier (SLC) family. The former are primary active transporters, using energy from ATP hydrolysis to transport substrates actively across the membrane, whereas the latter transport their substrates either down the gradient across the membrane, as facilitative transporters, or against the gradient across the membrane, such as secondary active transporters. This study focuses on Organic Cation Transporter 1 (OCT1) encoded by the SLC22A1 gene which is a member of the SLC family.^[44]

In 1994 the Organic Cation Transporter 1 (OCT1) was cloned from rat kidney as the first identified transporter of the SLC22 transporter family, which belongs now to the major facilitator superfamily (MFS), whose transporters enable import or export of target substrates by being either uniporters, symporters, or antiporters.^[45] The SLC22 family consists of two major clades OAT (organic anion transporter) and OCT (organic cation transporter). Both can be further divided into three subclades, designated as OAT, OAT-like, OAT-related or OCT, OCTN (organic cation/carnitine transporter), and OCT/OCTN-related (Table 1).^[46] They are mostly known to be polyspecific, accepting compounds of different size and molecular structure (Fig. 4). However, exact amino acids involved in binding and/or translocation of the various OCT1 substrates and providing polyspecificity are still unclear. Recent efforts have shown that these transporters are critically involved in drug disposition regarding absorption, tissue distribution, metabolism, and excretion events (ADME) of diverse cationic compounds such as nutrients and clinically relevant drugs.^[47,48,49]

It is known that OCT1 is highly expressed in the liver, mainly in the basolateral membrane of hepatocytes mediating the uptake of weak basic and cationic substances from the blood. Nevertheless, it is worth mentioning that OCT1 is also expressed in the intestine, kidney, and brain, as well as other members of the SLC22 family have tissue-specific roles. Moreover, although OCT1 was shown to be polyspecific, the human organic cation transporter 1 still possesses a strong selectivity for its ligands.^[50]

Table 1: The evolution of SLC22 transporters. Adapted from [46]



It is noteworthy that OCTs transport endogenous substrates such as choline, adrenaline, noradrenaline, dopamine, and thiamine possessing important physiological functions. OCTs do also transport therapeutic drugs such as (i) quinine, which is used for treating malaria, (ii) anti-retroviral drugs like lamivudine, zalcitabine, pentamidine, and trimethoprim, (iii) metformin for controlling blood sugar in diabetic patients, and (iv) the anticancer drugs including imatinib, anthracyclines, oxaliplatin and sorafenib (Fig. 4). [51,52,53,54,55,56,57,58,59,60,61,62,63] Alongside structurally diverse lipophilic organic cations of endogenous or xenobiotic origin, OCT transport for prototypic cations such as tetraethylammonium (TEA⁺) and 1-methyl-4-phenylpyridinium (MPP⁺) is also proven. [45,64] Other than that, OCT1's emerging role in cancer, is believed to be of benefit two-fold: suitable inhibitors can serve as a beneficial approach to arrest the growth of proliferating cancer cells by limiting their high energy demand. In other cases, it might be helpful to stimulate the expression and activity of this uptake transporter in cancer cells by increasing drug entry to enable the rapid destruction of cancer cells. [65,66,67,68] This already indicates the importance of OCT1 as a classical off-target, influencing the pharmacokinetics of many drugs and potentially leading to drug-drug interactions and toxicity.

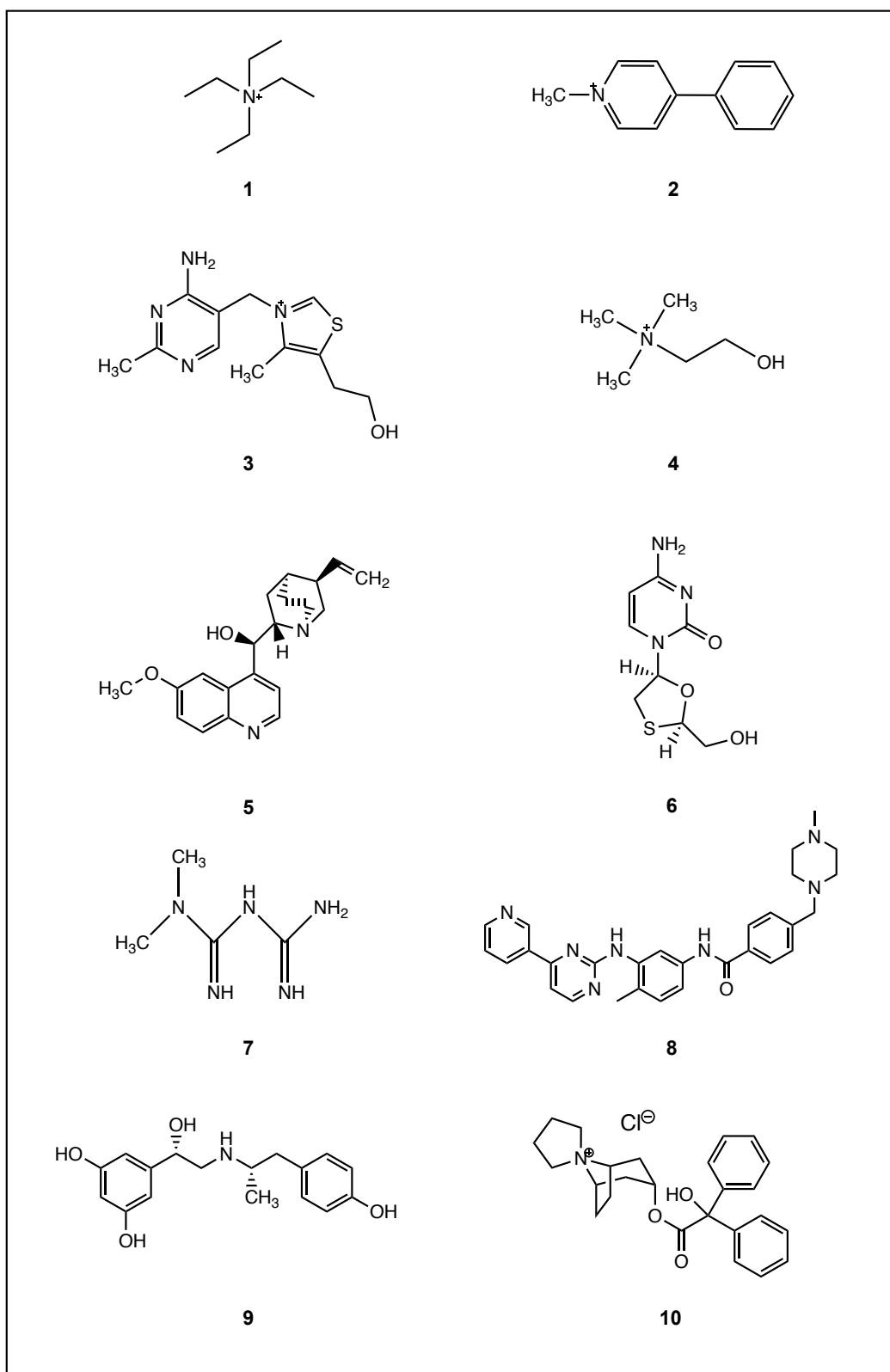
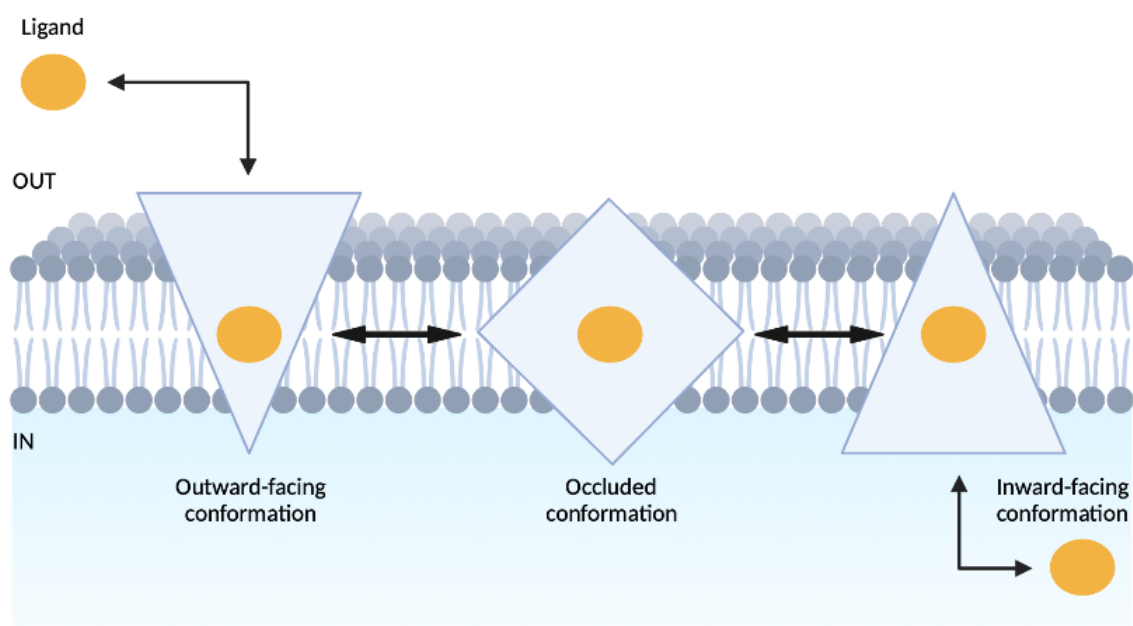


Figure 4: Chemical structure of substrates transported by OCT1. 1) Tetraethylammonium (TEA^+), prototypic cation. 2) 1-methyl-4-phenylpyridinium (MPP^+), prototypic cation. 3) Thiamine, endogenous compound involved in biosynthetic pathway and neurotransmission. 4) Choline, endogenous compound involved in biosynthetic pathway and neurotransmission. 5) Quinine, anti-malarial drug to treat *Plasmodium falciparum*. 6) Lamivudine, antiretroviral drug used for the treatment of HIV-1 infection. 7) Metformin, anti-diabetic drug used to lower blood sugar in those with type 2 diabetes. 8) Imatinib, anti-cancer drug used for chronic myelogenous leukemia (CML) and acute lymphocytic leukemia (ALL). 9) Fenoterol, β_2 -adrenergic drug used in asthma. 10) Trosipium, used to treat overactive bladder.

The required transport mechanism of the OCT1 protein's facilitated diffusion has been proposed to happen due to the binding of the substrate into a large outward open cleft of the transporter, which then closes to occlude the substrate. This occluded conformation is then followed by the opening of the inward-facing side of the cleft to channel the substrate into the cell. The transporter repeats the so called trans-zero transport cycle by returning into the outward-facing conformation (Scheme 10).^[69]



Scheme 10: Illustration of the ligand transport cycle through conformation changes by the organic cation transporter 1.

These conformational changes are provided by specific movements of amino acid residues within the 12 predicted transmembrane alpha helices (TMHs) with intracellular NH₂ and COOH termini (Fig. 5). Between TMH1 and TMH2 is a large extracellular loop that contains four or six cysteine residues, which may form disulfide bridges to stabilize the loop and at least three asparagine residues providing sites for N-glycosylation. A smaller intracellular loop is located between TMH6 and TMH7 that carries consensus sites for phosphorylation by several protein kinases. Egenberger *et al.* showed through fluorescence labeling, that TMHs 5, 8, and 11 were altered by substrate binding indicating large conformational changes during transport by rOCT1. At the same time, they could demonstrate amino acids (Cys474, Asp475 both in TMH11) being responsible for binding of TEA⁺ (tetraethylammonium⁺), a common chemical substrate, whereas the bending of TMH11 at Gly477 and/or Gly478 is supposed to be important for transport-related structural changes.^[70]

Other than that, it has been shown in extensive mutagenesis of rOCT1, that Phe160 (TMH2), Trp218 (TMH4), and Asp475 (TMH11) are in central parts and directly involved in binding of organic cations during transport, whereas mutations of several other amino acids located in more peripheral regions like Tyr222 (TMH4), Thr226 (TMH4), Arg440 (TMH10), Leu447 (TMH10), Gln448 (TMH10) also led to changes in affinity and/or selectivity of substrates. Thus, this already suggests that OCT1 needs to undergo multiple and rapid structural changes to achieve its transport functions.

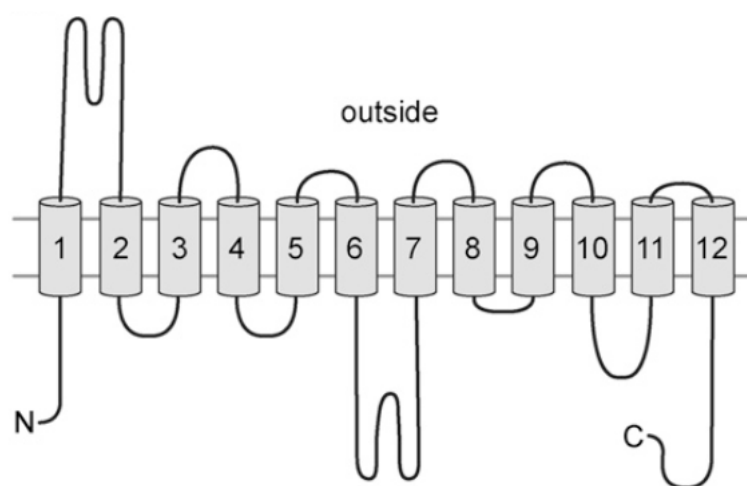
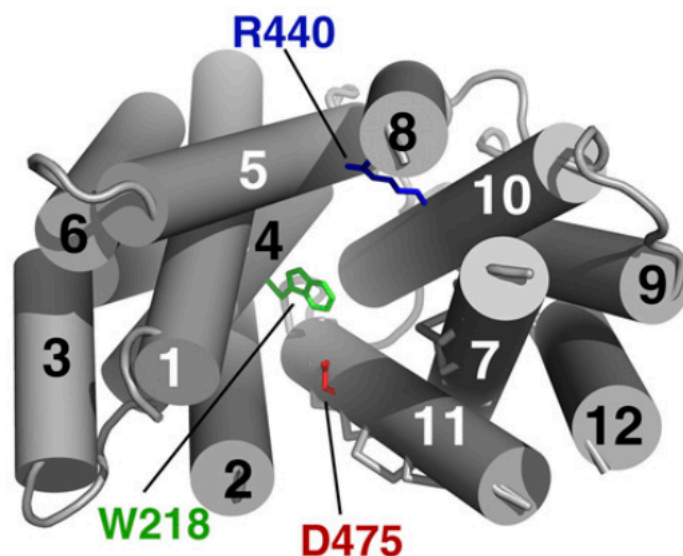


Figure 5: Predicted membrane topology of human OCTs (hOCT1, hOCT2, hOCT3, hOCTN1, hOCTN2). Adapted from [45]

Gorboulev *et al.* [71] performed a mutagenesis study in rat organic cation transporter 1 (rOCT1) early in 1999 to elucidate the role of Asp475 for the transport of organic cations. Point mutations of Asp75, located in the presumed 11th membrane spanning α -helix of rOCT1 (Fig. 6), with arginine, asparagine, or glutamate showed its crucial role for cation selectivity. The Asp475Glu mutant of rOCT1 showed the most promising effects on apparent K_m and V_{max} values. Here, the V_{max} values for choline, TEA⁺, MPP⁺, and N¹-methylnicotinamide were reduced by 89 to 98%, as well as the apparent K_m values were decreased for choline by 15-fold, TEA⁺ by 8-fold, and N¹-methylnicotinamide by 4-fold). More interestingly, the same mutation resulted also in an affinity increase for specific cations (n-tetraalkyl ammonium compounds) with increasing alkyl chain length, indicating that Asp475 may be localized close to the cation binding site or at a nearby protein domain and stabilizing the conformation of the cation binding site through an ionic interaction with another intramembraneous protein domain. [45,71]

outward-open, from outside



inward-open, from inside

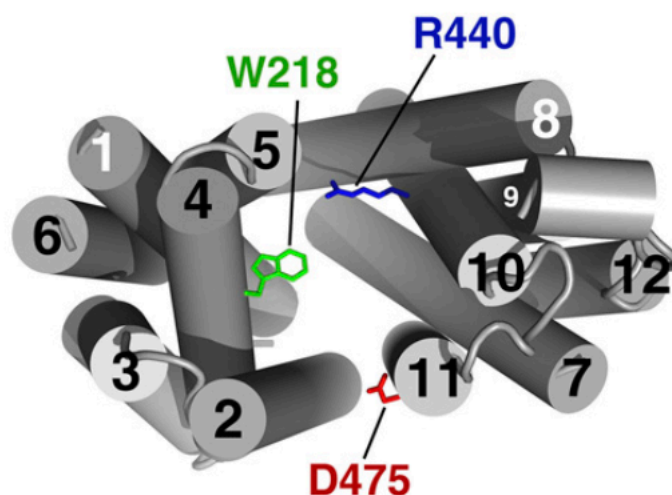


Figure 6: View of the modeled outward-open (upper panel) and inward-open (lower panel) binding cleft of rOCT1, with labeled amino acids (Trp218, Arg440, and Asp475) located in the inner parts. Adapted from ^[45]

The provided features underline the importance and promising role of the organic cation uptake transporter OCT1. Unfortunately, there still are some limits and uncertainties. So far, it remains unknown how OCT1 recognizes a broad array of ligands and whether this involves specific modifications and interactions with other proteins. Since many substrates differ in sizes and structures, it is expected that crystallization studies of OCT1 with key ligands might provide useful information on the responsible amino acid residues for the polyspecificity.

Another unexplored field is whether OCT1 has interacting partners when cells are in a resting state and exposed to ligands such as anticancer agents. Since it is known that many membrane proteins have interacting partners, the previously reported list of physical partners for OCT1 remains undiscovered.

Lastly, there remains the question of whether OCT1 can directly deliver ligands onto the DNA such as anthracyclines.

No matter how promising the role of OCT1 as a potential cancer drug target seems, there still are many challenges to overcome. This detailed abstract should provide funders scientific evidence of this key uptake transporter's potential role in future drug discovery projects.

Recent efforts of Meyer, Marleen J., *et al.* have shown strong differences in the affinity for metformin and thiamine between human and mouse OCT1. The study reports that the cellular uptake of both compounds was significantly lower in human than in mouse OCT1. Consequently, mouse models could lead to an overestimation of the effects of OCT1 on hepatic concentration in humans. As a result, this represents a strong limitation of using rodent animal models for predictions of OCT1-related pharmacokinetics and efficacy in humans. ^[72]

1.7.1 Human OCT1

The human OCT (hOCT) 1 was cloned and characterized in 1997, three years after the first cloning of OCT1. Its gene (SLC22A1) is located on the chromosome 6q26 and shares seventy-eight percent amino acid identity with rat OCT (rOCT) 1, and seventy-seven percent identity with mOCT1 orthologs. Just as rOCT1, hOCT1 appear to have transport activity for various organic cations with diverse molecular structures transporting in a sodium- and proton-independent manner, mediating electrogenic cellular influx and efflux of organic cations under trans-zero conditions, which are driven by substrate concentration gradients and membrane potential. ^[45] To this day, there is no solved crystal structure of mammalian MFS transporters affecting their research. Currently ongoing studies of hOCT1 are based on 3D structures generated from homology models, which derived from bacterial and fungal transporters. Since the amino acid identity of the reported inward-open conformation ^[73] and the outward-open conformation ^[74] for hOCT1 is below 20%, predictions and conclusions regarding molecular interaction of substrates with single amino acids are restricted. Therefore, our molecular understanding is rather based on mutagenesis analysis. By single-point mutations, K_m (Michaelis-Menten constant) and K_D (dissociation constant) values were determined to interpret substrate recognition and transport mechanisms. However, this approach comes along with limitations in the interpretation. Binding measurements do not allow to distinguish between binding to the outward-open or inward-open transporter conformation, moreover the exchange of an amino acid may exhibit an indirect effect on cation binding to a nearby or distant residue.

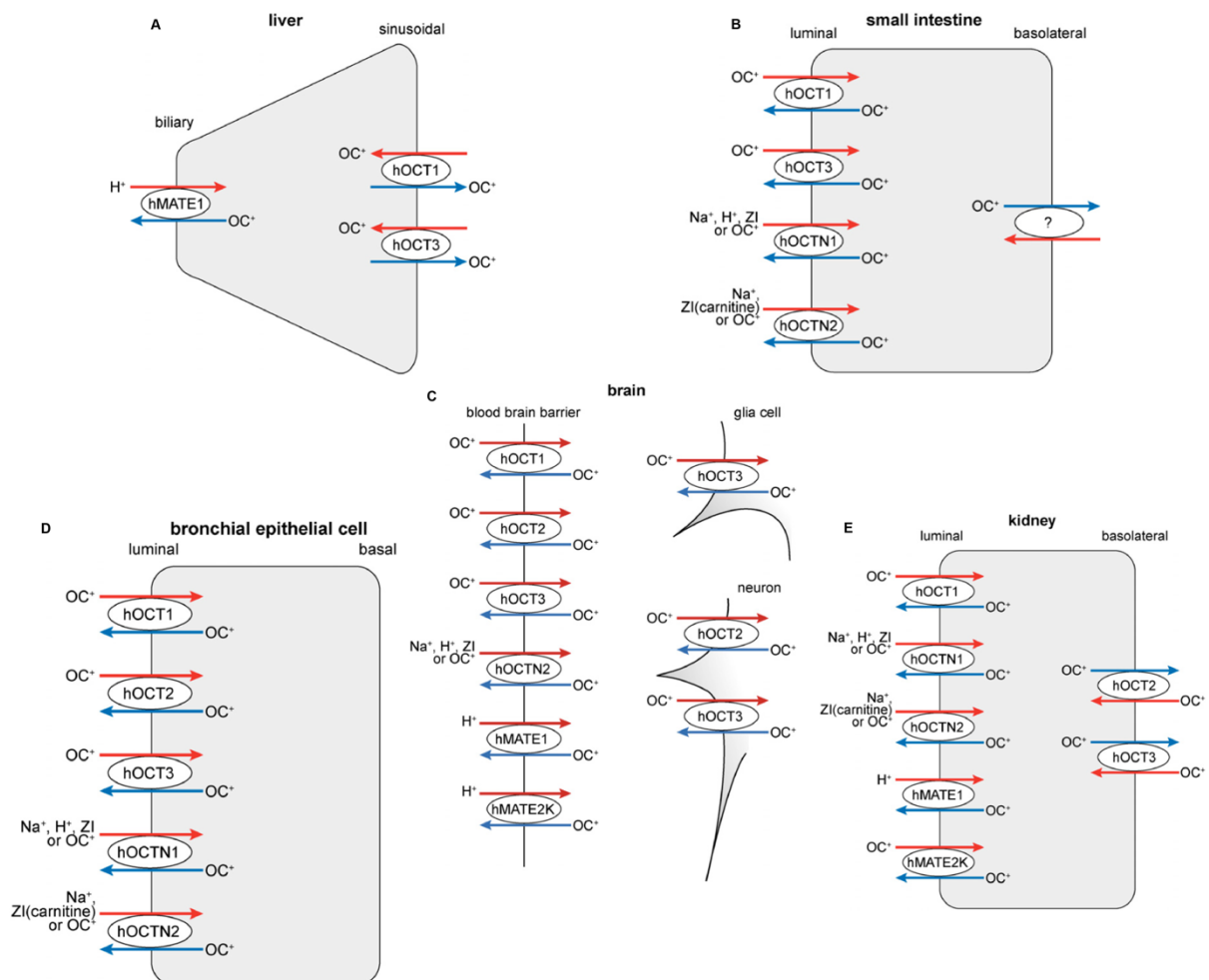
hOCT1 is strongly expressed in the liver and distributed in various other organs and tissues, such as eye, brain, small intestine, kidney, lung, urinary bladder, heart, placenta, and skeletal muscle at much lower levels. ^[45] Scheme 11 illustrates the location of OCTs in the following tissues: liver, small intestine, brain, lung, and kidney. In the liver, hOCT1 was exclusively localized at the sinusoidal membrane of human hepatocytes and it is mainly responsible for the uptake of organic cations from the portal vein but may also mediate release of organic cations into the portal vein. ^[75]

The first step of organic cation absorption takes place in small intestinal enterocytes, where hOCT1 is in the brush-border membrane (BBM). From there, hOCT1 is not only mediating the absorption but also the efflux of organic cations performing electroneutral cation exchange. ^[45]

In renal proximal tubules, hOCT1 is in the BBM, mediating reabsorption of organic cations from the tubular lumen. [76,77]

Even in lung, hOCT1 has been localized to the luminal membrane of ciliated bronchial epithelial cells. Here, hOCT1 is enabling the absorption of inhaled cationic drugs. [78,79,80]

Lastly, in human brain hOCT1 is expressed in brain microvessels, which are primarily comprised of endothelial cells. On the one hand, hOCT1 is involved in uptake of endogenous compounds (choline, L-carnitine, and thiamine) and of cationic drugs (metformin, morphine, and sulpiride) across the blood brain barrier (BBB) but also, on the other hand it may participate in the removal of organic cations from brain.



Scheme 11: Location of OCTs in A) hepatocytes (liver), B) small intestinal enterocytes, C) in brain, D) bronchial epithelial cell (lung), and E) tubular cells (kidney). Adapted from [45]

Recent efforts have shown that hOCT1 downregulation is linked to several diseases. Evidence has been provided on protein and/or mRNA level that hOCT1 is expressed in various tumors, such as breast cancer, colon cancer, cholangiocarcinoma, hepatocellular carcinoma, lung non-small cell carcinoma, myeloid leukemia cells, and esophageal cancer (Table 2).^[45] As tumors are known for altered expression levels of certain proteins, hOCT1 showed similar behavior in different organs. In cholangiocarcinoma and hepatocellular carcinoma^[61,81,82,83] expression of hOCT1 was decreased. The reduced expression levels of hOCT1 in hepatocellular carcinoma were correlated with promoter methylation^[82] and negatively with tumor malignancies^[80,81] Regarding hepatocellular carcinoma, it is known that the reduced expression of hOCT1 has a decreased response rate towards sorafenib and poor patient survival^[61,84] Therefore, hOCT1 gene expression is clinically relevant for proper response to sorafenib, as well as other anticancer drugs that are transported by hOCT1 such as imatinib, irinotecan, paclitaxel, and anthracyclines^[58,62,85,86] That's why scientists have recently proposed that hOCT1 should be amongst the crucial drug targets used for pharmacogenomic analyses.

Table 2: Expression of human organic cation transporter 1 (hOCT1) in tumors in different organs detected on mRNA and/or protein level. +, expression; d, decreased expression in tumor versus respective organ; s, similar expression in tumor and respective organ. Adapted from^[45]

Cancerous Tissue, Localization	hOCT1
Breast cancer	+
Buccal squamosal cell carcinoma	
Colon cancer	+, s
Cholangiocarcinoma	+, d
Glioblastoma	
Hepatocellular carcinoma	+, d
Lung non-small cell carcinoma	+, s
Myeloid leukemia	+
Esophageal cancer	+, s
Ovary cancer	
Prostate cancer	
Rectal cancer	
Renal cell carcinoma	
Stomach cancer	
Uterin cancer	

It is noteworthy, that even though the transporter OCT1 has such an impact on different organs, its specific functions of individual drugs in humans are still understood inadequately. The main reason is due to difficulties in reproducing organ-specific functions, such as intestinal absorption or secretion, biliary excretion, tubular reabsorption, and excretion in *in vivo* experiments from rodents to humans because of species differences in expression, membrane location, regulation, and substrate specificity.^[45]

1.8 Aims and Objectives

Similar differences in transport kinetics were observed with the anticholinergic drug trospium and the β_2 -adrenergic agonist fenoterol. Fenoterol is transported with 8.8-fold higher v_{\max} by mouse than by human OCT1, but mouse OCT1 has an 8.1-fold lower K_M . Using chimeras, the group of Prof. Tzvetkov was able to show that the amino acid difference of Tyr36 (mouse)-to-Cys36 (human) confers these differences in the transport kinetics of fenoterol. On the other hand, trospium is transported with 4.5-fold higher v_{\max} by human than by mouse OCT1, but human OCT1 has a 7.5-fold lower K_M . The amino acid difference of Phe32 (human)-to-Leu32 (mouse) confirmed this different transport kinetics of trospium.

Other than that, mutation of Phe159Ala (human) resulted in substantial increase in v_{\max} for fenoterol, but also a decrease in affinity. The same mutation in mouse OCT1 (Phe160Ala) revealed opposite effects, meaning a decrease in v_{\max} but an increase in K_M . It is believed that due to spatial proximity of Phe32 and Phe159 the findings could be mechanistically related.

The current work aims to understand the experimental findings of our collaborators using computational methods. Structure-based methods such as docking will provide us most valuable binding poses to identify possible moieties in the substrates that interact with Phe32 and Tyr36 among both organisms. Our homology model could provide insights into the spatial proximity of Phe159 to generate hypotheses how Phe159 and Tyr36 interact with each other.

2 Methods

2.1 PyMOL for molecular visualization

PyMOL (available at <https://pymol.org/2/>) [The PyMOL Molecular Graphics System, Version 2.4.2 Schrödinger, LLC] has been mostly used for 3D visualization of the ligand, the macromolecule, and the protein-ligand complex. Here, different stereo visualization modes (e.g., lines, sticks, cartoon) were used, to conceive much more 3D information of the entity. PyMOL supports macromolecule editing, which was used to perform rotamer analysis (Wizard > Mutagenesis > Protein) to set a specific residue's side-chain angle. Protein structure analysis enabled the alignment (Action > Align > Align to molecule > "Object") of two proteins from different sources.

2.2 Discovery Studio Visualizer

If not stated otherwise, all runs are further visualized and analyzed in Discovery Studio Visualizer (DSV), a software developed and distributed by Dassault Systèmes BIOVIA (available at <https://discover.3ds.com/discovery-studio-visualizer-download>). The conformation is loaded into DSV by drag and drop. The next step is to visualize amino acid residues of hOCT1/mOCT1, which are near fenoterol or Trospium (Scripts > Ligand Interactions > Show Ligand Binding Site Atoms). Afterwards, the residues are labeled in DSV (Structure > Labels > Add, Choose "AminoAcid" in the Object parameter). The final step is to display receptor-ligand interactions among the amino acids and the ligand (In the "Tools" widget on the left > View Interactions > Ligand Interactions). The results are summarized in a 2D diagram, visualizing all different type of interactions in a color-coded manner (In the "Tools" widget on the left > View Interactions > Show 2D Diagram).

2.3 Molecular Docking using AutoDock 4

The predicted protein structure of human OCT1 (hOCT1) was obtained by the AlphaFold Protein Structure Database (available at <https://alphafold.ebi.ac.uk>), a new data resource based on an AI system developed by DeepMind and the EMBL-European Bioinformatics Institute (EMBL-EBI).^[87] The highly accurate protein model was selected due to its very high pLDDT score (pLDDT > 90), a per-residue confidence score from 0 to 100, in the binding region and due to residues resolved in close proximity with $90 > \text{pLDDT} \geq 70$ model confidence (Varadi et al., 2021).^[88] Hence, the structural models of human OCT1 (UniProt ID: O15245) and mouse OCT1 (UniProt ID: O08966) were downloaded in PDB format and used for molecular docking studies in AutoDock 4.2.6. Protein preparation was performed in AutoDock Tools, a graphical user interface tool (GUI) from the AutoDock suite, which was originally designed and implemented by Dr. Oleg Trott in the Molecular Graphics Lab (MGL, <https://autodock.scripps.edu/>) and is now maintained and developed by the Forli Lab at Scripps Research (<http://www.scripps.edu/>), formerly known as The Scripps Research Institute (TSRI). After uploading the PDB file in AutoDock Tools (File > Read Molecule > hOCT1.pdb), the protein structure is prepared for molecular docking by adding polar hydrogens (Edit > Hydrogens > Add), applying Kollman charges (Edit > Charges > Add Kollman Charges) and save the protein in PDBQT format (Grid > Macromolecule > Choose > hOCT1).

The structures of fenoterol and trospium were obtained by PubChem (available at <https://pubchem.ncbi.nlm.nih.gov>), a free accessible chemical database maintained by the National Center for Biotechnology Information (NCBI). The 3D conformers (Pubchem CID – fenoterol: 3343, Trospium: 5284632) were downloaded as an SDF file for further ligand preparation steps. The molecular structures were uploaded in MarvinSketch (File > open > Fenoterol), a private cheminformatics and bioinformatics software company (available for download at <https://chemaxon.com/products/marvin/download>). The protonation state of the ligands was calculated by the pK_a plugin (Calculations > Protonation > pK_a, Suppl. Fig. 1), using the default parameters in the pK_a options window. According to the calculation results of the microspecies distribution, the one with the correct formal charge at pH 7.4 was selected, its explicit hydrogen atoms were added and then saved as a PDB file. The prepared PDB file was uploaded in AutoDock Tools (File > Read Molecule > Fenoterol/Trospium) and focused for the upcoming preparation (Ligand > Input > Choose > Fenoterol/Trospium > Select

Molecule for AutoDock 4). The next steps are performed as for the protein by adding polar hydrogens and charges, with the only difference that Gasteiger charges are added. In the next step, AutoDock Tools detects the central atom of the ligand and uses it as the root (Ligand > Torsion Tree > Detect Root). AutoDock Tools also provides insights into the number of rotatable and active bonds in the ligand to select which rotatable bonds should be considered (Ligand > Torsion Tree > Choose Torsions), but for this approach we maintained the default. The prepared ligand structure was saved for AutoDock 4 as a PDBQT file (Ligand > Output > Save as PDBQT). The next approach describes how the grid parameter file (GPF) was generated, which describes the binding site of the protein. To generate a GPF, you have to define the potential binding region with a grid box by its x-, y-, z-coordinates (Grid > Grid Box). The next step is to save these parameters in the grid options window (File > Close saving current) and then save the GPF in the AutoDock Tools window (Grid > Output > Save GPF). For further docking studies with the same protein, you can save this grid dimension parameters in a separated txt file (Grid > Grid Box > File > Output grid dimension file). In the following step a docking parameter file (DPF) is generated, which provides exact information about the docking run in terms of which docking algorithm is used, how many runs are performed, which map files to use, what the maximum allowable initial energy is, and many more. First, you need to set the protein rigid filename in ADT to specify the stem of the gridmap filenames (Docking > Macromolecule > Set Rigid Filename). The same has to be applied for the ligand whose parameters can be adjusted in the AutoDpf4 Ligand Parameters widget, but for this docking run we maintained the defaults (Docking > Ligand > Choose > Fenoterol > Select Ligand, AutoDpf4 Ligand Parameter window > accept). For this docking approach we have applied the Genetic Algorithm (GA) (Docking > Search Parameters > Genetic Algorithm) with 100 GA runs and a population size of 300 for better sampling of the 3D space, while other parameters are by default. In the docking parameters you could choose which random number generator to use and set the energy outside the grid, next to the maximum allowable initial energy but we have used the defaults (Docking > Docking Parameters > Accept/Close). The output of the DPF was saved for a Lamarckian Genetic Algorithm (LGA) docking, which is a hybrid of the GA method with the adaptive Local Search (LS) method together (Docking > Output > Lamarckian GA). Before we perform docking with AutoDock 4 we have to run the AutoGrid command, where we set the program pathname of AutoGrid4 and the parameter filename for the

GPF (Run > Run AutoGrid > Launch). To start AutoDock 4 from the ADT GUI we have to set here the program pathname for AutoDock4 and the parameter filename of the DPF (Run > Run AutoDock > Launch). After the docking run is completed, all generated results are reported in the “.dlg” file, providing a clustering histogram outlining the energies of the docked structures and their similarities to each other, which is measured by computing the root-mean-square-deviation (RMSD) between the coordinates of the atoms. AutoDock clusters the docked results at 0.5 Å by default, ordering all the conformations by docked energy, from lowest to highest. The lowest energy conformation represents the first cluster. If the next conformation is within the RMSD tolerance, it is added to the first cluster, otherwise it is the first member of a new cluster. The docking runs are analyzed in ADT to visualize the binding site and binding conformation of the protein-ligand complex (Analyze > Docking > Open > Choose “.dlg” file, Analyze > Macromolecule > Open > Choose hOCT1, Analyze > Conformations > Play). The most promising conformation is saved for further analysis as a PDBQT file by clicking the Ampersand button in the conformation player (Ampersand button > Write Complex). If not stated otherwise, results are visualized and analyzed in PyMOL or in Discovery Studio Visualizer.

2.4 Molecular Docking using AutoDock Vina

Ligand and protein preparation for molecular docking in AutoDock Vina (Dr. Oleg Trott, MGL; Forli lab, Center for Computational Structural Biology) was performed as previously described in 2.1.1. The grid parameters, also known as the search space, were provided by Dr. Alzbeta Tuerkova, former PhD student who was working on the same target. The following grid parameters (size in the x, y, z, directions and center of the x, y, z, coordinates) were applied:

```
--center_x 55.44 --center_y 51.45 --center_z 53.44 --size_x 40 --size_y 40 --size_z 30
```

AutoDock Vina requires as an input the receptor file and the ligand file in pdbqt format. In addition to it, the number of CPU (central processing units) was increased to ten, the exhaustiveness (intensive search for the global minimum and other binding modes) was also increased to ten and the num_modes parameter (maximum number of binding modes to generate) was increased to twenty. All these parameters were summarized in a configuration file (config.txt). Required tools for AutoDock Vina that need to be installed corresponding your operating system are AutoDock MGL Tools (<http://mgltools.scripps.edu/>) and AutoDock Vina (<https://vina.scripps.edu/downloads>) itself. Molecular docking is performed in AutoDock Vina through command line. First, you open the command prompt and change the directory to the folder containing all prepared files together. Then you paste the path of the folder where AutoDock Vina is saved, which is mostly in the C: drive and add the executable file (vina.exe) to the path. Then, in the same command the protein and the ligand have to be defined, as well as the config file, the log file, and the output file. ("C:\Program Files (x86)\The Scripps Research Institute\Vina\vina.exe --receptor protein.pdbqt --ligand ligand.pdbqt --config config.txt --log log.txt --out output.pdbqt"). After pressing enter, the run will start and after finishing the docking approach, AutoDock Vina will print all binding modes found with its corresponding affinity values as a table in the command prompt. In the folder all prepared files, are now the log and output file added. The first is opened in a code editor to get a broader insight into all binding modes and affinities, whereas the output file is further analyzed in PyMol to visualize the newly generated binding conformations, if not stated otherwise.

3 Results

3.1 Transport kinetics of fenoterol and trospium comparing hOCT1 and mOCT1

The motivation of this study is based on the experimental data generated by Prof. Tzvetkov and Dr. Meyer, our collaborators from the University of Greifswald. Together, our aim was to study the differences in OCT1 function by comparing the differences in transport kinetics of the β 2-adrenergic drug fenoterol (Fig. 4) and the anticholinergic drug trospium (Fig. 4) between human and mouse OCT1. The experimental results aim to identify not just regions but also single amino acids in the OCT1 protein that confer the species differences to get a deeper insight of the mechanism driving OCT1 polyspecificity. [89]

Concentration-dependent measurements showed strong differences in the uptake kinetics between human and mouse OCT1, such as transport capacity (v_{\max}) and affinity (K_M). Fenoterol was transported with an 8.1-fold higher affinity by human than by mouse OCT1 (Fig. 8B). Interestingly, the capacity was 8.8-fold lower (data not shown), turning human OCT1 into a high affinity low-capacity transporter of fenoterol and vice versa for mouse OCT1, respectively. Trospium, on the other hand, was transported with a 9.0-fold higher capacity (data not shown) and 10.6-fold lower affinity by hOCT1 (Fig. 8D). Therefore, human OCT1 is observed as a low affinity high-capacity and mOCT1 as a high affinity low-capacity transporter of trospium.

The next approach, undertaken by Prof. Tzvetkov and colleagues, was to identify regions conferring differences in substrate selectivity between human and mouse OCT1 using chimeric constructs. Human and mouse OCT1 differ in 124 amino acids, which represent 22% of their sequence (Suppl. Fig. 35). Since the different amino acids are consistently distributed throughout the entire protein (Fig. 7), there is no possibility to observe any trend for a specific region providing the species differences.

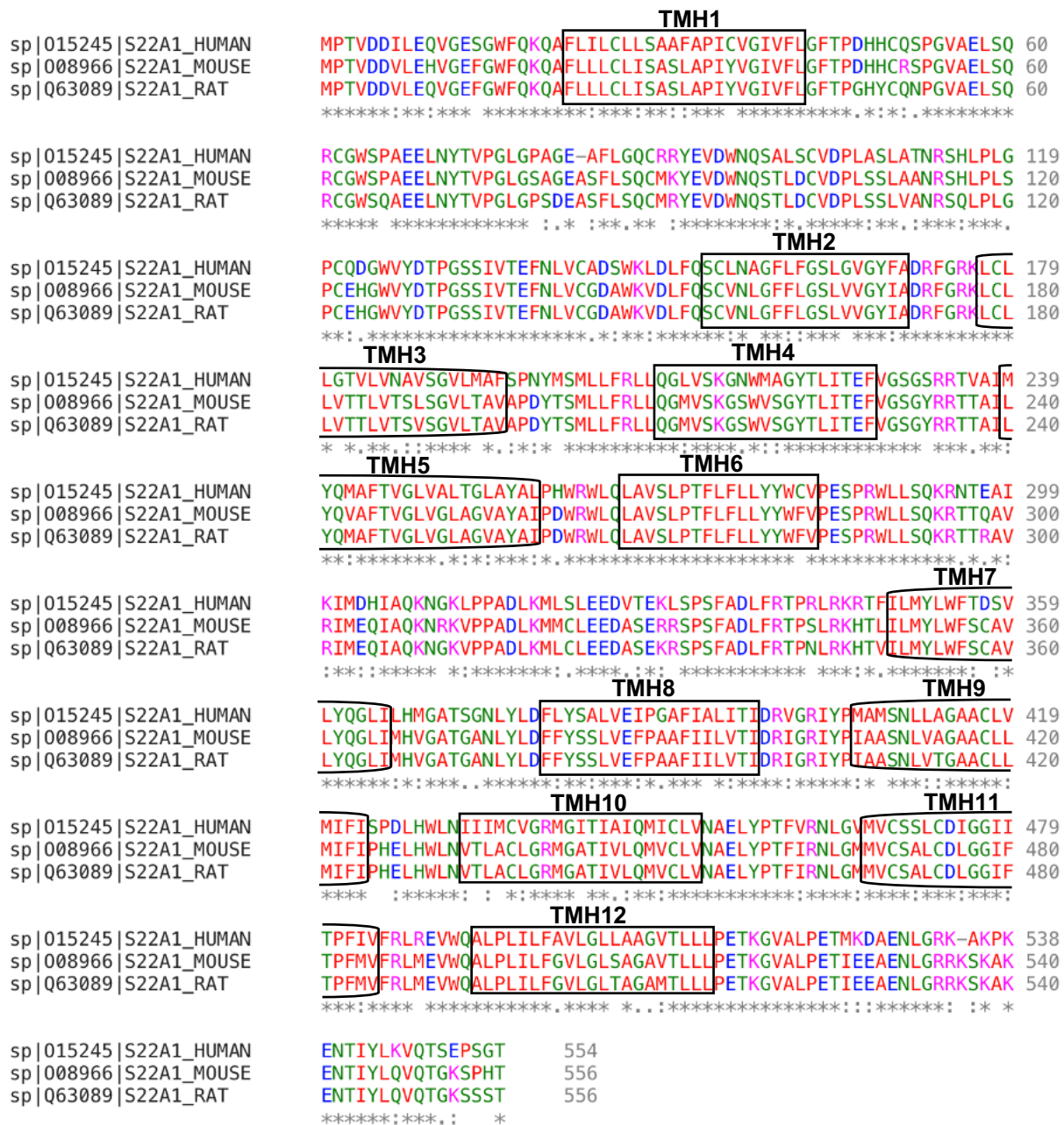


Figure 7: Protein alignment of human, mouse, and rat OCT1 using the multiple sequence alignment tool Clustal Omega. ^[90] Transmembrane helices (TMH) 1 to 12 are shown in boxes.

Meyer *et al.* generated high-resolution chimeric constructs carrying substitutions of single TMHs. Interestingly, the only chimera showing any difference in the uptake kinetics was the introduction of mouse TMH1 into human OCT1. On the one hand, it significantly increased fenoterol uptake compared to the human wild type whereas, on the other hand, trospium uptake was significantly decreased to levels even lower than mOCT1. Therefore, further studies were focused on TMH1 as an important determining region for the differences in uptake between mouse and human OCT1. Protein alignment of human and mouse OCT1 showed five different amino acids in

TMH1 (Fig. 7, Suppl. Fig. 35). Each amino acid of one species was mutated to the residue of the other species and then fenoterol uptake was analyzed. The substitution of cysteine at codon 36 to tyrosine (Cys36Tyr) increased fenoterol uptake of hOCT1 by 4.8-fold (Fig. 8A). More interestingly, the reverse substitution (Tyr36Cys) in mOCT1 reduced fenoterol uptake by 90%, resulting in uptake levels comparable to hOCT1 (Fig. 8A). However, they showed that other mutations in TMH1 did not influence fenoterol uptake.

Besides identifying Cys36 as the responsible residue in human OCT1 conferring the high affinity for fenoterol, the ligand was further analyzed on its functional groups. Fenoterol's structure is composed of two phenol rings, which are connected by a linker containing an amino group, a hydroxyl group, and a methyl group. Structurally similar compounds of the class of β 2-adrenergics between human and mouse OCT1 were compared and analyzed by the so-called "ligand-structure walking", leading to the hypothesis, that not only the presence of two phenol rings, but also the distance of the second aromatic ring to the positive charge of the protonatable amino group is responsible for the affinity. In summary, it supports the thought of a direct interaction of Cys36 with the second phenol ring of fenoterol.

Next, like fenoterol, Meyer *et al.* generated chimeric constructs, showing again TMH1 as the key transmembrane domain for the differences in trospium uptake between human and mouse OCT1. [89] Then, they analyzed once again single amino acid substitutions in TMH1 on trospium uptake, indicating the mutation of phenylalanine at codon 32 to leucine (Phe32Leu) as determinant for transport kinetics. This substitution decreased trospium uptake by 79% in hOCT1 (Fig. 8C) to even lower uptake levels of mOCT1. More interestingly, the reverse substitution in mOCT1, Leu32Phe, increased trospium uptake by 7-fold, surpassing the uptake of the human ortholog by 2.8-fold at the same concentration (Fig. 8C). Other mutations within the TMH1 had no impact on the uptake of trospium, not even substitution of codon 36. The same behavior was observed for substitution of codon 32 for fenoterol uptake. These results strongly indicate substrate-specific activity of these amino acid residues.

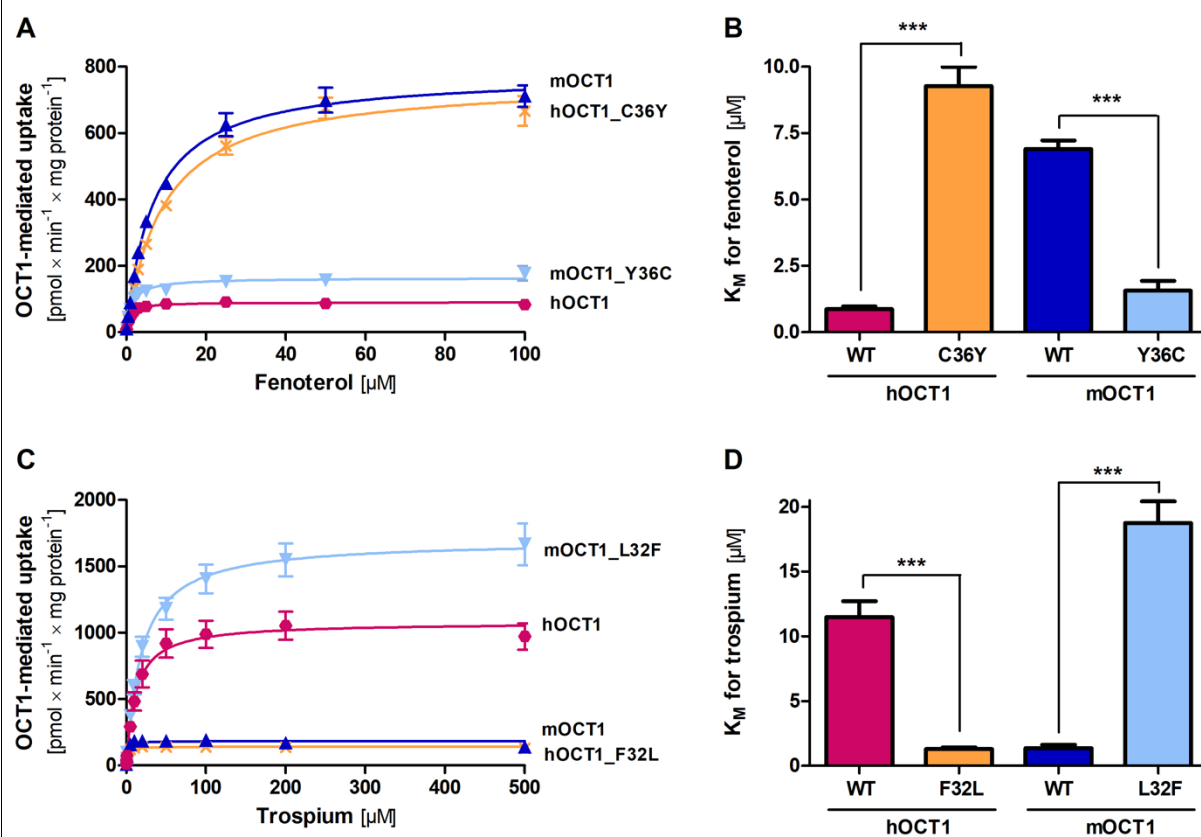


Figure 8: The role of TMH1 in transport kinetics comparing fenoterol and trospium of human and mouse OCT1 with its crucial amino acid differences. A) OCT1-mediated uptake of fenoterol with substituting effect at codon 36 – C36Y in human and Y36C in mouse OCT1. B) Shown are the absolute K_M values for fenoterol of the data shown in A. C) OCT1-mediated uptake of trospium with substituting effect at codon 32 – F32L in human and L32F in mouse OCT1. D) Shown are the absolute K_M values for trospium of the data shown in C. Adapted from ^[89]

3.2 Molecular docking via AutoDock Vina

Based on the experimental findings of the diverse transport kinetics for fenoterol and trospium, computational analysis such as structure-based methods were applied to obtain a better understanding. Substrate-specific effects of the amino acids at codon 32 (Phe32 in human and Leu32 in mouse OCT1) and codon 36 (Cys36 in human and Tyr36 in mouse OCT1) conferring the differences in uptake kinetics in terms of maximal velocity and affinity for fenoterol and trospium were analyzed through molecular docking in AutoDock Vina. Molecular docking provided us not just insights of the preferred orientation of the ligands, it enabled us to study possible interactions between the molecules and amino acids of the OCT1 orthologs.

The first docking approach was performed in an unbiased manner, meaning that no other modification was carried out other than stated in the methods. Hereby, we used the homology models for hOCT1 and mOCT1 already generated by our former colleague Dr. Alzbeta Tuerkova for previous studies. The final models are based on the crystal structure of the human glucose 3 transporter (GLUT3; Protein Data Bank identifier (PDB ID) 4zw9) adopting an outward-occluded conformation, which is reasonable for the investigation of substrate binding.^[72] In the following the best three ranked binding poses are analyzed.

The best ranked pose in the first run has a binding affinity of -7.2 kcal/mol (Table 3). Fenoterol is binding into the active site of hOCT1 in a U-shaped manner, the aromatic rings directed to the extracellular membrane, whereas the positively charged nitrogen pointing to the inward (Fig. 9). The oxygen of the phenyl ring containing two hydroxyl groups is stabilized by two polar interactions. It provides the role for both a hydrogen bond donor and a hydrogen bond acceptor for Gln362 and Gly363. The hydroxyl group in the linker part connecting the two aromatic rings shows a polar interaction with Gly477. Additionally, the positively charged nitrogen is forming an intermolecular H-bond with the sidechain of Asp357. Next to the second phenol ring containing only one hydroxy group, a network of pi-pi interactions with the aromatic residues between Phe32, Phe244, and Trp217, as well as cation-pi interactions between Phe32 and Lys214 are present. More importantly, Phe32 (3.6 Å) and the crucial Cys36 (3.3 Å) interaction both stabilize the ring either through a pi-pi interaction with Phe32 or via a pi-sulfur interaction.

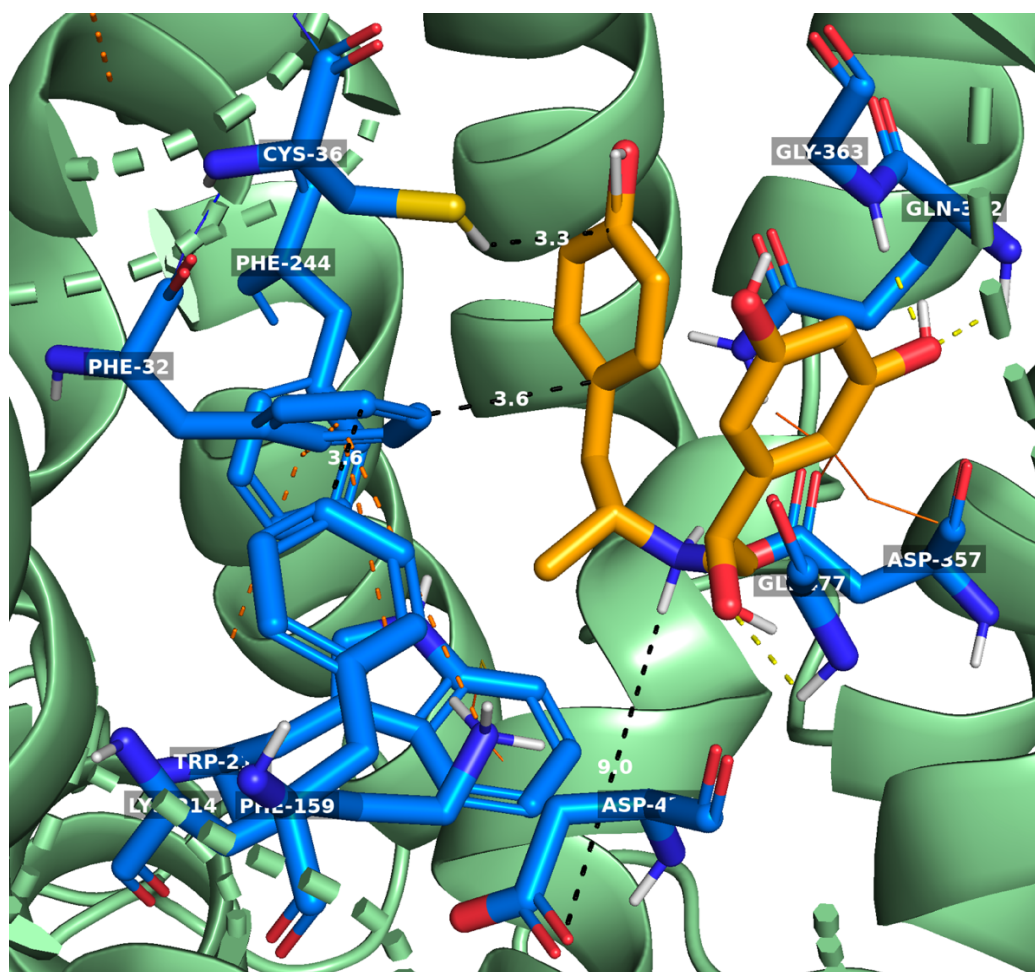


Figure 9: Molecular docking of fenoterol into hOCT1 by AutoDock Vina. Shown is here the best binding pose of fenoterol (orange) in hOCT1 (green) regarding the binding affinity out of ten conformations. Polar interactions are shown by yellow dashed lines. The distance of amino acids in close proximity are shown in black dashed lines with its respective value in white. Pi-Pi interactions are displayed by orange dashed lines. Heteroatoms are color-coded as well: red – oxygen, blue – nitrogen, yellow – sulfur.

The second best ranked pose in this run has an affinity of -7.0 kcal/mol (Table 3). The root means square deviation upper bound (RMSD u.b.) has a value of 1.804 and the RMSD lower bound (RMSD l.b.) has a value of 2.867. As in the first conformation, fenoterol is bound to the active site of hOCT1 in a U-shaped manner but more loosely. The aromatic ring possessing two OH-groups in fenoterol is more shifted towards TMH11, whereas the second phenol ring points more towards TMH1 (Fig. 10). The phenyl ring close to TMH11 is stabilized by three intermolecular H-bonds with Asp357, Gln362, and Gly363. In the linker part, both the hydroxyl group and the positively charged nitrogen form a H-bond with Asp357. Like in the first binding pose, Cys36 has the same distance (3.3 Å) stabilizing the second phenol ring via a pi-sulfur interaction. The distance to Phe32 (3.9 Å) is slightly increased still enabling a stabilization effect through pi-pi stacking.

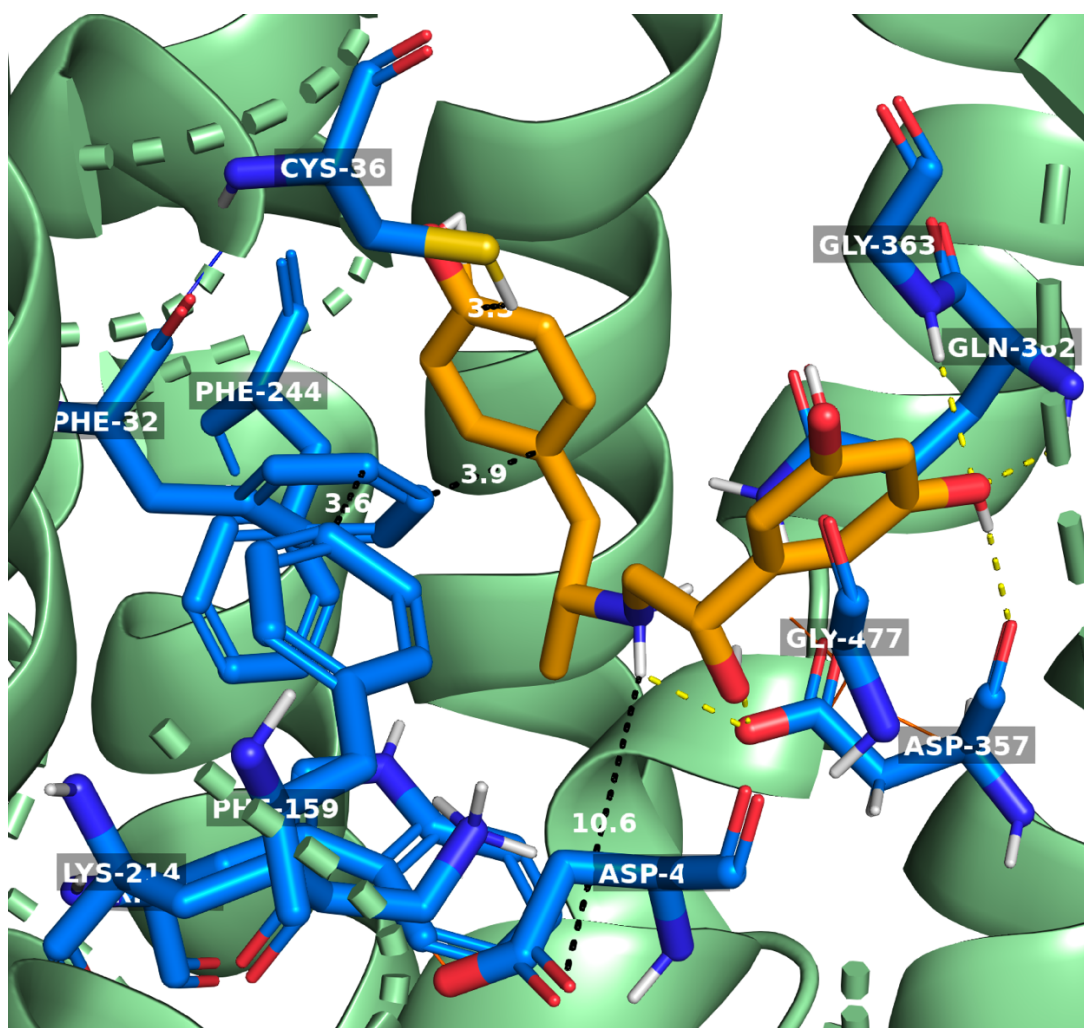


Figure 10: Molecular docking of fenoterol into hOCT1 by AutoDock Vina. Shown is here the second best binding pose of fenoterol (orange) in hOCT1 (green) regarding the binding affinity out of ten conformations. Polar interactions are shown by yellow dashed lines. The distance of amino acids in close proximity are shown by black dashed lines with its respective value in white. Pi-Pi interactions are displayed by orange dashed lines. Heteroatoms are color-coded as well: red – oxygen, blue – nitrogen, yellow – sulfur.

The third best binding pose has the same affinity as the second one, differing only in the RMSD values. The RMSD u.b. is 1.743 and the RMSD l.b. is 2.698 (Table 3). Unlike the first two poses, the third conformation seems to be more asymmetric (Fig 11). The phenyl group possessing two OH-groups is flipped to the inward of the active site due to the stabilizing intermolecular H-bond interaction with Asn156. The other conventional H-bonds between the positively charged nitrogen and Asp357 and between the hydroxy group in the linker part and Gln362 are still conserved. The minor difference is observed in the distance of the crucial pi-sulfur interaction (5.1 Å), whereas the distance to Phe32 stayed in the same range (3.8 Å).

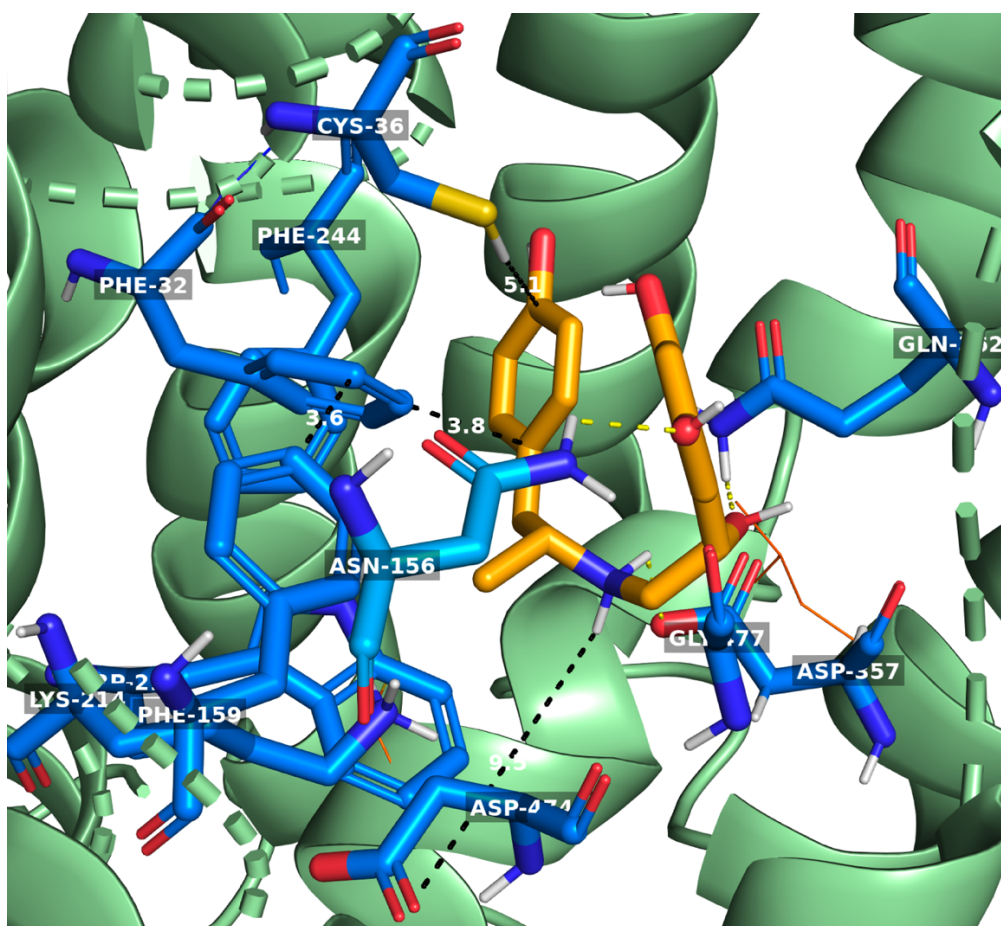


Figure 11: Molecular docking of fenoterol into hOCT1 by AutoDock Vina. Shown is here the third best binding pose of fenoterol (orange) in hOCT1 (green) regarding the binding affinity out of ten conformations. Polar interactions are shown by yellow dashed lines. The distance of amino acids in close proximity are shown by black dashed lines with its respective value in white. Pi-Pi interactions are displayed by orange dashed lines. Heteroatoms are color-coded as well: red – oxygen, blue – nitrogen, yellow – sulfur.

mode	affinity	dist from best mode	
	(kcal/mol)	rmsd l.b.	rmsd u.b.
1	-7.2	0.000	0.000
2	-7.0	1.804	2.867
3	-7.0	1.743	2.698
4	-6.9	2.857	6.667
5	-6.8	1.788	2.482
6	-6.7	3.235	5.072
7	-6.6	2.803	5.007
8	-6.6	2.153	5.834
9	-6.6	3.283	4.743
10	-6.6	3.243	5.042

Table 3: Binding affinities and RMSD values of fenoterol in hOCT1 analyzed by AutoDock Vina. Root mean square deviation (RMSD) values measuring the average between atoms of a position relative to the best fitting position, are calculated using only movable heavy atoms. Two variants of RMSD metrics are provided, rmsd l.b. (RMSD lower bound) and rmsd u.b. (RMSD upper bound). They differ in how the atoms are matched in the distance calculation; rmsd u.b. matches each atom in one conformation with itself in the other conformation, ignoring any symmetry; rmsd l.b. matches each atom in one conformation with the closest atom of the same element type in the other conformation.

The same settings were applied to the docking approach for fenoterol into mOCT1. As previously done, the best three poses are shown and analyzed.

The best ranked binding pose provides an affinity of -8.3 kcal/mol (Table 4). The conformation fits in the active site of mOCT1 in a U-shape opening towards the TMH7. Stabilizing effects are provided to the phenol ring possessing two hydroxy groups by the side chains of Asn157 and Gly478 via H-bond interactions (Fig. 12). The OH-group in the linker part shows intermolecular H-bond interactions with Lys215. This interaction is stabilized through cation-pi interactions between Lys215 and Trp-218. Since the two phenol rings point towards TMH7, the positively charged nitrogen is closer to Phe160 (3.6 Å) enabling cation-pi interactions. More interestingly, the determining substitution at codon 36, Tyr36, seems to be in close proximity to the second phenol ring (4.0 Å) allowing possible pi-pi stackings, as well as the aromatic ring of Phe245 (4.1 Å).

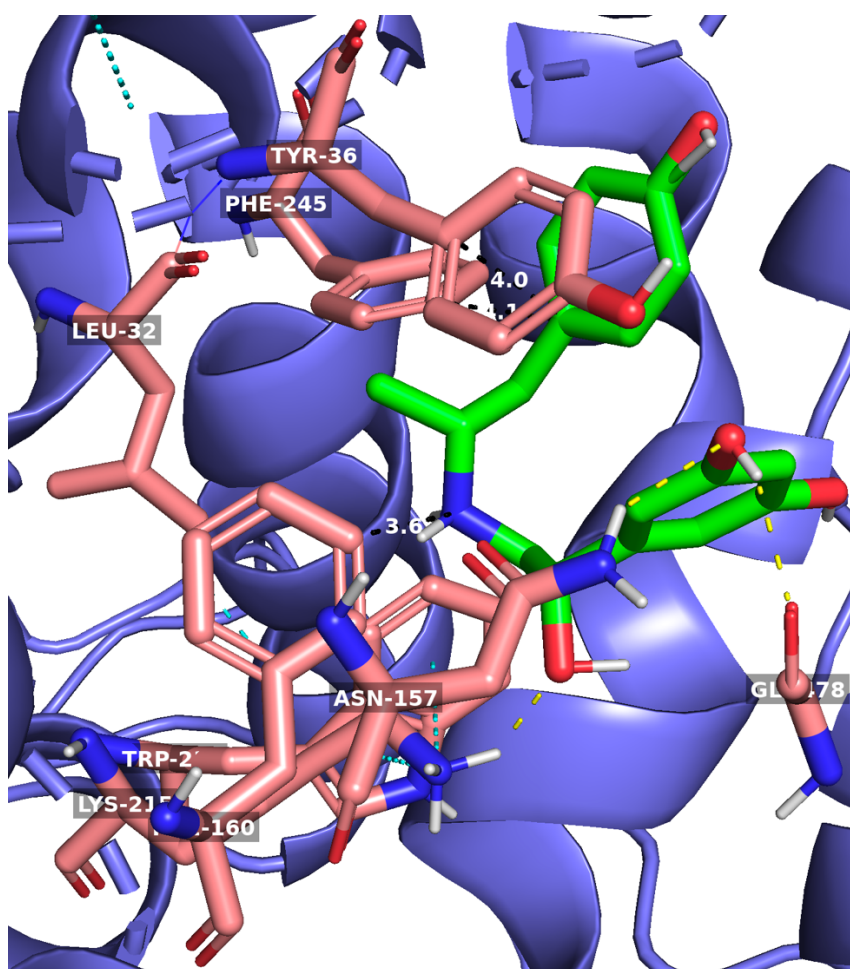


Figure 12: Molecular docking of fenoterol into mOCT1 by AutoDock Vina. Shown is here the best binding pose of fenoterol (green) in mOCT1 (purple) regarding the binding affinity out of ten conformations. Polar interactions are shown by yellow dashed lines. The distance of amino acids in close proximity are shown by black dashed lines with its respective value in white. Pi-Pi interactions are displayed by cyan dashed lines. Heteroatoms are color-coded as well: red – oxygen, blue – nitrogen, yellow – sulfur.

The second binding pose has an affinity of -8.2 kcal/mol (Table 4) with the exact same conformation and orientation (Fig. 13), which is confirmed by the RMSD u.b (1.746) and l.b. (0.149) values. This pose shows no intermolecular polar interactions between the phenol rings and other amino residues except the stabilizing effects of Tyr36 and Phe245 with the same distances. Also, the possible cation-pi interaction between the positively charged nitrogen and Phe160 is maintained (3.5 Å). The only observable intermolecular interaction was between the hydroxy group of the linker and the residues Lys215 and Cys474, stabilizing the ligand as a HBD and HBA.

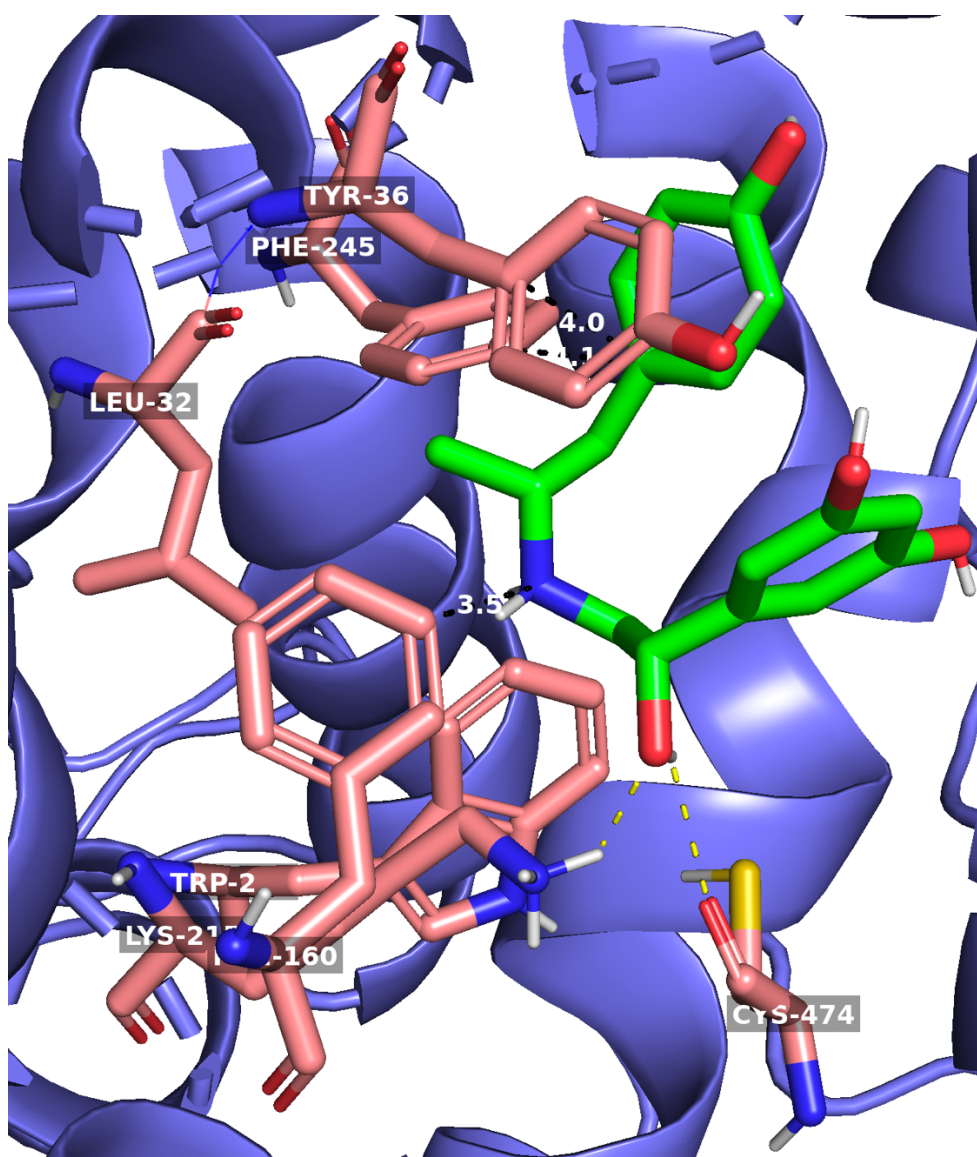


Figure 13: Molecular docking of fenoterol into mOCT1 by AutoDock Vina. Shown is here the second best binding pose of fenoterol (green) in mOCT1 (purple) regarding the binding affinity out of ten conformations. Polar interactions are shown by yellow dashed lines. The distance of amino acids in close proximity are shown by black dashed lines with its respective value in white. Pi-Pi interactions are displayed by cyan dashed lines. Heteroatoms are color-coded as well: red – oxygen, blue – nitrogen, yellow – sulfur.

The third best binding pose shows an affinity of -8.0 kcal/mol. Unlike the first two poses, this conformation differs again in its orientation towards TMH11 (Fig. 14). This is underlined by the high RMSD u.b. (4.848) and l.b. (2.451) values (Table 4). The stabilizing H-bond interactions between Lys215 and Cys474 are conserved with the only difference, that the hydroxy group of the phenyl ring possessing two OH-groups is the new interacting partner. Other than that, the other hydroxy group on the same phenol ring shows a H-bond interaction with Asn157. The other parts of fenoterol show no polar interaction, since its orientation has changed, the distances are increased.

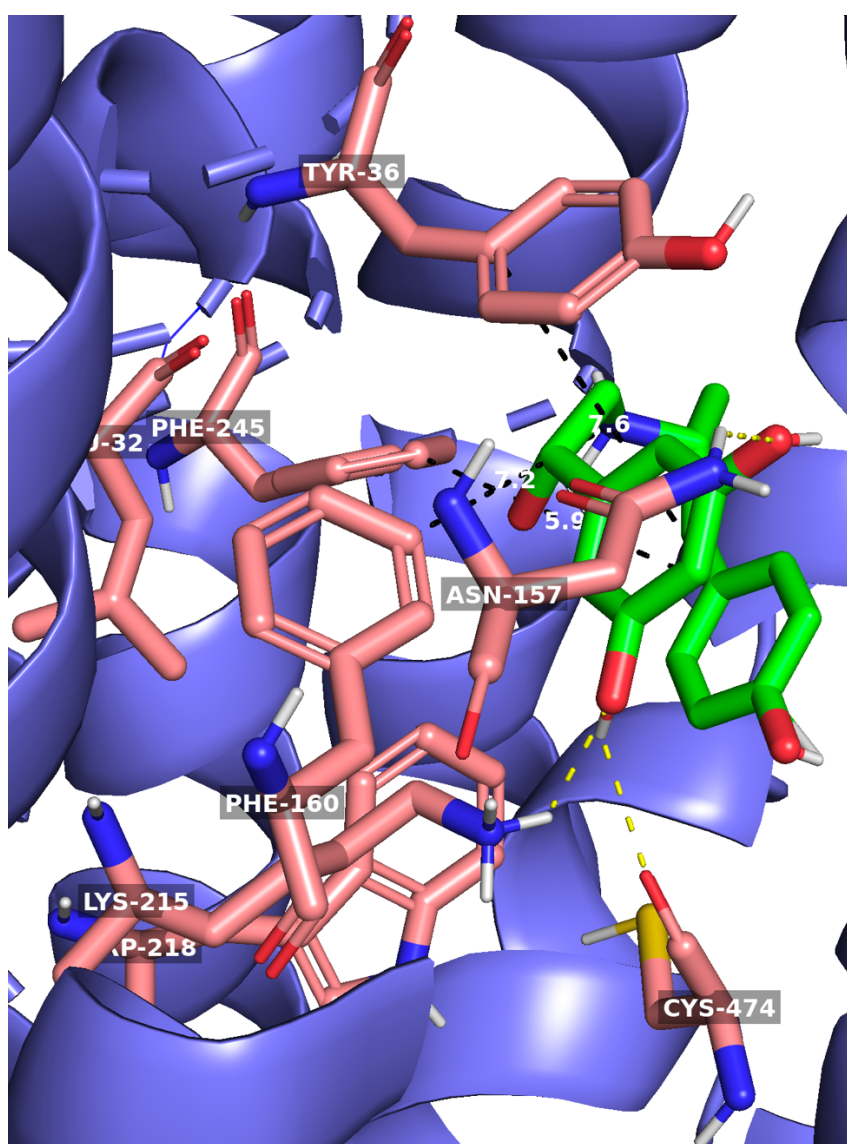


Figure 14: Molecular docking of fenoterol into mOCT1 by AutoDock Vina. Shown is here the third best binding pose of fenoterol (green) in mOCT1 (purple) regarding the binding affinity out of ten conformations. Polar interactions are shown by yellow dashed lines. The distance of amino acids in close proximity are shown by black dashed lines with its respective value in white. Pi-Pi interactions are displayed by cyan dashed lines. Heteroatoms are color-coded as well: red – oxygen, blue – nitrogen, yellow – sulfur.

mode	affinity	dist from best mode	
	(kcal/mol)	rmsd l.b.	rmsd u.b.
1	-8.3	0.000	0.000
2	-8.2	0.149	1.746
3	-8.0	2.451	4.848
4	-7.9	2.238	4.762
5	-7.9	2.033	4.598
6	-7.9	2.308	4.573
7	-7.7	2.193	3.828
8	-7.6	2.295	4.363
9	-7.5	2.623	5.080
10	-7.5	2.865	4.457

Table 4: Binding affinities and RMSD values of fenoterol in mOCT1 analyzed by AutoDock Vina. Root mean square deviation (RMSD) values measuring the average between atoms of a position relative to the best fitting position, are calculated using only movable heavy atoms. Two variants of RMSD metrics are provided, rmsd l.b. (RMSD lower bound) and rmsd u.b. (RMSD upper bound). They differ in how the atoms are matched in the distance calculation; rmsd u.b. matches each atom in one conformation with itself in the other conformation, ignoring any symmetry; rmsd l.b. matches each atom in one conformation with the closest atom of the same element type in the other conformation.

Next, we performed molecular docking in the exact same manner for trospium to first hOCT1 and then mOCT1. Like previously, the best three binding poses are illustrated and analyzed. The best docked binding pose has an affinity of -8.2 kcal/mol (Table 5). Trospium is in the middle of the active site with its boat conformation of the cycloheptane ring pointing towards the extracellular membrane and the two benzyl rings directed towards the intracellular membrane (Fig. 15). The conformation is stabilized by two intermolecular H-bonds. The first one is formed between the hydroxy group of trospium and the amino group of Gln362. In the second H-bond, the oxygen in the linker part of trospium shows HBA activity with Gly363. As already observed for fenoterol, the benzyl rings seem to be stabilized through a network of pi-pi and cation-pi interactions between Phe32, Lys214, Trp217, Phe244. No interaction was observed neither from the crucial Cys36 residue, nor from the essential Asp474 residue. Nevertheless, it seems that Phe159 provides additional stabilizing effect, enabling pi-pi interactions with the close benzyl ring of trospium (3.3 Å).

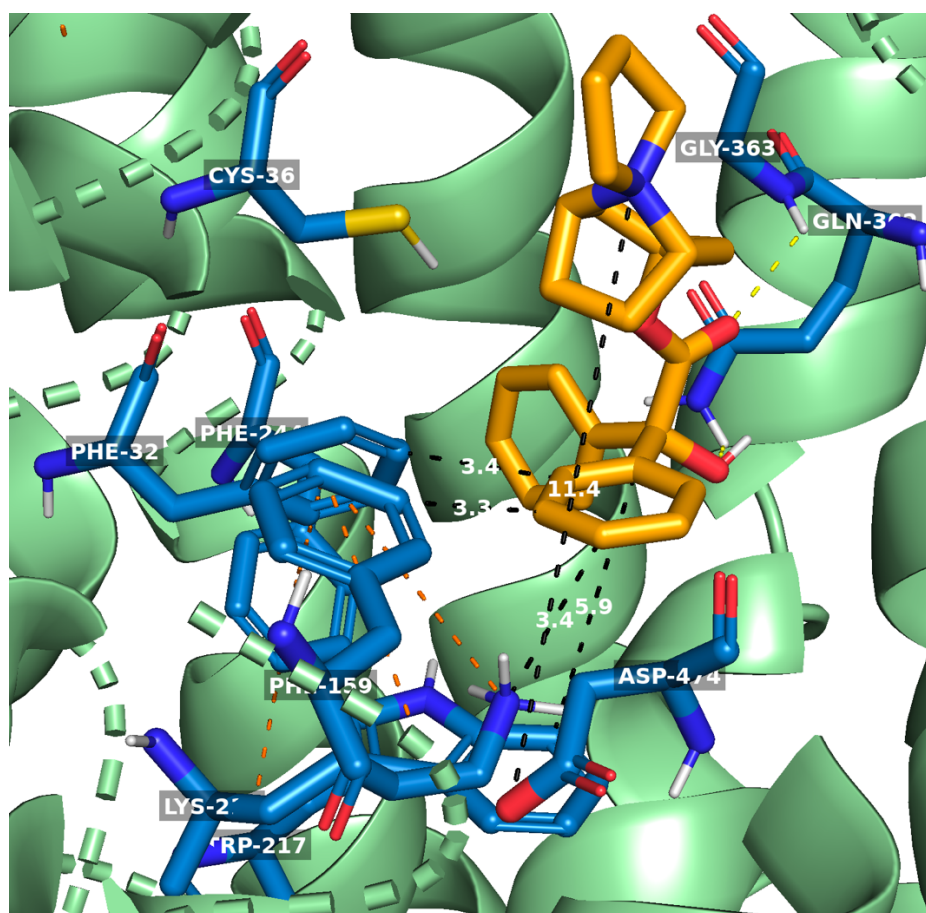


Figure 15: Molecular docking of trospium into hOCT1 by AutoDock Vina. Shown is here the best binding pose of trospium (orange) in hOCT1 (green) regarding the binding affinity out of ten conformations. Polar interactions are shown by yellow dashed lines. The distance of amino acids in close proximity are shown by black dashed lines with its respective value in white. Pi-Pi interactions are displayed by orange dashed lines. Heteroatoms are color-coded as well: red – oxygen, blue – nitrogen, yellow – sulfur.

The next two binding poses show no polar interaction after docking (Fig. 16 and 17). The second best ranked pose has an affinity of -7.3 kcal/mol with RMSD u.b. 2.448 and RMSD l.b. 7.362. Similarly, the third best ranked conformation shows an affinity of -7.2 kcal/mol towards hOCT1 with RMSD u.b. 1.551 and RMSD l.b. 3.956 (Table 5). Compared to the first conformation, the second pose underwent a 180° rotation, the benzyl rings being on top and the cycloheptane ring shifted towards the intracellular membrane. The third pose has a similar conformation to the best ranked one with a minor difference in the conformation of the cycloheptane ring and the orientation of the two benzyl rings. Here, the cycloheptane ring seems to be oriented in a twist-boat conformation and one of the benzyl rings points more towards the TMH7. For the second pose, it is observed a short distance between the crucial Cys36 and one benzyl group (3.6 Å) suggesting a sulfur-pi interaction.

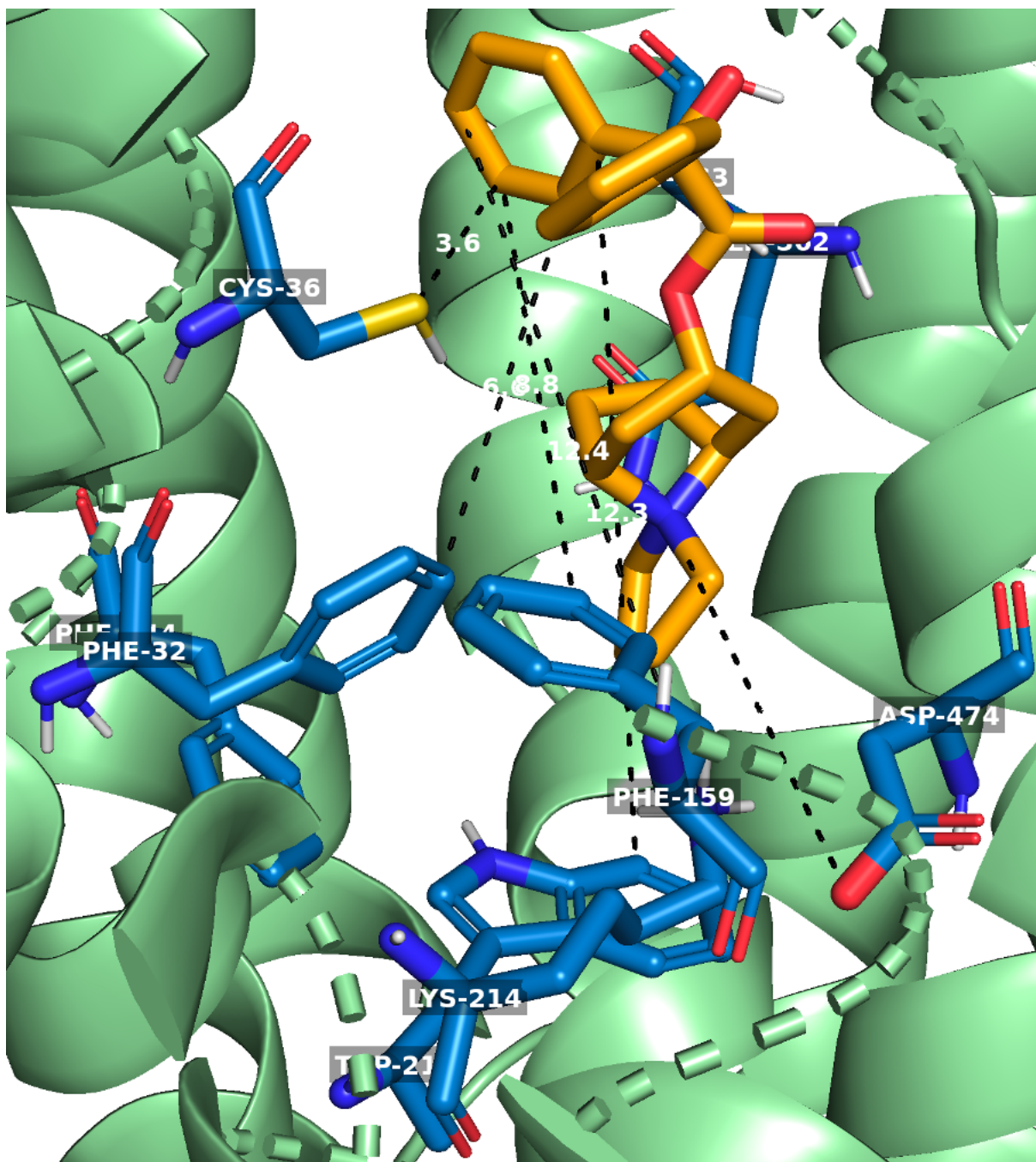


Figure 16: Molecular docking of trospium into hOCT1 by AutoDock Vina. Shown is here the second best binding pose of trospium (orange) in hOCT1 (green) regarding the binding affinity out of ten conformations. Polar interactions are shown by yellow dashed lines. The distance of amino acids in close proximity are shown by black dashed lines with its respective value in white. Pi-Pi interactions are displayed by orange dashed lines. Heteroatoms are color-coded as well: red – oxygen, blue – nitrogen, yellow – sulfur.

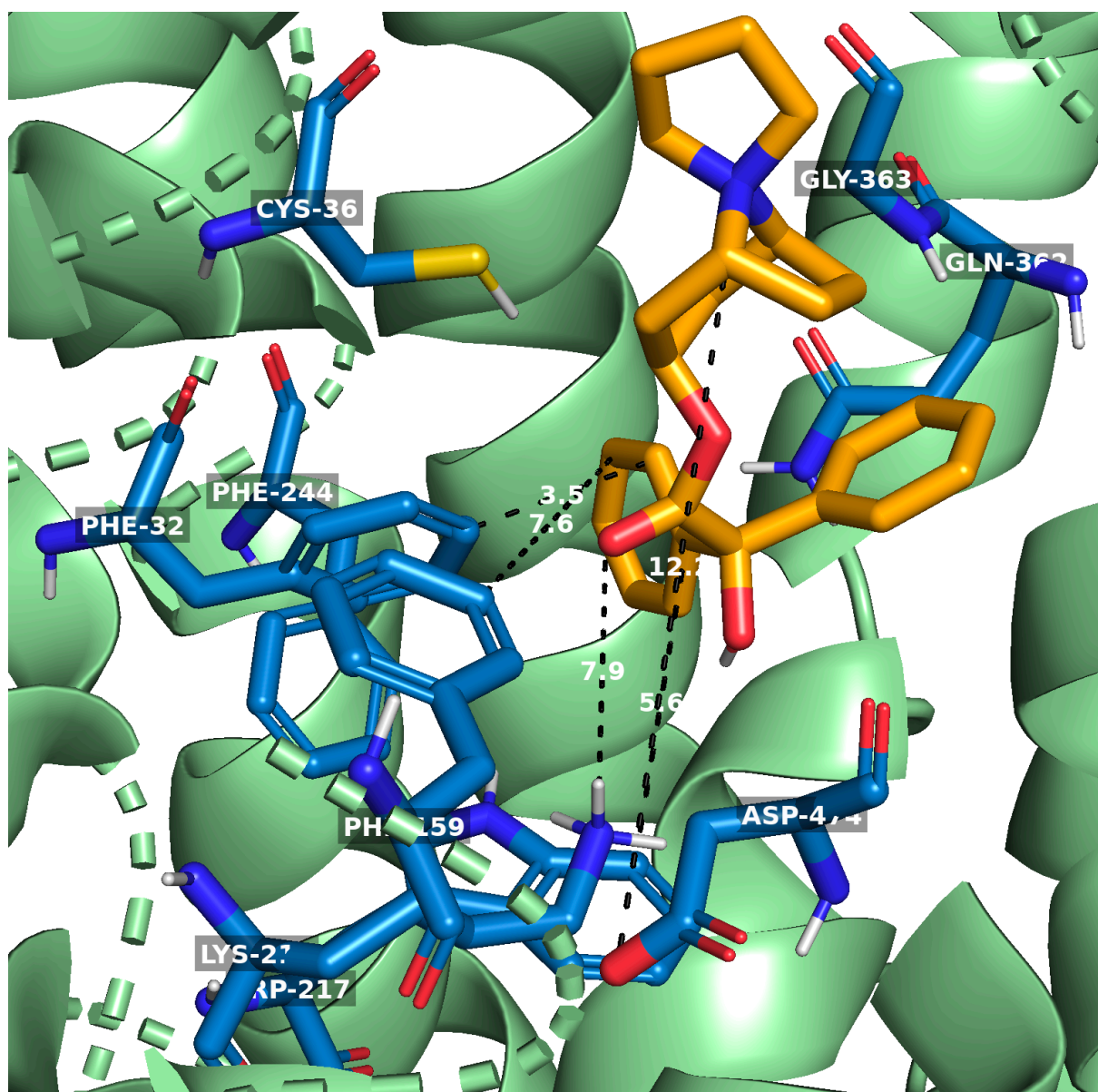


Figure 17: Molecular docking of trospium into hOCT1 by AutoDock Vina. Shown is here the third best binding pose of trospium (orange) in hOCT1 (green) regarding the binding affinity out of ten conformations. Polar interactions are shown by yellow dashed lines. The distance of amino acids in close proximity are shown by black dashed lines with its respective value in white. Pi-Pi interactions are displayed by orange dashed lines. Heteroatoms are color-coded as well: red – oxygen, blue – nitrogen, yellow – sulfur.

mode	affinity (kcal/mol)	dist from best mode	
		rmsd l.b.	rmsd u.b.
1	-8.2	0.000	0.000
2	-7.4	2.448	7.362
3	-7.3	1.551	3.956
4	-7.2	2.909	5.637
5	-7.1	2.630	7.074
6	-7.1	2.505	6.796
7	-6.9	13.115	15.236
8	-6.8	12.839	14.687
9	-6.6	3.079	6.428
10	-6.6	13.073	14.729

Table 5: Binding affinities and RMSD values of trospium in hOCT1 analyzed by AutoDock Vina. Root mean square deviation (RMSD) values measuring the average between atoms of a position relative to the best fitting position, are calculated using only movable heavy atoms. Two variants of RMSD metrics are provided, rmsd l.b. (RMSD lower bound) and rmsd u.b. (RMSD upper bound). They differ in how the atoms are matched in the distance calculation; rmsd u.b. matches each atom in one conformation with itself in the other conformation, ignoring any symmetry; rmsd l.b. matches each atom in one conformation with the closest atom of the same element type in the other conformation.

In the best ranked docking pose for trospium docked into mOCT1 no polar interactions were observed (Fig. 18). It has an affinity of -9.8 kcal/mol towards mOCT1 (Table 6). The conformation is stabilized more horizontally compared to the results in hOCT1. Even though there was no intermolecular interaction detected, one benzyl ring is very close to the already mentioned pi-pi network of mOCT1. It seems that the aromatic ring is stabilized by pi-pi and cation-pi interactions between Tyr36 (3.6 Å), Phe160 (4.0 Å), Lys215 (4.1 Å), Trp218 (3.5 Å), Phe245 (4.1 Å). Interestingly, no interaction between the essential Asp475 was observed again.

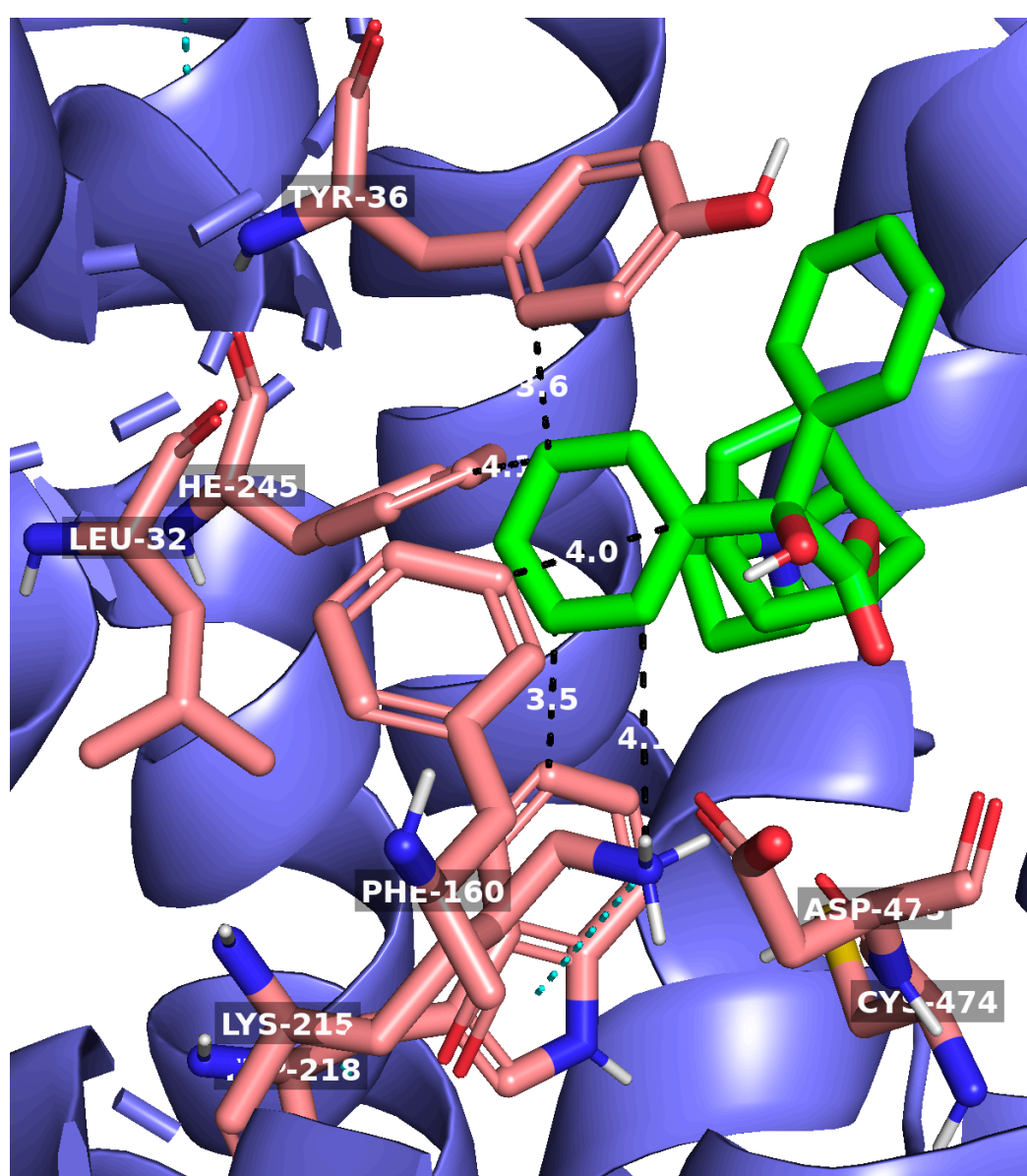


Figure 18: Molecular docking of trospium into mOCT1 by AutoDock Vina. Shown is here the best binding pose of trospium (green) in mOCT1 (purple) regarding the binding affinity out of ten conformations. Polar interactions are shown by yellow dashed lines. The distance of amino acids in close proximity are shown by black dashed lines with its respective value in white. Pi-Pi interactions are displayed by orange dashed lines. Heteroatoms are color-coded as well: red – oxygen, blue – nitrogen, yellow – sulfur.

The second best ranked pose has an affinity of -8.7 kcal/mol to mOCT1 (Table 6). Its RMSD values are following: RMSD u.b 1.769 and RMSD l.b. 2.408. The conformation is similar to the first pose except its longer distance to the pi-pi network of TMH2 and TMH4 (Fig. 19). This enables stabilizing effects from TMH7. Here, the oxygen in the linker part forms an intermolecular H-bond with Gly364. Since the positively charged nitrogen is trapped in the back, the distance to Asp475 makes it impossible to form an interaction.

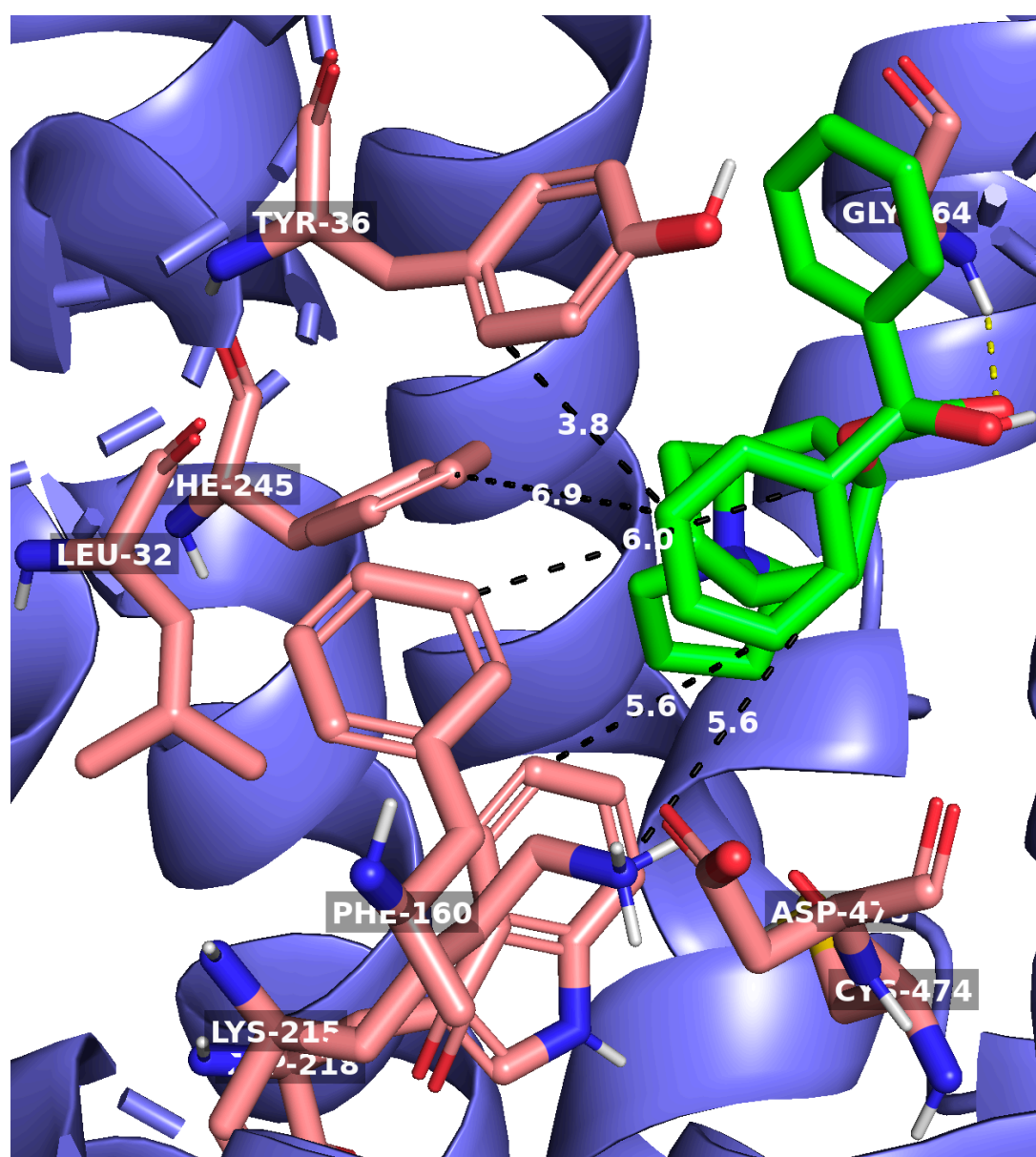


Figure 19: Molecular docking of trospium into mOCT1 by AutoDock Vina. Shown is here the second best binding pose of trospium (green) in mOCT1 (purple) regarding the binding affinity out of ten conformations. Polar interactions are shown by yellow dashed lines. The distance of amino acids in close proximity are shown by black dashed lines with its respective value in white. Pi-Pi interactions are displayed by orange dashed lines. Heteroatoms are color-coded as well: red – oxygen, blue – nitrogen, yellow – sulfur.

As already observed in the first pose, the third best ranked binding shows no polar interactions (Fig. 20). Its more linear conformation shows an affinity of -8.6 kcal/mol (Table 6). Since the cycloheptane ring is more shifted towards the intracellular membrane and the second benzyl ring is pointing more towards the TMH11, it explains the increased RMSD values. RMSD u.b is 1.905 and l.b. is 4.414. The black dashed lines indicate also that the benzyl rings have flipped position compared to the first pose.

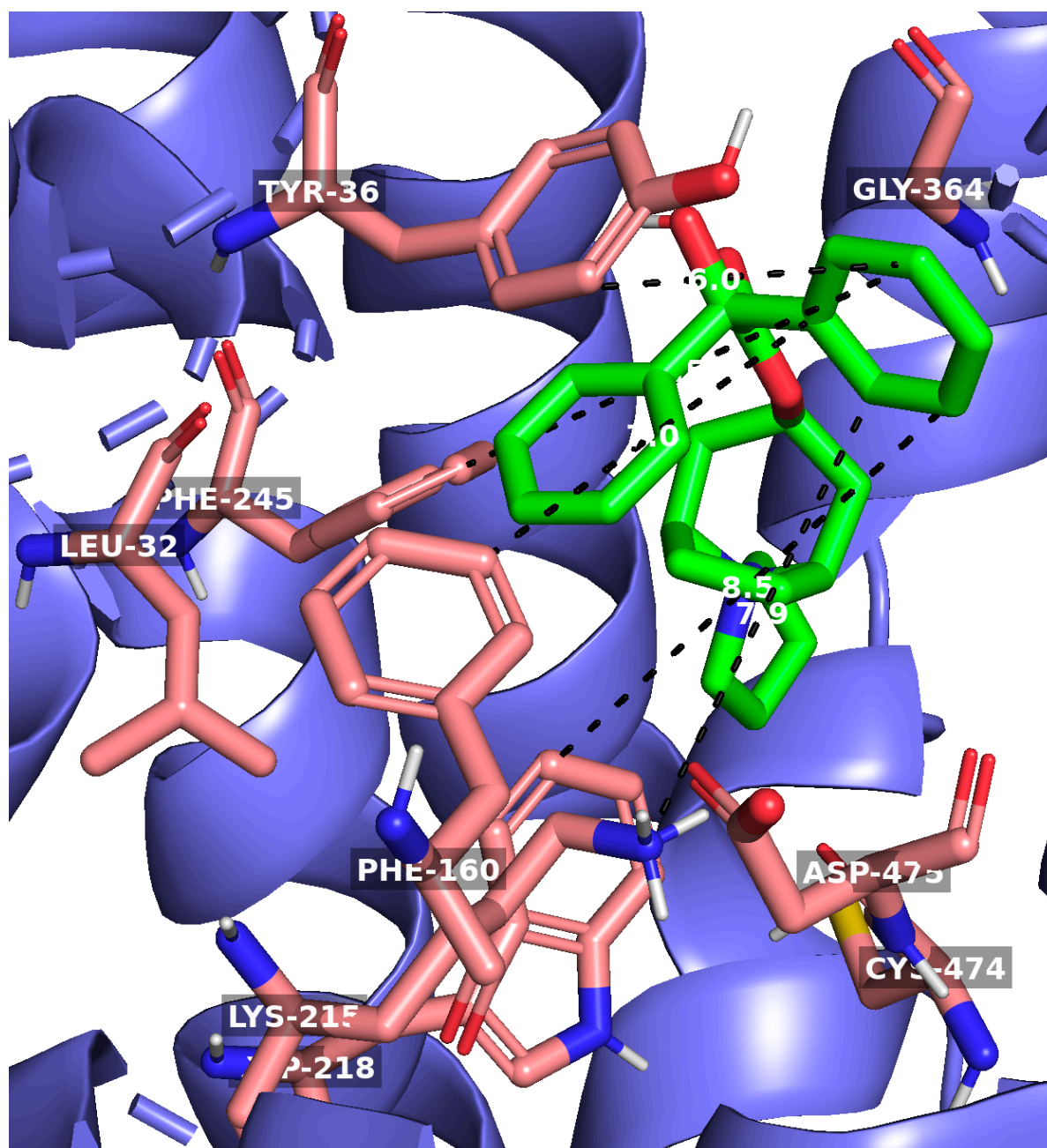


Figure 20: Molecular docking of trospium into mOCT1 by AutoDock Vina. Shown is here the best binding pose of trospium (green) in mOCT1 (purple) regarding the binding affinity out of ten conformations. Polar interactions are shown by yellow dashed lines. The distance of amino acids in close proximity are shown by black dashed lines with its respective value in white. Pi-Pi interactions are displayed by orange dashed lines. Heteroatoms are color-coded as well: red – oxygen, blue – nitrogen, yellow – sulfur.

mode	affinity (kcal/mol)	dist from best mode	
		rmsd l.b.	rmsd u.b.
1	-9.8	0.000	0.000
2	-8.7	1.769	2.408
3	-8.6	1.905	4.414
4	-7.8	2.296	6.222
5	-7.7	1.947	3.123
6	-7.6	2.930	6.002
7	-7.6	13.239	15.955
8	-7.2	1.949	6.069
9	-7.2	16.733	19.491
10	-7.2	16.681	18.555

Table 6: Binding affinities and RMSD values of trospium in mOCT1 analyzed by AutoDock Vina. Root mean square deviation (RMSD) values measuring the average between atoms of a position relative to the best fitting position, are calculated using only movable heavy atoms. Two variants of RMSD metrics are provided, rmsd l.b. (RMSD lower bound) and rmsd u.b. (RMSD upper bound). They differ in how the atoms are matched in the distance calculation; rmsd u.b. matches each atom in one conformation with itself in the other conformation, ignoring any symmetry; rmsd l.b. matches each atom in one conformation with the closest atom of the same element type in the other conformation.

3.2.1 Rotamer docking of fenoterol into hOCT1 using AutoDock Vina

Even though various intermolecular interactions have been reported throughout several docking runs, the one interaction that is pharmacologically proven [45,69,71], Asp474, hasn't been shown a single time neither for fenoterol nor for trospium in both organisms. Since this residue is confirmed to be essential for OCT1 cation interaction, a new rotamer has been created for hOCT1 (Fig. 21 and 22) and mOCT1 (Fig. 23 and 24). PyMol has a mutagenesis wizard enabling either substitutions or rotations for the residue of your choice. Since we only wanted to change the side chain orientation of Asp474, we ignored the mutations. For each amino acid exists several rotamers, which are ordered according to their frequencies of occurrence in the protein, shown as a percentage in the mutagenesis panel (not depicted in Fig. 21 – 24). For Asp474 out of 7 different rotamers the third one was chosen based on its direction towards the binding site with an occurrence rate of 5.0% compared to 3.3% of the older orientation. Since the new orientation comes with steric clashes (red disks), a second rotamer change has been performed for Lys214, giving Asp474 more spacial freedom to move and interact. Here, the new occurrence rate has changed from 2.3% to 1.8%.

In analogy to hOCT1, the same approach was applied for Asp475 and Lys215 in mOCT1 (Fig. 23 and 24). The occurrence rate of Asp475 has changed from 9.8% to 63.9% by choosing the first orientation out of six. The new rotamer of Lys215 comes with a new value of 10.8% compared to 1.9% of the previous orientation.

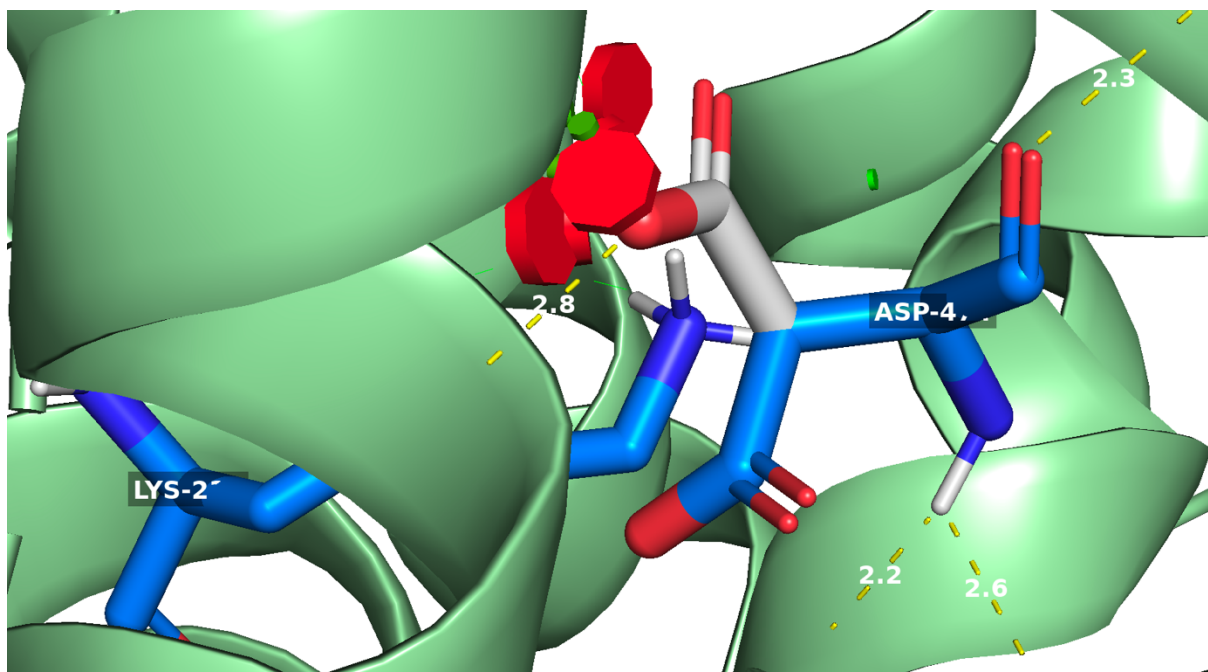


Figure 21: New orientation (rotamer) of Asp474 in hOCT1. The old side chain of Asp474 (blue) has been rotated more towards the active side. The new rotamer is represented in grey. The visible disks indicate pairwise overlap of van der Waals radii. Small green disks are shown when atoms are almost in contact or slightly overlapping. Large red discs indicate significant van der Waals overlap. The yellow dashed lines represent polar interactions with its distance.

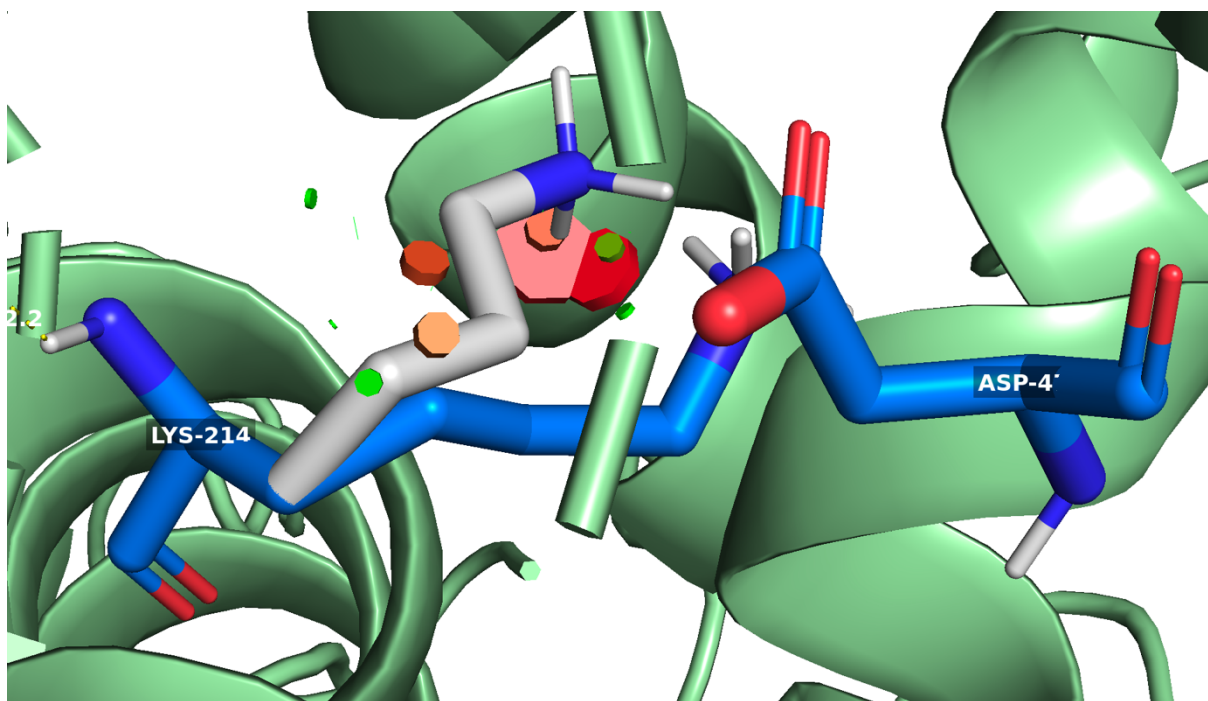


Figure 22: New orientation (rotamer) of Lys214 in hOCT1. The old side chain of Lys214 (blue) has been rotated more towards the active side. The new rotamer is represented in grey. The visible disks indicate pairwise overlap of van der Waals radii. Small green disks are shown when atoms are almost in contact or slightly overlapping. Large red discs indicate significant van der Waals overlap. The yellow dashed lines represent polar interactions with its distance.

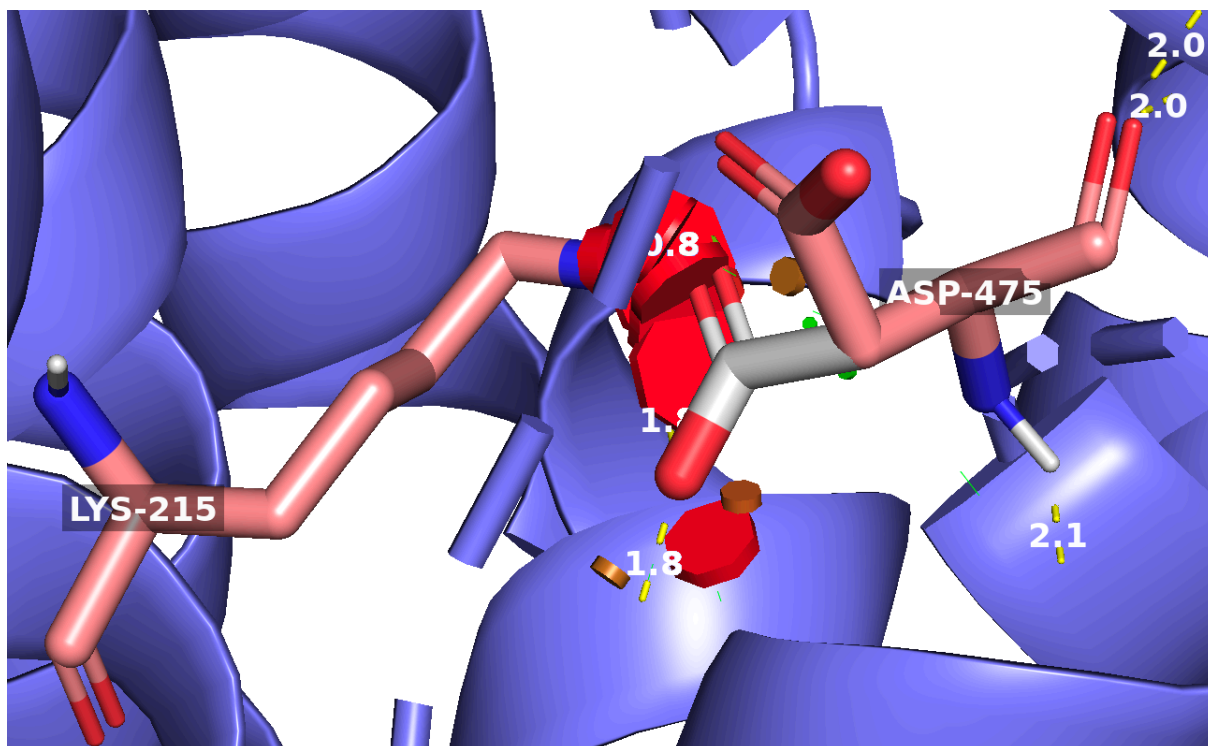


Figure 23: New orientation (rotamer) of Asp475 in mOCT1. The old side chain of Asp475 (salmon) has been rotated more towards the active side. The new rotamer is represented in grey. The visible disks indicate pairwise overlap of van der Waals radii. Small green disks are shown when atoms are almost in contact or slightly overlapping. Large red discs indicate significant van der Waals overlap. The yellow dashed lines represent polar interactions with its distance.

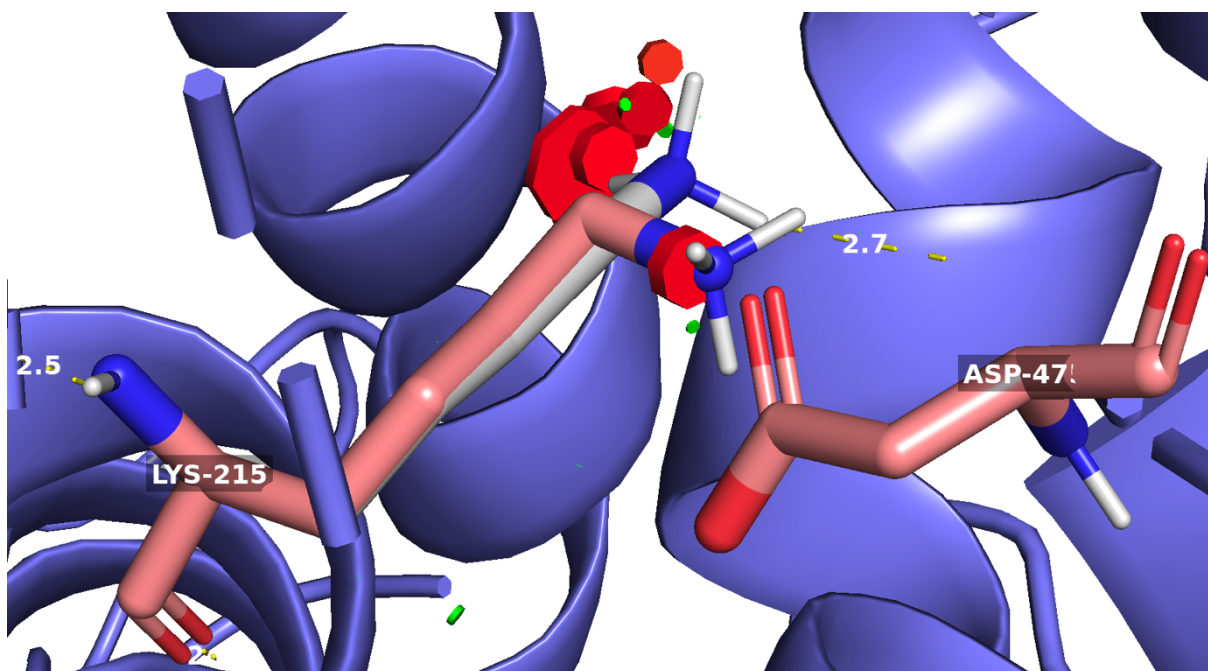


Figure 24: New orientation (rotamer) of Lys215 in mOCT1. The old side chain of Lys215 (salmon) has been rotated more towards the active side. The new rotamer is represented in grey. The visible disks indicate pairwise overlap of van der Waals radii. Small green disks are shown when atoms are almost in contact or slightly overlapping. Large red discs indicate significant van der Waals overlap. The yellow dashed lines represent polar interactions with its distance.

The following docking approach contains the new orientations of Asp474 and Lys214 in hOCT1 with fenoterol. Since four of the top five listed poses have an affinity of -7.0 kcal/mol (Table 7) the fifth conformation was selected, as it provides the crucial intermolecular interaction with Asp474 (Fig. 25). Its RMSD u.b 3.441 and RMSD l.b. 2.412. The hydroxy group of the phenyl ring containing two OH-groups is stabilized by Asp475 functioning as an HBD. Next, TMH7 stabilizes the linker part by forming two intermolecular interactions. Here, the backbone of Asp357 forms two H-bonds at the same time, firstly with the positively charged nitrogen and secondly with the hydrogen group right next to it. The second interaction of TMH7 comprises the H-bond formed again between the hydroxy group in the linker part and Gln362. Other than that, it seems that fenoterol is close by TMH1 and TMH2 being embedded in the pi-pi network. Possible formed pi interactions are the pi-sulfur interaction between Cys36 and the second phenol ring (3.9 Å), pi-pi interaction between Phe32 and the second phenol ring (3.9 Å), a cation-pi interaction between the positively charged nitrogen and Phe32 (4.6 Å), and a cation-pi interaction between the positively charged nitrogen and Trp217 (3.9 Å).

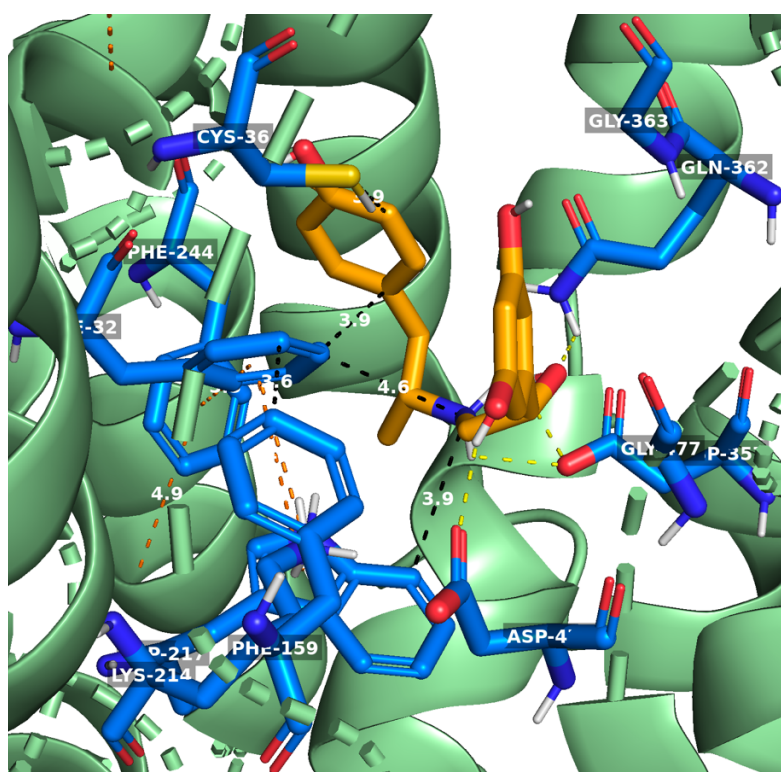


Figure 25: Molecular docking of fenoterol into hOCT1 by AutoDock Vina. Shown is here the fifth best binding pose of fenoterol (orange) in hOCT1 (green) with the new orientations of Asp474 and Lys214 regarding the binding affinity out of ten conformations. Polar interactions are shown by yellow dashed lines. The distance of amino acids in close proximity are shown by black dashed lines with its respective value in white. Pi-Pi interactions are displayed by orange dashed lines. Heteroatoms are color-coded as well: red – oxygen, blue – nitrogen, yellow – sulfur.

The best ranked docking pose of the same run has a binding affinity of -7.2 kcal/mol (Table 7). Its conformation is U-shaped as the fifth one with the minor difference both phenol rings being straightened more to the extracellular membrane (Fig. 26). Three different intermolecular interactions have been visualized by PyMol. Two of them, Asp357 and Gly363, are provided by TMH7 and the last one, Gly477, is formed by TMH11. Gly363 forms a H-Bond with one of the hydroxy groups of the phenyl ring, whereas the positively charged nitrogen is stabilized by a H-bond with Asp357. The hydroxy group of the linker part is also stabilized by a conventional H-bond with Gly477. Regarding the network of pi-pi interactions, fenoterol has almost the same distance to the side chains: Cys36 (4.5 Å), Phe32 (3.7 Å), Trp218 (4.3 Å).

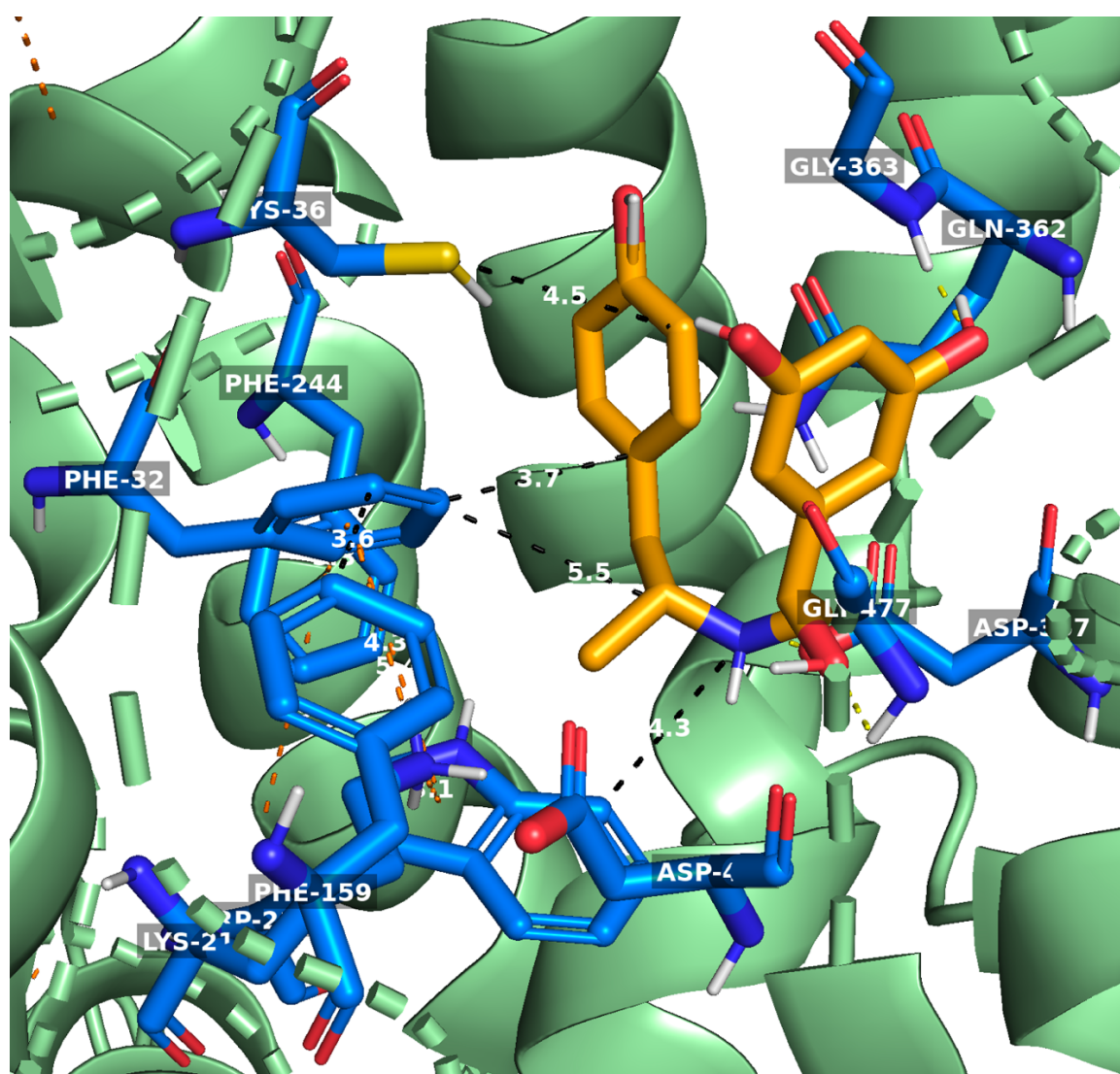


Figure 26: Molecular docking of fenoterol into hOCT1 by AutoDock Vina. Shown is here the best ranked binding pose of fenoterol (orange) in hOCT1 (green) with the new orientations of Asp474 and Lys214 regarding the binding affinity out of ten conformations. Polar interactions are shown by yellow dashed lines. The distance of amino acids in close proximity are shown by black dashed lines with its respective value in white. Pi-Pi interactions are displayed by orange dashed lines. Heteroatoms are color-coded as well: red – oxygen, blue – nitrogen, yellow – sulfur.

The second best ranked docking pose has the same affinity as the fifth (Table 7). Its RMSD values are following: RMSD u.b 3.124 and RMSD l.b. 2.427. The similar binding affinity is supported by its comparable U-shaped conformation (Fig. 27). Hence, the intermolecular interactions of the fifth docking pose are conserved except the important H-bond with Asp474, as the hydrogen of the hydroxy group in the second pose is rotated away. As seen in the fifth conformation, the second pose is in close proximity to TMH1 and TMH2. This facilitates stabilizing effects through pi interactions: such as pi-sulfur interaction with Cys36 (3.9 Å), pi-pi interaction with Phe32 (3.9 Å), and cation-pi interactions with Phe32 (4.7 Å) or Trp217 (3.7 Å).

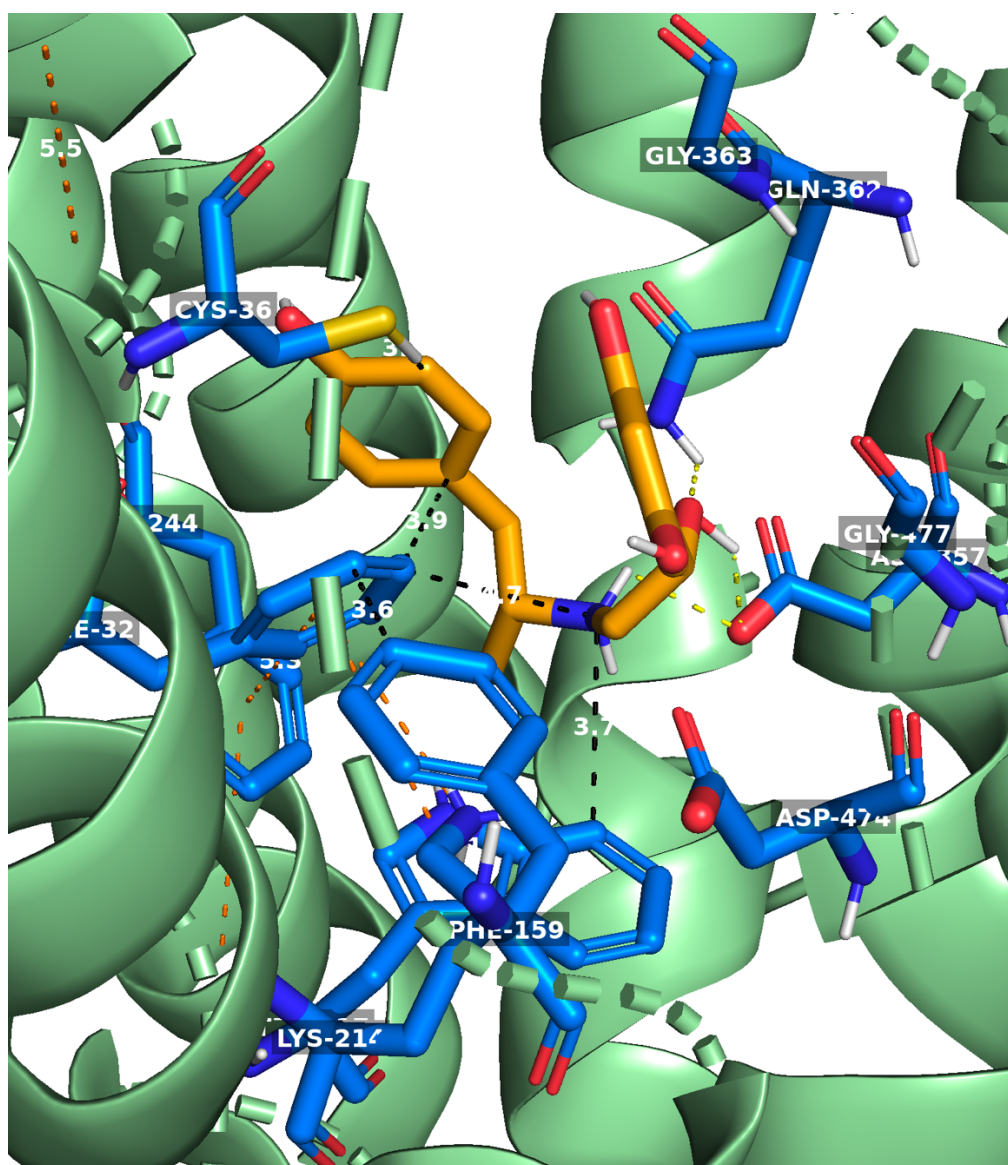


Figure 27: Molecular docking of fenoterol into hOCT1 by AutoDock Vina. Shown is here the second best ranked binding pose of fenoterol (orange) in hOCT1 (green) with the new orientations of Asp474 and Lys214 regarding the binding affinity out of ten conformations. Polar interactions are shown by yellow dashed lines. The distance of amino acids in close proximity are shown by black dashed lines with its respective value in white. Pi-Pi interactions are displayed by orange dashed lines. Heteroatoms are color-coded as well: red – oxygen, blue – nitrogen, yellow – sulfur.

mode	affinity (kcal/mol)	dist from best mode	
		rmsd l.b.	rmsd u.b.
1	-7.2	0.000	0.000
2	-7.0	2.427	3.124
3	-7.0	0.526	2.079
4	-7.0	1.769	2.801
5	-7.0	2.412	3.441
6	-6.9	2.854	5.271
7	-6.9	1.736	2.414
8	-6.9	2.447	6.391
9	-6.9	2.812	4.916
10	-6.8	2.304	3.717

Table 7: Binding affinities and RMSD values of fenoterol in hOCT1 with new rotamers analyzed by AutoDock Vina. Root mean square deviation (RMSD) values measuring the average between atoms of a position relative to the best fitting position, are calculated using only movable heavy atoms. Two variants of RMSD metrics are provided, rmsd l.b. (RMSD lower bound) and rmsd u.b. (RMSD upper bound). They differ in how the atoms are matched in the distance calculation; rmsd u.b. matches each atom in one conformation with itself in the other conformation, ignoring any symmetry; rmsd l.b. matches each atom in one conformation with the closest atom of the same element type in the other conformation.

3.2.2 Rotamer docking of fenoterol into mOCT1 using AutoDock Vina

In the same manner, molecular docking has been performed for fenoterol with mOCT1 with new orientations of Asp475 and Lys215. Out of ten conformations the best docked pose has an affinity of -8.1 kcal/mol (Table 8). Its U-shaped conformation towards the extracellular membrane is also preserved. PyMol has analyzed five polar contacts, which derived from TMH2, TMH4, TMH7, and TMH11 (Fig. 28). The hydroxy group containing two OH-groups of fenoterol is stabilized by H-bonds of the side chains Asn157 and Gly478. Additionally, Lys215 and Asp475 are forming H-bonds with the hydroxy group of the linker. The OH-group of the other phenol ring is stabilized by HBD interaction with Gly364. In a sandwich manner Tyr36 is forming a pi-pi interaction with the second phenol ring of fenoterol (3.6 Å). As the U-shape pushes the positively charged nitrogen into the cavity of Phe160 (3.6 Å), Lys215 (3.6 Å), and Trp218 (3.7 Å) cation-pi interactions enable stabilizing effects.

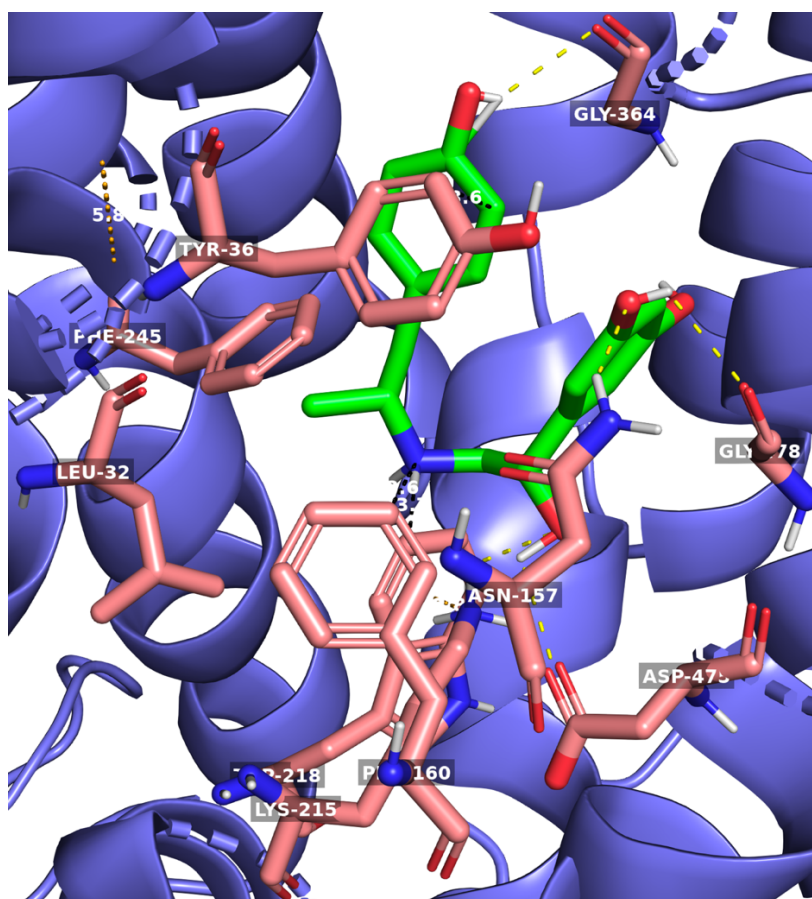


Figure 28: Molecular docking of fenoterol into mOCT1 by AutoDock Vina. Shown is here the best ranked binding pose of fenoterol (green) in mOCT1 (purple) with the new orientations of Asp475 and Lys215 regarding the binding affinity out of ten conformations. Polar interactions are shown by yellow dashed lines. The distance of amino acids in close proximity are shown by black dashed lines with its respective value in white. Pi-Pi interactions are displayed by orange dashed lines. Heteroatoms are color-coded as well: red – oxygen, blue – nitrogen, yellow – sulfur.

The second best ranked pose has an affinity of -7.9 kcal/mol (Table 8) with following RMSD values: u.b. 4.582 and l.b. 2.001. The RMSD values are supported by the shift of the second phenol ring from the extracellular membrane towards TMH2 and TMH4 (Fig. 29). Except Asp475, all other intermolecular interactions are preserved. The minor difference is the hydroxy group of the linker being the new interaction partner for Gly364. As the positively charged nitrogen is in the upper part of the active site, distances to possible pi interactions are highly increased. Instead, the shifted second phenol ring is stabilized through pi-pi interactions by Tyr36 (3.9 Å), Phe160 (3.6 Å), and through cation-pi interaction Lys214 (3.4 Å).

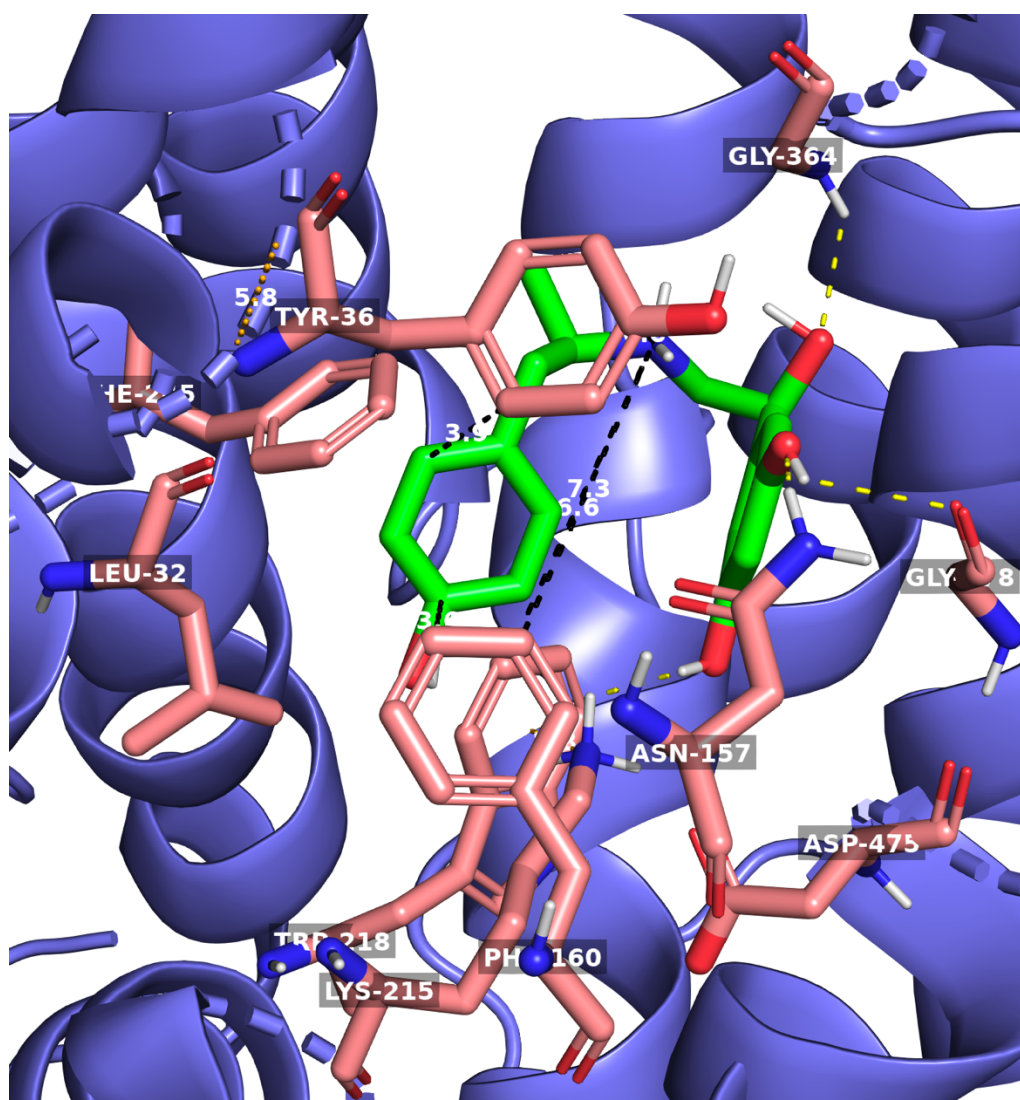


Figure 29: Molecular docking of fenoterol into mOCT1 by AutoDock Vina. Shown is here the second best ranked binding pose of fenoterol (green) in mOCT1 (purple) with the new orientations of Asp475 and Lys215 regarding the binding affinity out of ten conformations. Polar interactions are shown by yellow dashed lines. The distance of amino acids in close proximity are shown by black dashed lines with its respective value in white. Pi-Pi interactions are displayed by orange dashed lines. Heteroatoms are color-coded as well: red – oxygen, blue – nitrogen, yellow – sulfur.

Since the third and fourth best ranked pose differ only 0.1 kcal/mol in affinity (Table 8) the latter was chosen for analysis, as it provides the crucial interaction with Asp475 (Fig. 30). The conformation to the second pose is almost similar with following RMSD values: u.b. 4.374 and l.b. 2.033. Newly introduced stabilizing effects come from the H-bond formed between one of the two hydroxy groups of the phenol ring with Cys474. The network of pi interactions is again preserved with similar distances.

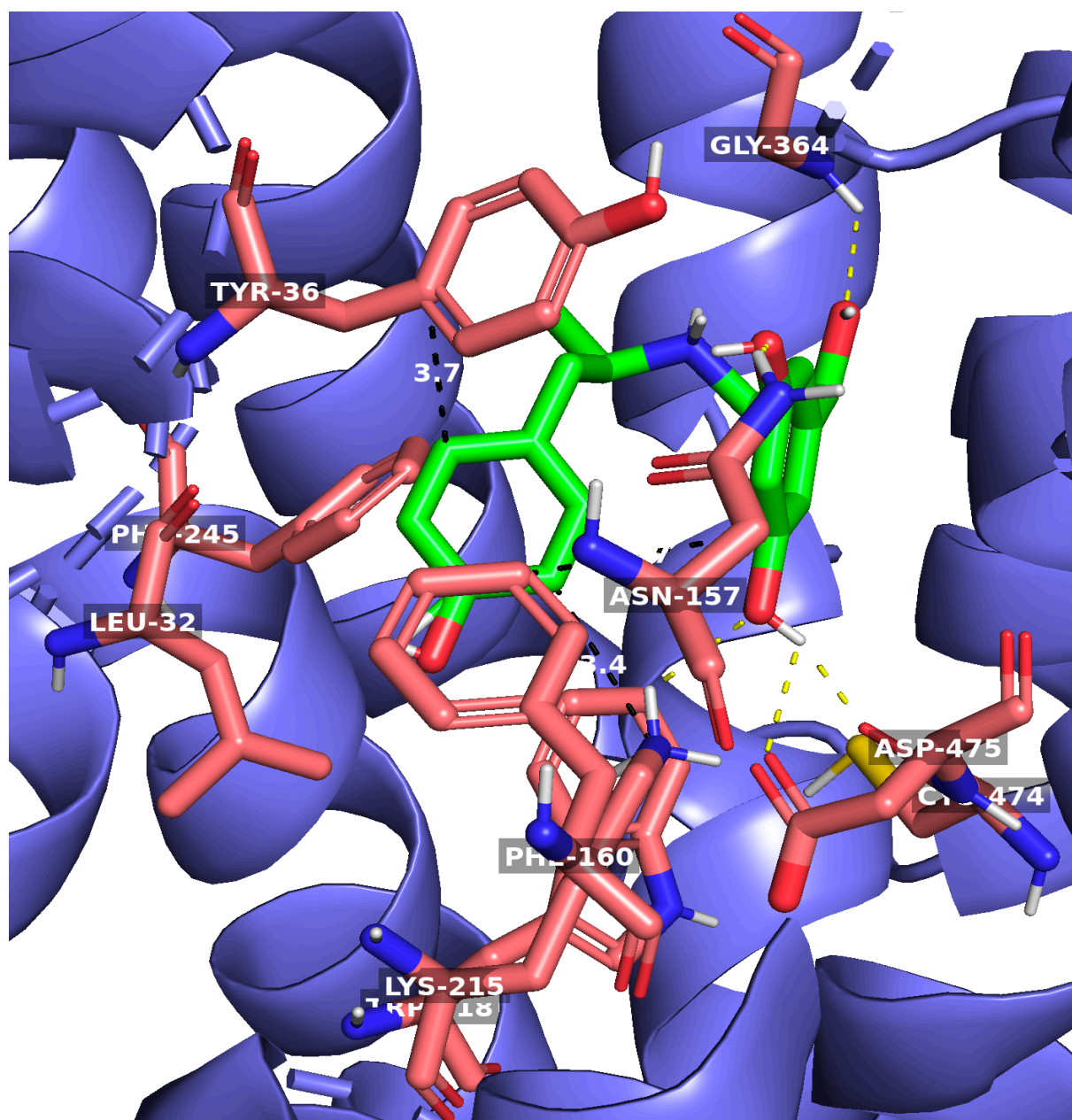


Figure 30: Molecular docking of fenoterol into mOCT1 by AutoDock Vina. Shown is here the fourth best ranked binding pose of fenoterol (green) in mOCT1 (purple) with the new orientations of Asp475 and Lys215 regarding the binding affinity out of ten conformations. Polar interactions are shown by yellow dashed lines. The distance of amino acids in close proximity are shown by black dashed lines with its respective value in white. Pi-Pi interactions are displayed by orange dashed lines. Heteroatoms are color-coded as well: red – oxygen, blue – nitrogen, yellow – sulfur.

mode	affinity (kcal/mol)	dist from best mode	
		rmsd l.b.	rmsd u.b.
1	-8.1	0.000	0.000
2	-7.9	2.001	4.582
3	-7.9	2.274	4.538
4	-7.8	2.033	4.374
5	-7.8	2.475	4.963
6	-7.8	2.340	4.509
7	-7.7	2.114	3.726
8	-7.6	2.152	3.789
9	-7.6	2.545	3.948
10	-7.5	2.845	4.407

Table 8: Binding affinities and RMSD values of fenoterol in mOCT1 with new rotamers analyzed by AutoDock Vina. Root mean square deviation (RMSD) values measuring the average between atoms of a position relative to the best fitting position, are calculated using only movable heavy atoms. Two variants of RMSD metrics are provided, rmsd l.b. (RMSD lower bound) and rmsd u.b. (RMSD upper bound). They differ in how the atoms are matched in the distance calculation; rmsd u.b. matches each atom in one conformation with itself in the other conformation, ignoring any symmetry; rmsd l.b. matches each atom in one conformation with the closest atom of the same element type in the other conformation.

3.2.3 Rotamer docking of trospium into hOCT1 using AutoDock Vina

The next step was to perform molecular docking of trospium into hOCT1 with the new rotamers of Asp474 and Lys214. The best ranked conformation has an affinity of -8.6 kcal/mol (Table 9). The orientation is as following: the positively charged nitrogen is pointing towards the extracellular membrane, whereas the aromatic rings are directed towards the TMH5 and TMH11 (Fig. 31). This conformation is stabilized by two polar intermolecular interactions, both derived from TMH7. The hydroxy group in the linker part of trospium forms a H-bond with the side chain of Gln362 and the oxygen of the linker interacts as an HBA with Gly363. As the benzyl rings are close to the network of pi interactions, stabilizing effects occur by Cys36 (5.0 Å), Phe32 (4.0 Å), Lys214 (3.6 Å), and Trp 217 (5.2 Å).

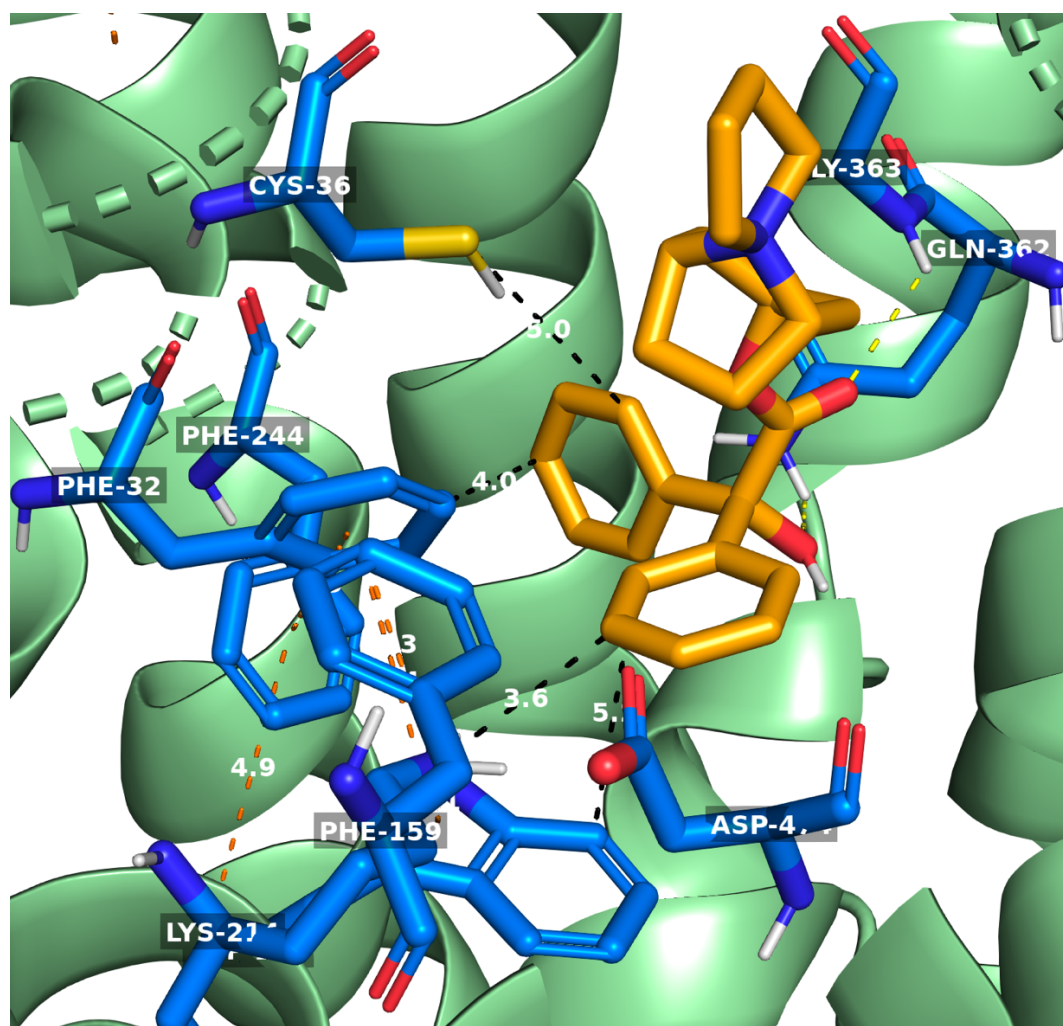


Figure 31: Molecular docking of trospium into hOCT1 by AutoDock Vina. Shown is here the best ranked binding pose of trospium (orange) in hOCT1 (green) with the new orientations of Asp474 and Lys214 regarding the binding affinity out of ten conformations. Polar interactions are shown by yellow dashed lines. The distance of amino acids in close proximity are shown by black dashed lines with its respective value in white. Pi-Pi interactions are displayed by orange dashed lines. Heteroatoms are color-coded as well: red – oxygen, blue – nitrogen, yellow – sulfur.

The second best ranked binding pose has an affinity of -7.7 kcal/mol (Table 9). Its conformation has rotated 180° (Fig. 32), the positively charged nitrogen being at the bottom and the aromatic rings at the top towards the extracellular membrane. Therefore, the RMSD values have changed accordingly: u.b. 7.318 and l.b. 2.525. Interestingly, this pose shows no single polar interaction. Nevertheless, pi-sulfur interaction of Cys36 (3.5 \AA), cation-pi interactions of Phe32 (4.1 \AA), Phe159 (4.9 \AA), and Trp217 (6.4 \AA) contribute to the stabilizing effects.

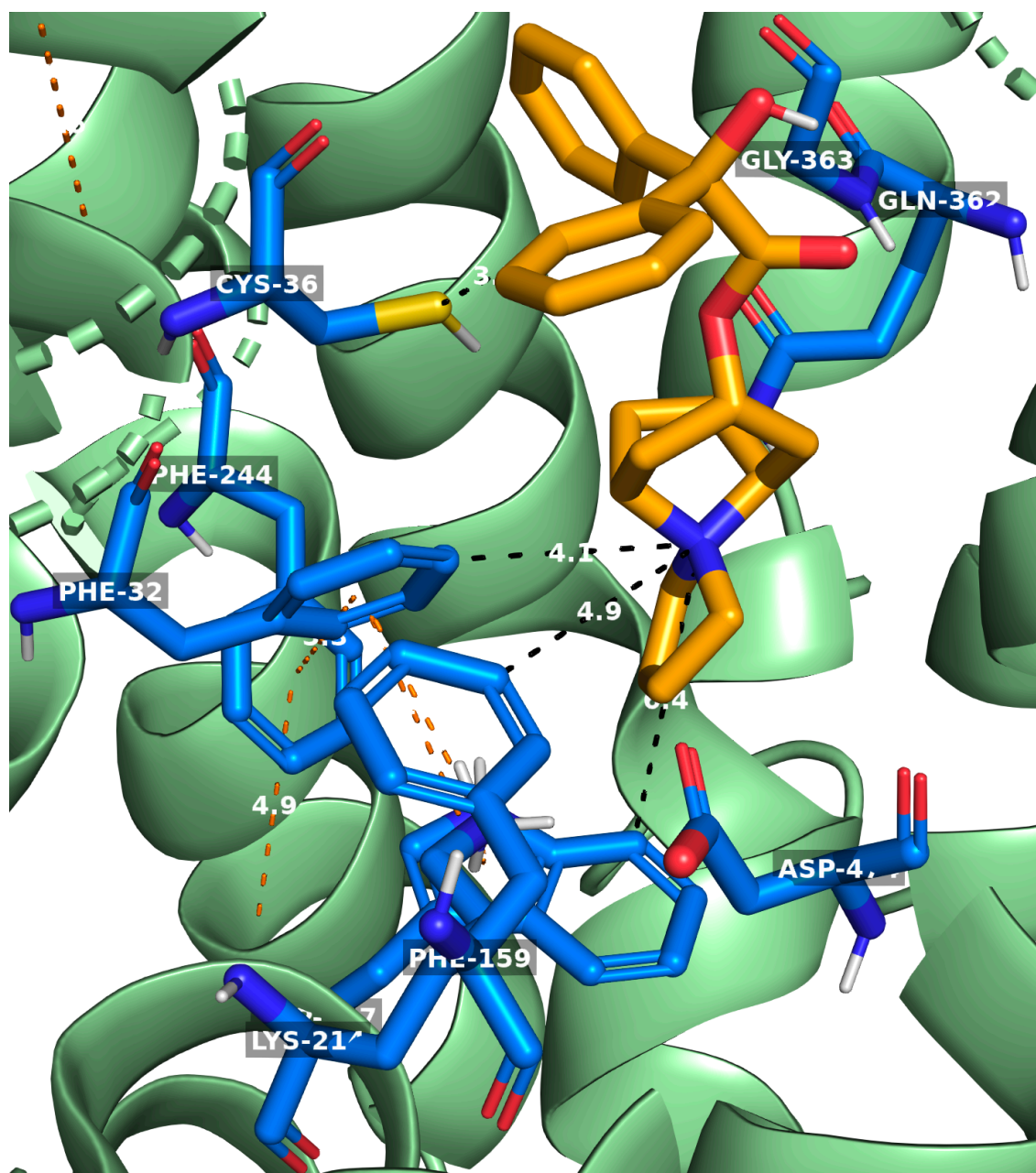


Figure 32: Molecular docking of trospium into hOCT1 by AutoDock Vina. Shown is here the second best ranked binding pose of trospium (orange) in hOCT1 (green) with the new orientations of Asp474 and Lys214 regarding the binding affinity out of ten conformations. Polar interactions are shown by yellow dashed lines. The distance of amino acids in close proximity are shown by black dashed lines with its respective value in white. Pi-Pi interactions are displayed by orange dashed lines. Heteroatoms are color-coded as well: red – oxygen, blue – nitrogen, yellow – sulfur.

The third best ranked conformation of Trospium has an affinity of -7.5 kcal/mol to hOCT1 (Table 9). Compared to the first two conformations, this one is placed horizontally in the active site. The RMSD values are as following: u.b 5.644 and l.b. 2.864. Trospium is stabilized by two intermolecular interactions arising from TMH5 and TMH7 (Fig. 33). Both H-bonds are formed by two glutamine side chains, Gln241 and Gln362 interacting with the oxygen of the linker. Additionally, one of the aromatic rings is stabilized by pi-sulfur interaction of Cys36 (3.6 Å) and pi-pi interaction of Phe32 (4.4 Å).

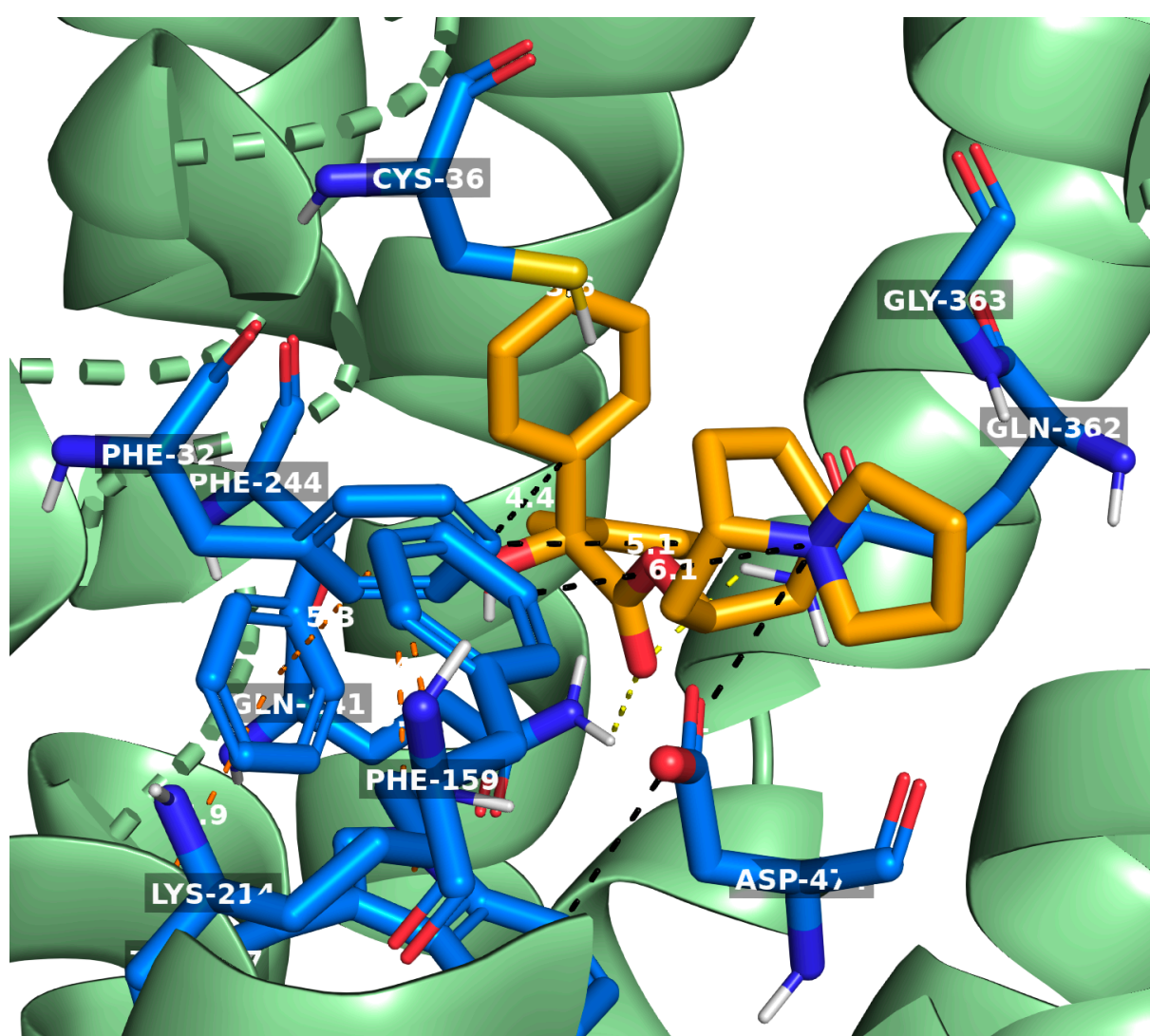


Figure 33: Molecular docking of trospium into hOCT1 by AutoDock Vina. Shown is here the third best ranked binding pose of trospium (orange) in hOCT1 (green) with the new orientations of Asp474 and Lys214 regarding the binding affinity out of ten conformations. Polar interactions are shown by yellow dashed lines. The distance of amino acids in close proximity are shown by black dashed lines with its respective value in white. Pi-Pi interactions are displayed by orange dashed lines. Heteroatoms are color-coded as well: red – oxygen, blue – nitrogen, yellow – sulfur.

mode	affinity (kcal/mol)	dist from best mode	
		rmsd l.b.	rmsd u.b.
1	-8.6	0.000	0.000
2	-7.7	2.525	7.318
3	-7.5	2.864	5.644
4	-7.4	2.680	7.062
5	-7.4	2.517	6.898
6	-7.3	3.346	6.042
7	-7.1	13.071	15.195
8	-7.1	12.872	14.245
9	-6.9	12.763	14.497
10	-6.7	2.498	6.585

Table 9: Binding affinities and RMSD values of trospium in hOCT1 with new rotamers analyzed by AutoDock Vina. Root mean square deviation (RMSD) values measuring the average between atoms of a position relative to the best fitting position, are calculated using only movable heavy atoms. Two variants of RMSD metrics are provided, rmsd l.b. (RMSD lower bound) and rmsd u.b. (RMSD upper bound). They differ in how the atoms are matched in the distance calculation; rmsd u.b. matches each atom in one conformation with itself in the other conformation, ignoring any symmetry; rmsd l.b. matches each atom in one conformation with the closest atom of the same element type in the other conformation.

3.2.4 Rotamer docking of trospium into mOCT1 using AutoDock Vina

In the next approach Trospium was docked into mOCT1 with the new rotamers Asp475 and Lys215. Out of ten poses the three best ranked structures were further analyzed with affinity values of -9.8, -8.8, and -8.7 kcal/mol (Table 10). The only structure showing polar interactions was the second pose, being stabilized by H-bonds of Gly364, which is in the TMH7 (Fig. 35). Regarding the conformations, the first and second pose share similar orientations, with the two benzyl rings opened to the extracellular membrane and located in the region of TMH1 and TMH2, whereas the nitrogenous bicyclic ring is embedded between TMH5 and TMH7 (Fig. 34 and 35). The distances of the second and third conformation vary with the following RMSD values: u.b. 2.420 and l.b. 1.775 for the second pose; u.b. 4.418 and l.b. 1.900 for the third pose. The network of pi-pi and cation-pi interactions range from 3.5 – 3.8 Å in the first binding pose. As the two benzyl rings from the second conformation are more shifted to the right (TMH7) the distances are increased, varying from 3.7 – 5.6 Å. In the third conformation the hydroxy group and the oxygen of the linker are pointing to the extracellular membrane, which flipped the benzyl rings again to the inside, which led to distances of 3.4 – 4.4 Å (Fig. 36).

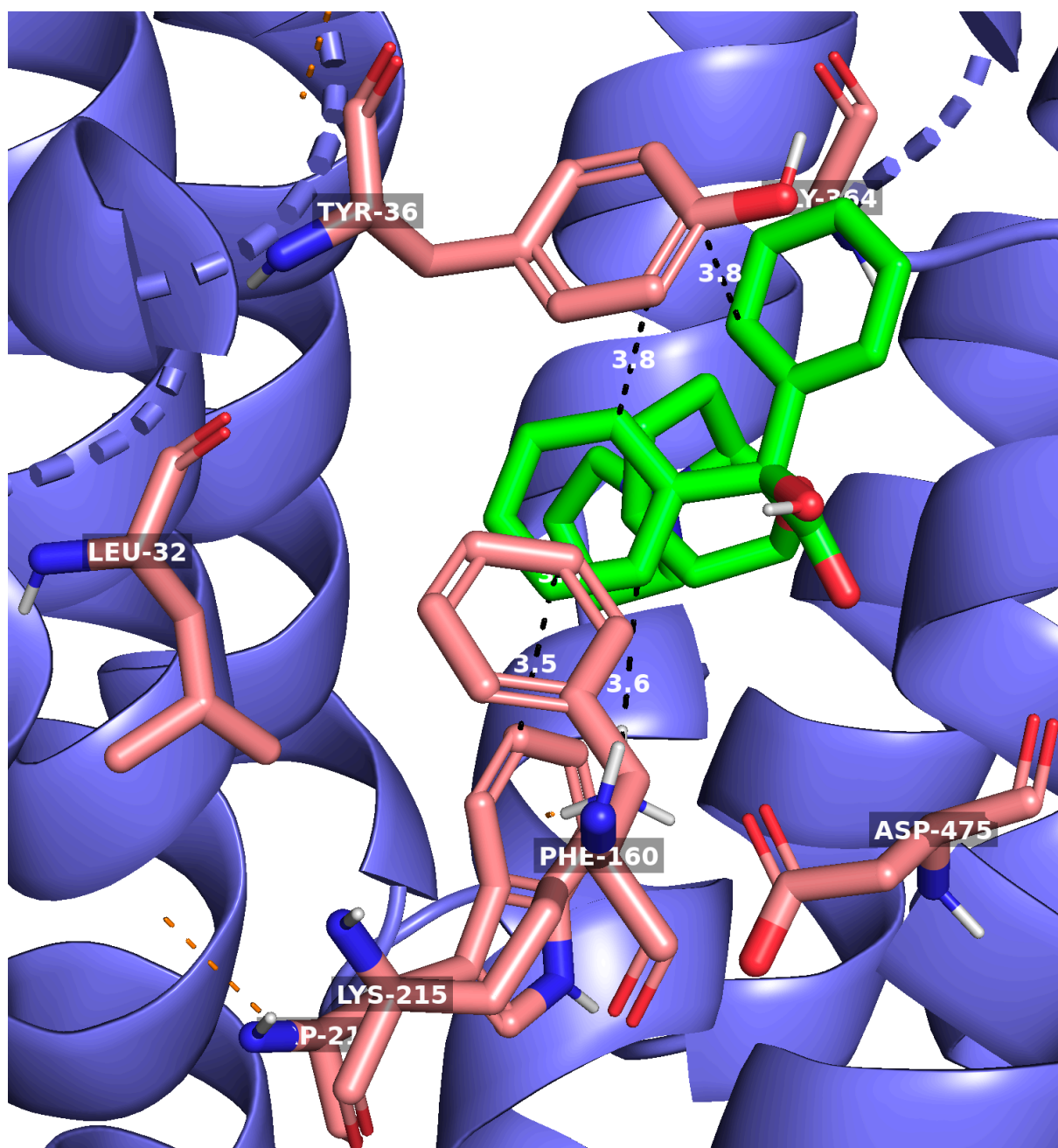


Figure 34: Molecular docking of trospium into mOCT1 by AutoDock Vina. Shown is here the best ranked binding pose of trospium (green) in mOCT1 (purple) with the new orientations of Asp475 and Lys215 regarding the binding affinity out of ten conformations. Polar interactions are shown by yellow dashed lines. The distance of amino acids in close proximity are shown by black dashed lines with its respective value in white. Pi-Pi interactions are displayed by orange dashed lines. Heteroatoms are color-coded as well: red – oxygen, blue – nitrogen, yellow – sulfur.

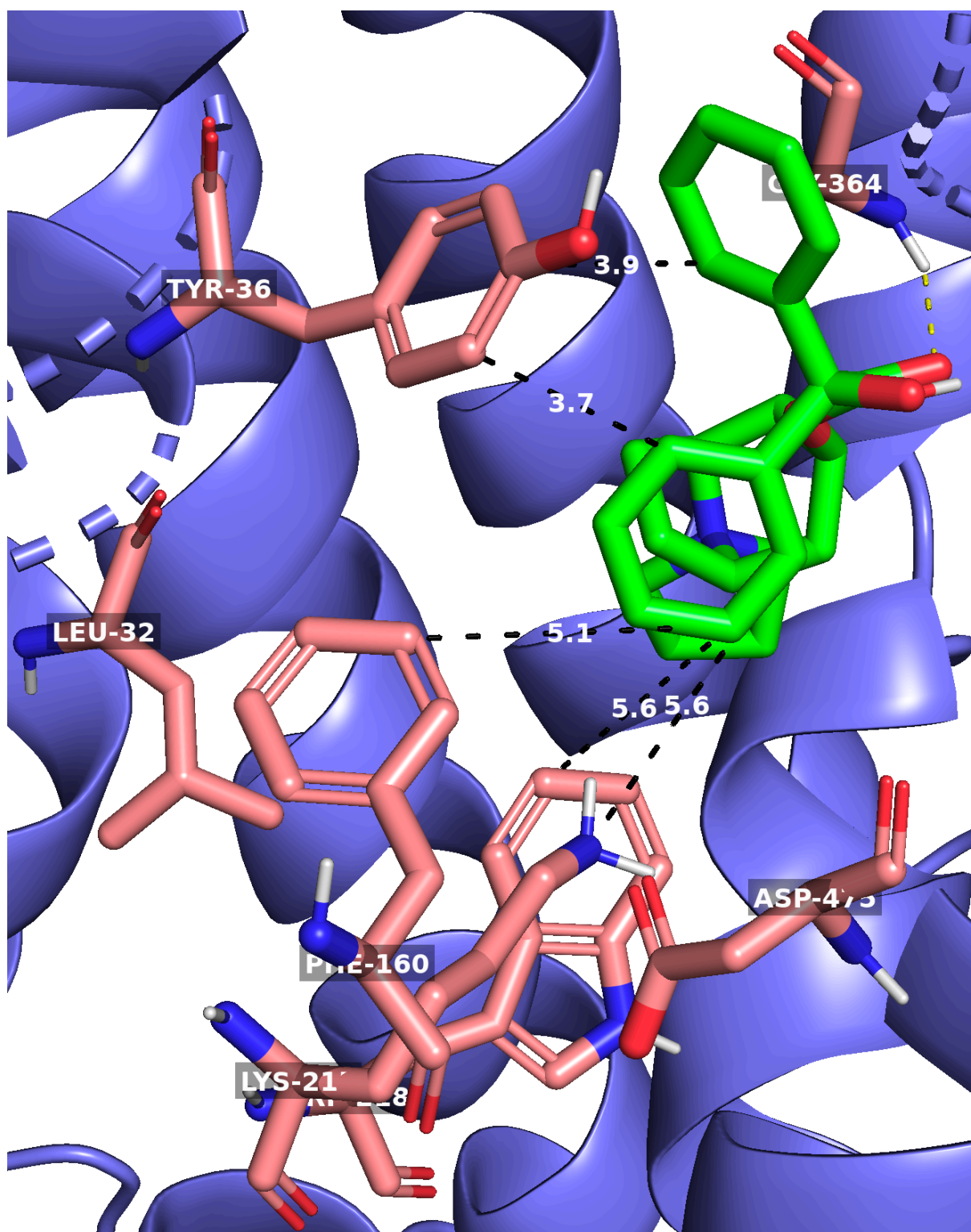


Figure 35: Molecular docking of trospium into mOCT1 by AutoDock Vina. Shown is here the second best ranked binding pose of trospium (green) in mOCT1 (purple) with the new orientations of Asp475 and Lys215 regarding the binding affinity out of ten conformations. Polar interactions are shown by yellow dashed lines. The distance of amino acids in close proximity are shown by black dashed lines with its respective value in white. Pi-Pi interactions are displayed by orange dashed lines. Heteroatoms are color-coded as well: red – oxygen, blue – nitrogen, yellow – sulfur.

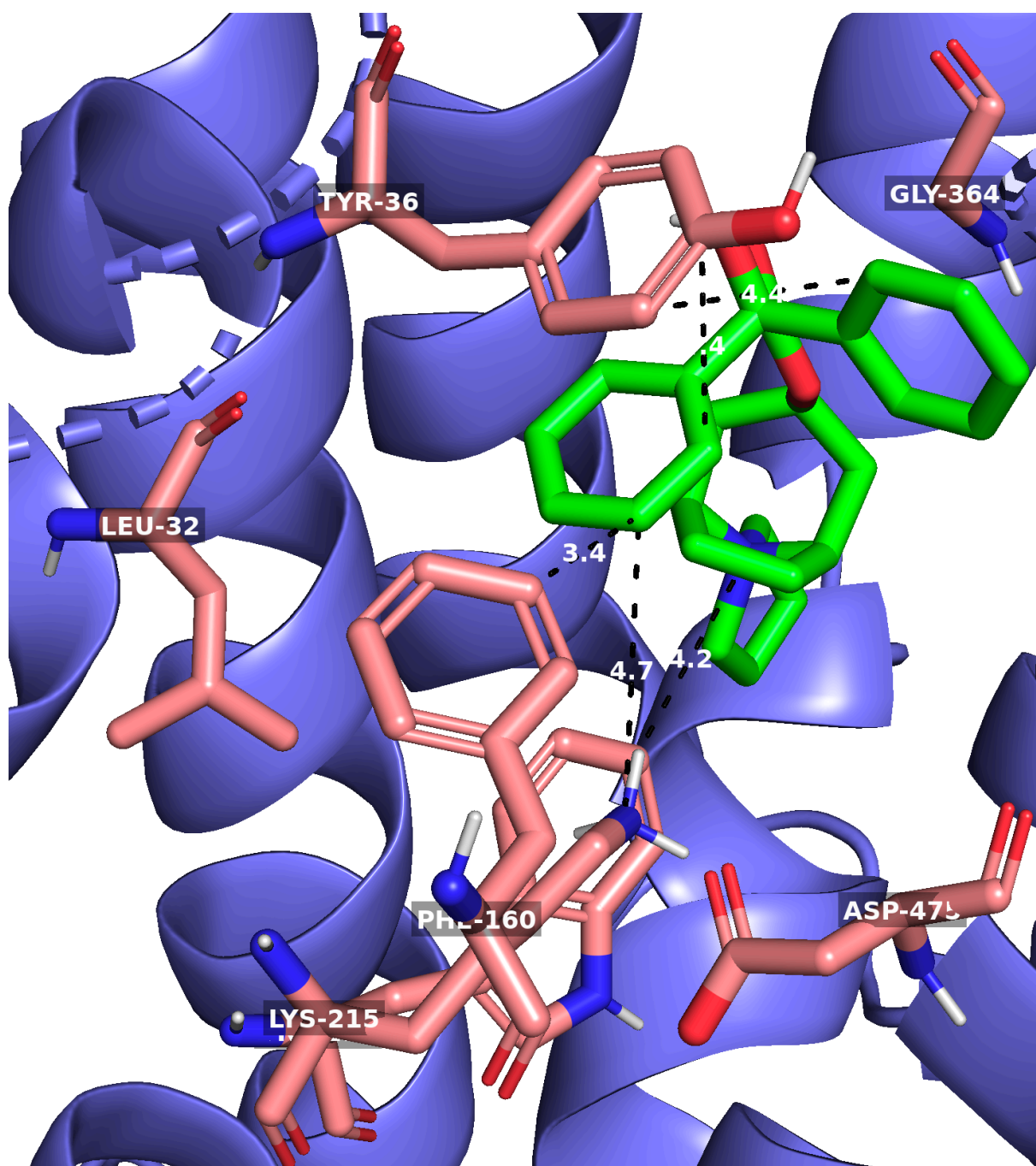


Figure 36: Molecular docking of trospium into mOCT1 by AutoDock Vina. Shown is here the third best ranked binding pose of trospium (green) in mOCT1 (purple) with the new orientations of Asp475 and Lys215 regarding the binding affinity out of ten conformations. Polar interactions are shown by yellow dashed lines. The distance of amino acids in close proximity are shown by black dashed lines with its respective value in white. Pi-Pi interactions are displayed by orange dashed lines. Heteroatoms are color-coded as well: red – oxygen, blue – nitrogen, yellow – sulfur.

mode	affinity (kcal/mol)	dist from best mode	
		rmsd l.b.	rmsd u.b.
1	-9.8	0.000	0.000
2	-8.8	1.775	2.420
3	-8.7	1.900	4.418
4	-8.3	1.724	2.624
5	-8.0	2.950	5.361
6	-7.9	1.714	2.812
7	-7.9	1.836	2.631
8	-7.6	2.409	3.711
9	-7.6	13.258	15.983
10	-7.6	2.499	4.227

Table 10: Binding affinities and RMSD values of trospium in mOCT1 with new rotamers analyzed by AutoDock Vina. Root mean square deviation (RMSD) values measuring the average between atoms of a position relative to the best fitting position, are calculated using only movable heavy atoms. Two variants of RMSD metrics are provided, rmsd l.b. (RMSD lower bound) and rmsd u.b. (RMSD upper bound). They differ in how the atoms are matched in the distance calculation; rmsd u.b. matches each atom in one conformation with itself in the other conformation, ignoring any symmetry; rmsd l.b. matches each atom in one conformation with the closest atom of the same element type in the other conformation.

As the rotamer docking approach hasn't provided reasonable results in both ligands regarding the interaction of the positively charged nitrogen with Asp475, concerns have arisen about this method in general and the homology models. In the meantime, DeepMind and EMBL's European Bioinformatics Institute (EMBL-EBI) have collaborated to create the AlphaFold Protein Structure Database (AlphaFold DB). AlphaFold DB is an openly accessible, extensive database providing high-accuracy protein-structure predictions, which are generated by an artificial intelligence system.^[87,88] Since our collaborators prioritized the human OCT model for further analyses we first compared our previous homology model with the one from AlphaFold DB (Fig. 37 B). As AlphaFold represents its models according to a per-residue confidence score (pLDDT) in different color codes (Fig. 37 A), we then visualized both structures and investigated the crucial residue at codon 474 using PyMol. Comparing the orientation, it is clear that the Asp 474 of the AlphaFold model (Fig. 38 A and B in green) is pointing into the active site, whereas our native homology model (Fig. 38 A in light blue) is oriented in the opposite direction.

Only our protein structure model with new rotamers has the same orientation (Fig. 38 B light blue). By using the align function in PyMol we performed a sequence alignment of both protein structures. This was followed by a structural superposition and cycles of refinement to reject structural outliers found during the fit. Out of 456 aligned atoms, 384 atoms were analyzed after 5 refinement cycles with a total RMSD score of 3.176 Å (Table 11).

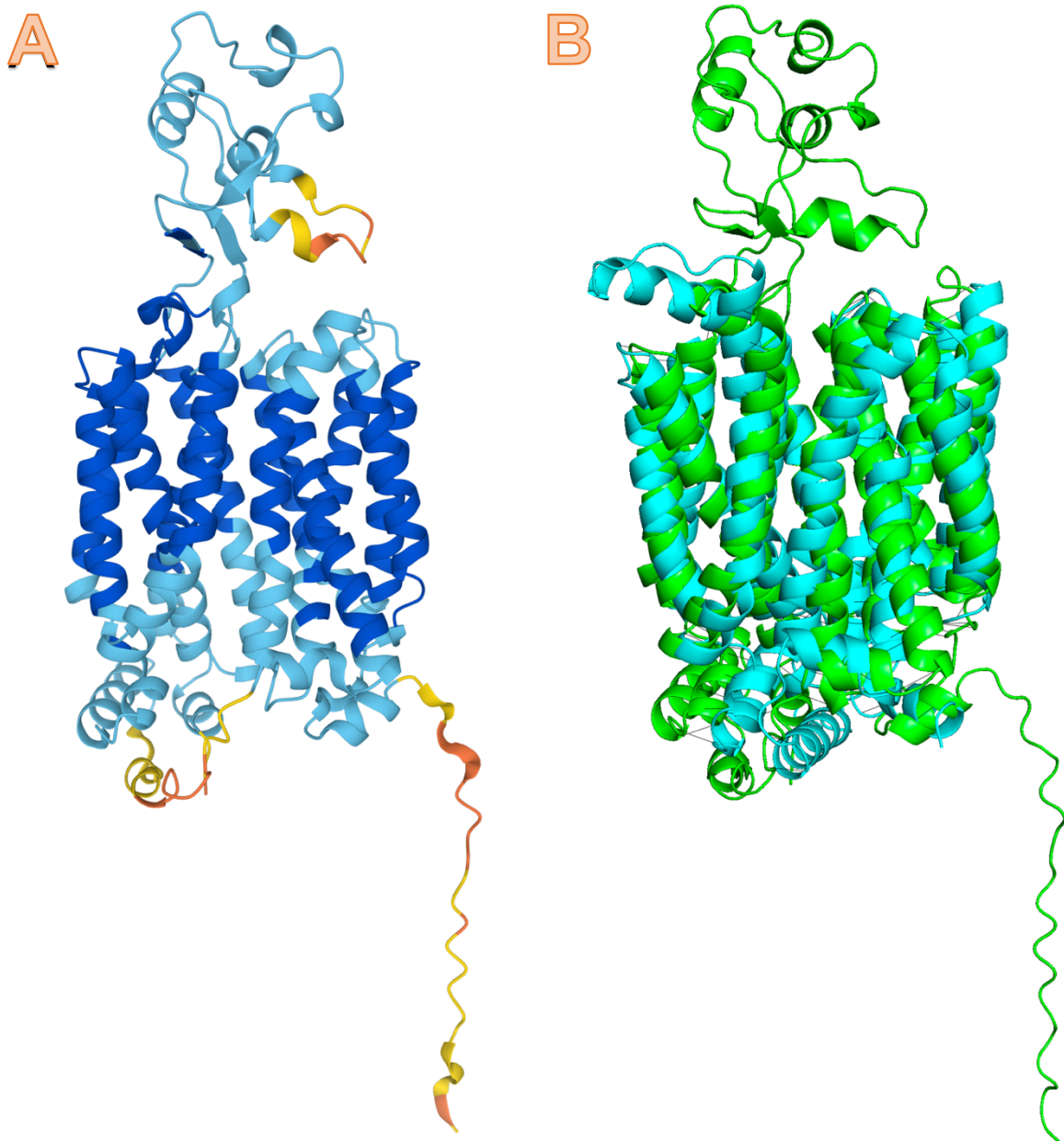


Figure 37: A) AlphaFold 3D structure prediction of hOCT1 (UniProt ID: O15245). AlphaFold produces a per-residue confidence score (pLDDT) between 0 and 100. Regions below 50 pLDDT may be unstructured in isolation. Model confidence is color-coded: Very high (pLDDT > 90) – dark blue; Confident (90 > pLDDT > 70) – light blue; Low (70 > pLDDT > 50) – yellow; Very low (pLDDT < 50) – orange. B) hOCT1 protein structures of AlphaFold (green) and our own generated homology model (blue) were aligned using PyMol.

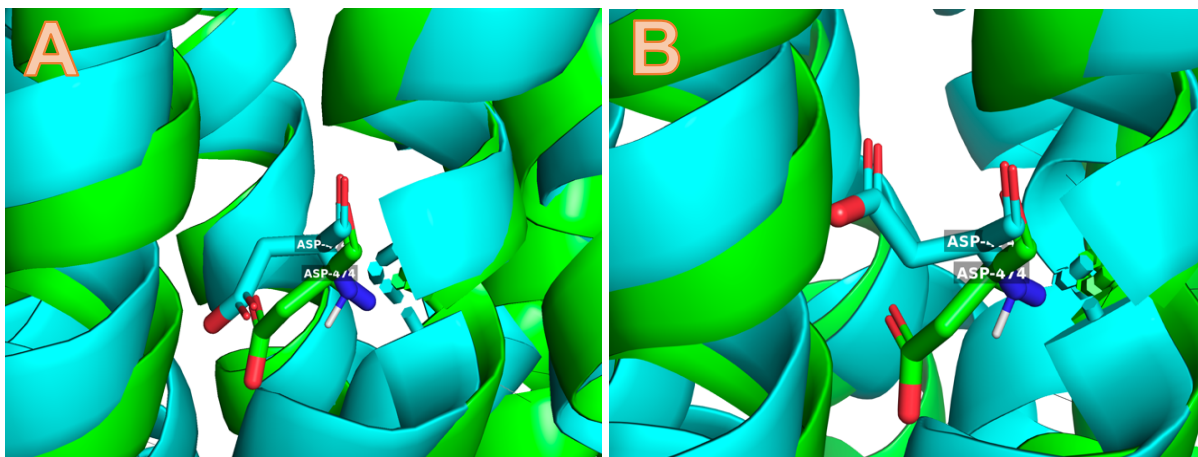


Figure 38: Detailed insight into the alignment of the hOCT1 protein structure from AlphaFold DB (UniProt ID: O15245) with our homology model using PyMol. A) Difference in the orientation of Asp474 from the AlphaFold DB model (green) and our native homology model (light blue). B) Difference in the orientation of Asp474 from the AlphaFold model (green) and our homology model with new rotamers (light blue).

```

Match: assigning 554 x 456 pairwise scores.
MatchAlign: aligning residues (554 vs 456)...
MatchAlign: score 2314.500
ExecutiveAlign: 456 atoms aligned.
ExecutiveRMS: 29 atoms rejected during cycle 1 (RMSD=6.61).
ExecutiveRMS: 24 atoms rejected during cycle 2 (RMSD=4.45).
ExecutiveRMS: 16 atoms rejected during cycle 3 (RMSD=3.59).
ExecutiveRMS: 2 atoms rejected during cycle 4 (RMSD=3.22).
ExecutiveRMS: 1 atoms rejected during cycle 5 (RMSD=3.19).
Executive: RMSD = 3.176 (384 to 384 atoms)

```

Table 11: Structural alignment with PyMol. Our native homology model was aligned to the protein structure model of human OCT1 from AlphaFold DB (UniProt ID: O15245) using the “align” command in PyMol. The RMSD (Root Mean Square Deviation) of the aligned atoms after outlier rejection is reported.

3.2.5 Molecular Docking of fenoterol into hOCT1 from AlphaFold DB using AutoDock Vina

After the investigation of the two protein models, we took advantage of the high-accuracy protein structure model of hOCT1 from AlphaFold DB for further analyses. Since its active site is predicted with very high confidence (Fig. 37 A, dark blue region) we believe that based on the per-residue confidence metric this predicted model will provide reasonable results during the next round of molecular docking using AutoDock Vina. Additionally, we increased the number of possible binding modes from ten to twenty as we do not want to miss any conformation showing the essential interaction with Asp474.

Out of twenty binding poses the two best ranked conformations have an affinity of -7.8 kcal/mol (Table 12). The conformation of the first pose is directed with its two phenol rings to the intracellular region in a U-shape, whereas the positively charged nitrogen is oriented towards the extracellular region of TMH2 (Fig. 39). This pose is stabilized by two conventional H-bonds formed by two glutamine residues. The hydroxy group of the phenol ring in the back is forming two intermolecular interactions, one H-bond is formed with the side chain of Gln241 (TMH5) and the other one is formed with the side chain of Gln447 (TMH10). Additionally, this conformation is stabilized again by a network of pi-pi interactions. Starting with the phenol ring in the back being stabilized by Phe244 through pi-pi interactions (3.8 Å). The positively charged nitrogen is forming pi-pi interactions with Phe32 (3.7 Å), Phe159 (5.0 Å), and Trp217 (5.5 Å). The second phenol ring is stabilized by cation-pi interactions of Lys214 (4.8 Å) and pi-pi interactions of Trp217 (3.9 Å) and Trp354 (3.9 Å).

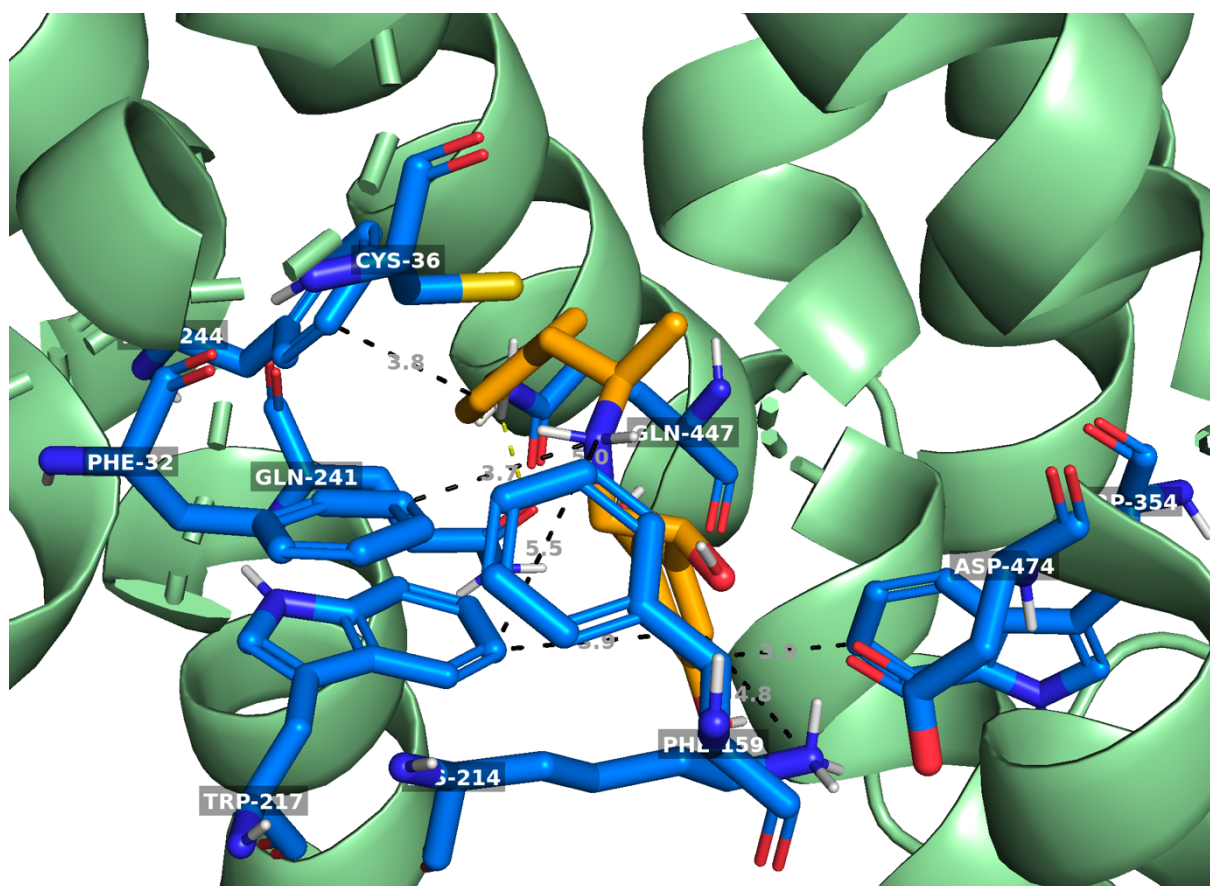


Figure 39: Molecular docking of fenoterol into hOCT1 from AlphaFold DB using AutoDock Vina. Shown is here the best ranked binding pose of fenoterol (orange) in hOCT1 (green) regarding the binding affinity out of 20 conformations. Polar interactions are shown by yellow dashed lines. The distance of amino acids in close proximity are shown by black dashed lines with its respective value in grey. Pi-Pi interactions are displayed by orange dashed lines. Heteroatoms are color-coded as well: red – oxygen, blue – nitrogen, yellow – sulfur.

As earlier stated, the second best pose has the same performance in terms of affinity (Table 12). However, the conformation is much more linearized compared to the previous pose (Fig. 40). The functional groups are in the same region, just stretched over the whole active site. These results following RMSD values: u.b. 4.571 Å and l.b. 2.969 Å. Also, the same OH-group as before forms two intermolecular H-bonds. Since the phenol group containing this hydroxy group is more shifted to TMH8, it is stabilized by Glu386 serving as an HBD. The second H-bond is formed by Thr245, which is in the TMH5 right next to TMH8. On the opposite side, the phenyl group containing two hydroxy groups is stabilized by a conventional H-bond of Asn156. Other than that, the distances of pi-pi or cation-pi interactions are increased, ranging now from 5 to 8 Å.

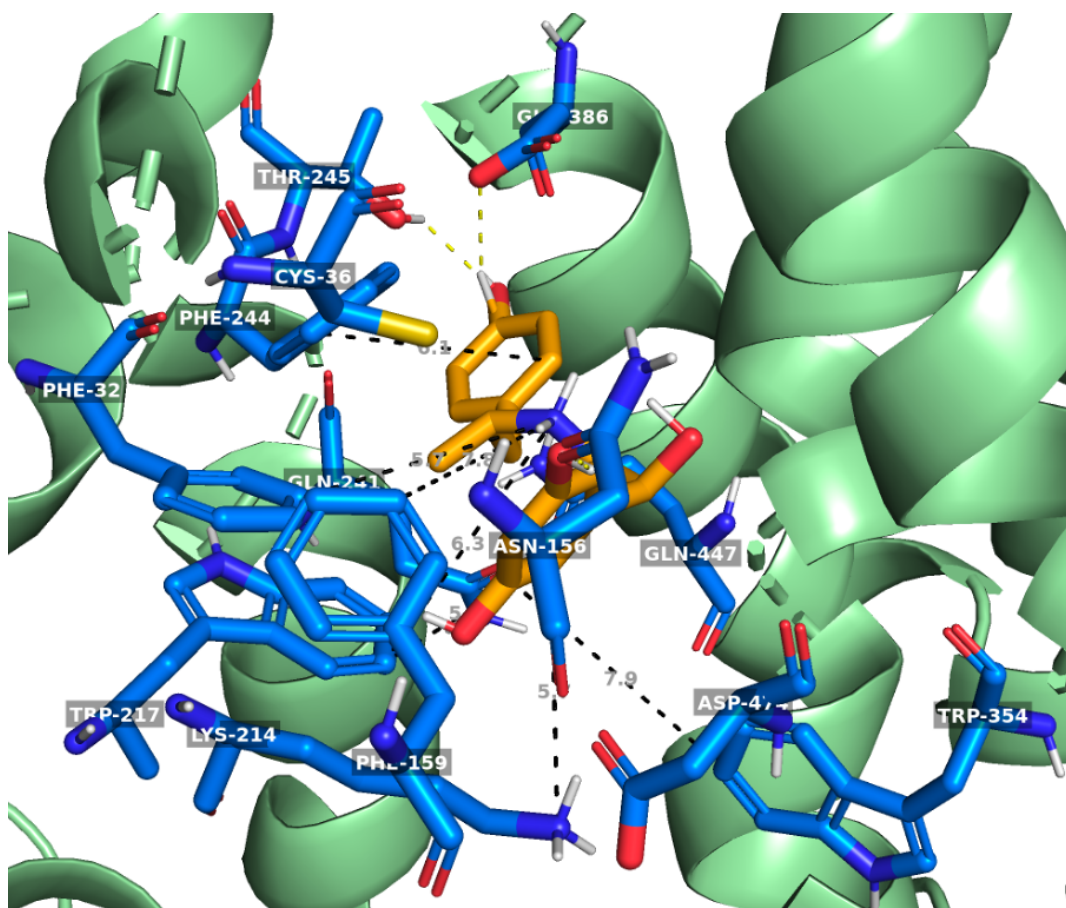


Figure 40: Molecular docking of fenoterol into hOCT1 from AlphaFold DB using AutoDock Vina. Shown is here the second best ranked binding pose of fenoterol (orange) in hOCT1 (green) regarding the binding affinity out of 20 conformations. Polar interactions are shown by yellow dashed lines. The distance of amino acids in close proximity are shown by black dashed lines with its respective value in grey. Pi-Pi interactions are displayed by orange dashed lines. Heteroatoms are color-coded as well: red – oxygen, blue – nitrogen, yellow – sulfur.

The next binding pose was chosen based on the interaction formed with Asp474. The fifteenth ranked conformation has an affinity of -7.2 kcal/mol (Table 12). As the second best ranked pose this conformation is also in a linearized shape bound in the active site (Fig. 41). This explains similar RMSD values such as: u.b. 4.671 Å and l.b. 2.840 Å. The main stabilizing effects derive from the phenol ring containing two hydroxy groups. One of them is interacting with the side chain Asn156 (TMH2) as an HBD, whereas the other OH-group forms two H-bonds with Lys214 (TMH4) and Asp474 (TMH11). The same phenol ring can be stabilized through a T-shaped pi-pi interaction by Phe159 (3.8 Å). The other aromatic ring can also be stabilized through a parallel displaced pi-pi interaction by Phe244 (4.3 Å). The positively charged nitrogen seems to be stabilized by Phe244 (4.2 Å), Phe32 (5.1 Å), and Trp217 (5.2 Å). Other amino residues are too far away to form any stabilizing effects.

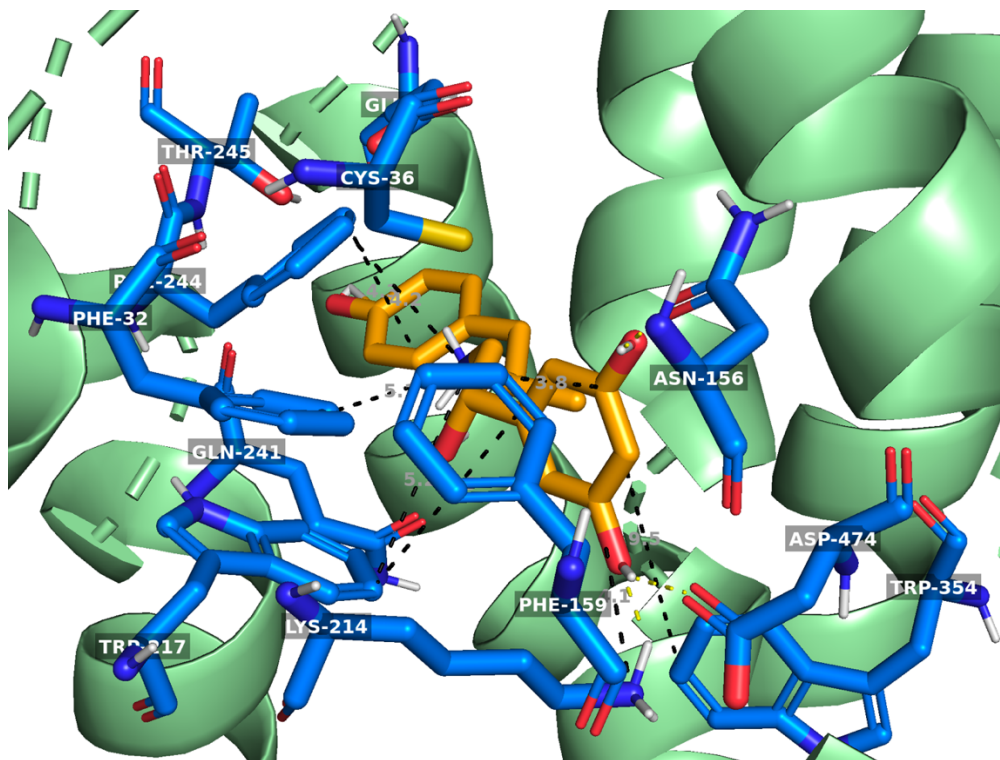


Figure 41: Molecular docking of fenoterol into hOCT1 from AlphaFold DB using AutoDock Vina. Shown is here the fifteenth best ranked binding pose of fenoterol (orange) in hOCT1 (green) regarding the binding affinity out of 20 conformations. Polar interactions are shown by yellow dashed lines. The distance of amino acids in close proximity are shown by black dashed lines with its respective value in grey. Pi-Pi interactions are displayed by orange dashed lines. Heteroatoms are color-coded as well: red – oxygen, blue – nitrogen, yellow – sulfur.

mode	affinity (kcal/mol)	dist from best mode	
		rmsd l.b.	rmsd u.b.
1	-7.8	0.000	0.000
2	-7.8	2.969	4.571
3	-7.7	0.062	2.017
4	-7.7	1.659	2.671
5	-7.7	1.705	2.973
6	-7.7	2.979	4.703
7	-7.6	2.151	3.654
8	-7.6	2.534	4.286
9	-7.5	2.036	3.241
10	-7.5	2.541	4.579
11	-7.5	2.731	3.633
12	-7.4	2.672	6.699
13	-7.3	2.180	4.338
14	-7.2	2.075	2.883
15	-7.2	2.840	4.671
16	-7.2	2.864	6.947
17	-7.2	2.212	4.580
18	-7.0	3.084	6.051
19	-7.0	1.745	4.838
20	-6.9	1.677	5.512

Table 12: Binding affinities and RMSD values of fenoterol in hOCT1 from AlphaFold DB analyzed by AutoDock Vina. Root mean square deviation (RMSD) values measuring the average between atoms of a position relative to the best fitting position, are calculated using only movable heavy atoms. Two variants of RMSD metrics are provided, rmsd l.b. (RMSD lower bound) and rmsd u.b. (RMSD upper bound). They differ in how the atoms are matched in the distance calculation; rmsd u.b. matches each atom in one conformation with itself in the other conformation, ignoring any symmetry; rmsd l.b. matches each atom in one conformation with the closest atom of the same element type in the other conformation.

3.2.6 Molecular Docking of trospium into hOCT1 from AlphaFold DB

Next, we performed molecular docking of trospium in the same manner as it was performed for fenoterol. Unfortunately, none of the twenty poses showed any intermolecular interaction within the active side. The three best docked conformations have all in common that the nitrogenous bicyclic ring is near the TMH5 in the back, whereas the two benzyl rings are at the opposite side of the binding cavity close to TMH11. Minor differences occur in the flipping direction of the two aromatic rings among the three conformations. Stabilizing effects are provided mainly by cation-pi interactions between Phe244 and the positively charged nitrogen and between the side chain of Lys214 and one of the aromatic rings. Distances vary from 3.6 Å up to 4.6 Å (Fig. 42 A, B, and C). The binding affinity of the best ranked pose is -8.9 kcal/mol, of the second best ranked pose is -8.1 kcal/mol and of the third best ranked pose is -7.7 kcal/mol (Table 13).

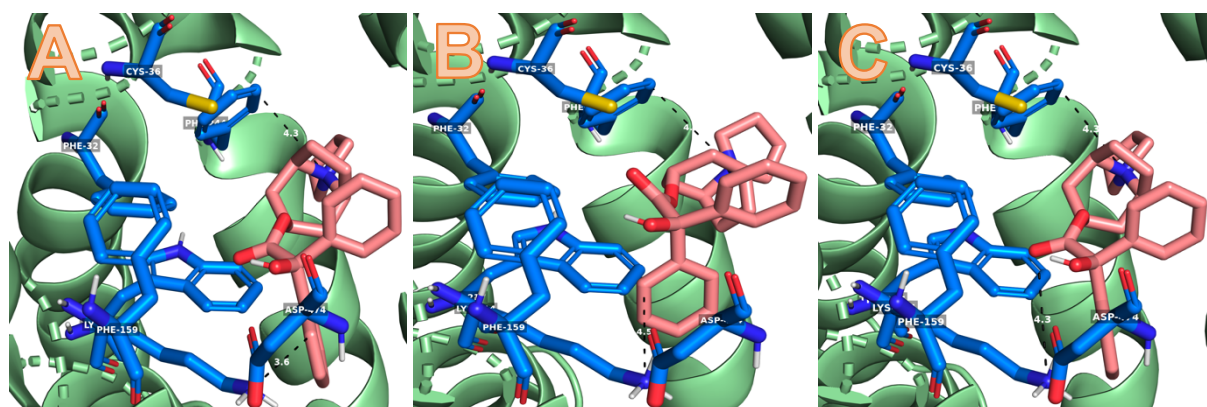


Figure 42: Molecular docking of trospium into hOCT1 from AlphaFold DB using AutoDock Vina. Shown are here the three best ranked binding poses of trospium (salmon) in hOCT1 (green) regarding the binding affinity out of 20 conformations. Polar interactions are shown by yellow dashed lines. The distance of amino acids in close proximity are shown by black dashed lines with its respective value in grey. Pi-Pi interactions are displayed by orange dashed lines. Heteroatoms are color-coded as well: red – oxygen, blue – nitrogen, yellow – sulfur.

mode	affinity (kcal/mol)	dist from best mode	
		rmsd l.b.	rmsd u.b.
1	-8.9	0.000	0.000
2	-8.1	1.258	2.112
3	-7.7	1.598	3.660
4	-7.7	1.798	4.226
5	-7.6	1.718	3.007
6	-7.5	1.948	6.101
7	-7.5	1.443	2.271
8	-7.4	1.365	3.562
9	-7.4	11.437	13.562
10	-7.3	1.496	2.756
11	-7.3	1.658	2.974
12	-7.3	10.971	13.420
13	-7.3	1.590	4.044
14	-7.3	0.984	1.870
15	-7.2	11.923	13.932
16	-7.2	1.675	3.797
17	-7.2	11.118	13.800
18	-7.1	10.740	13.789
19	-7.0	11.614	13.805
20	-7.0	11.186	13.334

Table 13: Binding affinities and RMSD values of fenoterol in hOCT1 from AlphaFold DB analyzed by AutoDock Vina. Root mean square deviation (RMSD) values measuring the average between atoms of a position relative to the best fitting position, are calculated using only movable heavy atoms. Two variants of RMSD metrics are provided, rmsd l.b. (RMSD lower bound) and rmsd u.b. (RMSD upper bound). They differ in how the atoms are matched in the distance calculation; rmsd u.b. matches each atom in one conformation with itself in the other conformation, ignoring any symmetry; rmsd l.b. matches each atom in one conformation with the closest atom of the same element type in the other conformation.

3.2.7 Flexible Docking of fenoterol into hOCT1 from AlphaFold DB using AutoDock Vina

Molecular docking of both ligands with the encouraging human OCT1 protein structure of AlphaFold DB didn't provide the interaction regarding Asp474. Since the protein was kept rigid in all performed docking approaches using AutoDock Vina, a new strategy using flexible docking was applied. Therefore, amino residues in close proximity of fenoterol, which showed increased interactions in previous results were kept flexible to investigate their orientation based on the ligands binding and conformation.

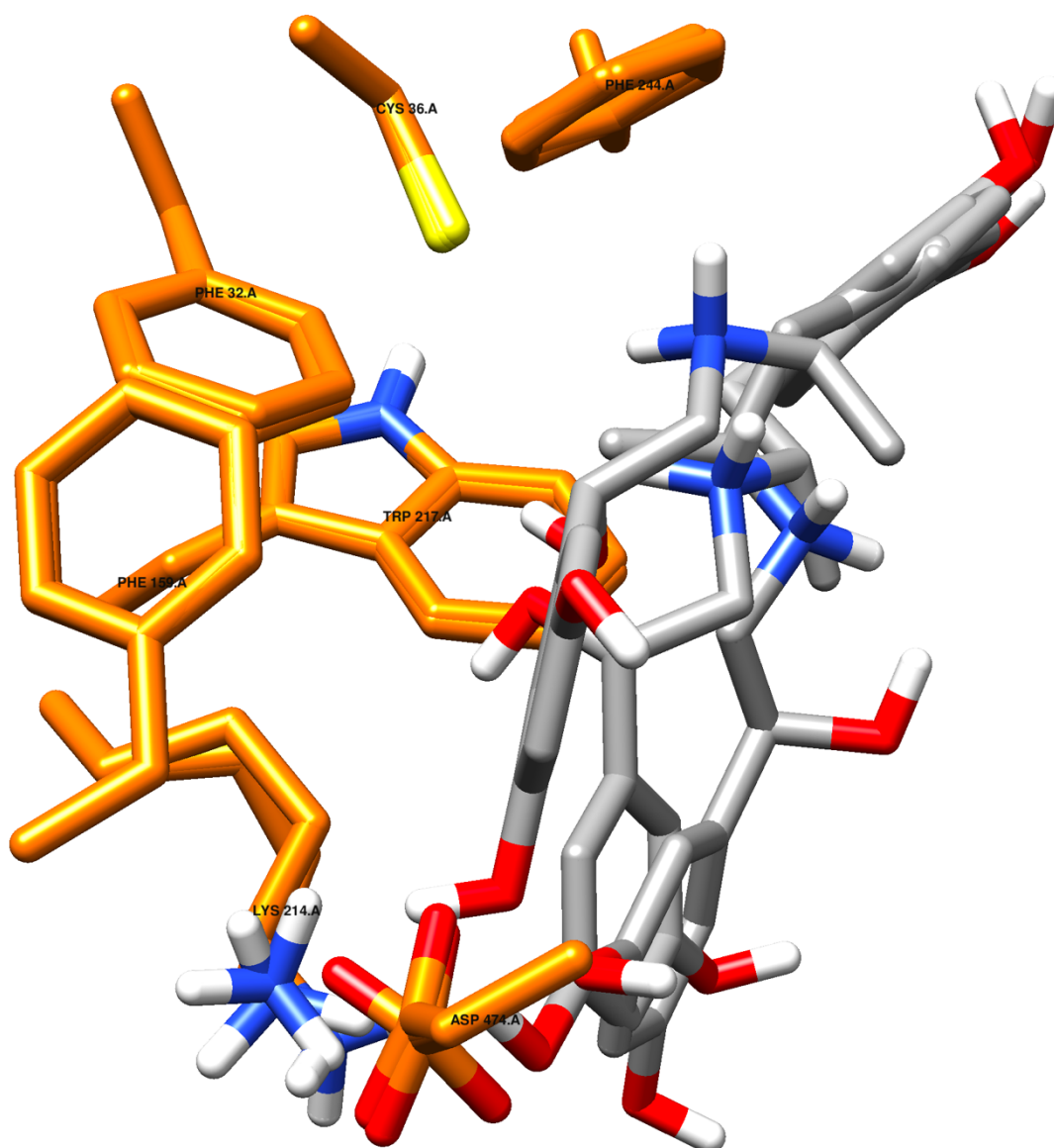


Figure 43: Overview of the three best ranked conformations during flexible docking of fenoterol (grey) in hOCT1 using AutoDock Vina. Following amino residues (orange) orientation are shown: Phe32, Cys36, Phe159, Lys214, Phe244, Asp474. The protein structure is hidden, seen are only the amino acids and the ligand, which are overlaid.

Following amino acids were kept flexible during docking: Phe32, Cys36, Phe159, Lys214, Trp217, Phe244, and Asp474. These residues are in TMH1, TMH2, TMH4, TMH5, and TMH11 and the remaining residues of the protein are kept rigid for molecular docking. Flexible docking was performed in a similar manner using AutoDock Vina. Out of 20 poses the three best ranked conformations were analyzed based on their binding affinity and interactions. At the beginning, flexible residues were visualized regarding their orientations during the docking approaches using Chimera. Thus, rigid parts of the protein were hidden, whereas the molecular structure of fenoterol and flexible residues were displayed and overlaid (Fig. 43). Beginning with the ligand, even though the binding affinity differ only 0.3 kcal/mol from the best ranked (-8.5 kcal/mol) to the third best (-8.2 kcal/mol) ranked conformation, the structures do not overlay perfectly. Nevertheless, their structural orientation is similar with the phenol ring having two hydroxy group directed to Lys214, and Asp474, the linker part with the positively charged nitrogen is more embedded in the middle of the active site, whereas the other phenol ring is anchored in the back. The behavior of the involved flexible amino acids differs from residue to residue. Phe32, Cys36, Phe159, and Phe244 almost didn't change their orientation during docking, as all three structures are perfectly overlaid. For Lys214 and Asp474 the side chain changed its orientation based on the ligands position in the active site to form an interaction.

The best ranked binding pose is stabilized by four different types of interactions. The hydroxy groups at the two phenol rings of fenoterol form a conventional H-bond with Glu386 (TMH8) and Asp474 (TMH11). The phenol group anchored close to TMH8 is stabilized by a pi-pi stacked interaction with Phe244. Cys473 is forming a pi-alkyl interaction with the other phenol ring. The same phenol ring is also stabilized by van der Waals forces from Lys214. Additionally, fenoterol is stabilized by intramolecular van der Waals forces, which is formed by the hydrogen of the positively charged nitrogen and the hydroxy group in the linker part (Fig. 44, Supp. Fig. 2).

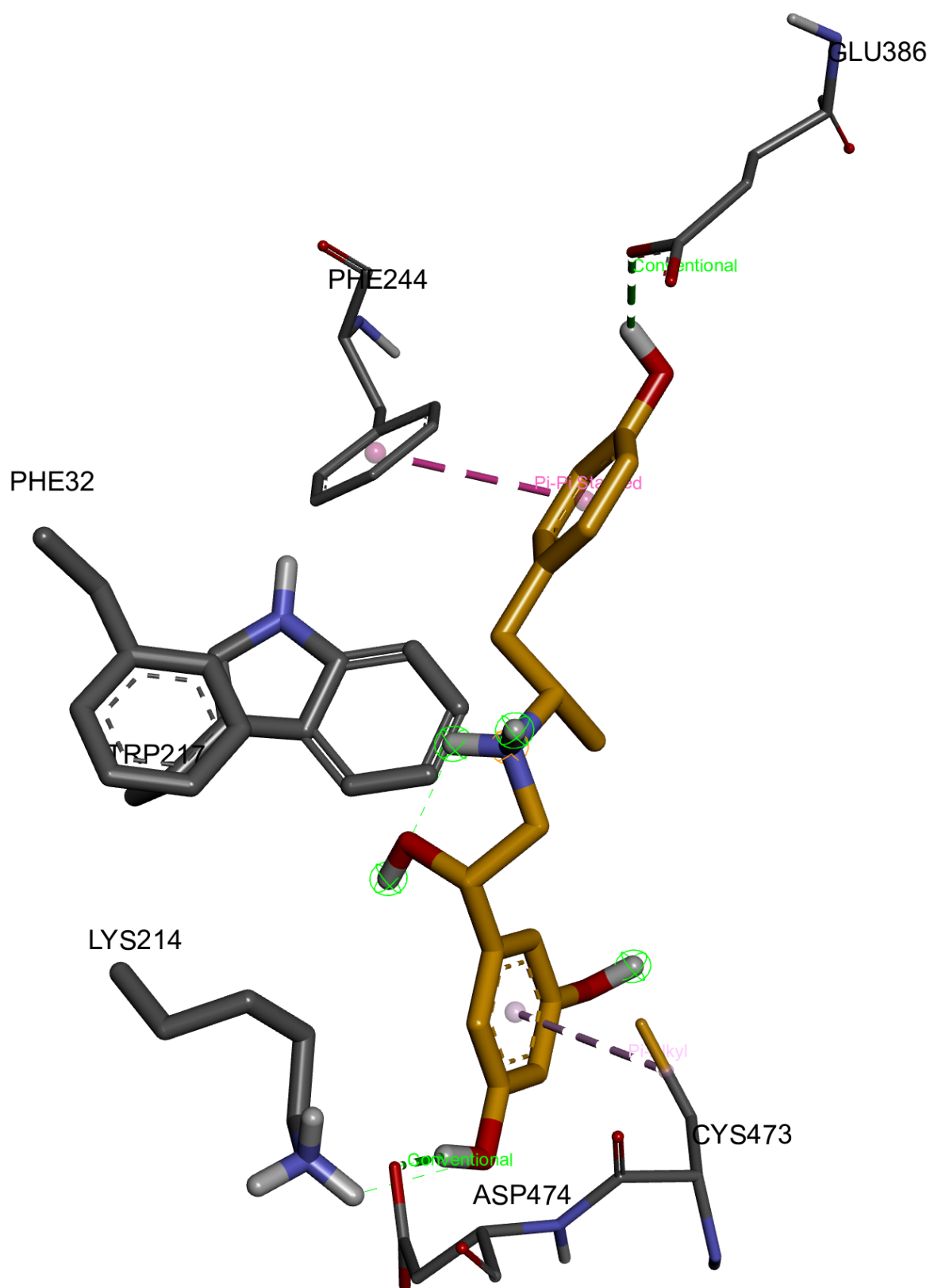


Figure 44: Flexible docking of fenoterol into hOCT1 from AlphaFold DB using AutoDock Vina. Shown is here the best ranked binding pose of fenoterol (orange) in hOCT1 out of 20 conformations regarding the binding affinity with its interacting amino residues (grey) in 3D. Following interactions are color-coded: Conventional H-bonds – green bold lines, van der Waals forces – thin green lines, Pi-Alkyl – pink, Donor-Donor – red, Pi-Pi Stacked – purple, Pi-Donor; Pi-Sulfur – mint green, Pi-Sulfur – yellow, Pi-Cation – orange. Heteroatoms are color-coded as well: red – oxygen, blue – nitrogen, yellow – sulfur.

The second best ranked binding pose has an affinity of -8.4 kcal/mol (Table 14) and has following RMSD values: u.b. 2.088 Å and l.b. 1.392 Å. Fenoterol is stabilized by seven different types of interactions (Fig. 45, Supp. Fig. 3). The phenol ring close to TMH8 is again stabilized by conventional H-bonds from Glu386, as well as pi-pi stacked interactions by Phe244. The latter is forming a pi-cation interaction with the positively charged nitrogen, stabilizing the structure. The remaining interactions are formed with the second phenol ring such as a pi-sulfur interaction with Cys36, a pi-pi T-shaped interaction with Phe159, a pi-sulfur interaction with Cys473, and van der Waals forces with Lys214 and Asp474.

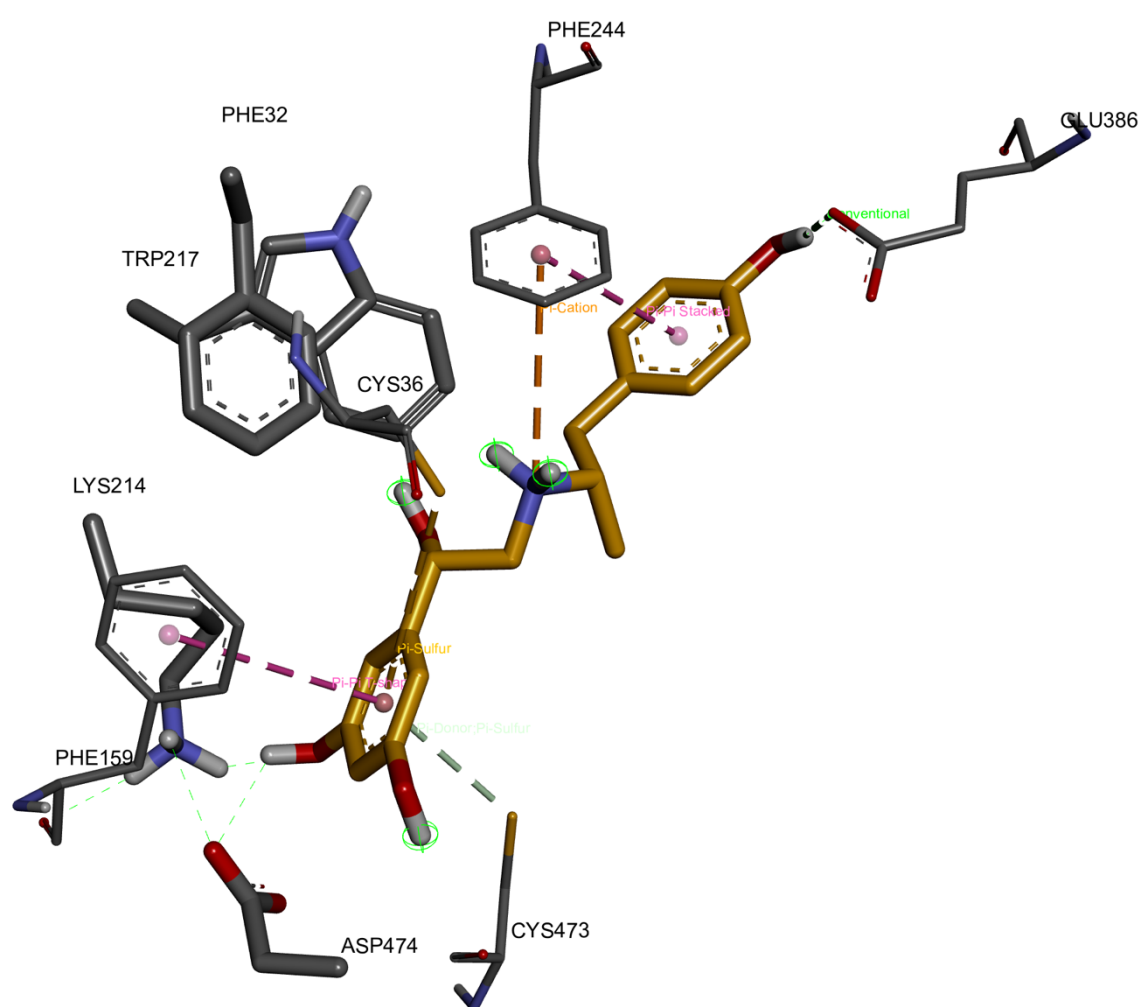


Figure 45: Flexible docking of fenoterol into hOCT1 from AlphaFold DB using AutoDock Vina. Shown is here the second best ranked binding pose of fenoterol (orange) in hOCT1 out of 20 conformations regarding the binding affinity with its interacting amino residues (grey). Following interactions are color-coded: Conventional H-bonds – green bold lines, van der Waals forces – thin green lines, Pi-Alkyl – pink, Donor-Donor – red, Pi-Pi Stacked – purple, Pi-Donor; Pi-Sulfur – mint green, Pi-Sulfur – yellow, Pi-Cation – orange. Heteroatoms are color-coded as well: red – oxygen, blue – nitrogen, yellow – sulfur.

The third best ranked binding conformation has an affinity of -8.2 kcal/mol (Table 14) and has following RMSD values: u.b. 1.779 Å and l.b. 0.941 Å providing a more similar orientation to the first binding pose. Its stabilizing effects are derived from five different types of interactions (Fig 46, Supp. Fig. 4). This time the phenol ring anchored in the back is stabilized by an intermolecular conventional H-bond from Gln447 located in the TMH10. Also, the same phenol ring is again stabilized by pi-pi stacked interactions from Phe244. The linker part is stabilizing itself by intramolecular donor-donor interaction between the hydroxy group and the hydrogen on the positively charged nitrogen. The second phenol ring is stabilized by following interactions: pi-alkyl (Cys473), intermolecular H-bond (Ser470), and van der Waals forces (Lys214).

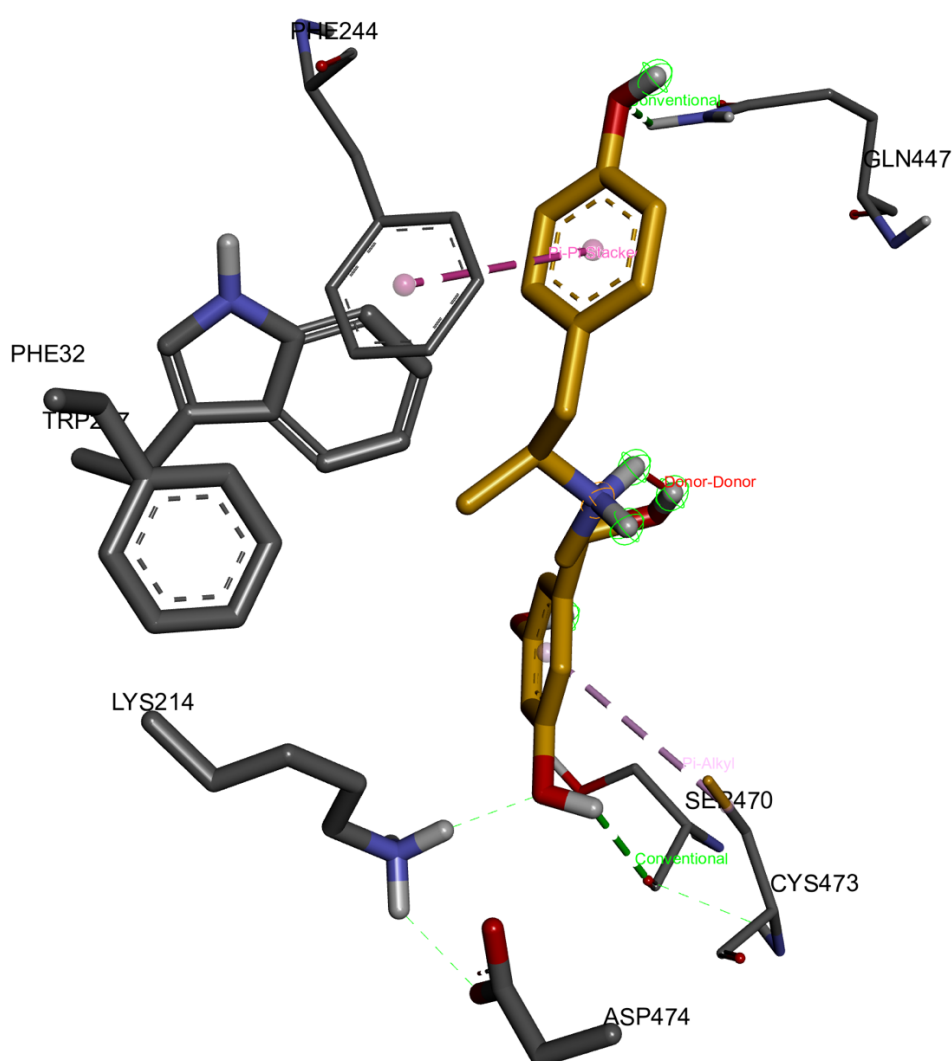


Figure 46: Flexible docking of fenoterol into hOCT1 from AlphaFold DB using AutoDock Vina. Shown is here the third best ranked binding pose of fenoterol (orange) in hOCT1 out of 20 conformations regarding the binding affinity with its interacting amino residues (grey). Following interactions are color-coded: Conventional H-bonds – green bold lines, van der Waals forces – thin green lines, Pi-Alkyl – pink, Donor-Donor – red, Pi-Pi Stacked – purple, Pi-Donor; Pi-Sulfur – mint green, Pi-Sulfur – yellow, Pi-Cation – orange. Heteroatoms are color-coded as well: red – oxygen, blue – nitrogen, yellow – sulfur.

mode	affinity (kcal/mol)	dist from best mode	
		rmsd l.b.	rmsd u.b.
1	-8.5	0.000	0.000
2	-8.4	1.392	2.088
3	-8.2	0.941	1.779
4	-8.0	1.408	2.501
5	-8.0	1.555	2.512
6	-7.7	1.247	5.439
7	-7.7	1.692	5.181
8	-7.6	1.404	2.356
9	-7.5	1.170	5.021
10	-7.1	1.670	2.640
11	-7.1	4.865	8.266
12	-7.1	4.021	7.332
13	-7.0	5.139	8.586
14	-6.9	5.389	8.779
15	-6.8	1.795	3.483
16	-6.8	1.701	4.778
17	-6.7	2.307	4.590
18	-6.7	4.228	7.006
19	-6.7	4.955	7.403
20	-6.7	1.614	5.295

Table 14: Binding affinities and RMSD values of fenoterol in hOCT1 from AlphaFold DB analyzed by flexible Docking using AutoDock Vina. Root mean square deviation (RMSD) values measuring the average between atoms of a position relative to the best fitting position, are calculated using only movable heavy atoms. Two variants of RMSD metrics are provided, rmsd l.b. (RMSD lower bound) and rmsd u.b. (RMSD upper bound). They differ in how the atoms are matched in the distance calculation; rmsd u.b. matches each atom in one conformation with itself in the other conformation, ignoring any symmetry; rmsd l.b. matches each atom in one conformation with the closest atom of the same element type in the other conformation.

3.2.8 Flexible Docking of fenoterol into mOCT1 from AlphaFold DB using AutoDock Vina

Subsequently, the same flexible docking approach was applied for fenoterol into mOCT1. The best ranked binding pose has an affinity of -9.0 kcal/mol (Table 15). Stabilizing effects are provided by seven different types of interactions (Fig. 47, Supp. Fig. 5). Starting with the phenol ring close to TMH8, Gln242 (TMH5) is forming an intermolecular H-bond, whereas Leu447 (TMH10) is stabilizing the ring with a pi-alkyl interaction. The linker is stabilized by Trp218 (TMH4), such as a pi-cation interaction with the positively charged nitrogen and a pi-sigma interaction with the neighboring methyl group. Tyr36 contributes also to stabilizing effects to the nitrogen by van der Waals forces. The second phenol ring containing two hydroxy groups is involved in following interactions: pi-alkyl and conventional H-bond (Cys451; TMH10), pi-pi T-shaped (Trp355; TMH7), pi-sulfur and conventional H-bond (Met467; TMH11), pi-alkyl (Val219; TMH4), carbon H-bond and conventional H-bond (Lys215, TMH4).

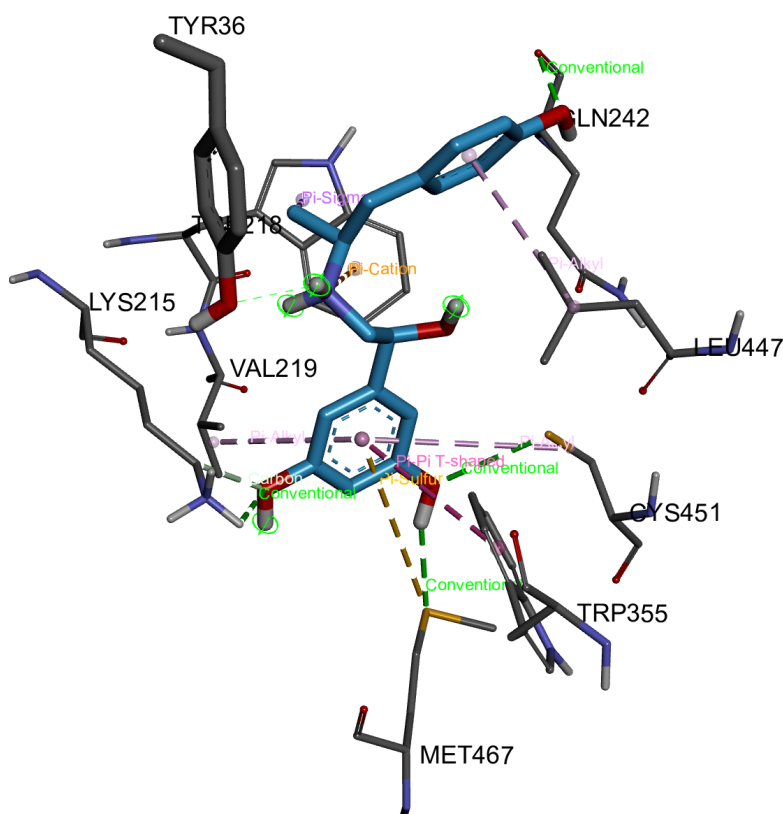


Figure 47: Flexible docking of fenoterol into mOCT1 from AlphaFold DB using AutoDock Vina. Shown is here the best ranked binding pose of fenoterol (blue) in hOCT1 out of 20 conformations regarding the binding affinity with its interacting amino residues (grey). Following interactions are color-coded: Conventional H-bonds – green bold lines, van der Waals forces – thin green lines, Pi-Alkyl – pink, Donor-Donor – red, Pi-Pi Stacked – purple, Pi-Donor; Pi-Sulfur – mint green, Pi-Sulfur – yellow, Pi-Cation – orange. Heteroatoms are color-coded as well: red – oxygen, blue – nitrogen, yellow – sulfur.

The second best ranked binding pose has also an affinity of -9.0 kcal/mol (Table 15). Its RMSD values are as following: u.b. 1.168 Å and l.b. 0.265 Å. The phenol ring with one hydroxy group is stabilized by pi-pi T-shaped (Tyr362; TMH7) and pi-sigma (Leu447; TMH10) interactions. Trp218 (TMH4) is forming three different interactions with three different parts of the ligand. Firstly, it is forming a pi-sigma interaction with the methyl in the linker part and secondly a pi-cation interaction with the positively charged nitrogen. Lastly, it provides stabilizing effects to the second phenol ring through pi-pi stacked interactions. Additional reactions formed for the same phenol ring are pi-sulfur and van der Waals forces (Cys451; TMH10), pi-pi T-shaped (Trp355; TMH7), pi-sulfur (Met467; TMH11), conventional H-bond (Ser471; TMH11), and carbon H-bond (Lys215; TMH4). Even though Cys451 is involved in so many reactions, Discovery Studio Visualizer indicate an unfavorable bump with the phenol ring (Fig. 48, Suppl. Fig. 6).

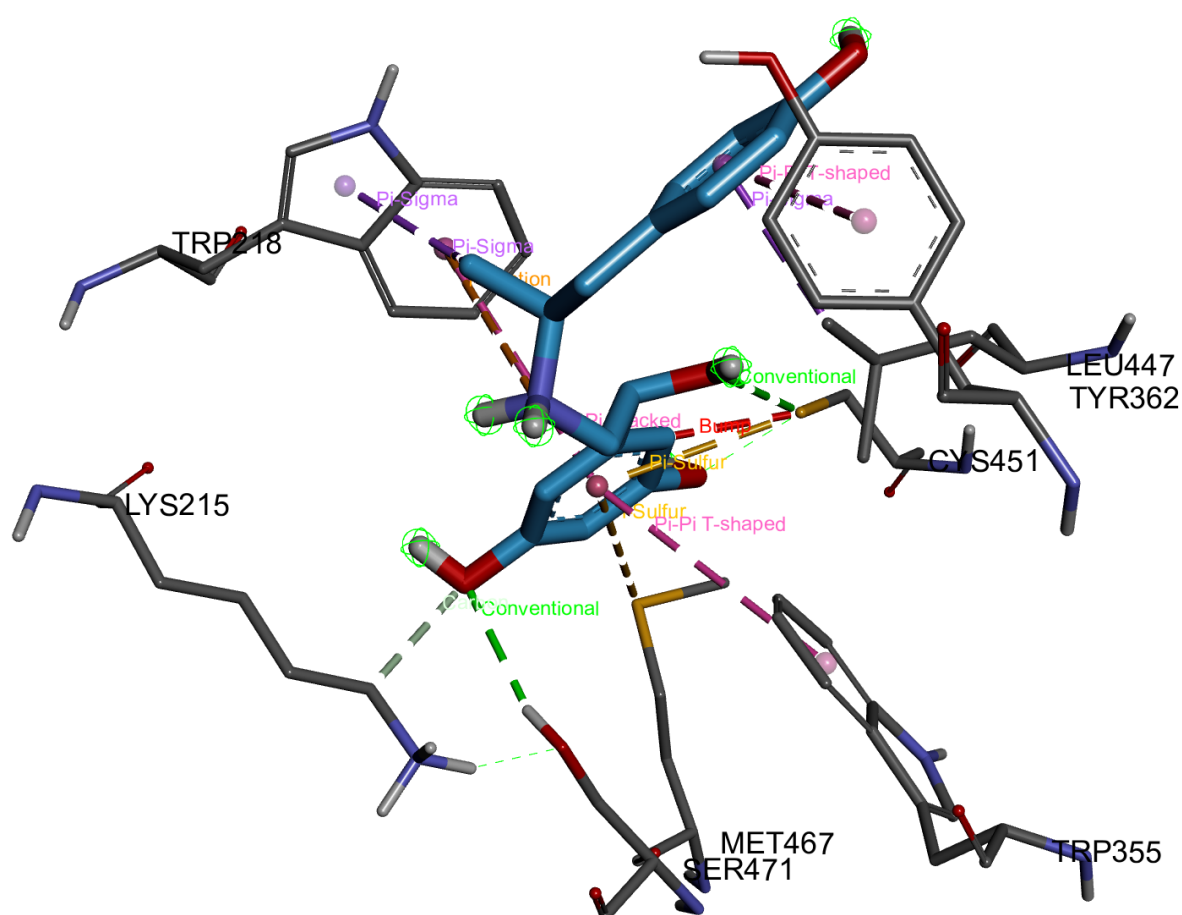


Figure 48: Flexible docking of fenoterol into mOCT1 from AlphaFold DB using AutoDock Vina. Shown is here the second best ranked binding pose of fenoterol (blue) in hOCT1 out of 20 conformations regarding the binding affinity with its interacting amino residues (grey). Following interactions are color-coded: Conventional H-bonds – green bold lines, van der Waals forces – thin green lines, Pi-Alkyl – pink, Donor-Donor – red, Pi-Pi Stacked – purple, Pi-Donor; Pi-Sulfur – mint green, Pi-Sulfur – yellow, Pi-Cation – orange. Heteroatoms are color-coded as well: red – oxygen, blue – nitrogen, yellow – sulfur.

The third best ranked binding pose has an affinity of -8.9 kcal/mol with the following RMSD values: u.b. 3.717 Å and l.b. 2.144 Å (Table 15). As previously observed, the phenol ring containing one hydroxy group is stabilized by pi-pi T-shaped (Tyr362; TMH7) and pi-sigma (Leu447; TMH10) interactions. Even though the linker part is left untouched, the second phenol ring is stabilized by several amino acids (Fig. 49, Suppl. Fig. 7). These include Ala359 (pi-alkyl; TMH7), Cys474 (pi-sulfur, TMH11), Gly478 (carbon H-bond, TMH11), ASN157 (conventional H-bond, TMH2), and Gln363 (conventional H-bond, TMH7).

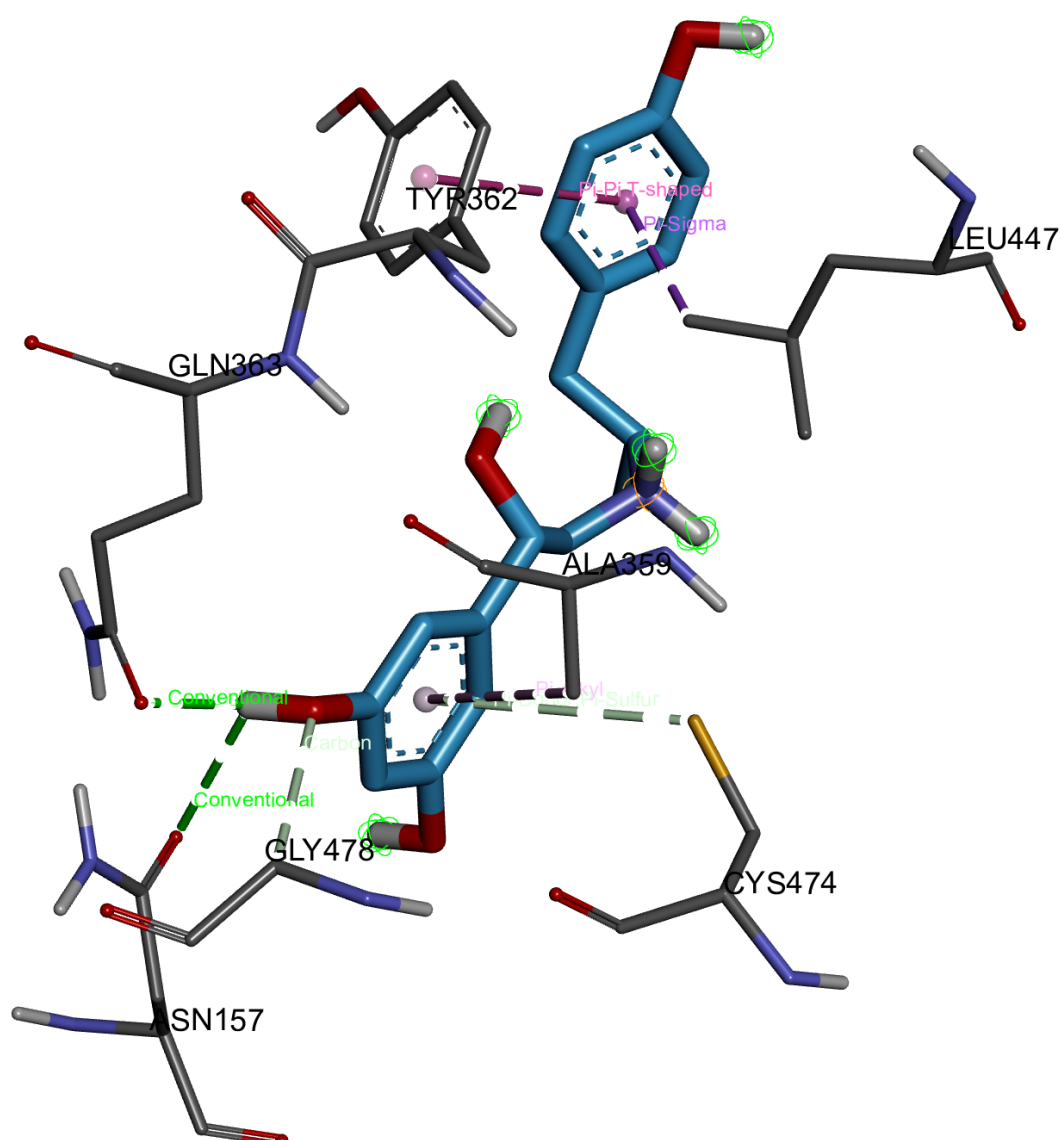


Figure 49: Flexible docking of fenoterol into mOCT1 from AlphaFold DB using AutoDock Vina. Shown is here the third best ranked binding pose of fenoterol (blue) in hOCT1 out of 20 conformations regarding the binding affinity with its interacting amino residues (grey). Following interactions are color-coded: Conventional H-bonds – green bold lines, van der Waals forces – thin green lines, Pi-Alkyl – pink, Donor-Donor – red, Pi-Pi Stacked – purple, Pi-Donor; Pi-Sulfur – mint green, Pi-Sulfur – yellow, Pi-Cation – orange. Heteroatoms are color-coded as well: red – oxygen, blue – nitrogen, yellow – sulfur.

mode	affinity (kcal/mol)	dist from best mode	
		rmsd l.b.	rmsd u.b.
1	-9.0	0.000	0.000
2	-9.0	0.265	1.168
3	-8.9	2.144	3.717
4	-8.8	1.868	3.462
5	-8.8	0.990	4.591
6	-8.8	1.956	3.589
7	-8.5	2.225	3.416
8	-8.5	1.740	3.421
9	-8.4	1.763	2.801
10	-8.3	1.254	1.913
11	-8.3	1.685	2.965
12	-8.2	1.317	4.386
13	-8.1	1.237	2.354
14	-8.0	1.785	3.411
15	-8.0	1.952	5.488
16	-7.9	1.822	3.518
17	-7.8	1.656	4.179
18	-7.8	1.948	4.455
19	-7.6	1.560	3.108
20	-7.5	1.866	4.012

Table 15: Binding affinities and RMSD values of fenoterol in hOCT1 from AlphaFold DB analyzed by flexible Docking using AutoDock Vina. Root mean square deviation (RMSD) values measuring the average between atoms of a position relative to the best fitting position, are calculated using only movable heavy atoms. Two variants of RMSD metrics are provided, rmsd l.b. (RMSD lower bound) and rmsd u.b. (RMSD upper bound). They differ in how the atoms are matched in the distance calculation; rmsd u.b. matches each atom in one conformation with itself in the other conformation, ignoring any symmetry; rmsd l.b. matches each atom in one conformation with the closest atom of the same element type in the other conformation.

As in the previous docking approach, the flexible amino residues were overlaid to investigate their directions based on the ligand's conformation (Fig. 50). For residues such as Phe245, Trp218, and Asp475 the positions are almost identical. The remaining amino acids Leu32, Tyr36, Phe160, and Lys215 provide minor differences in their orientation.

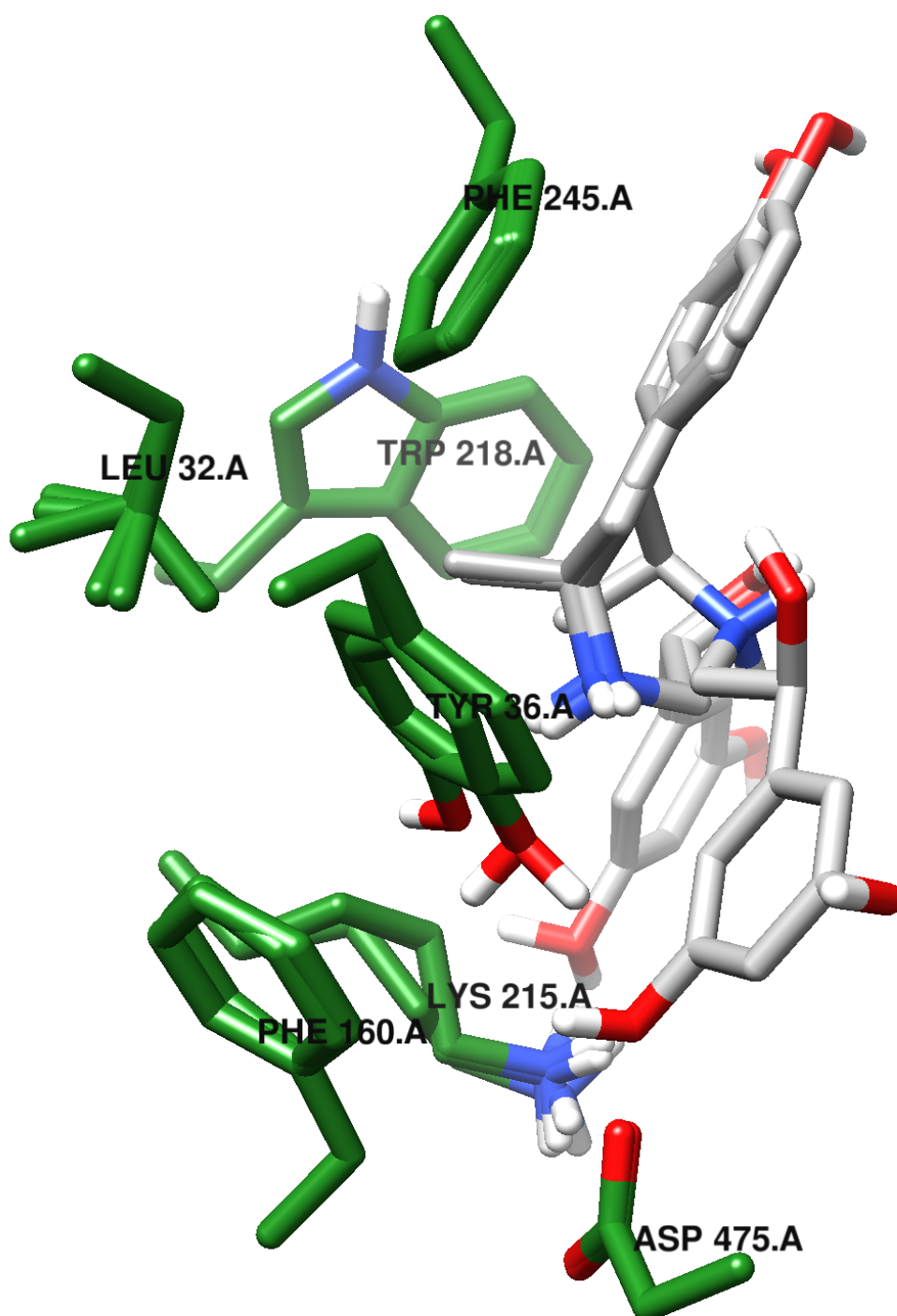


Figure 50: Overview of the three best ranked conformations during flexible docking of fenoterol (grey) in mOCT1 (green) using AutoDock Vina. Following amino residues orientation are shown: Phe32, Cys36, Phe159, Lys214, Phe244, Asp474. The protein structure is hidden, seen are only the amino acids and the ligand, which are overlaid.

3.2.9 Rotamer Docking of fenoterol into hOCT1 from AlphaFold DB using AutoDock Vina

As already performed in the previous docking approach for our own generated homology model, rotamer docking was done as the next step with hOCT1 structure from AlphaFold DB. Compared to previous process Lys214 was not changed, only the essential residue aspartate at codon 474 was reoriented. Therefore, the initial second pose with an occurrence rate of 20.2 % was changed to the first pose represented by an occurrence rate of 57.8% out of seven possible conformations. The first orientation shows only one small green disk indicating no atoms are in contact, whereas the new rotamer has three green disks, pointing towards atoms being almost in contact or slightly overlap (Fig. 51). Since no red disks are depicted, both orientations lack significant van der Waals overlap. This rotamer approach was performed for fenoterol and tropium with the hOCT1 protein structure from AlphaFold DB, to investigate differences in the interaction.

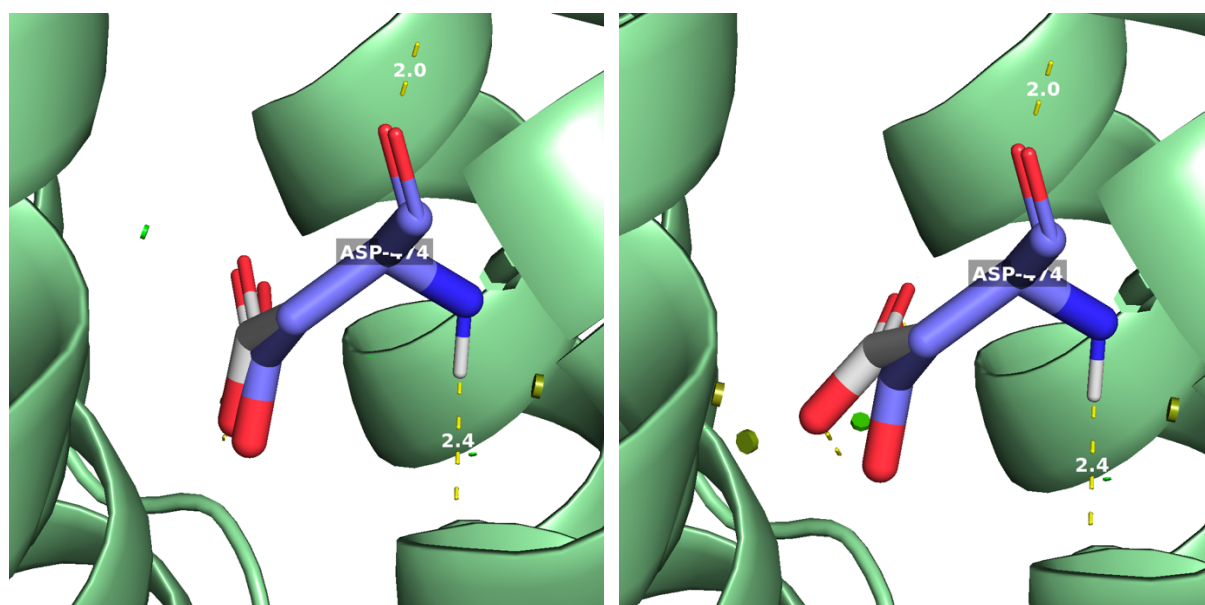


Figure 51: New orientation (rotamer) of Asp474 in hOCT1. The old side chain of Asp474 (blue) has been rotated more towards the active side. The new rotamer is represented in grey. The visible disks indicate pairwise overlap of van der Waals radii. Small green disks are shown when atoms are almost in contact or slightly overlapping. Large red discs indicate significant van der Waals overlap. The yellow dashed lines represent polar interactions with its distance.

The three best ranked conformations share the same binding affinity with -7.8 kcal/mol (Table 16). In the first binding pose three intermolecular H-bonds were observed. They are mainly formed with the hydroxy group of the phenol ring with one substituent. The reacting partners are Gln241 (TMH5) and Gln447 (TMH10). Since the ligand is docked into the active site in a U-shape, one of the two hydroxy group of the second phenol ring is forming an intermolecular H-bond with Gln241. Since both residues, Phe32 (3.7 Å) and Phe159 (5.0 Å) are close to the positively charged nitrogen cation- π interactions could have stabilizing effects to fenoterol. Additionally, the same type of interactions can be formed by Lys214 (4.8 Å) with the phenol ring having two OH-groups (Fig. 52).

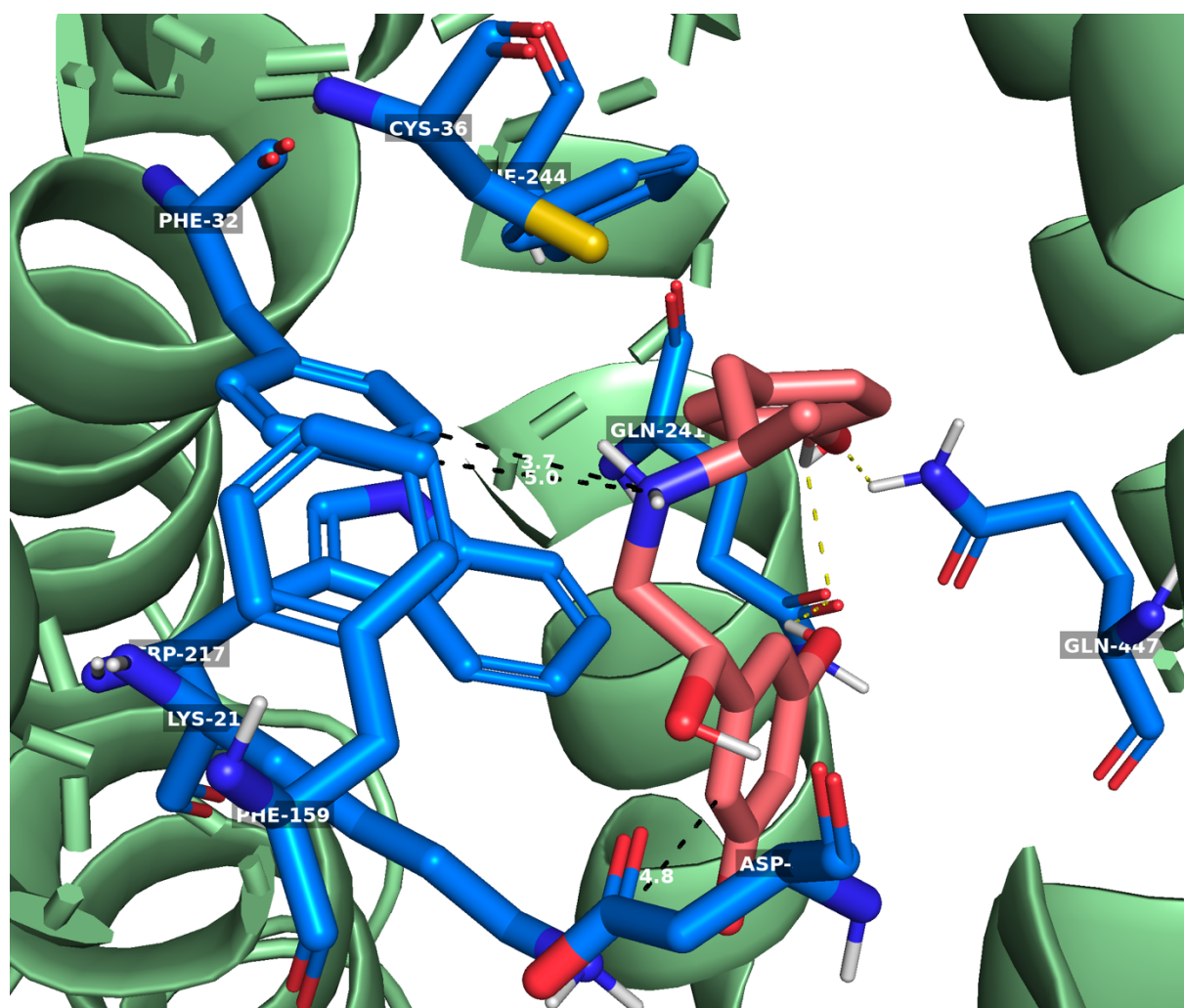


Figure 52: Molecular docking of fenoterol into hOCT1 from AlphaFold DB by AutoDock Vina. Shown is here the best ranked binding pose of fenoterol (salmon) in hOCT1 (green) with the new orientation of Asp474 regarding the binding affinity out of twenty conformations. Polar interactions are shown by yellow dashed lines. The distance of amino acids in close proximity are shown by black dashed lines with its respective value in white. Pi-Pi interactions are displayed by orange dashed lines. Heteroatoms are color-coded as well: red – oxygen, blue – nitrogen, yellow – sulfur.

The second best ranked binding conformation shows the same performance regarding binding affinity with the following RMSD values: 4.585 Å u.b. and 2.975 Å (Table 16). Compared to the first conformation this binding pose is binding in a more linear shape to the active site. This enables the hydroxy group of the one substituted phenol group to form polar interactions with Thr245 (TMH5). The distances of the previous residues have increased ranging from 5.7 Å to 8.0 Å. Nevertheless, pi-pi stacked interactions between Phe159 (TMH2, 3.5 Å) and the second phenol ring can stabilize the ligand (Fig. 53).

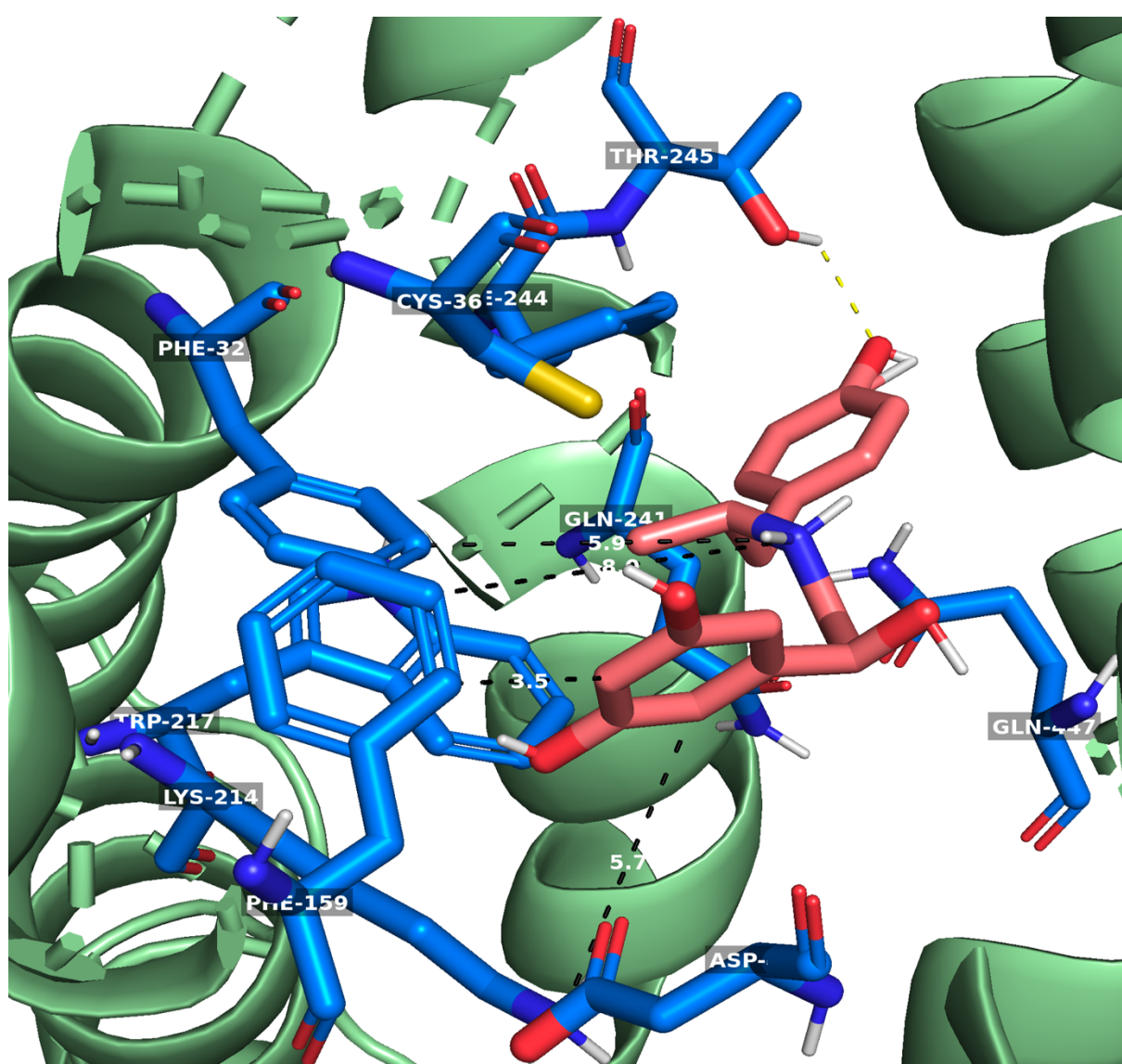


Figure 53: Molecular docking of fenoterol into hOCT1 from AlphaFold DB by AutoDock Vina. Shown is here the second best ranked binding pose of fenoterol (salmon) in hOCT1 (green) with the new orientation of Asp474 regarding the binding affinity out of twenty conformations. Polar interactions are shown by yellow dashed lines. The distance of amino acids in close proximity are shown by black dashed lines with its respective value in white. Pi-Pi interactions are displayed by orange dashed lines. Heteroatoms are color-coded as well: red – oxygen, blue – nitrogen, yellow – sulfur.

The third best ranked conformation shows following RMSD values: 2.019 u.b. and 0.112 Å l.b. (Table 16). Interestingly, the U-shape is almost similar to the first binding pose (Fig. 52, and 54). This explains the same binding affinity, the same interacting partners (Gln241 and Gln447), and similar distances to previous residues (Phe32, Phe159 and Lys214).

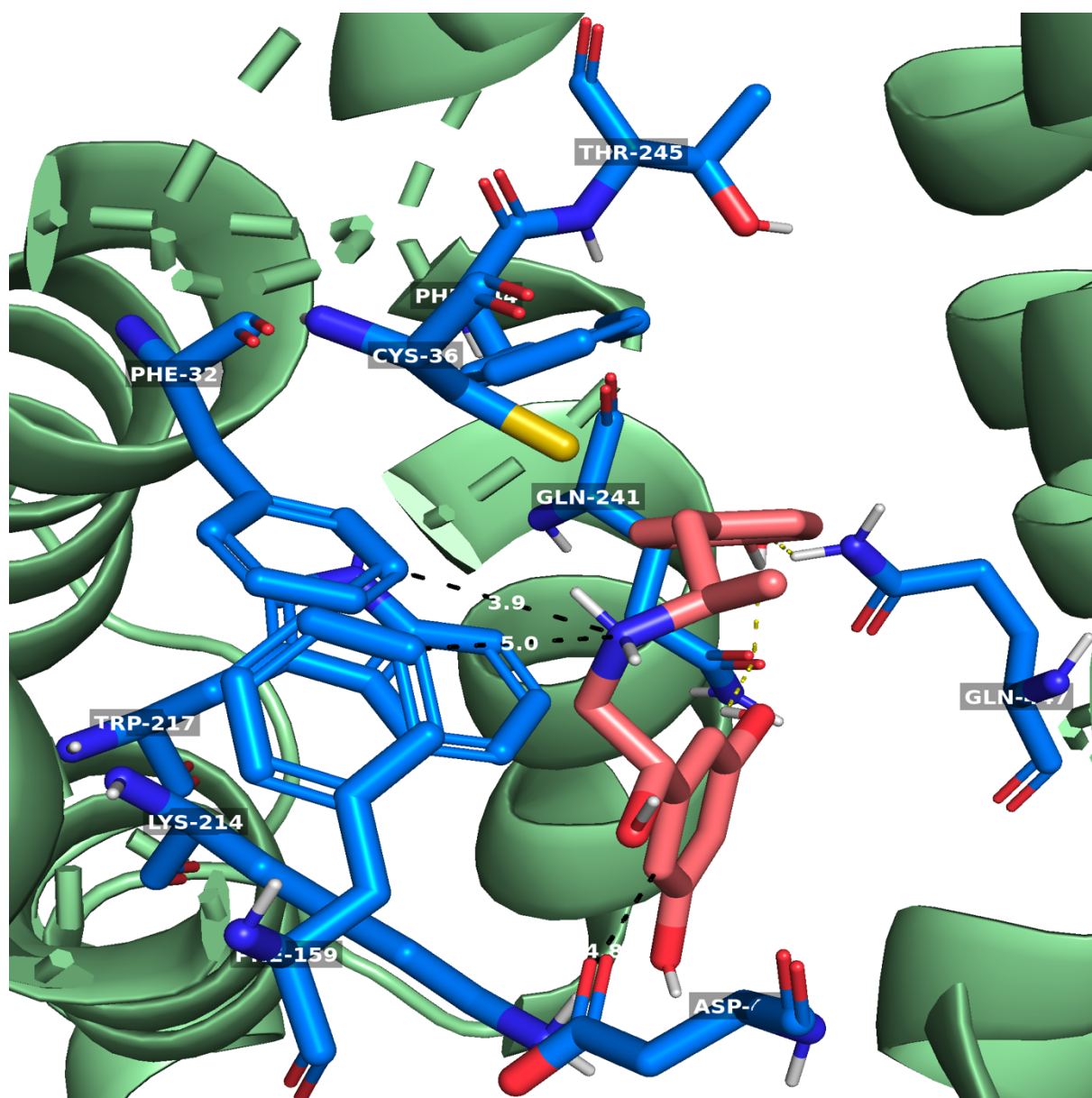


Figure 54: Molecular docking of fenoterol into hOCT1 from AlphaFold DB by AutoDock Vina. Shown is here the second best ranked binding pose of fenoterol (salmon) in hOCT1 (green) with the new orientation of Asp474 regarding the binding affinity out of twenty conformations. Polar interactions are shown by yellow dashed lines. The distance of amino acids in close proximity are shown by black dashed lines with its respective value in white. Pi-Pi interactions are displayed by orange dashed lines. Heteroatoms are color-coded as well: red – oxygen, blue – nitrogen, yellow – sulfur.

mode	affinity (kcal/mol)	dist from best mode	
		rmsd l.b.	rmsd u.b.
1	-7.8	0.000	0.000
2	-7.8	2.975	4.585
3	-7.8	0.112	2.019
4	-7.7	1.685	2.935
5	-7.7	2.996	4.687
6	-7.7	1.747	2.768
7	-7.6	2.128	3.495
8	-7.5	2.773	3.687
9	-7.5	2.027	3.093
10	-7.4	2.548	4.636
11	-7.4	2.503	4.434
12	-7.3	2.240	3.539
13	-7.3	2.677	6.679
14	-7.3	2.672	6.800
15	-7.2	2.189	4.609
16	-7.1	2.296	4.654
17	-7.1	1.699	2.373
18	-7.1	2.575	4.503
19	-7.1	2.320	4.175
20	-7.0	2.996	6.762

Table 16: Binding affinities and RMSD values of fenoterol in hOCT1 from AlphaFold DB analyzed by flexible Docking using AutoDock Vina. Root mean square deviation (RMSD) values measuring the average between atoms of a position relative to the best fitting position, are calculated using only movable heavy atoms. Two variants of RMSD metrics are provided, rmsd l.b. (RMSD lower bound) and rmsd u.b. (RMSD upper bound). They differ in how the atoms are matched in the distance calculation; rmsd u.b. matches each atom in one conformation with itself in the other conformation, ignoring any symmetry; rmsd l.b. matches each atom in one conformation with the closest atom of the same element type in the other conformation.

3.2.10 Rotamer Docking of trospium into hOCT1 from AlphaFold DB using AutoDock Vina

In the exact same manner rotamer docking was performed for trospium in the hOCT1 structure from AlphaFold DB using AutoDock Vina. Even though the setting was the same and docking was performed successfully, no polar interactions were detected in PyMol. Due to that, Discovery Studio Visualizer was used for visualization as in the flexible docking approach.

Out of 20 conformations the three best ranked binding poses regarding binding affinity were chosen for analysis and visualization. The best ranked binding pose has an affinity of -8.9 kcal/mol (Table 17). Trospium is stabilized by six intermolecular and one intramolecular interaction. Beginning with the intermolecular interactions Gln241 (TMH5) is forming a carbon hydrogen bond with the bicyclic ring. On the other hand, Phe244 (TMH5) stabilizes the ligand by a pi-cation interaction. The following intermolecular interactions are formed with the two benzyl rings: pi-alkyl (Ile446; TMH10), pi-donor hydrogen bond (Cys473; TMH11), pi-alkyl (Cys473; TMH11), and pi-pi stacked (Trp354; TMH7). Additionally, trospium is stabilizing itself by an intramolecular pi-alkyl interaction between one of the benzyl rings and the bicyclic ring (Fig. 55, Suppl. Fig. 8).

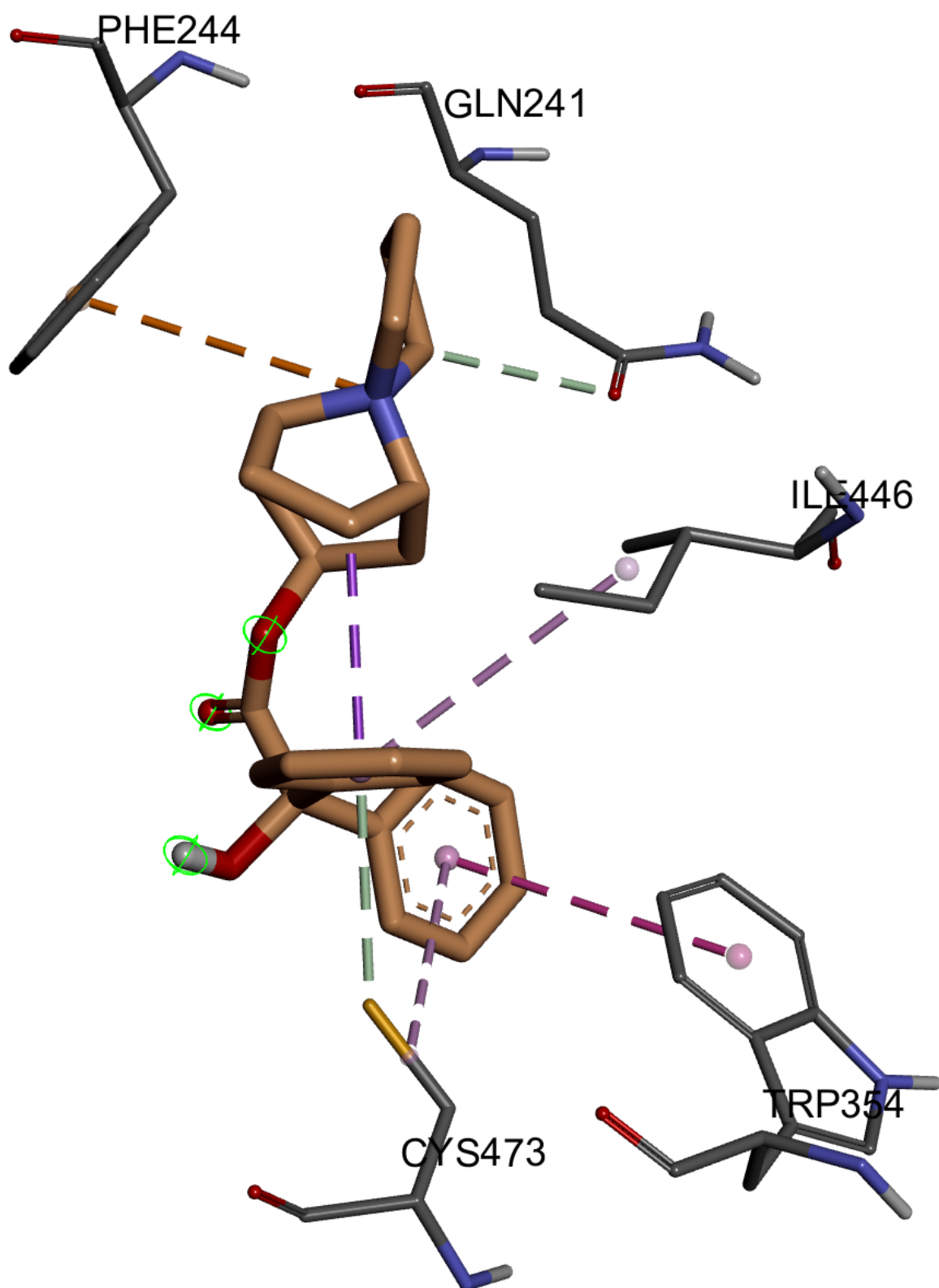


Figure 55: Molecular docking of trospium into hOCT1 from AlphaFold DB by AutoDock Vina. Shown is here the best ranked binding pose of trospium (orange) in hOCT1's interacting amino acids (gray) with the new orientation of Asp474 regarding the binding affinity out of twenty conformations. Following interactions are color-coded: Conventional H-bonds – green bold lines, van der Waals forces – thin green lines, Pi-Alkyl – pink, Donor-Donor – red, Pi-Pi Stacked – purple, Carbon Hydrogen bond; Pi-Donor Hydrogen Bond – mint green, Pi-Sulfur – yellow, Pi-Cation – orange. Heteroatoms are color-coded as well: red – oxygen, blue – nitrogen, yellow – sulfur.

The second best ranked binding pose has an affinity of -8.1 kcal/mol with the following RMSD values: 2.054 Å u.b. and 1.239 Å l.b. (Table 17). This conformation has a comparable shape and it is stabilized by nine intermolecular interactions. The interaction types and reaction partners of Gln241, Phe244, Ile446, and Cys473 are preserved. Newly formed interactions include a pi-cation interaction between Lys214 (TMH4) and a benzyl ring, as well as a pi-pi T-shaped interaction between Trp217 (TMH4) with the same aromatic ring. One of the two remaining interactions is formed by Met218 (TMH4), a pi-sulfur interaction with the benzyl ring. Cys36 (TMH1) is stabilizing the ligand with a conventional hydrogen bond formed with the oxygen in the linker part (Fig. 56, Supp. Fig. 9).

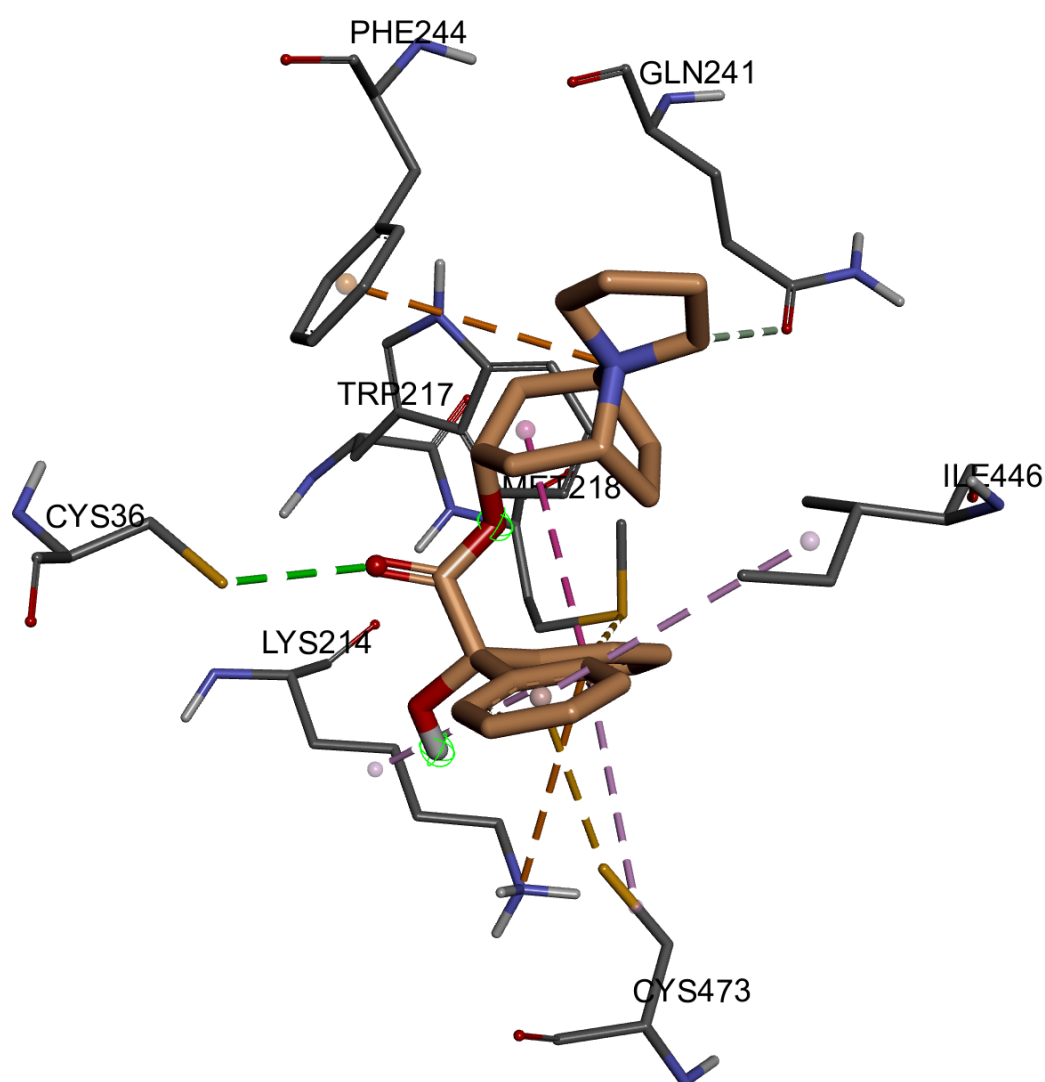


Figure 56: Molecular docking of trospium into hOCT1 from AlphaFold DB by AutoDock Vina. Shown is here the second best ranked binding pose of trospium (orange) in hOCT1's interacting amino acids (gray) with the new orientation of Asp474 regarding the binding affinity out of twenty conformations. Following interactions are color-coded: Conventional H-bonds – green bold lines, van der Waals forces – thin green lines, Pi-Alkyl – pink, Donor-Donor – red, Pi-Pi Stacked – purple, Carbon Hydrogen bond; Pi-Donor Hydrogen Bond – mint green, Pi-Sulfur – yellow, Pi-Cation – orange. Heteroatoms are color-coded as well: red – oxygen, blue – nitrogen, yellow – sulfur.

The third best ranked conformation has a binding affinity of -7.8 kcal/mol with following RMSD values: 3.658 Å u.b. and 1.596 Å l.b. (Table 17). Compared to the other two poses, this conformation has a different orientation of the linker part, the oxygen and hydroxyl group pointing more towards TMH10, and the two benzyl groups are directed more towards TMH4 and TMH11. As in the second binding pose, stabilizing effects by Lys214, Gln241, Phe244, Ile446, and Cys473 were preserved. Additional stabilizing effects are provided by Glu386 (TMH8) forming an intermolecular pi-cation interaction with the positively charged nitrogen (Fig. 57, Supp. Fig. 10).

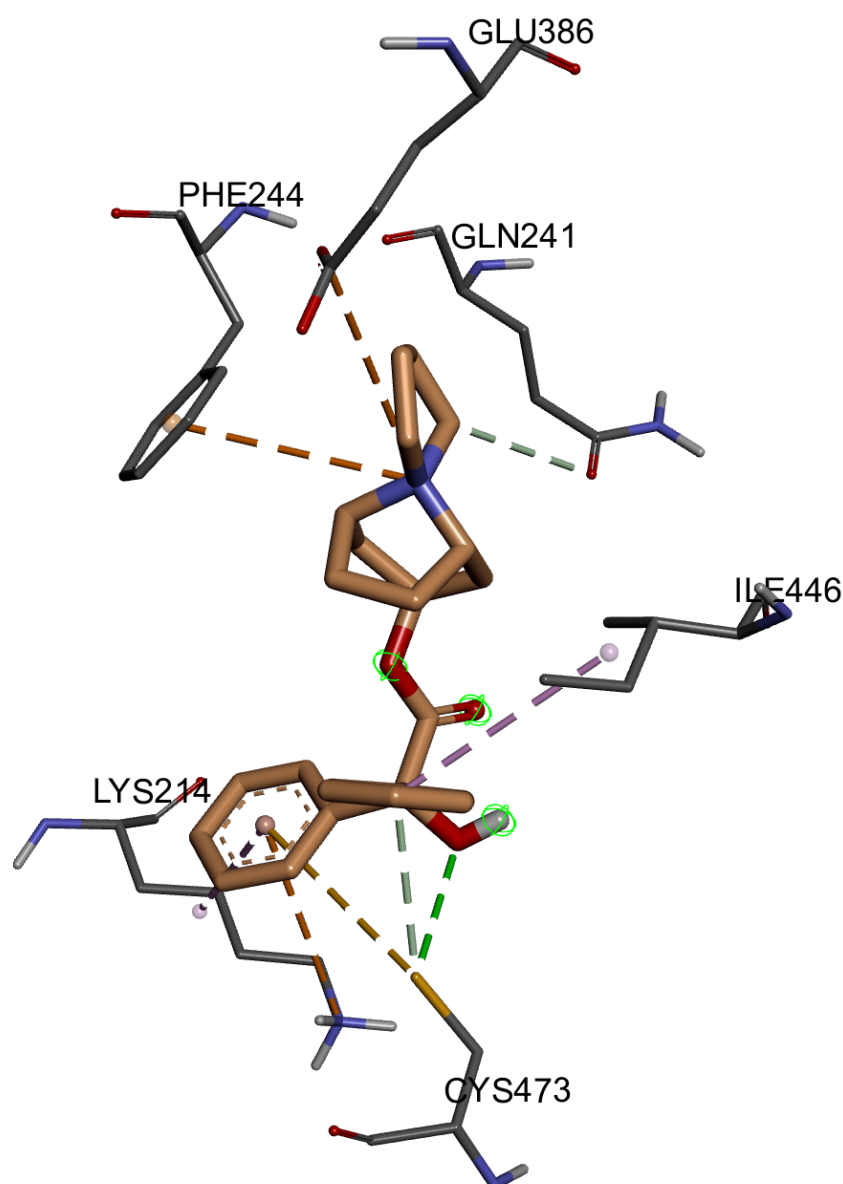


Figure 57: Molecular docking of trospium into hOCT1 from AlphaFold DB by AutoDock Vina. Shown is here the third best ranked binding pose of trospium (orange) in hOCT1's interacting amino acids (gray) with the new orientation of Asp474 regarding the binding affinity out of twenty conformations. Following interactions are color-coded: Conventional H-bonds – green bold lines, van der Waals forces – thin green lines, Pi-Alkyl – pink, Donor-Donor – red, Pi-Pi Stacked – purple, Carbon Hydrogen bond; Pi-Donor Hydrogen Bond – mint green, Pi-Sulfur – yellow, Pi-Cation – orange. Heteroatoms are color-coded as well: red – oxygen, blue – nitrogen, yellow – sulfur.

mode	affinity	dist from best mode	
	(kcal/mol)	rmsd l.b.	rmsd u.b.
1	-8.9	0.000	0.000
2	-8.1	1.239	2.054
3	-7.8	1.596	3.658
4	-7.7	1.801	4.232
5	-7.5	1.946	6.103
6	-7.4	10.822	13.530
7	-7.4	1.428	2.877
8	-7.4	11.439	13.564
9	-7.3	10.971	13.402
10	-7.3	11.126	13.159
11	-7.3	12.220	13.719
12	-7.2	1.581	4.055
13	-7.2	11.924	13.928
14	-7.2	11.132	13.805
15	-7.1	11.297	13.672
16	-7.1	1.794	4.053
17	-7.1	11.482	15.095
18	-7.0	10.768	13.816
19	-7.0	11.080	13.571
20	-6.9	11.249	13.340

Table 17: Binding affinities and RMSD values of trospium in hOCT1 from AlphaFold DB analyzed by rotamer Docking using AutoDock Vina. Root mean square deviation (RMSD) values measuring the average between atoms of a position relative to the best fitting position, are calculated using only movable heavy atoms. Two variants of RMSD metrics are provided, rmsd l.b. (RMSD lower bound) and rmsd u.b. (RMSD upper bound). They differ in how the atoms are matched in the distance calculation; rmsd u.b. matches each atom in one conformation with itself in the other conformation, ignoring any symmetry; rmsd l.b. matches each atom in one conformation with the closest atom of the same element type in the other conformation.

3.3 Molecular Docking via AutoDock4

None of the so far performed docking approaches provided reasonable results regarding the essential interaction between the positively charged nitrogen of the ligands and aspartate at codon 474. After performing different methods such as normal molecular docking and rotamer docking with our self-generated homology model, first doubts were raised due to insufficient results. That's why we took advantage of the high-accuracy protein structure model of hOCT1 and mOCT1 from AlphaFold DB for further analyses. Since the repeated docking approaches with the new model in normal docking, flexible docking, and rotamer docking were still not sufficient, concerns were raised about the docking program (AutoDock Vina) itself. Therefore, an alternative open-source docking engine, AutoDock 4, known as the initial docking program of the AutoDock suite, was used for upcoming molecular docking studies. For this purpose, a grid box of 40x40x40 grid points with grid spacing 0.375 Å was constructed at the active site of hOCT1 and mOCT1. The Lamarckian genetic algorithm (LGA) was employed with the default parameters; Number of GA runs were set to 100 and population size was set to 300. For both organisms 100 LGA runs were conducted for each ligand, which produced 400 output conformations in total. AutoDock 4.2 was used to perform clustering of binding conformations based on similarities regarding binding modes and affinities. The resulted 100 output conformations were clustered using an all-atom RMSD cut-off of 2.0 Å and the energetically most favored representative of the first four clusters were analyzed further.

3.3.1 Molecular Docking of fenoterol into hOCT1 from AlphaFold using AutoDock4

The first docking approach of fenoterol to hOCT1 from AlphaFold DB reports 27 distinct conformational clusters out of 100 runs, using a rmsd-tolerance of 2.0 Å. The number of multi-member conformational clusters are 21 out of 27 clusters (Table 18). Since cluster rank 4 has the highest frequency with 14 representative conformations and a mean binding energy of -4.81 kcal/mol run 80 was further analyzed. Run 80 has an estimated binding energy of -5.38 kcal/mol (Supp. Fig. 12), whose sum is composed of the final intermolecular energy -8.37 kcal/mol (vdW + Hbond + desolv + electrostatic energy), the final total internal energy -2.39 kcal/mol, and the torsional free energy 2.98 kcal/mol, and then subtracted from the unbound system's energy -2.39 kcal/mol. This pose is stabilized by 11 intermolecular interactions and two intramolecular

interaction (Fig. 58, Supp. Fig. 11). Out of 11 intermolecular interactions, there are six distinct types of interactions formed to stabilize fenoterol, whose conformation is horizontally U-shaped. The phenol ring containing one hydroxy group is stabilized by following types of interactions and reacting partners: pi-pi T-shaped interactions (Phe32; Trp217; Phe244) and pi-sulfur interaction (Cys36). The positively charged nitrogen in the linker part is forming an ionic interaction with Asp474 and Cys473 is forming H-bonds with the hydrogens of the respective amino group (-NH₂). Also, the OH-group of the linker part is stabilized by a conventional H-bond of Ser358. The aromatic ring composed of two hydroxy groups is stabilized by a network of interactions: pi-donor hydrogen bond (Cys473), conventional hydrogen bond (Trp354), and pi-sigma (Ile446). Additionally, the structure is stabilized by an intramolecular H-bond formed by two OH-groups of the oppositely located phenol rings and by an intramolecular T-shaped pi-pi interaction between the aromatic rings.

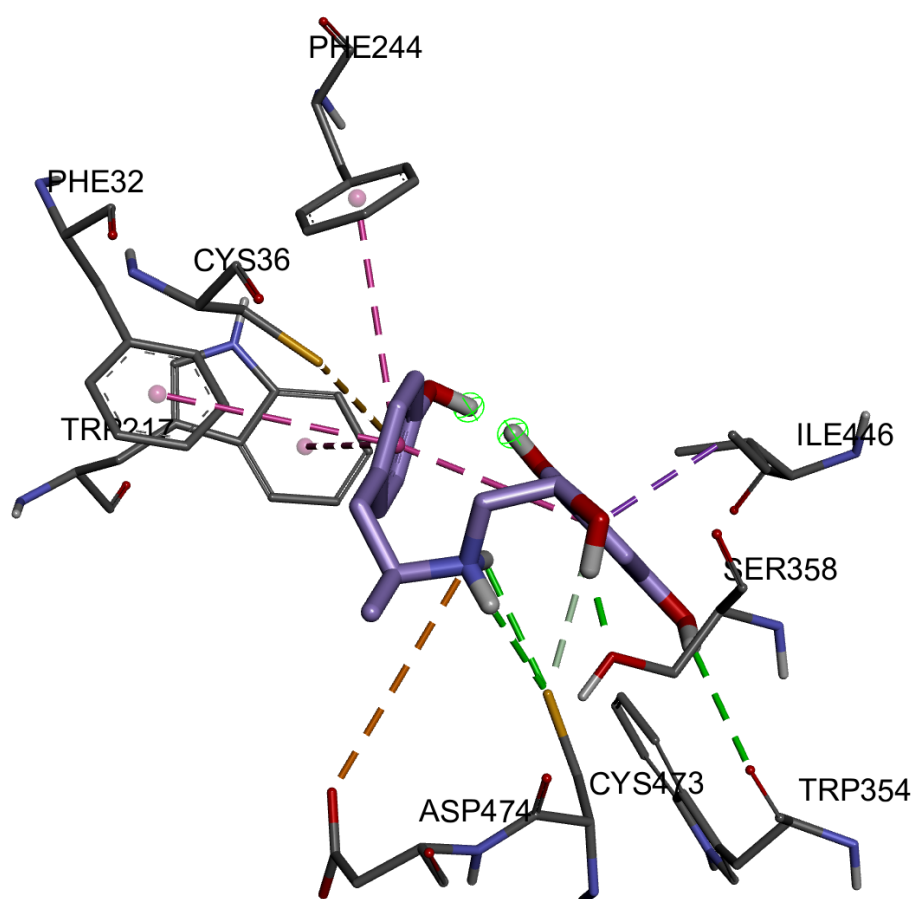


Figure 58: Molecular docking of fenoterol into hOCT1 from AlphaFold DB by AutoDock 4.2. Shown is here the third best ranked binding pose of fenoterol (purple) in hOCT1 out of 14 conformations from the cluster rank 4 with its interacting amino acids (gray) regarding the binding energy. Following interactions are color-coded: Conventional H-bonds – green bold lines, van der Waals forces – thin green lines, Pi-Alkyl – pink, Donor-Donor – red, Pi-Pi Stacked – purple, Carbon Hydrogen bond; Pi-Donor Hydrogen Bond – mint green, Pi-Sulfur – yellow, Pi-Cation – orange. Heteroatoms are color-coded as well: red – oxygen, blue – nitrogen, yellow – sulfur.

Next, the binding poses from cluster rank one to three with the lowest binding energy for each cluster are investigated. The best ranked conformation from the best ranked cluster, which is composed of four conformations in total, has an estimated binding energy of -6.22 kcal/mol (Supp. Fig. 14). Its sum is made up of the final intermolecular energy -9.20 kcal/mol (vdW + Hbond + desolv + electrostatic energy), the final total internal energy -1.15 kcal/mol, and the torsional free energy 2.98 kcal/mol, and then subtracted from the unbound system's energy -1.15 kcal/mol. Due to its linear shape compared to the previous conformation, the structure is stabilized in total by six intermolecular interactions, which are derived from four different types. The phenol ring consisting of one hydroxy group is stabilized by a pi-pi stacked interaction from Phe244 and by a conventional H-bond from Gln241. The methyl group between this aromatic ring and the positively charged nitrogen is forming a pi-sigma interaction with Tyr361. The phenol ring on the opposite side is stabilized by a pi-donor hydrogen bond from Cys473, whereas the two hydroxy groups linked to the aromatic ring are forming two conventional hydrogen bonds with Asp474 and Ser358 (Fig. 59, Supp. Fig. 13).

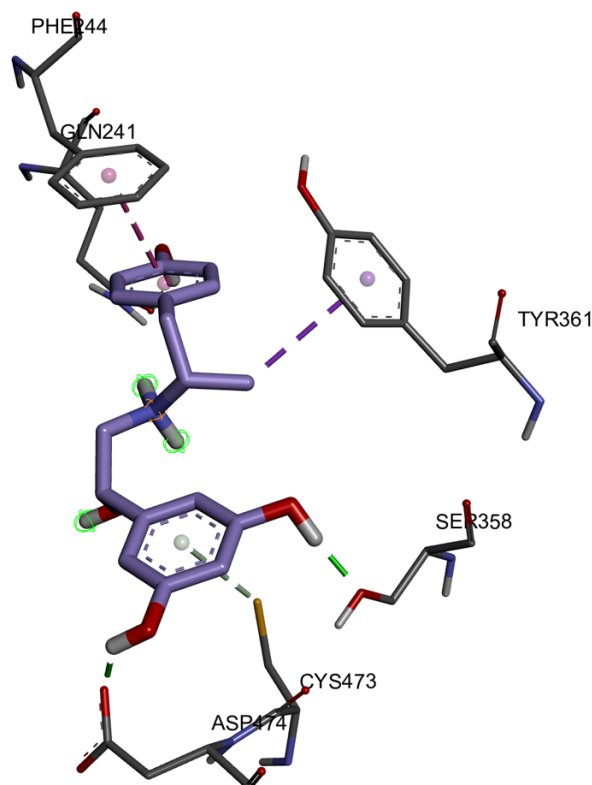


Figure 59: Molecular docking of fenoterol into hOCT1 from AlphaFold DB by AutoDock 4.2. Shown is here the best ranked binding pose of fenoterol (purple) in hOCT1 from cluster rank 1 with its interacting amino acids (gray) regarding the binding energy. Following interactions are color-coded: Conventional H-bonds – green bold lines, van der Waals forces – thin green lines, Pi-Alkyl – pink, Donor-Donor – red, Pi-Pi Stacked – purple, Carbon Hydrogen bond; Pi-Donor Hydrogen Bond – mint green, Pi-Sulfur – yellow, Pi-Cation – orange. Heteroatoms are color-coded as well: red – oxygen, blue – nitrogen, yellow – sulfur.

The best ranked binding pose out of five conformations in cluster rank 2 has an estimated binding energy of -6.10 kcal/mol (Supp. Fig. 16). Its sum is composed of the final intermolecular energy -9.08 kcal/mol (vdW + Hbond + desolv + electrostatic energy), the final total internal energy -1.98 kcal/mol, and the torsional free energy 2.98 kcal/mol, and then subtracted from the unbound system's energy -1.98 kcal/mol. Since this structure is binding the active site in a U-shape manner, the number of interactions is increased. In total, the conformation of fenoterol is stabilized by 14 intermolecular interactions (Fig. 60; Supp. Fig. 15), which are distinguished in seven different types. The phenol ring with the single OH-group is stabilized by a pi-pi stacked interaction with Tyr361 and by a pi-sulfur interaction with Cys36. The hydroxy group on this aromatic ring forms two conventional hydrogen bonds with Ser358 and Gln362. Nevertheless, an unfavorable donor-donor interaction between the side chain of Gln362 and the same OH-group was detected. The neighboring methyl group is stabilized by a pi-sigma interaction with Trp217. The hydroxy groups on the second phenol ring are forming conventional H-bonds with Cys36, Asn156, Gln362, Cys473, and Asp474. The phenol ring itself is stabilized by a pi-alkyl interaction (Cys473), by T-shaped pi-pi interaction (Phe159), and by a pi-sulfur interaction (Cys36).

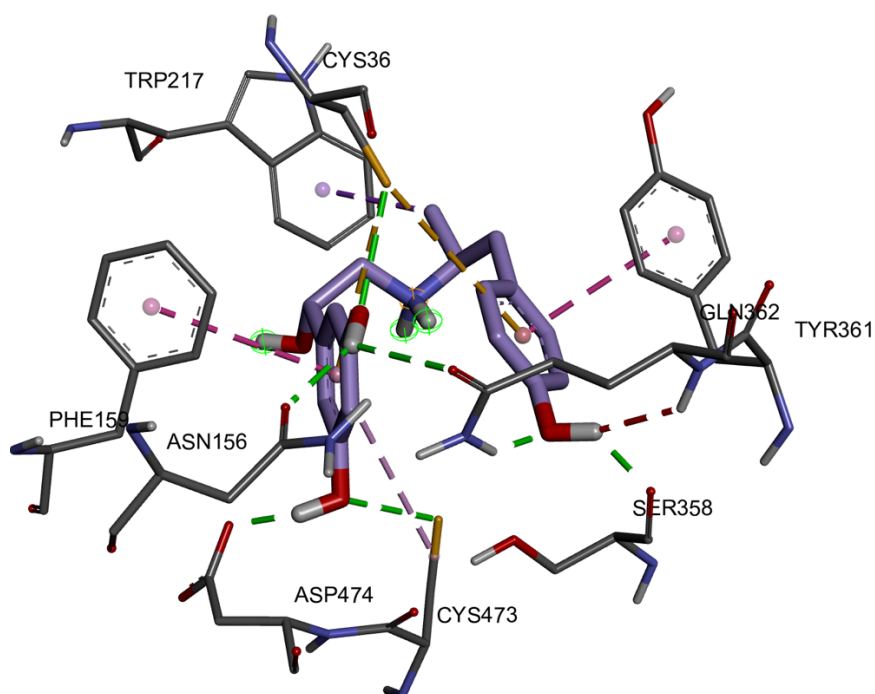


Figure 60: Molecular docking of fenoterol into hOCT1 from AlphaFold DB by AutoDock 4.2. Shown is here the best ranked binding pose of fenoterol (purple) in hOCT1 from cluster rank 2 with its interacting amino acids (gray) regarding the binding energy. Following interactions are color-coded: Conventional H-bonds – green bold lines, van der Waals forces – thin green lines, Pi-Alkyl – pink, Donor-Donor – red, Pi-Pi Stacked – purple, Carbon Hydrogen bond; Pi-Donor Hydrogen Bond – mint green, Pi-Sulfur – yellow, Pi-Cation – orange. Heteroatoms are color-coded as well: red – oxygen, blue – nitrogen, yellow – sulfur.

The best ranked binding pose out of seven conformations in cluster rank 3 has an estimated binding energy of -5.67 kcal/mol (Supp. Fig. 18). Its sum is made up of the final intermolecular energy -8.65 kcal/mol (vdW + Hbond + desolv + electrostatic energy), the final total internal energy -2.19 kcal/mol, and the torsional free energy 2.98 kcal/mol, and then subtracted from the unbound system's energy -2.19 kcal/mol. This U-shaped conformation has performed a 180° rotation compared to the previous conformation and is stabilized by ten intermolecular interactions and one intramolecular interaction (Fig. 61, Supp. Fig. 17). The single OH-group of the phenol ring forms a conventional H-bond with Asn156. The same phenol ring is stabilized intermolecularly by a T-shaped pi-pi interaction (Phe159), by two pi-alkyl interactions (Lys214, Cys473), and by a pi-sulfur interaction (Cys36). The positively charged nitrogen is stabilized by an intermolecular pi-cation interaction with Trp217, whereas the methyl group right next to it is forming an intramolecular pi-alkyl interaction with the second phenyl group. Also, the hydroxy group in the linker part is stabilized by a conventional hydrogen bond with Cys36. On the other hand, one of the OH-groups at the second phenol ring is forming a conventional H-bond with Ser358. The second phenol ring is stabilized by a pi-alkyl interaction with Cys473 and by a pi-sigma interaction with Ile446.

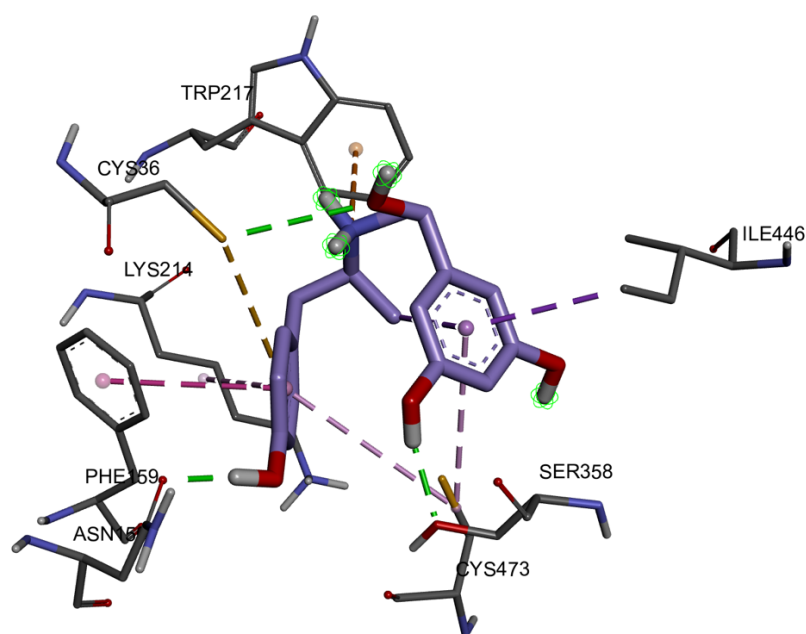


Figure 61: Molecular docking of fenoterol into hOCT1 from AlphaFold DB by AutoDock 4.2. Shown is here the best ranked binding pose of fenoterol (purple) in hOCT1 from cluster rank 1 with its interacting amino acids (gray) regarding the binding energy. Following interactions are color-coded: Conventional H-bonds – green bold lines, van der Waals forces – thin green lines, Pi-Alkyl – pink, Donor-Donor – red, Pi-Pi Stacked – purple, Carbon Hydrogen bond; Pi-Donor Hydrogen Bond – mint green, Pi-Sulfur – yellow, Pi-Cation – orange. Heteroatoms are color-coded as well: red – oxygen, blue – nitrogen, yellow – sulfur.

DPF> analysis

perform a ranked cluster analysis

CLUSTER ANALYSIS OF CONFORMATIONS

Number of conformations = 100

RMSD cluster analysis will be performed using the ligand atoms only (28 / 28 total atoms).

Outputting structurally similar clusters, ranked in order of increasing energy.

Number of distinct conformational clusters found = 27, out of 100 runs,
Using an rmsd-tolerance of 2.0 Å

CLUSTERING HISTOGRAM

Clus- ter Rank	Lowest Binding Energy	Run	Mean Binding Energy	Num in Clus	Histogram							
					5	10	15	20	25	30	35	
1	-6.22	5	-5.72	4	####							
2	-6.10	93	-5.34	5	#####							
3	-5.67	22	-5.16	7	#####							
4	-5.66	48	-4.81	14	#####							
5	-5.62	13	-4.94	5	#####							
6	-5.54	60	-5.54	1	#							
7	-5.34	71	-5.19	2	##							
8	-5.25	65	-4.38	6	#####							
9	-5.22	45	-4.65	4	####							
10	-5.18	72	-4.68	4	####							
11	-5.11	3	-4.96	2	##							
12	-5.04	15	-4.66	2	##							
13	-5.00	79	-4.59	4	####							
14	-4.96	70	-4.34	7	#####							
15	-4.91	47	-4.59	3	###							
16	-4.87	36	-4.78	2	##							
17	-4.86	85	-4.19	8	#####							
18	-4.55	62	-4.53	2	##							
19	-4.46	73	-4.18	5	#####							
20	-4.45	57	-4.45	1	#							
21	-4.44	89	-4.28	2	##							
22	-3.90	32	-3.66	2	##							
23	-3.85	78	-3.85	1	#							
24	-3.85	97	-3.70	4	####							
25	-3.79	55	-3.79	1	#							
26	-3.70	69	-3.70	1	#							
27	-3.56	42	-3.56	1	#							

Number of multi-member conformational clusters found = 21, out of 100 runs.

Table 18: Cluster analysis of conformations after molecular docking of fenoterol into hOCT1 from AlphaFold DB using AutoDock 4.2. Shown is here the summary of pose clustering and binding energy from the docking log file (dlg).

3.3.2 Molecular Docking of trospium into hOCT1 from AlphaFold DB using AutoDock4

As described for fenoterol in the same manner, binding conformations of trospium to hOCT1 from Alpha Fold DB with the lowest binding energy of the respective four best ranked clusters are investigated in detail (Table 19). The best ranked binding pose out of five conformations in the first cluster rank has an estimated binding energy of -10.07 kcal/mol (Supp. Fig. 20). Its sum is composed of the final intermolecular energy -11.86 kcal/mol (vdW + Hbond + desolv + electrostatic energy), the final total internal energy -1.89 kcal/mol, and the torsional free energy 1.79 kcal/mol, and then subtracted from the unbound system's energy -1.89 kcal/mol. This conformation is stabilized by five different intermolecular interactions. The aromatic rings in the back are stabilized by a pi-pi stacked interaction with Phe244 and a pi-sigma interaction with Ile446. The carbonyl group in the linker part is forming a conventional H-bond with Cys36. The crucial aspartate at codon 474 is stabilizing trospium in two ways: by an ionic interaction with the positively charged nitrogen and by a carbon hydrogen bond with the bicyclic ring (Fig. 62; Supp. Fig. 19).

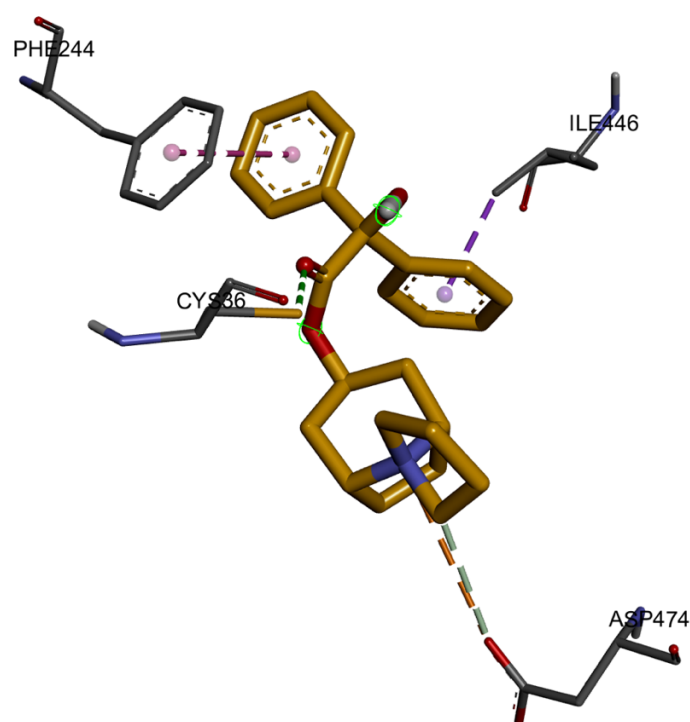


Figure 62: Molecular docking of trospium into hOCT1 from AlphaFold DB by AutoDock 4.2. Shown is here the best ranked binding pose of trospium (orange) in hOCT1 from cluster rank 1 with its interacting amino acids (gray) regarding the binding energy. Following interactions are color-coded: Conventional H-bonds – green bold lines, van der Waals forces – thin green lines, Pi-Alkyl – pink, Donor-Donor – red, Pi-Pi Stacked – purple, Carbon Hydrogen bond; Pi-Donor Hydrogen Bond – mint green, Pi-Sulfur – yellow, Pi-Cation – orange. Heteroatoms are color-coded as well: red – oxygen, blue – nitrogen, yellow – sulfur.

The best ranked docking pose out of 74 conformations in the second cluster rank has an estimated binding affinity of -9.39 kcal/mol (Supp. Fig. 22). Its sum is made up of the final intermolecular energy -11.18 kcal/mol (vdW + Hbond + desolv + electrostatic energy), the final total internal energy -2.83 kcal/mol, and the torsional free energy 1.79 kcal/mol, and then subtracted from the unbound system's energy -2.83 kcal/mol. Even though its RMSD value of 6.069 Å to the reference structure is quite high, the number of conformations in this cluster indicates the likelihood of this conformation. It is stabilized by eight intermolecular interactions and two intramolecular interactions. The latter is composed of a pi-sigma interaction, which is formed by the bicyclic ring and the aromatic ring and an ionic interaction between the positively charged nitrogen and the same aromatic ring. The exact same benzyl group is furthermore involved in a pi-sigma interaction (Ile446), a pi-alkyl interaction (Cys473), and a T-shaped pi-pi interaction (Tyr361). Moreover, the neighboring aromatic ring is stabilized by a pi-pi stacked interaction with Phe244. Carbon H-bond interactions of Asn156 and Asp474 provide stabilizing effects to the bicyclic ring. Additionally, the positively charged nitrogen forms an ionic bond with the essential Asp474 (Fig. 63, Supp. Fig. 21).

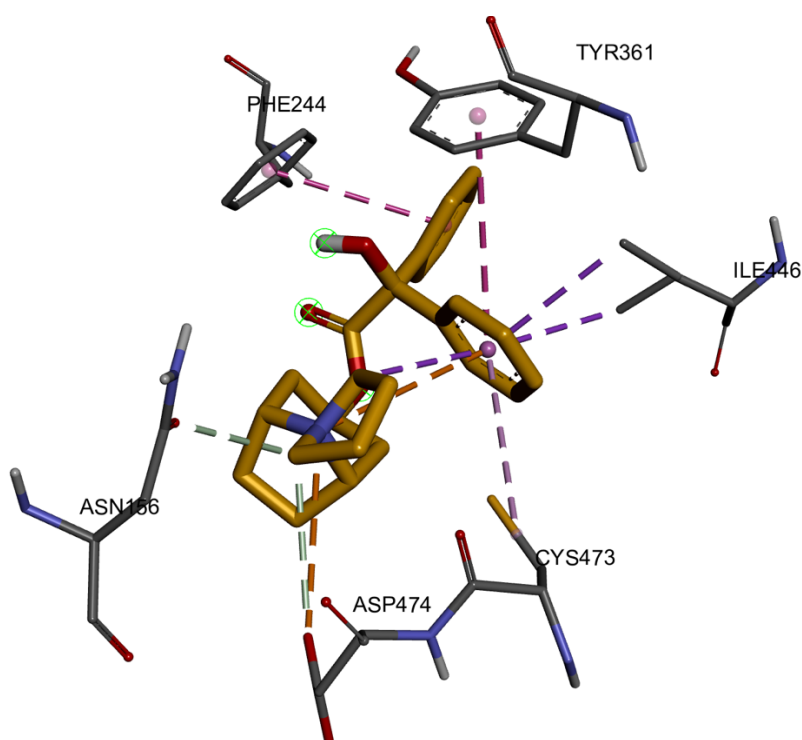


Figure 63: Molecular docking of trospium into hOCT1 from AlphaFold DB by AutoDock 4.2. Shown is here the best ranked binding pose of trospium (orange) in hOCT1 from cluster rank 2 with its interacting amino acids (gray) regarding the binding energy. Following interactions are color-coded: Conventional H-bonds – green bold lines, van der Waals forces – thin green lines, Pi-Alkyl – pink, Donor-Donor – red, Pi-Pi Stacked – purple, Carbon Hydrogen bond; Pi-Donor Hydrogen Bond – mint green, Pi-Sulfur – yellow, Pi-Cation – orange. Heteroatoms are color-coded as well: red – oxygen, blue – nitrogen, yellow – sulfur.

Next, the best ranked binding pose out of 16 different conformations in the third cluster rank with an estimated binding affinity of -9.31 kcal/mol (Supp. Fig. 24) is analyzed. Its total is the sum of the final intermolecular energy -11.10 kcal/mol (vdW + Hbond + desolv + electrostatic energy), the final total internal energy -2.38 kcal/mol, and the torsional free energy 1.79 kcal/mol, which is then subtracted from the unbound system's energy -2.38 kcal/mol. Compared to the second pose this structure underwent a 180° rotation, letting the boat conformation of the cycloheptane ring point towards the extracellular membrane, whereas the two aromatic rings are directed more to the intracellular membrane. In total, eight intermolecular interactions enable stabilizing effects of trospium. Pi-sigma and pi-cation interactions are investigated between Phe244, the cycloheptane ring and the positively charged nitrogen. The aromatic rings are stabilized by following interactions: pi-sulfur (Met218; Cys473), pi-alkyl (Lys214), pi-cation (Lys214), and pi-donor H-bond (Cys473). The carbonyl group in the linker part is forming a conventional H-bond with Cys36 (Fig. 64, Suppl. Fig. 23).

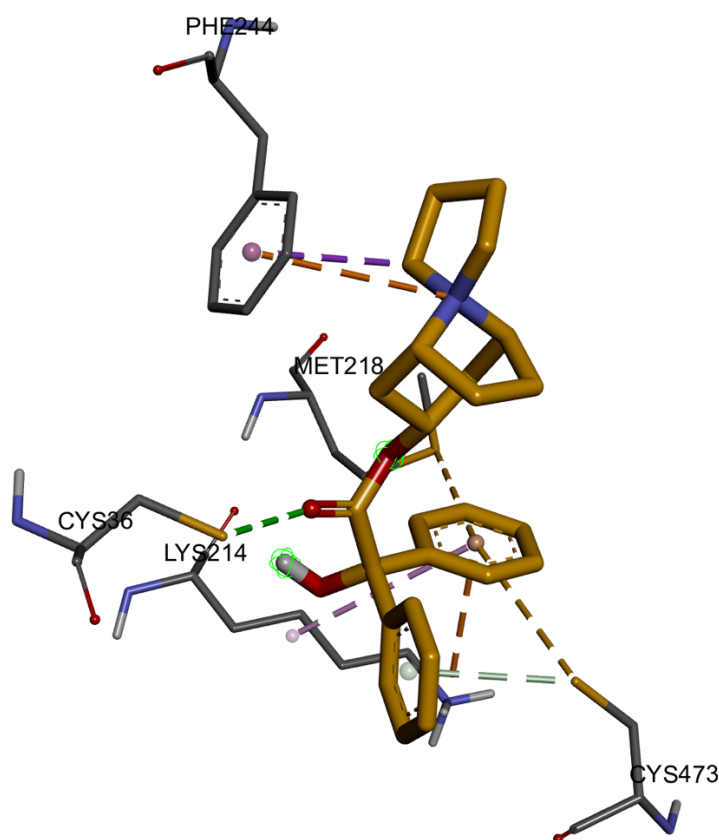


Figure 64: Molecular docking of trospium into hOCT1 from AlphaFold DB by AutoDock 4.2. Shown is here the best ranked binding pose of trospium (orange) in hOCT1 from cluster rank 3 with its interacting amino acids (gray) regarding the binding energy. Following interactions are color-coded: Conventional H-bonds – green bold lines, van der Waals forces – thin green lines, Pi-Alkyl – pink, Donor-Donor – red, Pi-Pi Stacked – purple, Carbon Hydrogen bond; Pi-Donor Hydrogen Bond – mint green, Pi-Sulfur – yellow, Pi-Cation – orange. Heteroatoms are color-coded as well: red – oxygen, blue – nitrogen, yellow – sulfur.

Lastly, the only binding pose of cluster rank four having an estimated binding affinity of -8.96 kcal/mol (Suppl. Fig. 26) is investigated in detail. Its sum is composed of the final intermolecular energy -10.74 kcal/mol (vdW + Hbond + desolv + electrostatic energy), the final total internal energy -2.56 kcal/mol, and the torsional free energy 1.79 kcal/mol, and then subtracted from the unbound system's energy -2.56 kcal/mol. Trospium's structure is comparable to the conformations of the first and second cluster rank, being stabilized by six intermolecular interactions and one intramolecular interaction. The latter is formed by a pi-cation interaction between the positively charged nitrogen and the aromatic ring. Additionally, the crucial amino residue aspartate at codon 474 provides also stabilizing effects to the positively charged nitrogen by an ionic interaction. Furthermore, interactions such as pi-pi stacked (Phe244), pi-sigma (Ile446), pi-alkyl (Ile446; Cys473), and pi-pi T-shaped (Tyr361) add stabilizing effects to molecular structure of trospium (Fig. 65, Suppl. Fig. 25).

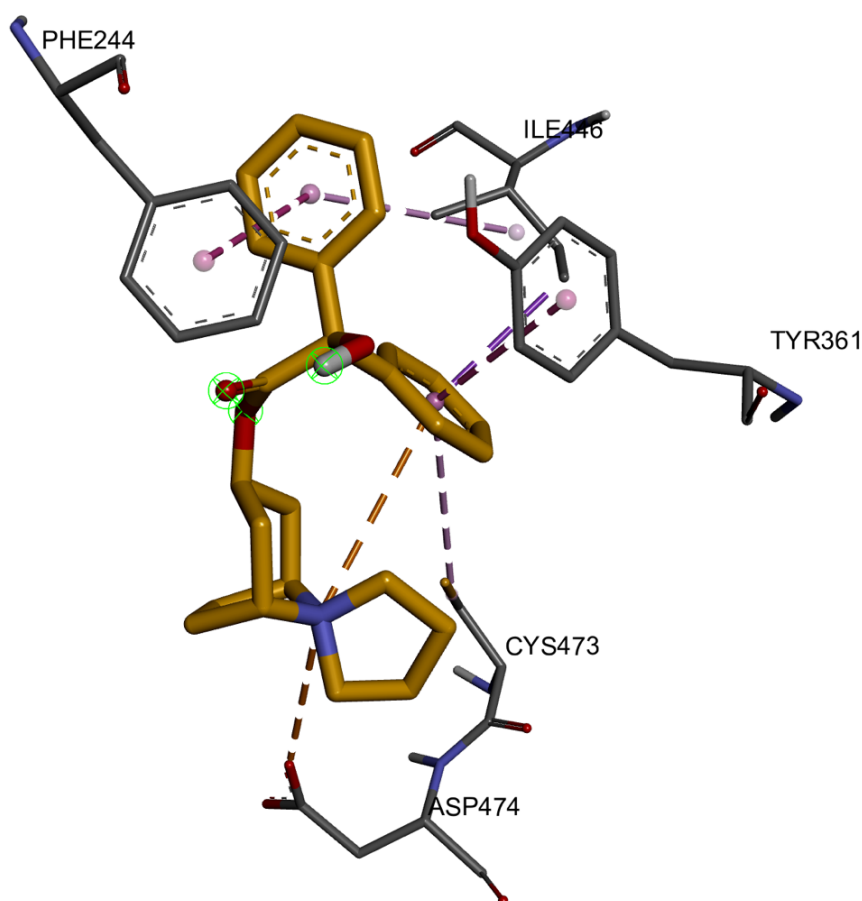


Figure 65: Molecular docking of trospium into hOCT1 from AlphaFold DB by AutoDock 4.2. Shown is here the best ranked binding pose of trospium (orange) in hOCT1 from cluster rank 4 with its interacting amino acids (gray) regarding the binding energy. Following interactions are color-coded: Conventional H-bonds – green bold lines, van der Waals forces – thin green lines, Pi-Alkyl – pink, Donor-Donor – red, Pi-Pi Stacked – purple, Carbon Hydrogen bond; Pi-Donor Hydrogen Bond – mint green, Pi-Sulfur – yellow, Pi-Cation – orange. Heteroatoms are color-coded as well: red – oxygen, blue – nitrogen, yellow – sulfur.

DPF> analysis # perform a ranked cluster analysis

CLUSTER ANALYSIS OF CONFORMATIONS

Number of conformations = 100

RMSD cluster analysis will be performed using the ligand atoms only (30 / 30 total atoms).

Outputting structurally similar clusters, ranked in order of increasing energy.

Number of distinct conformational clusters found = 7, out of 100 runs,
Using an rmsd-tolerance of 2.0 A

CLUSTERING HISTOGRAM

Clus- ter Rank	Lowest Binding Energy	Run	Mean Binding Energy	Num in Clus	Histogram							
					5	10	15	20	25	30	35	
1	-10.07	3	-9.62	5	#####							
2	-9.39	13	-8.93	74	#####	#####	#####	#####	#####	#####	#####	#####
3	-9.31	39	-8.88	16	#####							
4	-8.96	86	-8.96	1	#							
5	-8.56	5	-8.47	2	##							
6	-8.11	8	-8.11	1	#							
7	-7.54	52	-7.54	1	#							

Number of multi-member conformational clusters found = 4, out of 100 runs.

Table 19: Cluster analysis of conformations after molecular docking of trospium into hOCT1 from AlphaFold DB using AutoDock 4.2. Shown is here the summary of pose clustering and binding energy from the docking log file (dlg).

3.3.3 Molecular Docking of fenoterol into mOCT1 from AlphaFold DB using AutoDock4

The same docking approach was applied for fenoterol into mOCT1 (UniProt: O08966) using AutoDock 4.2. Here, out of 18 different cluster ranks (Table 20) four are further analyzed based on their free binding energy and interactions. Cluster rank 1 consists of 37 different conformations, the best one (pose 88) having an estimated free binding energy of -6.40 kcal/mol (Suppl. Fig. 28). This value is composed of the final intermolecular energy -9.38 kcal/mol (vdW + Hbond + desolv + electrostatic energy), the final total internal energy -1.69 kcal/mol, and the torsional free energy 2.98 kcal/mol, and then subtracted from the unbound system's energy -1.69 kcal/mol. The U-shape of trospium enables nine intermolecular interactions and one intramolecular interaction, which both contribute to this estimated free binding energy. The phenol ring containing one hydroxy group is stabilized by two pi-pi stacked interactions from Trp218, by one pi-sulfur interaction from Cys451, and by one Carbon H-bond with Lys215. The upwards tending positively charged nitrogen is stabilized by a pi-cation interaction with Phe245. Remaining interactions providing stabilizing effects to either the second phenol ring or its OH-groups are: Pi-sulfur (Cys474), Pi-Pi stacked (Tyr36), Conventional H-Bond (Asp475), Pi-Alkyl (Lys215), and Carbon H-Bond (Phe160). Additionally, both phenol rings are able to stabilize themselves by an intramolecular pi-pi stacked interaction due to their shape (Fig. 66; Suppl. Fig. 27).

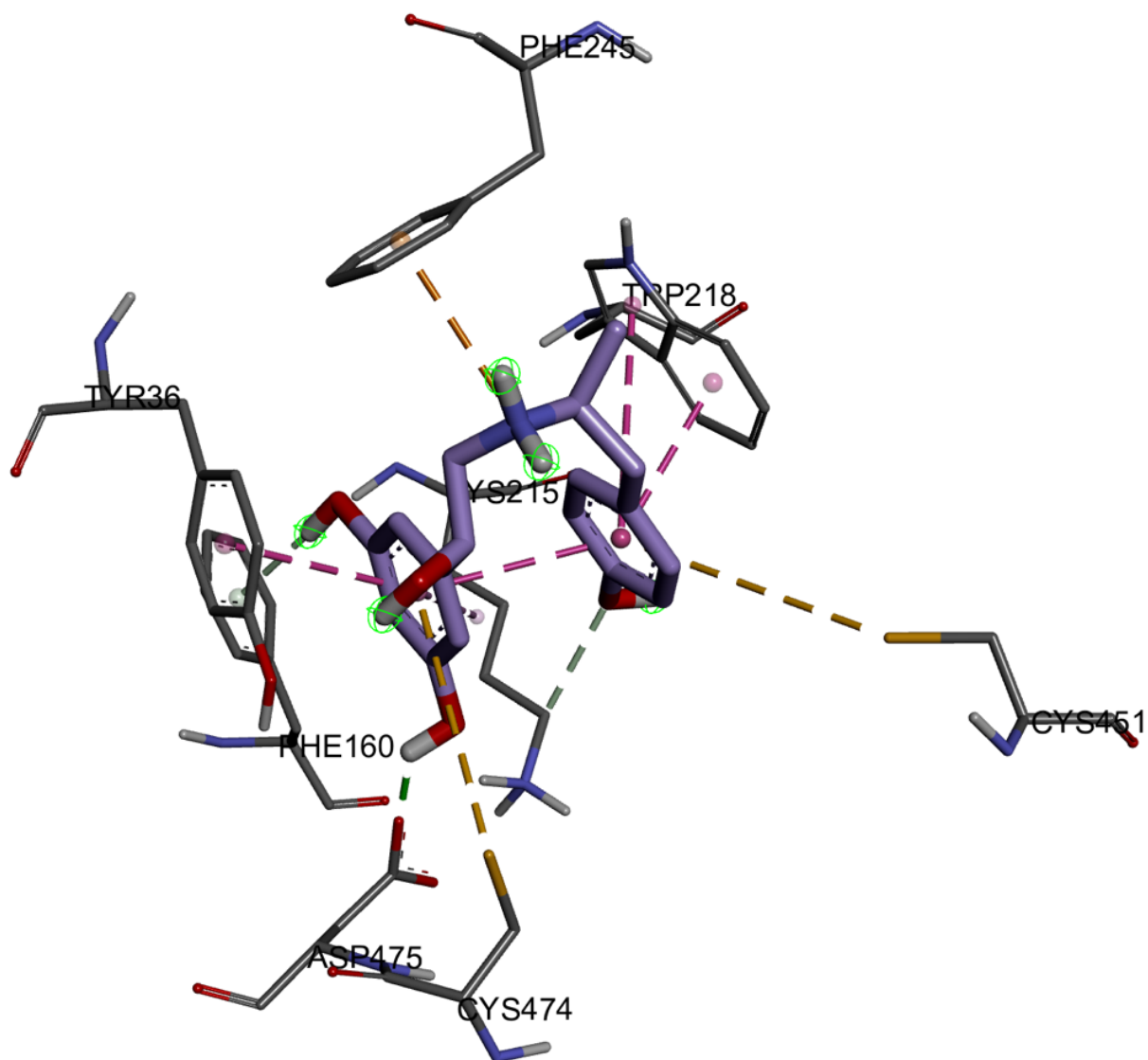


Figure 66: Molecular docking of fenoterol into mOCT1 from AlphaFold DB by AutoDock 4.2. Shown is here the best ranked binding pose of fenoterol (purple) in mOCT1 from cluster rank 1 with its interacting amino acids (gray) regarding the binding energy. Following interactions are color-coded: Conventional H-bonds – green bold lines, van der Waals forces – thin green lines, Pi-Alkyl – pink, Donor-Donor – red, Pi-Pi Stacked – purple, Carbon Hydrogen bond; Pi-Donor Hydrogen Bond – mint green, Pi-Sulfur – yellow, Pi-Cation – orange. Heteroatoms are color-coded as well: red – oxygen, blue – nitrogen, yellow – sulfur.

The best ranked pose (pose 8) in cluster rank two out of three conformation has an estimated binding affinity of -6.37 kcal/mol (Suppl. Fig. 30). Its sum is made up of the final intermolecular energy -9.36 kcal/mol (vdW + Hbond + desolv + electrostatic energy), the final total internal energy -2.11 kcal/mol, and the torsional free energy 2.98 kcal/mol, and then subtracted from the unbound system's energy -2.11 kcal/mol. Even though this structure is not in a U-shape, it is involved in 12 intermolecular interactions and one intramolecular interaction (Fig. 67, Suppl Fig. 29). As already seen in the previous conformation, both phenol rings are stabilizing themselves by an intramolecular pi-pi stacked interaction. Moreover, the single substituted phenol ring is trapped in a network of pi-pi stacked and T-shaped interactions (Tyr36, Trp218, and Phe245) as well as stabilized by a pi-sigma interaction with Leu32. The positively charged nitrogen is forming a conventional H-bond with Gln242 and the neighboring hydroxy group in the linker part is stabilized by the same type of interaction with Cys451. The OH-groups on the second phenol ring are forming H-bonds with Tyr36 and Asp475, whereas the aromatic ring itself is stabilized by a T-shaped pi-pi interaction (Trp355), by a pi-donor H-bond (Cys474), and by a pi-alkyl interaction (Leu447).

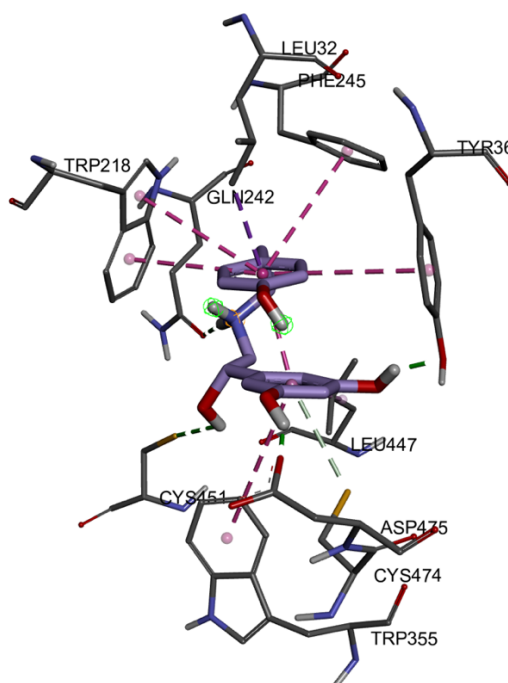


Figure 67: Molecular docking of fenoterol into mOCT1 from AlphaFold DB by AutoDock 4.2. Shown is here the best ranked binding pose of fenoterol (purple) in mOCT1 from cluster rank 2 with its interacting amino acids (gray) regarding the binding energy. Following interactions are color-coded: Conventional H-bonds – green bold lines, van der Waals forces – thin green lines, Pi-Alkyl – pink, Donor-Donor – red, Pi-Pi Stacked – purple, Carbon Hydrogen bond; Pi-Donor Hydrogen Bond – mint green, Pi-Sulfur – yellow, Pi-Cation – orange. Heteroatoms are color-coded as well: red – oxygen, blue – nitrogen, yellow – sulfur.

Next, the best ranked representative of cluster rank three is analyzed. Out of three different conformations this binding pose has an estimated free binding energy of -6.36 kcal/mol, which is the sum of the final intermolecular energy -9.35 kcal/mol (vdW + Hbond + desolv + electrostatic energy), the final total internal energy -1.03 kcal/mol, and the torsional free energy 2.98 kcal/mol, and then subtracted from the unbound system's energy -1.03 kcal/mol (Suppl. Fig. 32). The linear shape of this conformation enables nine intermolecular interactions but no intramolecular interaction. The single hydroxy group on the phenyl ring is forming two conventional H-bonds with Thr246 and Gln448. The aromatic ring itself is stabilized by a pi-pi stacked interaction with Phe245 and a pi-sigma interaction with Leu447. On the other side, the phenol ring containing two OH-groups is stabilized by two pi-alkyl interactions (Leu32, Lys215), a pi-pi stacked interaction (Tyr36), and a pi-sulfur interaction (Cys474). Additionally, the crucial aspartate at codon 475 forms a conventional H-bond with the hydroxy group on the phenyl ring (Fig. 68, Suppl. Fig. 31).

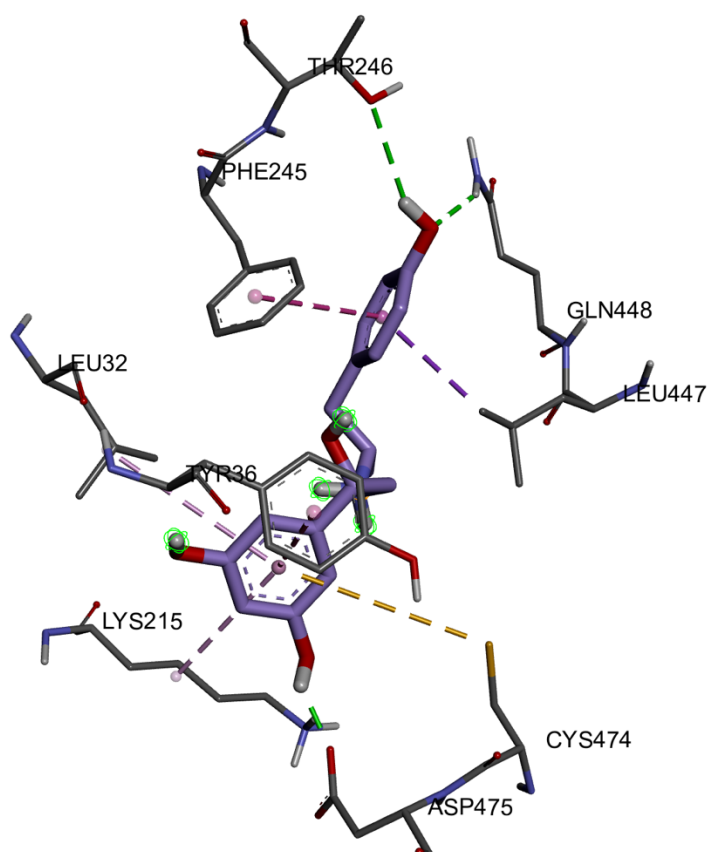


Figure 68: Molecular docking of fenoterol into mOCT1 from AlphaFold DB by AutoDock 4.2. Shown is here the best ranked binding pose of fenoterol (purple) in mOCT1 from cluster rank 3 with its interacting amino acids (gray) regarding the binding energy. Following interactions are color-coded: Conventional H-bonds – green bold lines, van der Waals forces – thin green lines, Pi-Alkyl – pink, Donor-Donor – red, Pi-Pi Stacked – purple, Carbon Hydrogen bond; Pi-Donor Hydrogen Bond – mint green, Pi-Sulfur – yellow, Pi-Cation – orange. Heteroatoms are color-coded as well: red – oxygen, blue – nitrogen, yellow – sulfur.

Lastly, the cluster rank providing the second largest number of representatives for one cluster is number seven. Out of 17 different conformations, binding pose nine provides an estimated binding affinity of -5.88 kcal/mol (Suppl. Fig. 34). Its sum is composed of the final intermolecular energy -8.86 kcal/mol (vdW + Hbond + desolv + electrostatic energy), the final total internal energy -1.98 kcal/mol, and the torsional free energy 2.98 kcal/mol, and then subtracted from the unbound system's energy -1.98 kcal/mol. The best ranked binding is involved in ten intermolecular interactions and one intramolecular interaction. Since the whole structure is again in a U-shape, the latter is formed again between the two phenol rings by a T-shaped pi-pi interaction. The phenol ring having one OH-group is also stabilized by a T-shaped pi-pi interaction (Phe245), as well as a pi-alkyl interaction (Leu447). Additionally, the hydroxy group is forming a conventional H-bond with Gln242. The phenol ring on the opposite site is stabilized by three different types of interactions through Lys215: pi-cation, pi-sigma, pi-alkyl, and by one pi-sulfur interaction through Cys474. Next to it, the OH-group is forming a conventional H-bond with Asp475. Interestingly, the positively charged nitrogen is stabilized by two pi-cation reactions, which are formed by Tyr36 and Asp475 (Fig. 69; Suppl. Fig. 33).

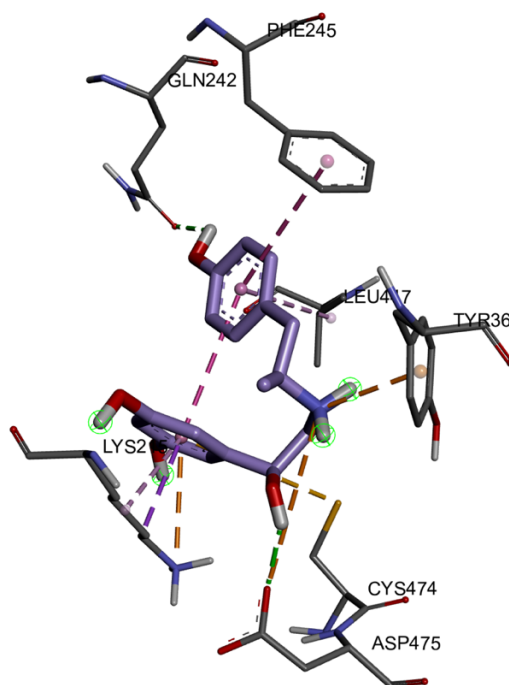


Figure 69: Molecular docking of fenoterol into mOCT1 from AlphaFold DB by AutoDock 4.2. Shown is here the best ranked binding pose of fenoterol (purple) in mOCT1 from cluster rank 7 with its interacting amino acids (gray) regarding the binding energy. Following interactions are color-coded: Conventional H-bonds – green bold lines, van der Waals forces – thin green lines, Pi-Alkyl – pink, Donor-Donor – red, Pi-Pi Stacked – purple, Carbon Hydrogen bond; Pi-Donor Hydrogen Bond – mint green, Pi-Sulfur – yellow, Pi-Cation – orange. Heteroatoms are color-coded as well: red – oxygen, blue – nitrogen, yellow – sulfur.

CLUSTER ANALYSIS OF CONFORMATIONS

Number of conformations = 100

RMSD cluster analysis will be performed using the ligand atoms only (28 / 28 total atoms).

Outputting structurally similar clusters, ranked in order of increasing energy.

Number of distinct conformational clusters found = 18, out of 100 runs,
Using an rmsd-tolerance of 2.0 Å

CLUSTERING HISTOGRAM

Cluster Rank	Lowest Binding Energy	Run	Mean Binding Energy	Number in Cluster	Histogram	
					5	10
1	-6.40	88	-5.63	37	#####	
2	-6.37	8	-5.24	3	###	
3	-6.36	47	-6.00	3	###	
4	-6.13	97	-5.47	2	##	
5	-6.12	99	-6.12	1	#	
6	-6.04	20	-5.95	3	###	
7	-5.88	9	-5.23	17	#####	
8	-5.80	96	-5.01	9	#####	
9	-5.62	41	-5.62	2	##	
10	-5.48	78	-5.01	2	##	
11	-5.41	57	-5.17	2	##	
12	-5.39	32	-4.96	9	#####	
13	-5.19	16	-5.19	1	#	
14	-4.96	64	-4.96	1	#	
15	-4.92	73	-4.92	1	#	
16	-4.91	28	-4.91	1	#	
17	-4.60	26	-4.32	5	#####	
18	-4.44	27	-4.44	1	#	

Number of multi-member conformational clusters found = 12, out of 100 runs.

Table 20: Cluster analysis of conformations after molecular docking of fenoterol into mOCT1 from AlphaFold DB using AutoDock 4.2. Shown is here the summary of pose clustering and binding energy from the docking log file (dlg).

3.3.4 Molecular Docking of trospium into mOCT1 from AlphaFold DB using AutoDock4

The last approach concluded molecular docking of trospium into mouse OCT1 (UniProt: O08966) from AlphaFold DB using AutoDock 4.2. The outcome was as following: 100 performed runs resulted in eight different cluster ranks, five of these being multi-member conformational clusters (Table 21). The first four cluster ranks had the highest number in representative poses, wherefore they were further analyzed for binding. The best ranked pose (run 64) out of 17 conformations from cluster rank 1 has an estimated binding energy of -11.02 kcal/mol. Its value is derived from the final intermolecular energy -12.81 kcal/mol (vdW + Hbond + desolv + electrostatic energy), the final total internal energy -1.44 kcal/mol, and the torsional free energy 1.79 kcal/mol, and then subtracted from the unbound system's energy -1.44 kcal/mol (Suppl. Fig. 36). The two benzyl rings are stabilized by following interactions: Pi-alkyl (Leu32; Lys215; Ala359; Cys474), pi-pi stacked (Phe160), pi-pi T-shaped (Tyr36), pi-donor hydrogen bond (Tyr36), and pi-anion (Asp475). Next to the rings, the hydroxyl group is forming an H-bond with Asp475. Additionally, the positively charged nitrogen is stabilized by a pi-cation interaction with Trp218 (Fig. 70, Suppl. Fig. 35).

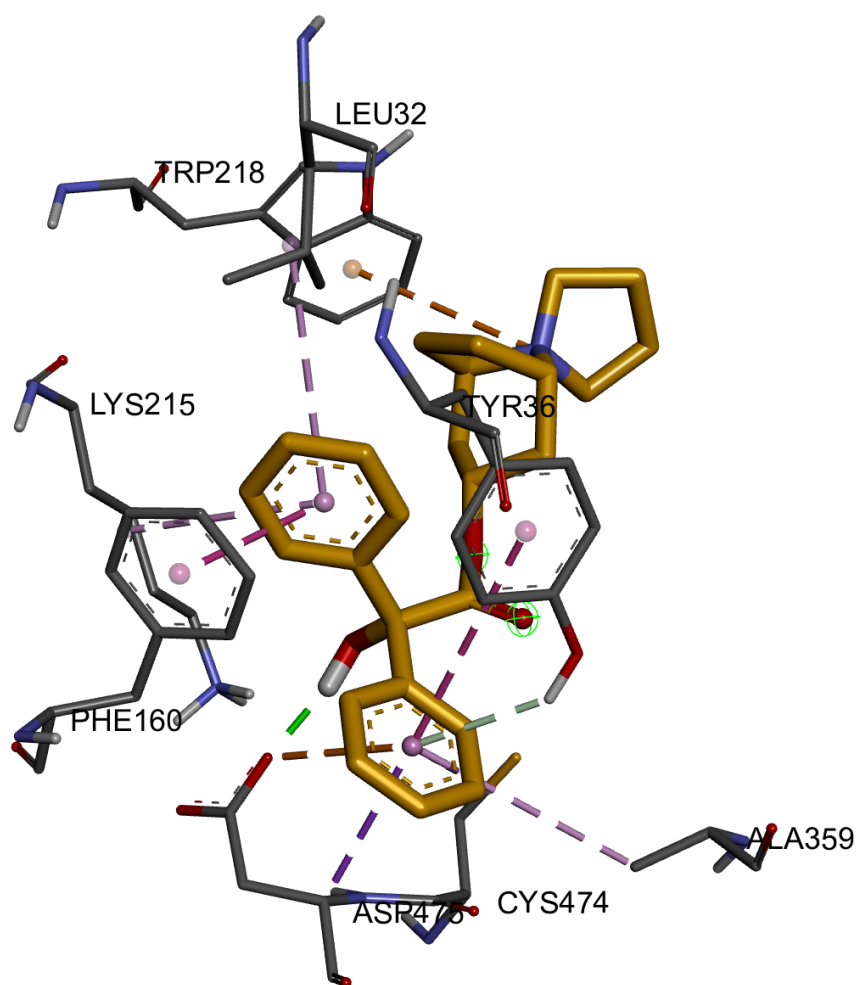


Figure 70: Molecular docking of trospium into mOCT1 from AlphaFold DB by AutoDock 4.2. Shown is here the best ranked binding pose of trospium (orange) in mOCT1 from cluster rank 1 with its interacting amino acids (gray) regarding the binding energy. Following interactions are color-coded: Conventional H-bonds – green bold lines, van der Waals forces – thin green lines, Pi-Alkyl – pink, Donor-Donor – red, Pi-Pi Stacked – purple, Carbon Hydrogen bond; Pi-Donor Hydrogen Bond – mint green, Pi-Sulfur – yellow, Pi-Cation – orange. Heteroatoms are color-coded as well: red – oxygen, blue – nitrogen, yellow – sulfur.

For cluster rank two, out of 16 conformations, the best ranked binding pose (60) has an estimated binding energy of -10.23 kcal/mol (Suppl. Fig. 38). Its value is composed of the final intermolecular energy -12.02 kcal/mol (vdW + Hbond + desolv + electrostatic energy), the final total internal energy -1.81 kcal/mol, and the torsional free energy 1.79 kcal/mol, and then subtracted from the unbound system's energy -1.81 kcal/mol. Compared to the structure of the first cluster, this conformation has undergone a 180° rotation. This enabled the cycloheptane to bind in close proximity of TMH11, which led to stabilizing effect of both an ionic interaction with the positively charged nitrogen and a carbon H-bond with the bicyclic ring by the crucial aspartate at codon 475. The majority of the remaining interactions are formed with the two aromatic rings: pi-pi stacked (Trp218; Phe245), pi-alkyl (Leu447), and pi-sulfur (Cys451). Moreover, this partly U-shaped pose facilitated an intramolecular pi-cation interaction between the positively charged nitrogen and one of the benzyl rings (Fig. 71, Suppl Fig. 37).

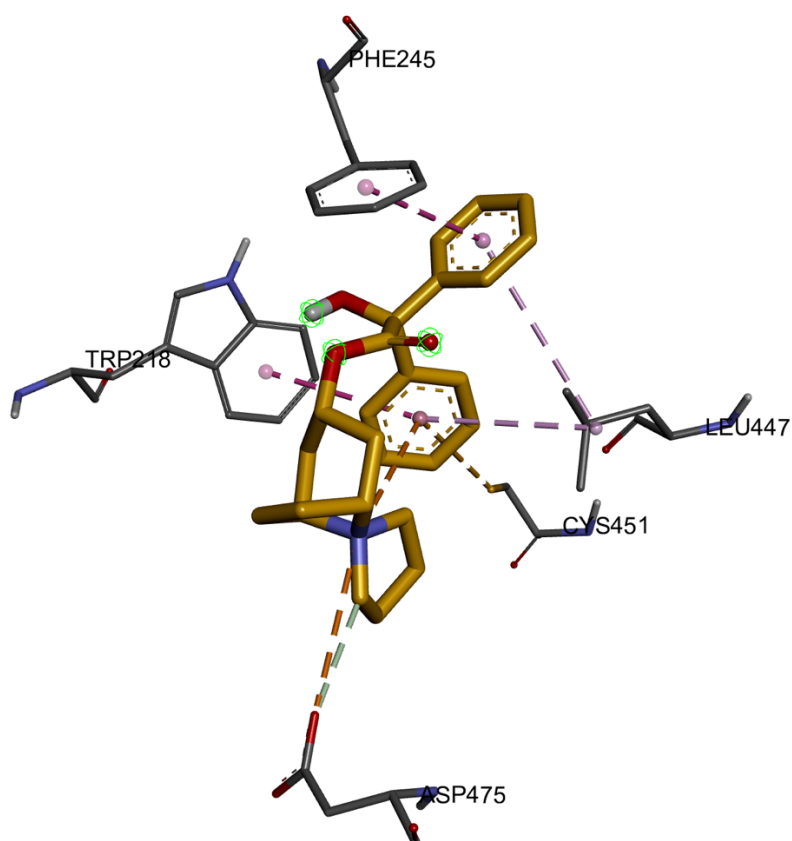


Figure 71: Molecular docking of trospium into mOCT1 from AlphaFold DB by AutoDock 4.2. Shown is here the best ranked binding pose of trospium (orange) in mOCT1 from cluster rank 2 with its interacting amino acids (gray) regarding the binding energy. Following interactions are color-coded: Conventional H-bonds – green bold lines, van der Waals forces – thin green lines, Pi-Alkyl – pink, Donor-Donor – red, Pi-Pi Stacked – purple, Carbon Hydrogen bond; Pi-Donor Hydrogen Bond – mint green, Pi-Sulfur – yellow, Pi-Cation – orange. Heteroatoms are color-coded as well: red – oxygen, blue – nitrogen, yellow – sulfur.

The third cluster rank had 20 representative conformations, whose best ranked pose (run 17) has an estimated binding energy of -9.82 kcal/mol (Suppl. Fig. 40). Its sum is made up of the final intermolecular energy -11.62 kcal/mol (vdW + Hbond + desolv + electrostatic energy), the final total internal energy -2.04 kcal/mol, and the torsional free energy 1.79 kcal/mol, and then subtracted from the unbound system's energy -2.04 kcal/mol. This binding conformation is similar to the first cluster rank with the minor difference, that the two aromatic rings lie in a horizontal manner in the binding pocket. Trospium is stabilized in total by ten intermolecular interactions, which are subdivided in five different types of interactions. The positively charged nitrogen of the cycloheptane ring is stabilized by a pi-cation ring with Phe245, being the only undergone interaction of the bicyclic ring. Most intermolecular interactions are provided by the two benzyl rings: pi-alkyl (Leu32; Lys215; Cys451), pi-pi T-shaped (Phe160; Trp218; Trp355), pi-sulfur (Met467), and pi-cation (Lys215). Moreover, the hydroxyl group in between those aromatic rings forms a conventional H-Bond with Lys215 (Fig. 72, Suppl. Fig. 39).

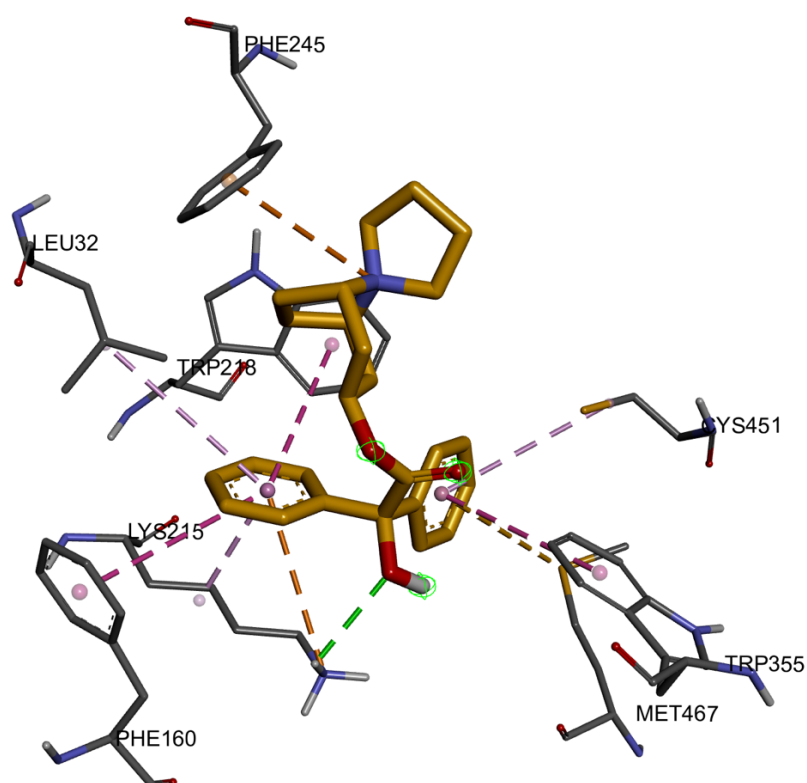


Figure 72: Molecular docking of trospium into mOCT1 from AlphaFold DB by AutoDock 4.2. Shown is here the best ranked binding pose of trospium (orange) in mOCT1 from cluster rank 3 with its interacting amino acids (gray) regarding the binding energy. Following interactions are color-coded: Conventional H-bonds – green bold lines, van der Waals forces – thin green lines, Pi-Alkyl – pink, Donor-Donor – red, Pi-Pi Stacked – purple, Carbon Hydrogen bond; Pi-Donor Hydrogen Bond – mint green, Pi-Sulfur – yellow, Pi-Cation – orange. Heteroatoms are color-coded as well: red – oxygen, blue – nitrogen, yellow – sulfur.

The fourth and last cluster rank being analyzed is with 40 conformations the cluster rank with the most representative poses among all eight listed (Table 21). Binding pose 20 is listed as the best ranked in this cluster with an estimated binding energy of -9.67 kcal/mol, whose total value is the sum of the final intermolecular energy -11.46 kcal/mol (vdW + Hbond + desolv + electrostatic energy), the final total internal energy -2.55 kcal/mol, and the torsional free energy 1.79 kcal/mol, which is then subtracted from the unbound system's energy -2.55 kcal/mol (Suppl Fig. 42). Out of eight interactions, seven intermolecular interactions and one intramolecular interaction provide stabilizing effects to the molecular structure. As this conformation is mimicking third cluster rank pose, the intermolecular pi-cation interaction between Phe245 and the positively charged nitrogen is maintained. Also, the aromatic rings are involved in the majority of interactions: pi-alkyl (Lys215; Ala359; Cys474), pi-pi T-shaped (Trp218), and pi-cation (Lys215). This time, the hydroxyl group between the benzyl rings forms a pi-lone pair interaction with Phe160. Lastly, an intramolecular pi-sigma interaction between one of the aromatic rings and the cycloheptane is enabling stabilizing effects (Fig. 73, Suppl. Fig. 41).

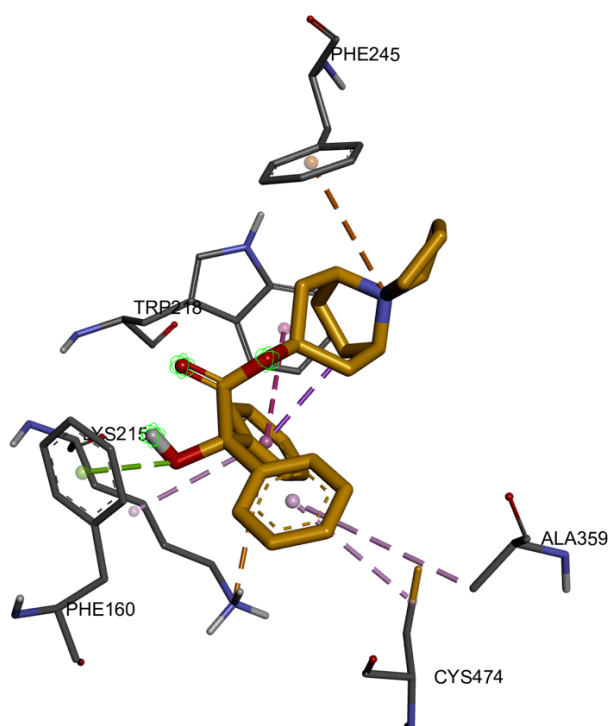


Figure 73: Molecular docking of trospium into mOCT1 from AlphaFold DB by AutoDock 4.2. Shown is here the best ranked binding pose of trospium (orange) in mOCT1 from cluster rank 4 with its interacting amino acids (gray) regarding the binding energy. Following interactions are color-coded: Conventional H-bonds – green bold lines, van der Waals forces – thin green lines, Pi-Alkyl – pink, Donor-Donor – red, Pi-Pi Stacked – purple, Carbon Hydrogen bond; Pi-Donor Hydrogen Bond – mint green, Pi-Sulfur – yellow, Pi-Cation – orange. Heteroatoms are color-coded as well: red – oxygen, blue – nitrogen, yellow – sulfur.

DPF> analysis

perform a ranked cluster analysis

CLUSTER ANALYSIS OF CONFORMATIONS

Number of conformations = 100

RMSD cluster analysis will be performed using the ligand atoms only (30 / 30 total atoms).

Outputting structurally similar clusters, ranked in order of increasing energy.

Number of distinct conformational clusters found = 8, out of 100 runs,
Using an rmsd-tolerance of 2.0 A

CLUSTERING HISTOGRAM

Clus-ter Rank	Lowest Binding Energy	Run	Mean Binding Energy	Num in Clus	Histogram							
					5	10	15	20	25	30	35	
1	-11.02	64	-9.72	17	#####							
2	-10.23	60	-9.42	16	#####							
3	-9.82	17	-9.15	20	#####							
4	-9.67	20	-9.12	40	#####							
5	-9.63	86	-9.37	4	####							
6	-9.29	28	-9.29	1	#							
7	-8.82	78	-8.82	1	#							
8	-7.94	39	-7.94	1	#							

Number of multi-member conformational clusters found = 5, out of 100 runs.

Table 21: Cluster analysis of conformations after molecular docking of trospium into mOCT1 from AlphaFold DB using AutoDock 4.2. Shown is here the summary of pose clustering and binding energy from the docking log file (dlg).

4 Discussion

In 1994, Gründemann *et al.* have isolated complementary DNA from rat kidney encoding a 556-amino-acid membrane protein, called OCT1 for the first time. ^[91] Since then, OCT1 (SLC22A1) is known to be the first identified transporter of the SLC22 family, that belongs to the major facilitator superfamily, possessing over 450 solute carriers or transporters, which are grouped into 52 families. Three years later, in 1997 hOCT1 was cloned exhibiting seventy-eight percent amino acid identity to rOCT1. ^[92] To date, it is known that in the liver, hOCT1 is expressed most abundantly in the sinusoidal membrane of hepatocytes, whereas at lower levels hOCT1 is distributed in various organs and tissues, such as eye, brain, small intestine, kidney, lung, urinary bladder, heart, placenta, and skeletal muscle. ^[45] hOCT1 operates as a facilitated diffusion system transporting structurally diverse organic cations, and uncharged compounds in a sodium- and proton-independent manner and mediating electrogenic cellular influx and efflux (uniport) of organic cations across the plasma membrane. ^[66] Due to its large impact on various physiologic functions in different organs and on pharmacokinetics of various drugs, this transporter was intensively explored regarding biochemical, physiologic, and pharmacological properties. The International Transporter Consortium, the American Food and Drug Administration (FDA) (<https://www.fda.gov/media/134582/download>), as well as the European Medicines Agency (EMA) (https://www.ema.europa.eu/en/documents/scientific-guideline/guideline-investigation-drug-interactions-revision-1_en.pdf) both have proposed preclinical in vitro testing of novel drugs for interaction with hOCT1 due to its clinical significance for pharmacokinetics of drugs. ^[65,68] These include its role in disposition, excretion, drug-drug interactions, and genetic polymorphism. Nevertheless, after two decades of research into OCT1's functional role, it remains uncertain what are the define substrates of this uptake transporter, how OCT1 recognizes and excretes a broad array of ligands, whether this involves specific modifications and interactions with other proteins, and its impact on organ-specific functions. Even though many data rely on experimental tests with *in vivo* models, measurements performed in rodents cannot be directly transferred to humans because of species differences in expression, membrane location, regulation, and substrate specificity between rodents and humans. ^[45,69]

As molecular understanding of ligand recognition and the mechanism by which OCT1 mediates substrate translocation into the cells are of great interests, *in silico* modeling of two approved drugs, fenoterol and trospium, was performed into human and mouse

OCT1. Given that transport kinetics in both substrates differ in each organism, structure-based methods were performed to investigate crucial interactions in the protein-ligand complex. ^[89] In this context, the present work aimed at characterizing single amino acids, which are involved in substrate interaction of OCT1 and confer the species differences so that a better understanding of OCT1 polyspecificity is given. Meyer *et al.* ^[89] reports fenoterol as the most affine substrate for hOCT1, confirming previous observations of Haberkorn *et al.* ^[93], whereas trospium was transported with the highest affinity by mOCT1. Site-directed mutagenesis on chimeric constructs provided insights into essential amino acid substitutions in transmembrane helix 1 conferring differences between human and mouse OCT1 substrate recognition. Point mutation of Cys36 (human) to Tyr36 (mouse) reversed uptake kinetics of fenoterol, whereas substitution of Leu32 (mouse) to Phe32 (human) decreased trospium's affinity in mOCT1. Nevertheless, even though both amino acids are in close proximity in TMH1 each substitution showed substrate-specific effects, as the Cys36Tyr substitution affected transport kinetics for fenoterol but not for trospium and vice versa in the substitution of codon 32. ^[89] Interestingly, only amino acids in TMH4, TMH10, and TMH11 provided functional role in OCT1 substrate recognition and ligand interaction by now. ^[71,73,94,95] Moreover, the majority of available data regarding structure-to-function relationships has been generated with the initially identified substrate TEA⁺ and MPP⁺ studying rat OCT1. As it is known, that human and rat OCT1 differ in 120 amino acids each of them can cause alterations in OCT1 function. ^[96] Since there is only little structure-to-function data available comparing rat and human OCT1, *in silico* analyses of this work should fill this lack of knowledge to get a better understanding of OCT1's polyspecificity.

4.1 Experimental findings with AutoDock Vina

The first approach was to perform molecular docking via AutoDock Vina to support experimental findings and to study protein-ligand interactions on a molecular level. In an unbiased manner both ligands were docked into our own generated homology models for human and mouse OCT1. Interestingly, the three best ranked conformations of fenoterol in mOCT1 (Table 4) showed a better performance in affinity compared to hOCT1 (Table 3), with the highest value of -8.3 kcal/mol in mOCT1 and -7.2 kcal/mol in hOCT1. Even if these are only minor differences, the findings do not confirm the 8.1-fold higher affinity in transport of fenoterol with hOCT1 in the experimental results. This could be due to the fact, that almost all conformations bind in a U-shaped manner in both organisms, enabling polar interactions with similar amino acids such as Asn156/157 (TMH2), or Gly477/478 (TMH11), the latter being located within a mechanistically important hinge domain in which substrate binding induces transport-related structural changes. ^[70] Polar interactions with Lys215 and Cys474 were observed several times in mOCT1 but not in hOCT1, whereas Gln362, Gly363, Asp357 have provided repeatedly stabilizing effects in hOCT1 but not in mOCT1. Many residues (Gln362, Gly363, and Gly477) are present in the defined binding regions of previous studies. ^[70,73] Given that AutoDock Vina shows only intramolecular pi interactions of the protein, possible intermolecular pi interactions with the ligand in close proximity were only able to visualize by measuring the distance. In literature cation-pi interactions can be formed up to a distance of 6 Å. ^[97] In both organisms Phe160 has a distance of 3.6 Å to the positively charged nitrogen of fenoterol, enabling stabilizing effects by cation-pi interaction, which is in the range according to literature and supports findings to be critical for the binding in rOCT1. ^[98,99,100] Other than that, Chen *et al.* ^[101] reports T-shaped pi-pi stacking interactions were experimentally found to occur up to a distance of 4.96 Å. In hOCT1 this interaction is provided by Phe32 with a distance ranging from 3.6 – 3.9 Å, which is replaced by leucine in mOCT1. Previous studies have concluded that pi-sulfur interactions occur at distances between 4 – 6 Å. ^[102,103] The distance of the crucial pi-sulfur interaction at codon 36 is between 3.3 – 5.1 Å supporting experimental results of Meyer *et al.*

Docking results of trospium comply with the experimental findings, having lower binding affinities in hOCT1 than in mOCT1 (Table 5, and 6). Given that the best ranked conformation in mOCT1 is surrounded by multiple residues forming pi-pi stacking interactions (Tyr36, Phe160, Trp218, Phe245) ranging from 3.5 – 4.1 Å, this gives

explanation on its high binding affinity (-9.8 kcal/mol). The suggested point mutation of Leu32Phe would provide even more stabilizing effects *in silico*, corresponding to the observed increase in trospium uptake. Controversially, in hOCT1 tyrosine is replaced by cysteine disabling the formation of the same network of pi-pi stacking interactions, as the substrate is further away and not in an advantageous conformation. Since the unbiased approach of molecular docking didn't provide the crucial interaction of Asp474 in human or Asp475 in mouse, we then decided to change its orientation in the protein model to increase its likelihood to interact with the ligand's positive charge, as it is suggested in previous mutagenesis studies and homology modeling efforts. [45, 70,71,95,104] However, the binding affinities of fenoterol in human and mouse OCT1 were according to the previous run (Table 7, and 8), contradicting with the experimental results. Interestingly, H-bond interactions with the essential aspartate residue at codon 474/475 were observed in both runs, indicating that the change in direction of the rotamer enabled the formation of stabilizing effects. Like the unbiased docking, amino acids being conserved in both organisms and forming polar interactions are: Gly363/364, Gly477/Gly478. The differences in residues are Asn157, Lys215, and Cys474, which are present in mOCT1 interaction, whereas Asp357 and Gln362 are present in hOCT1.

The rotamer docking approach in trospium provided binding affinities as seen in the point mutations, with the adjustment of even higher values in mOCT1 (Table 10). As Gly364 (mOCT1), Gln241 (hOCT1), Gln362 (hOCT1), and Gly363 (hOCT1) were the only observed polar interaction for the three best ranked binding poses, docking results indicate that stabilizing effects are mainly provided by pi-pi stacking interactions.

Our next approach was to take advantage of the high-accuracy protein structure model of hOCT1 from AlphaFold DB with its active site being predicted with very high confidence. First, both substrates were docked again in an unbiased manner into the hOCT1. Interestingly, calculated binding affinities (Table 12) for fenoterol by AutoDock Vina were elevated compared to previous approaches. Reasons could be due to newly introduced residues forming polar interactions such as Lys214, having a positively charged sidechain at physiological pH, Thr245, a polar amino acid with a neutral side chain and Glu386, having a negatively charged side chain at physiological pH (Fig. 39 – 41). Similarly, results for trospium showed also increased calculated binding affinities (Table 13) although not a single polar interaction was observed for the best three ranked binding poses.

The results indicate, that stabilizing effects are provided again by pi-pi stacking as it is the case for Phe244, which was suggested in previous studies. [73,104]

Second, in a new approach performing flexible docking certain residues (Phe32, Cys36, Phe159, Lys214, Trp217, Phe244, and Asp474) were kept flexible to allow for a greater measure of native flexibility or to reveal new conformations, since fully flexible docking methods can enhance pose predictions up to 80-95%. [105] An overlap of the docking results in fenoterol (Fig. 43) showed that almost all side chains stay rigid except Lys214 and Asp474 changing their directions. The flexible docking approach improved the binding affinity for fenoterol up to -8.5 kcal/mol (Table 14), suggesting that this method is a proper way to predict ligand binding by simulating the dynamic behavior for some protein side chains. In all the best ranked binding poses of fenoterol interactions like Cys36, Lys214, Phe244, Glu386, Cys473, and Asp474 are conserved (Fig. 44-46). The same trend regarding the binding affinity was observed in fenoterol with mOCT1 (Table 15). Flexible residues like Leu32, Tyr36, Phe160, and Lys215 changed their direction during the docking runs (Fig. 50). New residues add up to the already provided stabilizing effects, such as Trp355, Tyr362, Leu447, Cys451, and Met467, with Leu447 being in the predicted binding site in previous studies (Fig. 47 - 49). [71,94,98] In addition to intermolecular interactions with Asn157, Lys215, Trp218, and Cys474 the new residues could explain the increased affinity (-9.0 kcal/mol) to mOCT1.

Third and lastly, a rotamer docking approach following previous steps were applied for Asp474 to increase its occurrence rate and its orientation (Fig. 51). For fenoterol, repeating interactions showing polar contacts are Gln241 and Gln447 (Fig. 52 – 54), which both were suggested in other studies. [71,73,94,98] However, resulting binding affinities (Table 16) were lower (- 7.8 kcal/mol) compared to the flexible docking approach, which could be due to the less generated polar interactions. The results of the same approach with Trospium were visualized with Discovery Studio Visualizer since no polar interactions were detected in PyMol. DSV provided repeatedly different type of interactions from residues such as Lys214, Gln241, Phe244, Ile446, and Cys473 (Fig. 55 – 57). Interestingly, phenylalanine at codon 244 enabled stabilizing effects by cation-pi interaction with the positively charged nitrogen. This indicates again its important role in ligand binding and could be one of the reasons for its elevated binding affinity (-8.9 kcal/mol, Table 17).

4.2 Experimental findings with AutoDock 4

Several studies have confirmed through mutagenesis experiments, that the most remarkable amino acid residue of key importance for substrate binding and/or translocation is Asp475 in mouse OCT1. ^[96] It is stated that the interaction with the positive charge of the substrate plays an essential role. ^[71,94,95,98] Since this interaction was only seen for Trp218, Phe244, and Glu386 but not for Asp474/475 molecular docking was performed with AlphaFold's high-accuracy protein structure model using AutoDock 4. The first docking approach reports 27 different clusters for fenoterol in hOCT1. Out of these 27 clusters, cluster rank 4 has the highest number (14) of representative conformations, indicating that this binding pose has a promising role in the protein-ligand complex. Compared to AutoDock Vina, AutoDock 4 calculates a binding energy based on the torsional free energy, intermolecular energy, which is the sum of van der Waals forces, H-bond interactions, desolvation energy, and electrostatic energy, then subtracted from unbound system's energy. The lowest binding energy of the four best ranked binding poses range from -6.22 kcal/mol to -5.66 kcal/mol (Table 18). In the four highest ranked conformations the most prevalent residues forming interactions with the substrate are Cys36 (3), Phe159 (2), Trp217 (3), Phe244 (2), Ser358 (4), Ile446 (2), Cys473 (4), Asp474 (3) (Fig. 63 – 66). Interactions of most interest are Cys36 and Asp474 since both have been shown to be crucial in ligand uptake. However, it is suggested that Cys473 provides stabilizing effects by its pi-sulfur interaction, as it is present in all four conformations. Also, Ser358 seems to apply an important role in stabilizing the ligand by H-bond interactions in all four conformations. Additionally, it is obvious that fenoterol is embedded in various types of pi interactions, whether the residues are aromatic, aliphatic, acidic, or neutral. This broad range of interactions give first insights of OCT1 polyspecificity. ^[96]

Contrary to fenoterol, trospium provides only three out of seven cluster ranks with multi-member conformations in hOCT1. Cluster rank 2 has 74 representative binding modes out of 100 runs, indicating a reasonable orientation in the binding pocket. The lowest binding energies range from -10.07 kcal/mol to -9.31 kcal/mol (Table 19) for the best three ranks. Amino acid residues occurring frequently are Cys36 (2), Phe244 (4), Ile446 (3), Cys473 (3), Asp474 (3) (Fig. 61 – 64). Again, these residues were already provided in fenoterol, pointing to their importance in uptake kinetics. Interestingly, the suggested interaction at codon 32 is not present in none of the listed conformations.

This brings up two assumptions: it could be due to spatial reasons having not enough space to form an interaction with Phe32 due to its aromatic ring, or the aliphatic property in Leu32 is lacking in Phe32.

In mOCT1 the number of representative conformations for each cluster of fenoterol does not correlate to the calculated binding energy, meaning that multi-member conformational clusters are ranked at position one, seven, eight, twelve, and seventeen. This shows that the binding energy alone is not convincing enough, but the number of poses for each representative cluster, indicating the likelihood of this cluster, contributes as well. However, the lowest binding energy calculated by AutoDock 4 is at -6.40 kcal/mol (Table 20), contradicting the experimental results of Meyer *et al.* [89] Frequent residues forming various types of interactions are Leu32 (2) Tyr36 (4), Lys215 (3), Trp218 (2), Phe245 (4), Leu447(2), Cys474 (4), and Asp475 (4). Interestingly, Tyr36 is involved in all interactions of the four analyzed conformations, even though it is said that point mutation at codon 36 resulted in reverse uptake kinetics, resulting mOCT1 as a low affinity high-capacity transporter for fenoterol. Also, Phe245, Cys474, and Asp475 are present, suggesting that they contribute to this finding. Nevertheless, there is no clear trend confirming the observed experimental events, as most of the present amino acids form stabilizing effects in hOCT1.

Lastly, out of 100 runs performing molecular docking of trospium into mOCT1, the high affinity low-capacity transporter according to experimental results, cluster analysis of conformations yielded eight different cluster ranks, comprising five multi-member conformational clusters. The latter was distributed between the first four best ranked clusters having 17, 16, 20, and 40 members in each cluster rank, respectively. Again, stabilizing effects of Phe160, Lys215, Trp218, and Phe245 are very frequent. The crucial amino acid at codon 32 is also present in two out of four analyses, supporting experimental results by single point mutations. Interestingly, experimental findings correspond to the calculated binding energies as they're higher for mOCT1 (-11.02 kcal/mol) than to hOCT1 (-10.07 kcal/mol).

4.3 Concluding remarks

Eventually, the outcome of molecular docking using AutoDock 4 is different compared to AutoDock Vina. Even though AutoDock Vina's performance is much faster, it is restricted to polar contacts, showing only H-bond interactions, whereas AutoDock 4 executes slower, but provides various types of inter- and intramolecular interactions of the ligand-protein complex. Generally, it appears that certain residues occur repeatedly and interact with the respective substrate in a network, suggesting that not a single amino acid alone but together with several other residues they mediate substrate translocation into the cells. Given that the globally accepted interaction at codon 474 (human) and 475 (mouse) is present in quite a few bindings for both substrates, prior studies were confirmed once more. *In silico* analyses enabled us to confirm the experimentally identified interaction between the second phenol ring of fenoterol and Cys36 in hOCT1. Also, molecular docking suggested that two amino acids, Phe32, and Phe244, interact with the second ring of fenoterol. However, none was experimentally identified by Meyer *et al.*, but Gebauer *et al.* suggested Phe244 in a recent publication to be of interest for the (S, S) enantiomer of fenoterol. ^[106] In addition to that, both residues are supported in several binding conformations by a network of pi stacking interaction such as Phe159/Phe160, Lys214/215, and Trp217/218, indicating that they ensure stabilizing effects to the complex.

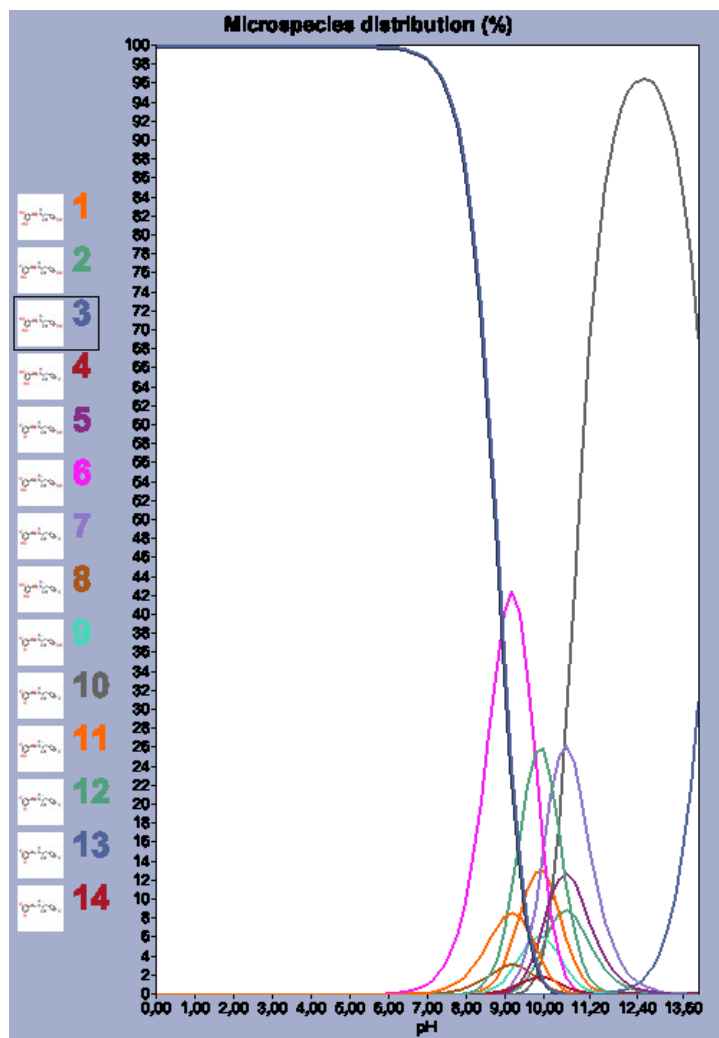
On the other hand, molecular docking provided the essential Leu32 interaction with trospium in mOCT1, which is of key importance for its high affinity. As seen before, the benzyl ring of the substrate is mostly embedded in a network of pi-pi and cation pi interactions by previously mentioned amino residues. Interestingly, Cys474 and Ala359 are in two of the four different clusters present at the same time, suggesting that both cooperate to stabilize one of the aromatic rings. As the interaction at codon 359 is not conserved in human OCT1, it is assumed that this interaction adds to its transport kinetics.

This work confirms the experimentally determined important amino acids in transmembrane helix 1 in OCT1 substrate recognition of Meyer *et al.* study, using *in silico* docking. Molecular docking supports the experimental identified interaction between the second phenol ring of fenoterol and Cys36 in hOCT1, as well as the crucial interaction between trospium and Leu32 in mOCT1. However, we should clarify that they were not present in all the conformations of the four cluster ranks with the highest binding affinity or highest number of representative poses. Thus, this shows that without experimental data, docking would not be able to clearly identify any of these essential residues for the high affinity interactions. Surprisingly, *in silico* docking has suggested new amino acids, such as Phe32 and Phe244 for fenoterol and Cys474 together with Ala359 for trospium, but none of them has been experimentally confirmed yet.

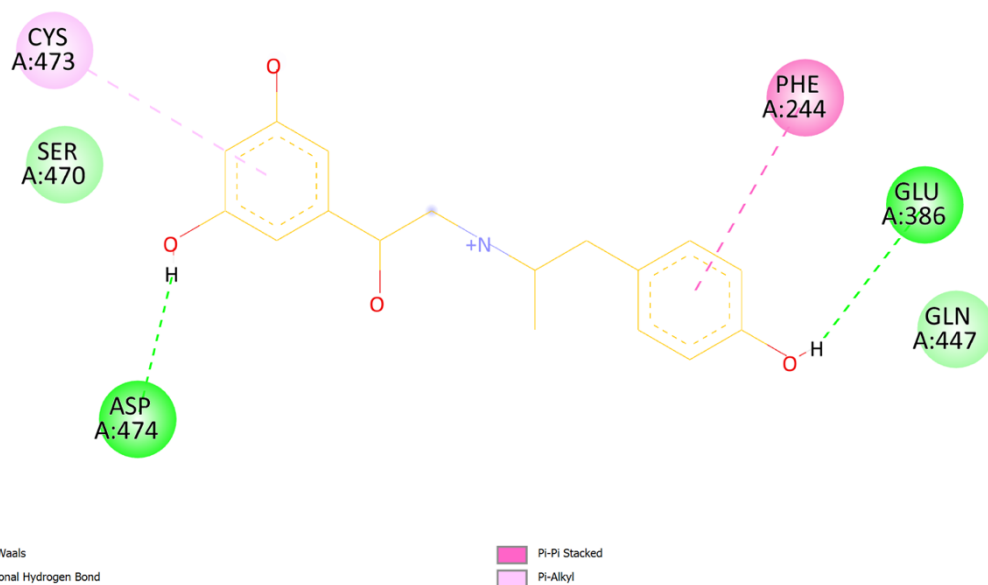
In conclusion, this study supports experimental findings for new amino acids being important for the mechanism of OCT1 polyspecificity. However, it is believed that not just single residues, but several are of importance as suggested with the network of pi-pi stacking interactions. Thus, this leaves space for a follow-up study, investigating other substrates using molecular docking. Also, it would be of interest to repeat all approaches with different grid boxes to redefine the search space of the ligand.

5 Appendix

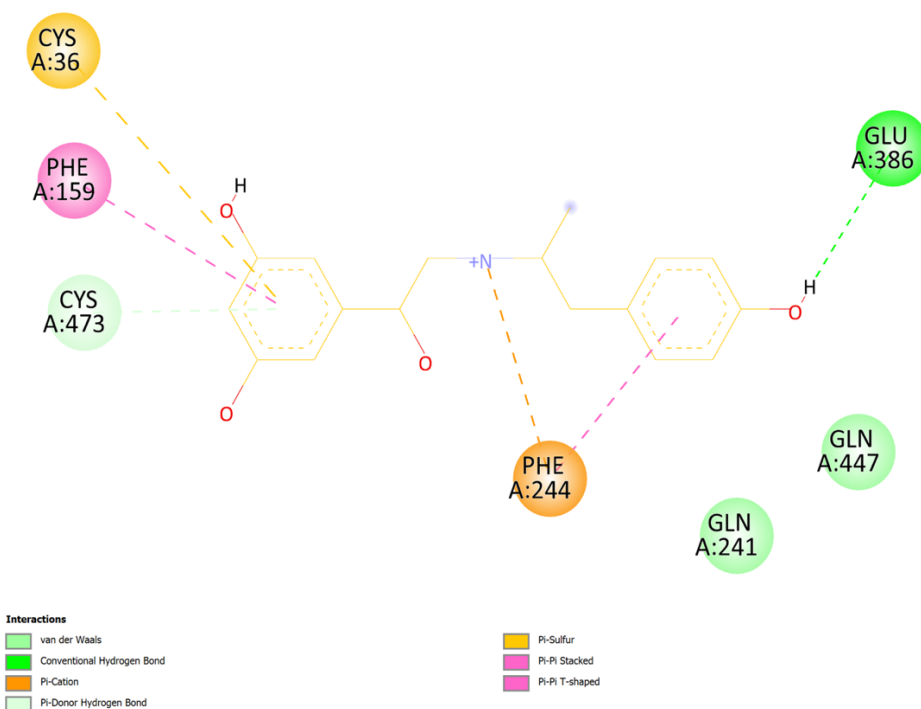
5.1 Supplementary Figures



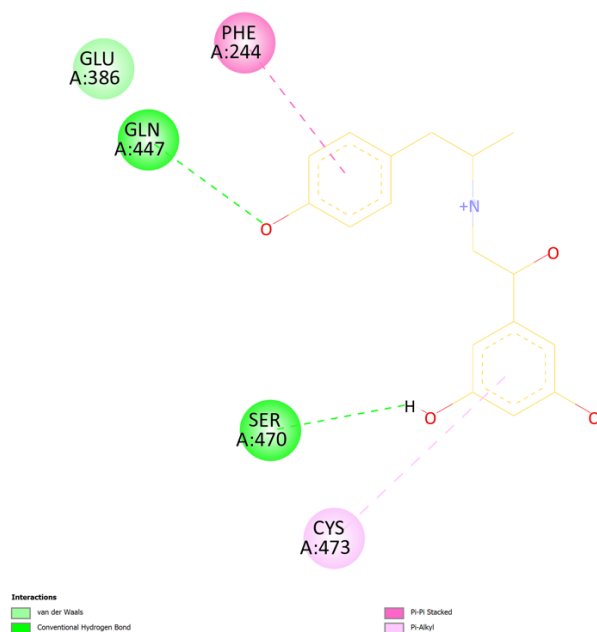
Supplemental Figure 1: Protonation states of fenoterol. Calculation results of microspecies distribution according to its pH.



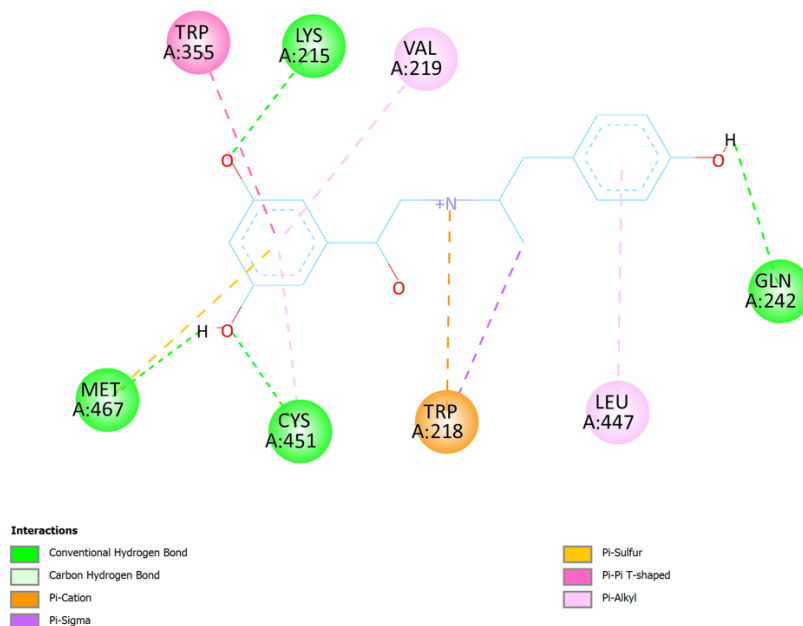
Supplemental Figure 2: Flexible docking of fenoterol into hOCT1 from AlphaFold DB using AutoDock Vina. Shown is here the best ranked binding pose of fenoterol (green) in hOCT1 out of 20 conformations regarding the binding affinity with its interacting amino residues (grey) in 2D. Following interactions are color-coded: Conventional H-bonds – green, Pi-Alkyl – pink, Donor-Donor – red, Pi-Pi Stacked – purple, Pi-Donor; Pi-Sulfur – mint green, Pi-Sulfur – yellow, Pi-Cation – orange. Heteroatoms are color-coded as well: red – oxygen, blue – nitrogen, yellow – sulfur.



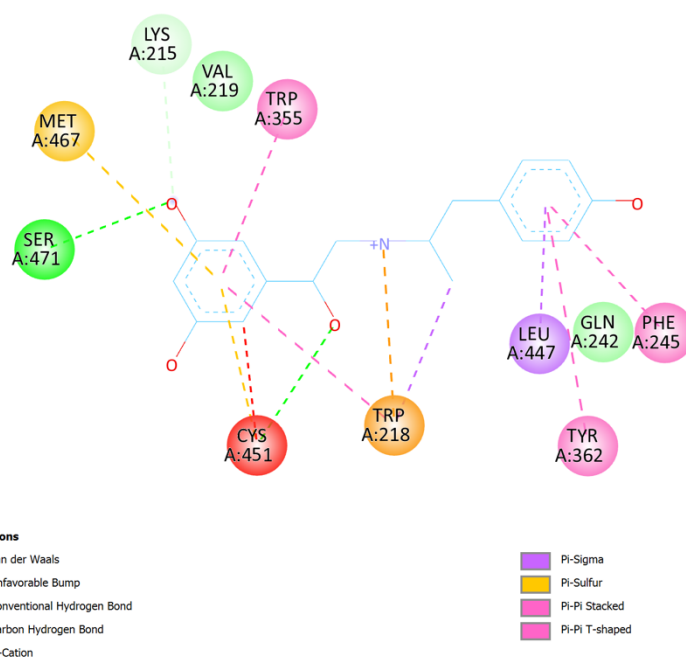
Supplemental Figure 3: Flexible docking of fenoterol into hOCT1 from AlphaFold DB using AutoDock Vina. Shown is here the second best ranked binding pose of fenoterol in hOCT1 out of 20 conformations regarding the binding affinity with its interacting amino residues in 2D. Following interactions are color-coded: Conventional H-bonds – green, Pi-Alkyl – pink, Donor-Donor – red, Pi-Pi Stacked – purple, Pi-Donor; Pi-Sulfur – mint green, Pi-Sulfur – yellow, Pi-Cation – orange. Heteroatoms are color-coded as well: red – oxygen, blue – nitrogen, yellow – sulfur.



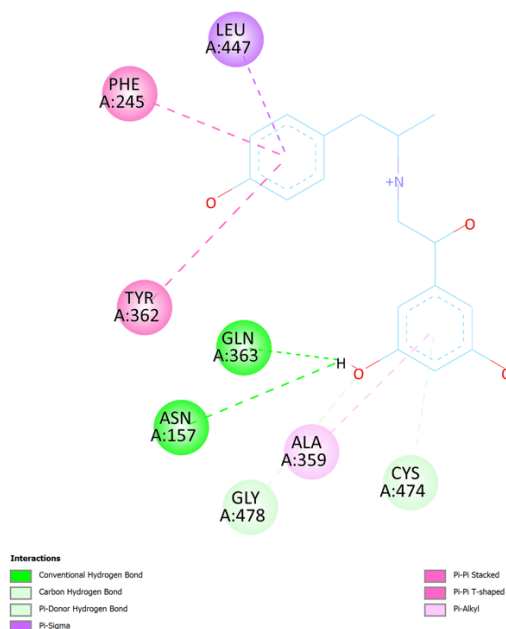
Supplemental Figure 4: Flexible docking of fenoterol into hOCT1 from AlphaFold DB using AutoDock Vina. Shown is here the third best ranked binding pose of fenoterol in hOCT1 out of 20 conformations regarding the binding affinity with its interacting amino residues in 2D. Following interactions are color-coded: Conventional H-bonds – green, Pi-Alkyl – pink, Donor-Donor – red, Pi-Pi Stacked – purple, Pi-Donor; Pi-Sulfur – mint green, Pi-Sulfur – yellow, Pi-Cation – orange. Heteroatoms are color-coded as well: red – oxygen, blue – nitrogen, yellow – sulfur.



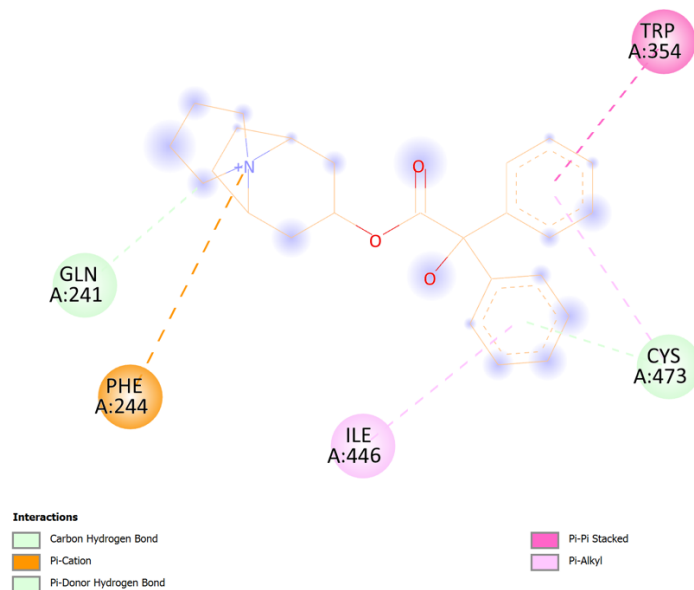
Supplemental Figure 5: Flexible docking of fenoterol into mOCT1 from AlphaFold DB using AutoDock Vina. Shown is here the best ranked binding pose of fenoterol in hOCT1 out of 20 conformations regarding the binding affinity with its interacting amino residues in 2D. Following interactions are color-coded: Conventional H-bonds – green, Pi-Alkyl – pink, Donor-Donor – red, Pi-Pi Stacked – purple, Pi-Donor; Pi-Sulfur – mint green, Pi-Sulfur – yellow, Pi-Cation – orange. Heteroatoms are color-coded as well: red – oxygen, blue – nitrogen, yellow – sulfur.



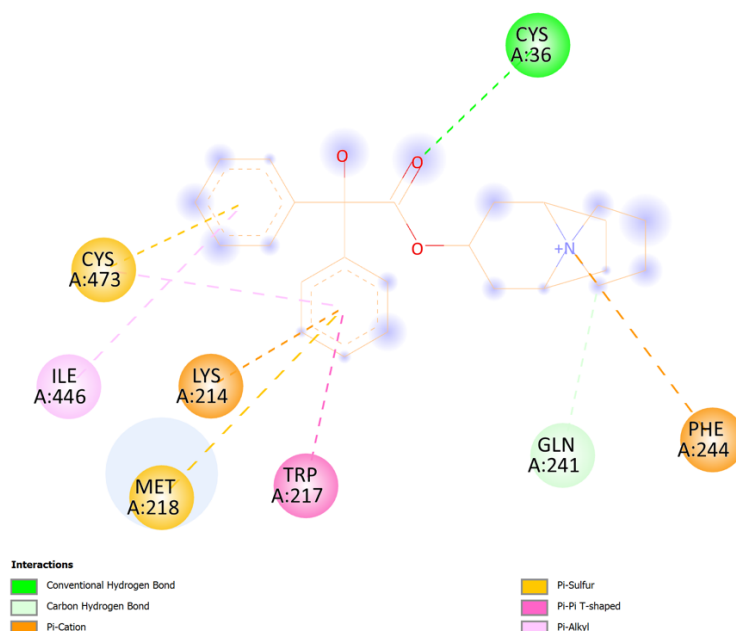
Supplemental Figure 6: Flexible docking of fenoterol into mOCT1 from AlphaFold DB using AutoDock Vina. Shown is here the second best ranked binding pose of fenoterol in hOCT1 out of 20 conformations regarding the binding affinity with its interacting amino residues in 2D. Following interactions are color-coded: Conventional H-bonds – green, Pi-Alkyl – pink, Donor-Donor – red, Pi-Pi Stacked – purple, Pi-Donor; Pi-Sulfur – mint green, Pi-Sulfur – yellow, Pi-Cation – orange. Heteroatoms are color-coded as well: red – oxygen, blue – nitrogen, yellow – sulfur.



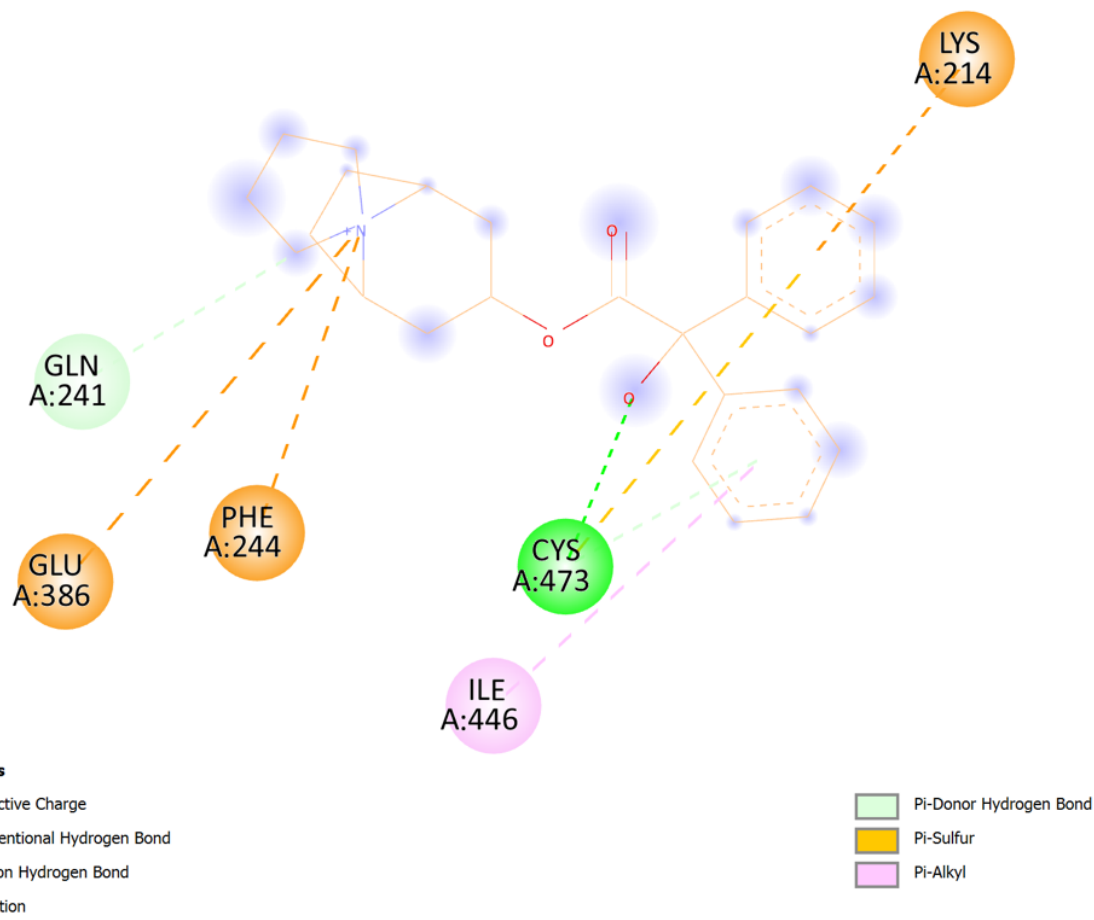
Supplemental Figure 7: Flexible docking of fenoterol into mOCT1 from AlphaFold DB using AutoDock Vina. Shown is here the third best ranked binding pose of fenoterol in hOCT1 out of 20 conformations regarding the binding affinity with its interacting amino residues in 2D. Following interactions are color-coded: Conventional H-bonds – green, Pi-Alkyl – pink, Donor-Donor – red, Pi-Pi Stacked – purple, Pi-Donor; Pi-Sulfur – mint green, Pi-Sulfur – yellow, Pi-Cation – orange. Heteroatoms are color-coded as well: red – oxygen, blue – nitrogen, yellow – sulfur.



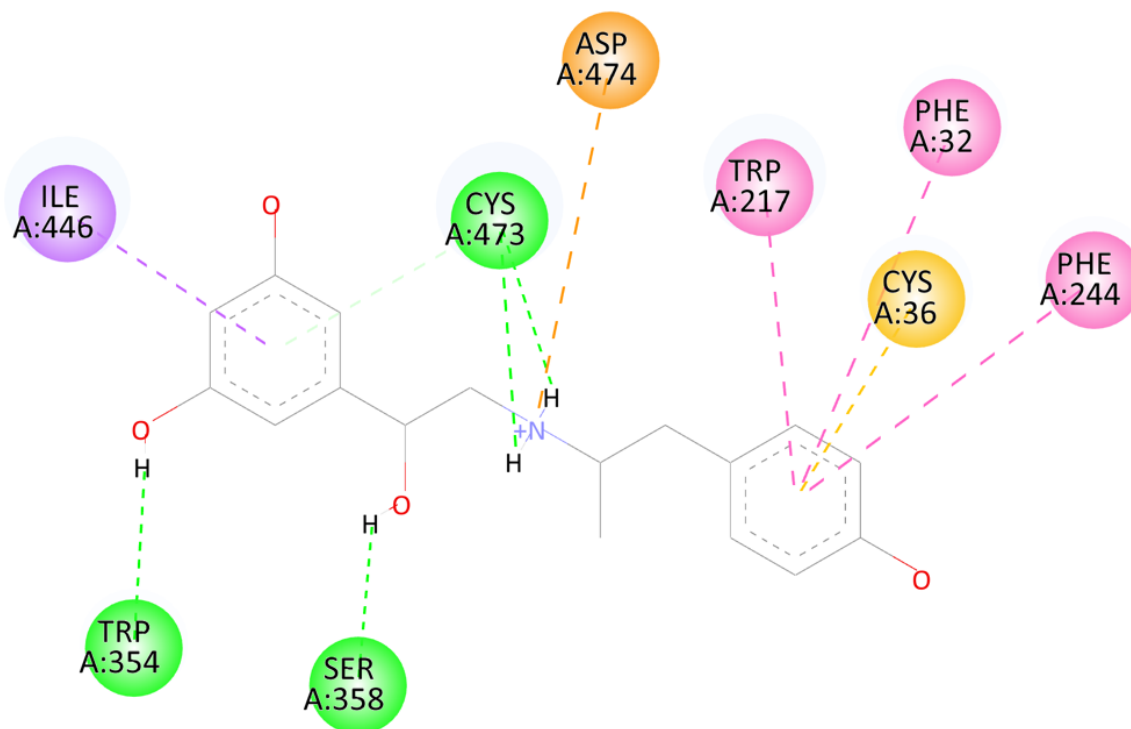
Supplemental Figure 8: Rotamer docking of trospium into hOCT1 from AlphaFold DB using AutoDock Vina. Shown is here the best ranked binding pose of trospium in hOCT1 out of 20 conformations regarding the binding affinity with its interacting amino residues in 2D. Following interactions are color-coded: Conventional H-bonds – green bold lines, van der Waals forces – thin green lines, Pi-Alkyl – pink, Donor-Donor – red, Pi-Pi Stacked – purple, Carbon Hydrogen bond; Pi-Donor Hydrogen Bond – mint green, Pi-Sulfur – yellow, Pi-Cation – orange. Heteroatoms are color-coded as well: red – oxygen, blue – nitrogen, yellow – sulfur.



Supplemental Figure 9: Rotamer docking of trospium into hOCT1 from AlphaFold DB using AutoDock Vina. Shown is here the second best ranked binding pose of trospium in hOCT1 out of 20 conformations regarding the binding affinity with its interacting amino residues in 2D. Following interactions are color-coded: Conventional H-bonds – green bold lines, van der Waals forces – thin green lines, Pi-Alkyl – pink, Donor-Donor – red, Pi-Pi Stacked – purple, Carbon Hydrogen bond; Pi-Donor Hydrogen Bond – mint green, Pi-Sulfur – yellow, Pi-Cation – orange. Heteroatoms are color-coded as well: red – oxygen, blue – nitrogen, yellow – sulfur.



Supplemental Figure 10: Rotamer docking of trospium into hOCT1 from AlphaFold DB using AutoDock Vina. Shown is here the second best ranked binding pose of trospium in hOCT1 out of 20 conformations regarding the binding affinity with its interacting amino residues in 2D. Following interactions are color-coded: Conventional H-bonds – green bold lines, van der Waals forces – thin green lines, Pi-Alkyl – pink, Donor-Donor – red, Pi-Pi Stacked – purple, Carbon Hydrogen bond; Pi-Donor Hydrogen Bond – mint green, Pi-Sulfur – yellow, Pi-Cation – orange. Heteroatoms are color-coded as well: red – oxygen, blue – nitrogen, yellow – sulfur.



Interactions

- Attractive Charge
- Conventional Hydrogen Bond
- Pi-Donor Hydrogen Bond

- Pi-Sigma
- Pi-Sulfur
- Pi-Pi T-shaped

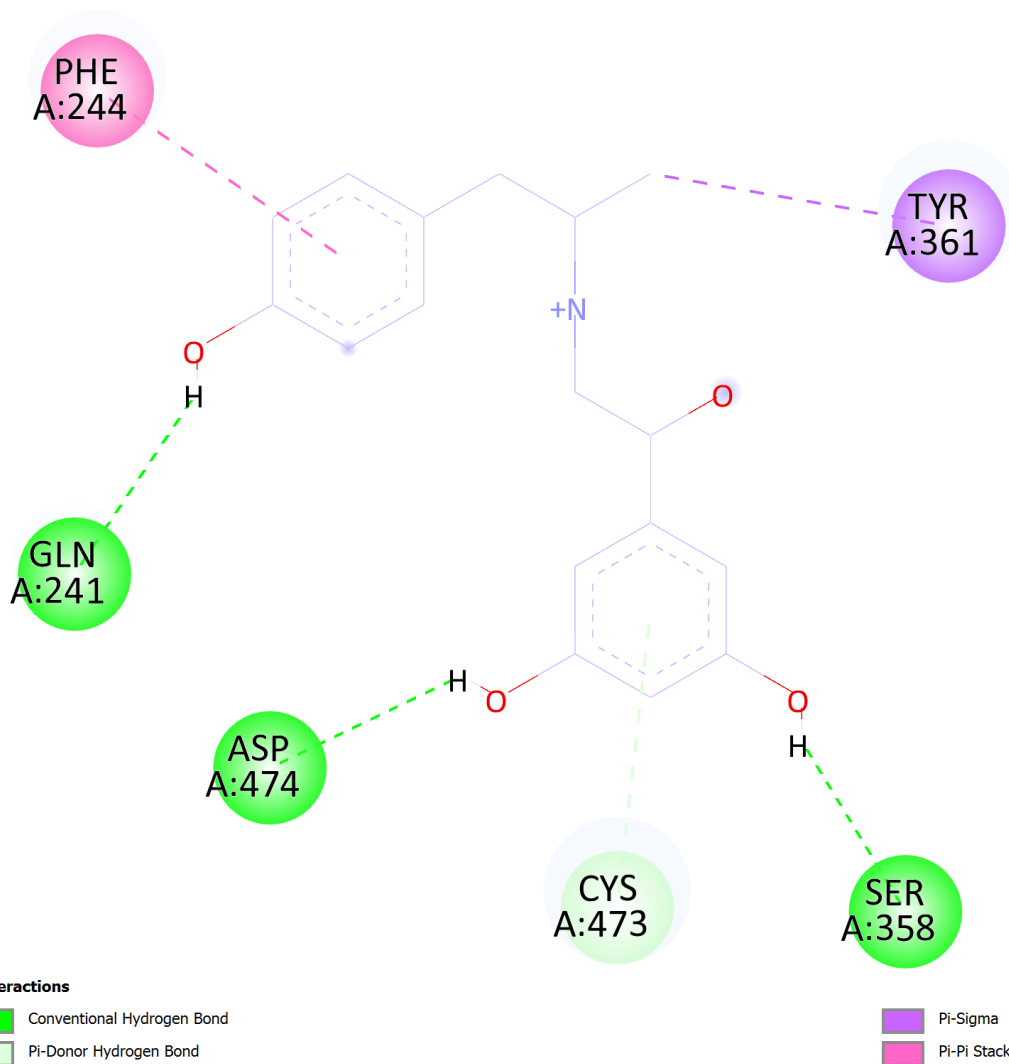
Supplemental Figure 11: Molecular docking of fenoterol into hOCT1 from AlphaFold DB using AutoDock 4.2. Shown is here the third best ranked binding pose of fenoterol in hOCT1 out of 14 conformations in cluster rank 4 regarding the binding energy with its interacting amino residues in 2D. Following interactions are color-coded: Conventional H-bonds – green bold lines, van der Waals forces – thin green lines, Pi-Alkyl – pink, Donor-Donor – red, Pi-Pi Stacked – purple, Carbon Hydrogen bond; Pi-Donor Hydrogen Bond – mint green, Pi-Sulfur – yellow, Pi-Cation – orange. Heteroatoms are color-coded as well: red – oxygen, blue – nitrogen, yellow – sulfur.

```

DOCKED: MODEL      80
DOCKED: USER      Run = 80
DOCKED: USER      DPF = ./AF_Fenoterol.dpf
DOCKED: USER
DOCKED: USER      Estimated Free Energy of Binding      = -5.38 kcal/mol [(1)+(2)+(3)-(4)]
DOCKED: USER      Estimated Inhibition Constant, Ki    = 113.19 uM (micromolar) [Temperature = 298.15 K]
DOCKED: USER
DOCKED: USER      (1) Final Intermolecular Energy      = -8.37 kcal/mol
DOCKED: USER          vdW + Hbond + desolv Energy      = -8.14 kcal/mol
DOCKED: USER          Electrostatic Energy            = -0.23 kcal/mol
DOCKED: USER      (2) Final Total Internal Energy      = -2.39 kcal/mol
DOCKED: USER      (3) Torsional Free Energy           = +2.98 kcal/mol
DOCKED: USER      (4) Unbound System's Energy [(2)]   = -2.39 kcal/mol

```

Supplemental Figure 12: Molecular docking of fenoterol into hOCT1 using AutoDock 4.2. Shown is here the binding energy of run 80 of cluster rank 4.



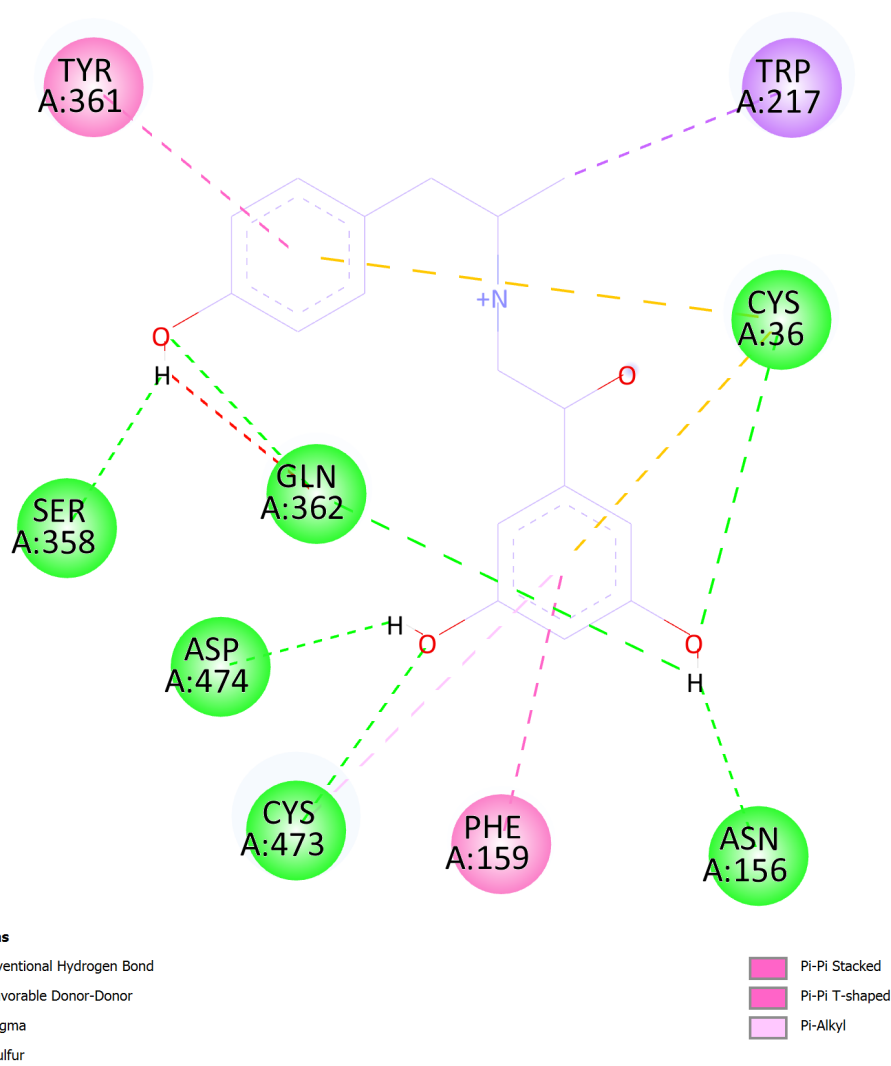
Supplemental Figure 13: Molecular docking of fenoterol into hOCT1 from AlphaFold DB using AutoDock 4.2. Shown is here the best ranked binding pose of fenoterol in hOCT1 out of 4 conformations in cluster rank 1 regarding the binding energy with its interacting amino residues in 2D. Following interactions are color-coded: Conventional H-bonds – green bold lines, van der Waals forces – thin green lines, Pi-Alkyl – pink, Donor-Donor – red, Pi-Pi Stacked – purple, Carbon Hydrogen bond; Pi-Donor Hydrogen Bond – mint green, Pi-Sulfur – yellow, Pi-Cation – orange. Heteroatoms are color-coded as well: red – oxygen, blue – nitrogen, yellow – sulfur.

```

MODEL          5
USER           Run = 5
USER           Cluster Rank = 1
USER           Number of conformations in this cluster = 4
USER
USER           RMSD from reference structure           = 5.272 A
USER
USER           Estimated Free Energy of Binding         = -6.22 kcal/mol [(1)+(2)+(3)-(4)]
USER           Estimated Inhibition Constant, Ki        = 27.54 uM (micromolar) [Temperature = 298.15 K]
USER
USER           (1) Final Intermolecular Energy         = -9.20 kcal/mol
USER               vdW + Hbond + desolv Energy         = -8.91 kcal/mol
USER               Electrostatic Energy                 = -0.30 kcal/mol
USER           (2) Final Total Internal Energy          = -1.15 kcal/mol
USER           (3) Torsional Free Energy                = +2.98 kcal/mol
USER           (4) Unbound System's Energy [(2)]       = -1.15 kcal/mol

```

Supplemental Figure 14: Molecular docking of fenoterol into hOCT1 using AutoDock 4.2. Shown is here the binding energy of run 5, the energetically most favored representative of cluster rank 1.

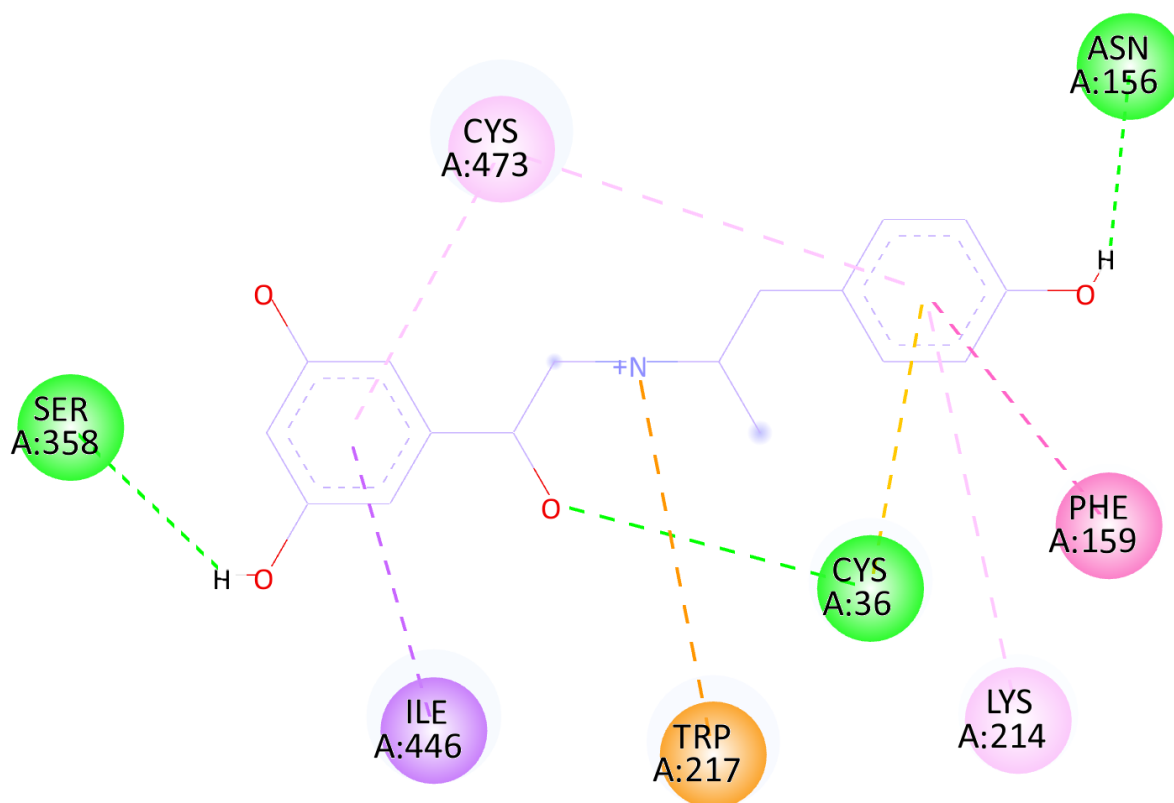


Supplemental Figure 15: Molecular docking of fenoterol into hOCT1 from AlphaFold DB using AutoDock 4.2. Shown is here the best ranked binding pose of fenoterol in hOCT1 out of 5 conformations in cluster rank 2 regarding the binding energy with its interacting amino residues in 2D. Following interactions are color-coded: Conventional H-bonds – green bold lines, van der Waals forces – thin green lines, Pi-Alkyl – pink, Donor-Donor – red, Pi-Pi Stacked – purple, Carbon Hydrogen bond; Pi-Donor Hydrogen Bond – mint green, Pi-Sulfur – yellow, Pi-Cation – orange. Heteroatoms are color-coded as well: red – oxygen, blue – nitrogen, yellow – sulfur.

```

MODEL          93
USER          Run = 93
USER          Cluster Rank = 2
USER          Number of conformations in this cluster = 5
USER          RMSD from reference structure          = 3.905 A
USER          Estimated Free Energy of Binding      = -6.10 kcal/mol [(1)+(2)+(3)-(4)]
USER          Estimated Inhibition Constant, Ki    = 34.05 uM (micromolar) [Temperature = 298.15 K]
USER          (1) Final Intermolecular Energy      = -9.08 kcal/mol
USER          vdW + Hbond + desolv Energy          = -8.83 kcal/mol
USER          Electrostatic Energy                 = -0.25 kcal/mol
USER          (2) Final Total Internal Energy       = -1.98 kcal/mol
USER          (3) Torsional Free Energy            = +2.98 kcal/mol
USER          (4) Unbound System's Energy [(2)]    = -1.98 kcal/mol
  
```

Supplemental Figure 16: Molecular docking of fenoterol into hOCT1 using AutoDock 4.2. Shown is here the binding energy of run 93, the energetically most favored representative of cluster rank 2.



Interactions

■ Conventional Hydrogen Bond
■ Pi-Cation
■ Pi-Sigma

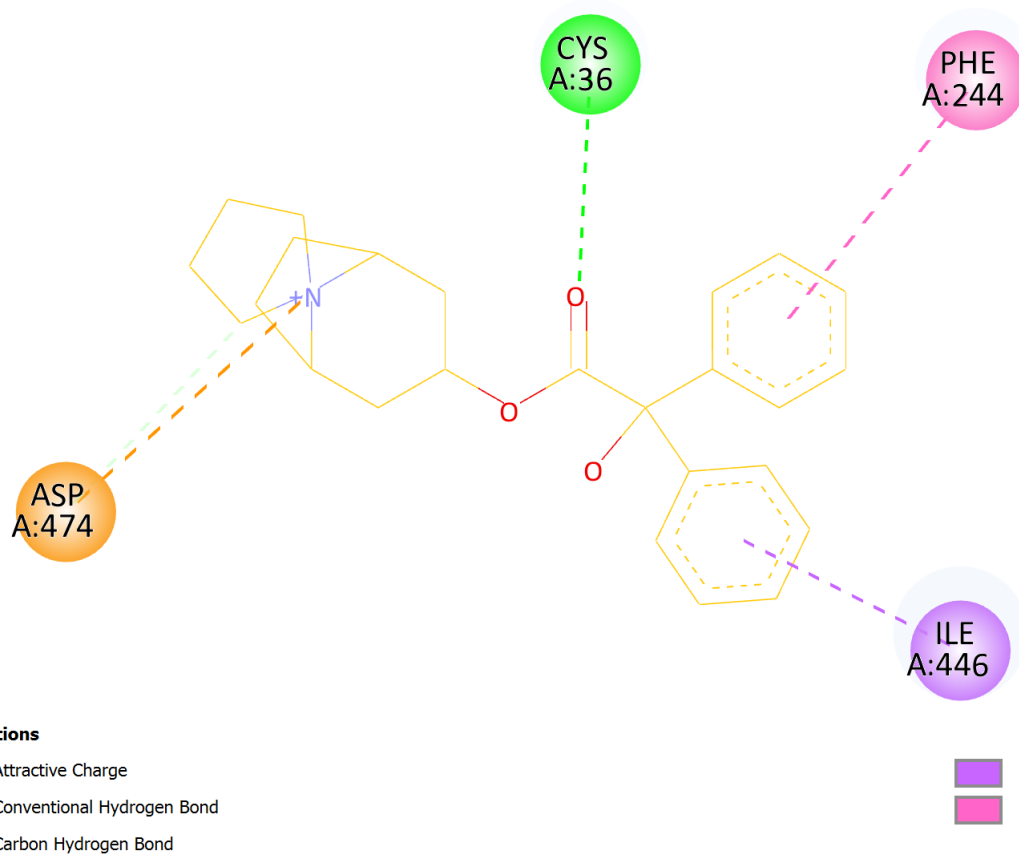
■ Pi-Sulfur
■ Pi-Pi T-shaped
■ Pi-Alkyl

Supplemental Figure 17: Molecular docking of fenoterol into hOCT1 from AlphaFold DB using AutoDock 4.2. Shown is here the best ranked binding pose of fenoterol in hOCT1 out of 7 conformations in cluster rank 3 regarding the binding energy with its interacting amino residues in 2D. Following interactions are color-coded: Conventional H-bonds – green bold lines, van der Waals forces – thin green lines, Pi-Alkyl – pink, Donor-Donor – red, Pi-Pi Stacked – purple, Carbon Hydrogen bond; Pi-Donor Hydrogen Bond – mint green, Pi-Sulfur – yellow, Pi-Cation – orange. Heteroatoms are color-coded as well: red – oxygen, blue – nitrogen, yellow – sulfur.

```

MODEL      22
USER      Run = 22
USER      Cluster Rank = 3
USER      Number of conformations in this cluster = 7
USER
USER      RMSD from reference structure      = 4.194 A
USER
USER      Estimated Free Energy of Binding   = -5.67 kcal/mol [(1)+(2)+(3)-(4)]
USER      Estimated Inhibition Constant, Ki = 70.37 uM (micromolar) [Temperature = 298.15 K]
USER
USER      (1) Final Intermolecular Energy   = -8.65 kcal/mol
USER      vdW + Hbond + desolv Energy       = -8.46 kcal/mol
USER      Electrostatic Energy              = -0.19 kcal/mol
USER      (2) Final Total Internal Energy    = -2.19 kcal/mol
USER      (3) Torsional Free Energy          = +2.98 kcal/mol
USER      (4) Unbound System's Energy [(2)] = -2.19 kcal/mol
  
```

Supplemental Figure 18: Molecular docking of fenoterol into hOCT1 using AutoDock 4.2. Shown is here the binding energy of run 22, the energetically most favored representative of cluster rank 3.

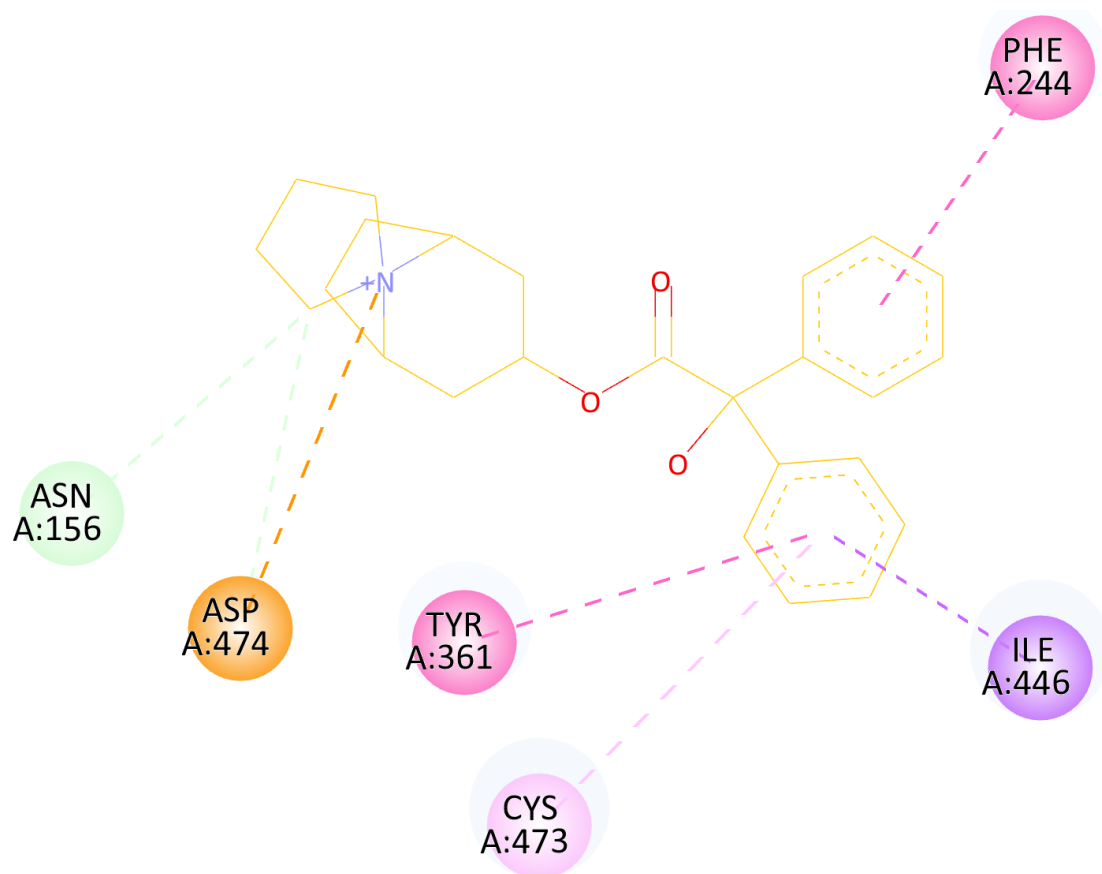


Supplemental Figure 19: Molecular docking of trospium into hOCT1 from AlphaFold DB using AutoDock 4.2. Shown is here the best ranked binding pose of trospium in hOCT1 out of 5 conformations in cluster rank 1 regarding the binding energy with its interacting amino residues in 2D. Following interactions are color-coded: Conventional H-bonds – green bold lines, van der Waals forces – thin green lines, Pi-Alkyl – pink, Donor-Donor – red, Pi-Pi Stacked – purple, Carbon Hydrogen bond; Pi-Donor Hydrogen Bond – mint green, Pi-Sulfur – yellow, Pi-Cation – orange. Heteroatoms are color-coded as well: red – oxygen, blue – nitrogen, yellow – sulfur.

```

MODEL          3
USER           Run = 3
USER           Cluster Rank = 1
USER           Number of conformations in this cluster = 5
USER
USER           RMSD from reference structure           = 5.890 A
USER
USER           Estimated Free Energy of Binding        = -10.07 kcal/mol  [(1)+(2)+(3)-(4)]
USER           Estimated Inhibition Constant, Ki      = 41.64 nM (nanomolar)  [Temperature = 298.15 K]
USER
USER           (1) Final Intermolecular Energy       = -11.86 kcal/mol
USER               vdW + Hbond + desolv Energy       = -11.56 kcal/mol
USER               Electrostatic Energy              = -0.30 kcal/mol
USER           (2) Final Total Internal Energy        = -1.89 kcal/mol
USER           (3) Torsional Free Energy              = +1.79 kcal/mol
USER           (4) Unbound System's Energy [(2)]     = -1.89 kcal/mol
  
```

Supplemental Figure 20: Molecular docking of trospium into hOCT1 using AutoDock 4.2. Shown is here the binding energy of run 3, the energetically most favored representative of cluster rank 1.



Interactions

 Attractive Charge
 Carbon Hydrogen Bond
 Pi-Sigma

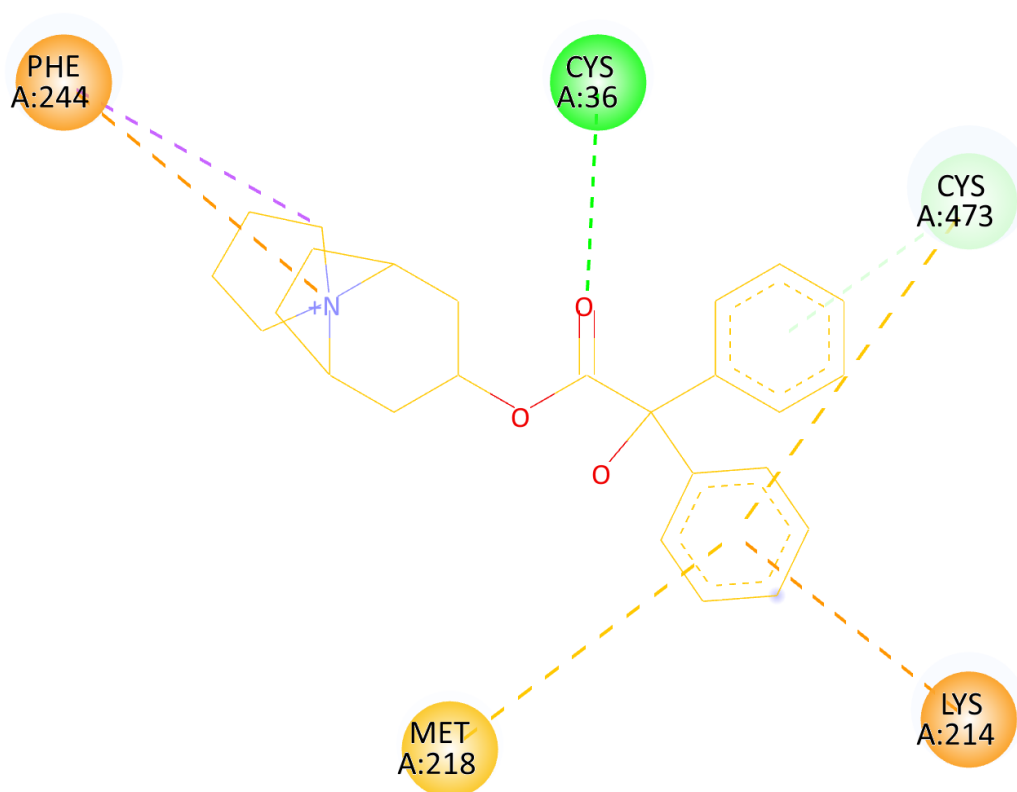
 Pi-Pi Stacked
 Pi-Pi T-shaped
 Pi-Alkyl

Supplemental Figure 21: Molecular docking of trospium into hOCT1 from AlphaFold DB using AutoDock 4.2. Shown is here the best ranked binding pose of trospium in hOCT1 out of 74 conformations in cluster rank 2 regarding the binding energy with its interacting amino residues in 2D. Following interactions are color-coded: Conventional H-bonds – green bold lines, van der Waals forces – thin green lines, Pi-Alkyl – pink, Donor-Donor – red, Pi-Pi Stacked – purple, Carbon Hydrogen bond; Pi-Donor Hydrogen Bond – mint green, Pi-Sulfur – yellow, Pi-Cation – orange. Heteroatoms are color-coded as well: red – oxygen, blue – nitrogen, yellow – sulfur.




```

MODEL      13
USER      Run = 13
USER      Cluster Rank = 2
USER      Number of conformations in this cluster = 74
USER
USER      RMSD from reference structure      = 6.069 A
USER
USER      Estimated Free Energy of Binding   = -9.39 kcal/mol [(1)+(2)+(3)-(4)]
USER      Estimated Inhibition Constant, Ki = 131.01 nM (nanomolar) [Temperature = 298.15 K]
USER
USER      (1) Final Intermolecular Energy   = -11.18 kcal/mol
USER          vdW + Hbond + desolv Energy   = -11.07 kcal/mol
USER          Electrostatic Energy         = -0.11 kcal/mol
USER      (2) Final Total Internal Energy   = -2.83 kcal/mol
USER      (3) Torsional Free Energy         = +1.79 kcal/mol
USER      (4) Unbound System's Energy [(2)] = -2.83 kcal/mol
  
```

Supplemental Figure 22: Molecular docking of trospium into hOCT1 using AutoDock 4.2. Shown is here the binding energy of run 13, the energetically most favored representative of cluster rank 2.



Interactions

	Conventional Hydrogen Bond
	Pi-Cation
	Pi-Donor Hydrogen Bond

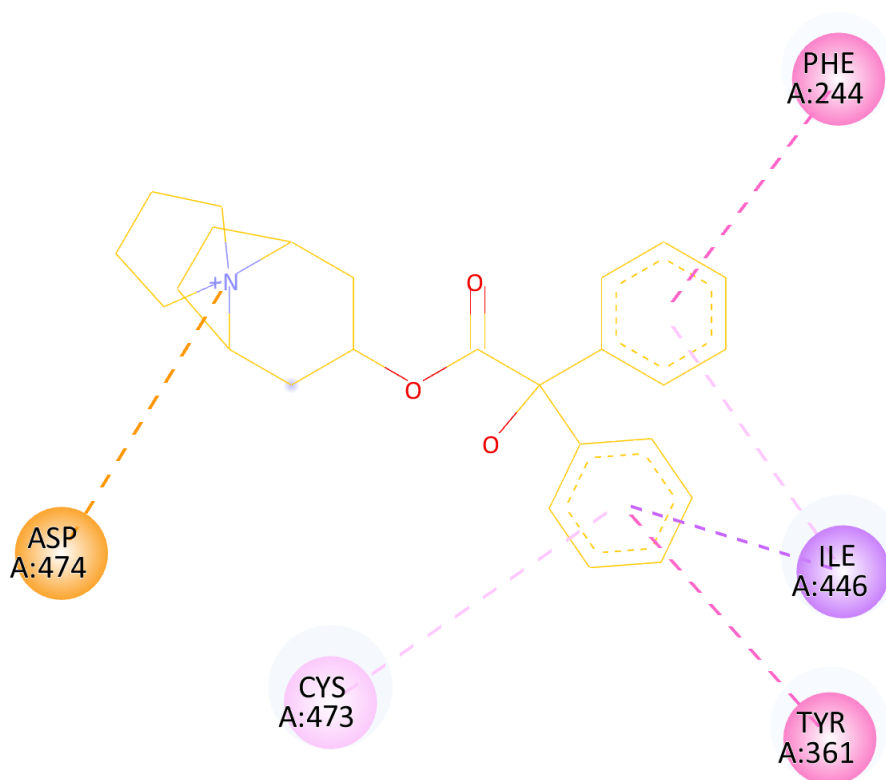
	Pi-Sigma
	Pi-Sulfur
	Pi-Alkyl

Supplemental Figure 23: Molecular docking of trospium into hOCT1 from AlphaFold DB using AutoDock 4.2. Shown is here the best ranked binding pose of trospium in hOCT1 out of 16 conformations in cluster rank 3 regarding the binding energy with its interacting amino residues in 2D. Following interactions are color-coded: Conventional H-bonds – green bold lines, van der Waals forces – thin green lines, Pi-Alkyl – pink, Donor-Donor – red, Pi-Pi Stacked – purple, Carbon Hydrogen bond; Pi-Donor Hydrogen Bond – mint green, Pi-Sulfur – yellow, Pi-Cation – orange. Heteroatoms are color-coded as well: red – oxygen, blue – nitrogen, yellow – sulfur.

```

MODEL      39
USER      Run = 39
USER      Cluster Rank = 3
USER      Number of conformations in this cluster = 16
USER
USER      RMSD from reference structure      = 6.348 A
USER
USER      Estimated Free Energy of Binding   = -9.31 kcal/mol  [(1)+(2)+(3)-(4)]
USER      Estimated Inhibition Constant, Ki  = 148.64 nM (nanomolar)  [Temperature = 298.15 K]
USER
USER      (1) Final Intermolecular Energy   = -11.10 kcal/mol
USER      vdW + Hbond + desolv Energy       = -10.88 kcal/mol
USER      Electrostatic Energy              = -0.23 kcal/mol
USER      (2) Final Total Internal Energy    = -2.38 kcal/mol
USER      (3) Torsional Free Energy          = +1.79 kcal/mol
USER      (4) Unbound System's Energy      [(2)] = -2.38 kcal/mol
  
```

Supplemental Figure 24: Molecular docking of trospium into hOCT1 using AutoDock 4.2. Shown is here the binding energy of run 39, the energetically most favored representative of cluster rank 3.



Interactions

■	Attractive Charge
■	Pi-Sigma
■	Pi-Pi Stacked

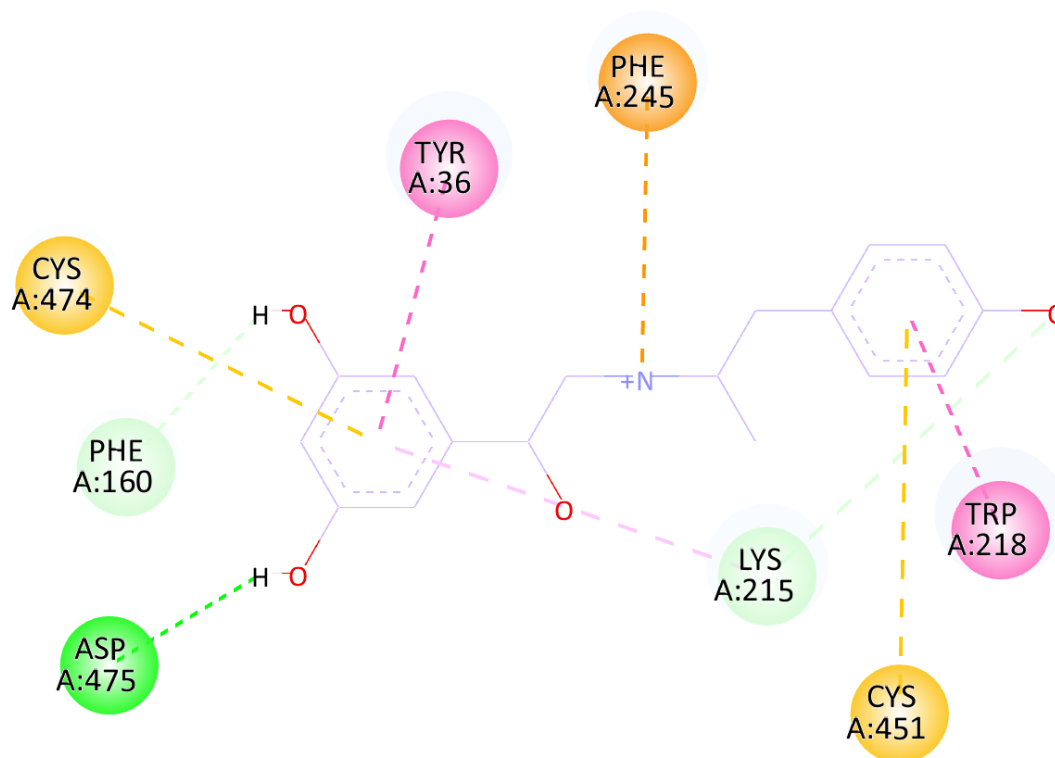
■	Pi-Pi T-shaped
■	Pi-Alkyl

Supplemental Figure 25: Molecular docking of trospium into hOCT1 from AlphaFold DB using AutoDock 4.2. Shown is here the best ranked binding pose of trospium in hOCT1 in cluster rank 4 regarding the binding energy with its interacting amino residues in 2D. Following interactions are color-coded: Conventional H-bonds – green bold lines, van der Waals forces – thin green lines, Pi-Alkyl – pink, Donor-Donor – red, Pi-Pi Stacked – purple, Carbon Hydrogen bond; Pi-Donor Hydrogen Bond – mint green, Pi-Sulfur – yellow, Pi-Cation – orange. Heteroatoms are color-coded as well: red – oxygen, blue – nitrogen, yellow – sulfur.

```

MODEL      86
USER      Run = 86
USER      Cluster Rank = 4
USER      Number of conformations in this cluster = 1
USER
USER      RMSD from reference structure      = 6.889 A
USER
USER      Estimated Free Energy of Binding   = -8.96 kcal/mol [(1)+(2)+(3)-(4)]
USER      Estimated Inhibition Constant, Ki  = 272.82 nM (nanomolar) [Temperature = 298.15 K]
USER
USER      (1) Final Intermolecular Energy   = -10.74 kcal/mol
USER      vdW + Hbond + desolv Energy       = -10.47 kcal/mol
USER      Electrostatic Energy              = -0.28 kcal/mol
USER      (2) Final Total Internal Energy   = -2.56 kcal/mol
USER      (3) Torsional Free Energy         = +1.79 kcal/mol
USER      (4) Unbound System's Energy      [(2)] = -2.56 kcal/mol
  
```

Supplemental Figure 26: Molecular docking of trospium into hOCT1 using AutoDock 4.2. Shown is here the binding energy of run 86, the energetically most favored representative of cluster rank 4.



Interactions

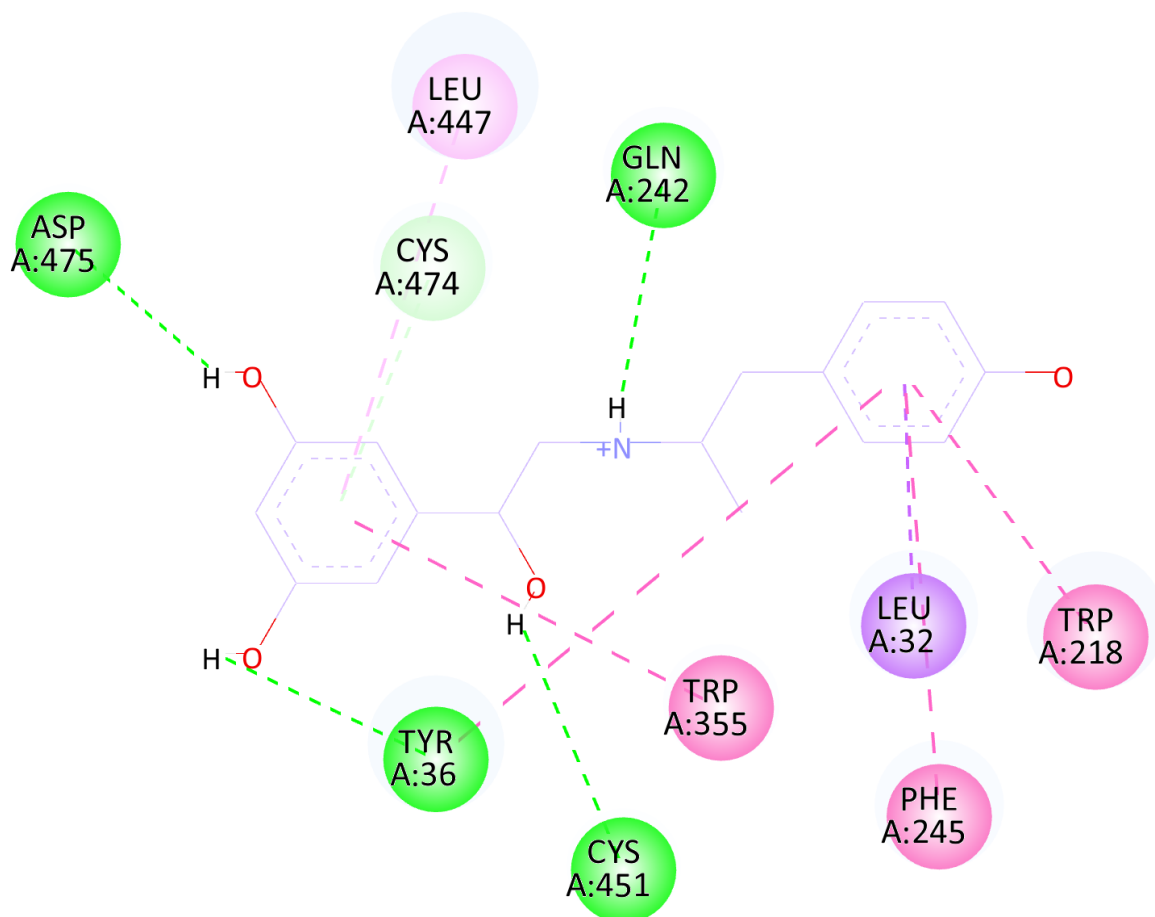
	Conventional Hydrogen Bond		Pi-Sulfur
	Carbon Hydrogen Bond		Pi-Pi Stacked
	Pi-Cation		Pi-Alkyl
	Pi-Donor Hydrogen Bond		

Supplemental Figure 27: Molecular docking of fenoterol into mOCT1 from AlphaFold DB using AutoDock 4.2. Shown is here the best ranked binding pose of fenoterol in mOCT1 out of 37 conformations in cluster rank 1 regarding the binding energy with its interacting amino residues in 2D. Following interactions are color-coded: Conventional H-bonds – green bold lines, van der Waals forces – thin green lines, Pi-Alkyl – pink, Donor-Donor – red, Pi-Pi Stacked – purple, Carbon Hydrogen bond; Pi-Donor Hydrogen Bond – mint green, Pi-Sulfur – yellow, Pi-Cation – orange. Heteroatoms are color-coded as well: red – oxygen, blue – nitrogen, yellow – sulfur.

```

MODEL      88
USER      Run = 88
USER      Cluster Rank = 1
USER      Number of conformations in this cluster = 37
USER
USER      RMSD from reference structure      = 4.573 A
USER
USER      Estimated Free Energy of Binding   = -6.40 kcal/mol [(1)+(2)+(3)-(4)]
USER      Estimated Inhibition Constant, Ki  = 20.41 uM (micromolar) [Temperature = 298.15 K]
USER
USER      (1) Final Intermolecular Energy   = -9.38 kcal/mol
USER      vdW + Hbond + desolv Energy       = -8.91 kcal/mol
USER      Electrostatic Energy              = -0.47 kcal/mol
USER      (2) Final Total Internal Energy    = -1.69 kcal/mol
USER      (3) Torsional Free Energy          = +2.98 kcal/mol
USER      (4) Unbound System's Energy [(2)] = -1.69 kcal/mol
  
```

Supplemental Figure 28: Molecular docking of fenoterol into mOCT1 using AutoDock 4.2. Shown is here the binding energy of run 88, the energetically most favored representative of cluster rank 1.



Interactions

■	Conventional Hydrogen Bond
■	Pi-Donor Hydrogen Bond
■	Pi-Sigma

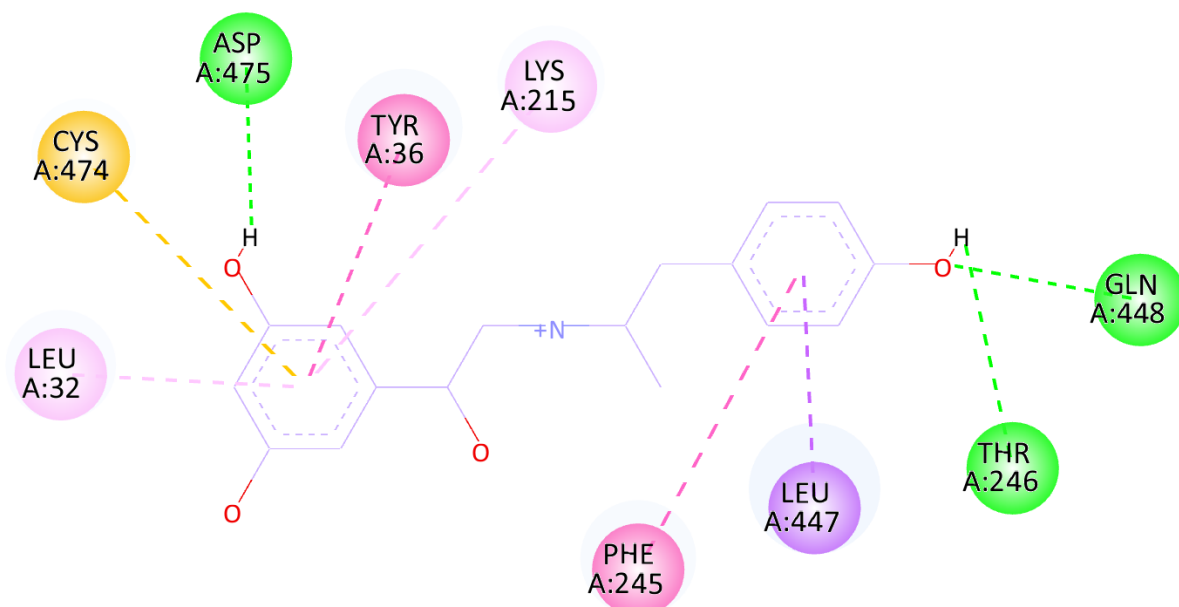
■	Pi-Pi Stacked
■	Pi-Pi T-shaped
■	Pi-Alkyl

Supplemental Figure 29: Molecular docking of fenoterol into mOCT1 from AlphaFold DB using AutoDock 4.2. Shown is here the best ranked binding pose of fenoterol in mOCT1 out of 3 conformations in cluster rank 2 regarding the binding energy with its interacting amino residues in 2D. Following interactions are color-coded: Conventional H-bonds – green bold lines, van der Waals forces – thin green lines, Pi-Alkyl – pink, Donor-Donor – red, Pi-Pi Stacked – purple, Carbon Hydrogen bond; Pi-Donor Hydrogen Bond – mint green, Pi-Sulfur – yellow, Pi-Cation – orange. Heteroatoms are color-coded as well: red – oxygen, blue – nitrogen, yellow – sulfur.

```

MODEL          8
USER           Run = 8
USER           Cluster Rank = 2
USER           Number of conformations in this cluster = 3
USER
USER           RMSD from reference structure           = 5.505 A
USER
USER           Estimated Free Energy of Binding        = -6.37 kcal/mol [(1)+(2)+(3)-(4)]
USER           Estimated Inhibition Constant, Ki       = 21.30 uM (micromolar) [Temperature = 298.15 K]
USER
USER           (1) Final Intermolecular Energy        = -9.36 kcal/mol
USER           vdW + Hbond + desolv Energy            = -8.91 kcal/mol
USER           Electrostatic Energy                   = -0.45 kcal/mol
USER           (2) Final Total Internal Energy        = -2.11 kcal/mol
USER           (3) Torsional Free Energy              = +2.98 kcal/mol
USER           (4) Unbound System's Energy [(2)]     = -2.11 kcal/mol
  
```

Supplemental Figure 30: Molecular docking of fenoterol into mOCT1 using AutoDock 4.2. Shown is here the binding energy of run 8, the energetically most favored representative of cluster rank 2.



Interactions

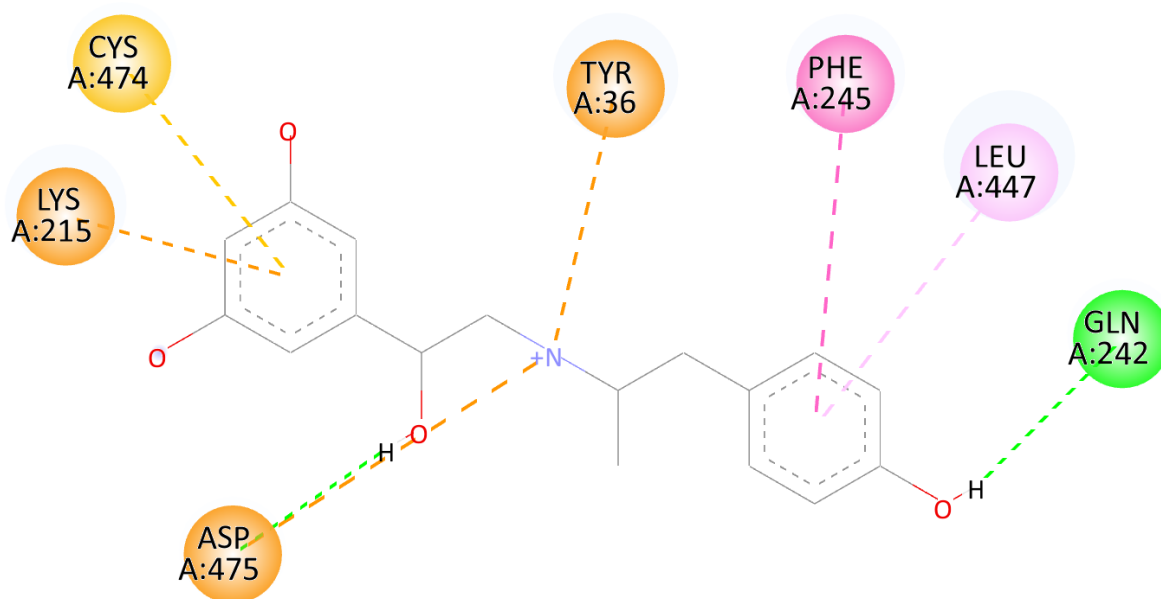
	Conventional Hydrogen Bond		Pi-Pi Stacked
	Pi-Sigma		Pi-Alkyl
	Pi-Sulfur		

Supplemental Figure 31: Molecular docking of fenoterol into mOCT1 from AlphaFold DB using AutoDock 4.2. Shown is here the best ranked binding pose of fenoterol in mOCT1 out of 3 conformations in cluster rank 3 regarding the binding energy with its interacting amino residues in 2D. Following interactions are color-coded: Conventional H-bonds – green bold lines, van der Waals forces – thin green lines, Pi-Alkyl – pink, Donor-Donor – red, Pi-Pi Stacked – purple, Carbon Hydrogen bond; Pi-Donor Hydrogen Bond – mint green, Pi-Sulfur – yellow, Pi-Cation – orange. Heteroatoms are color-coded as well: red – oxygen, blue – nitrogen, yellow – sulfur.

```

MODEL          47
USER           Run = 47
USER           Cluster Rank = 3
USER           Number of conformations in this cluster = 3
USER           RMSD from reference structure           = 5.316 A
USER           Estimated Free Energy of Binding       = -6.36 kcal/mol [(1)+(2)+(3)-(4)]
USER           Estimated Inhibition Constant, Ki      = 21.70 uM (micromolar) [Temperature = 298.15 K]
USER           (1) Final Intermolecular Energy       = -9.35 kcal/mol
USER           vdW + Hbond + desolv Energy           = -8.96 kcal/mol
USER           Electrostatic Energy                  = -0.38 kcal/mol
USER           (2) Final Total Internal Energy        = -1.03 kcal/mol
USER           (3) Torsional Free Energy              = +2.98 kcal/mol
USER           (4) Unbound System's Energy [(2)]     = -1.03 kcal/mol
  
```

Supplemental Figure 32: Molecular docking of fenoterol into mOCT1 using AutoDock 4.2. Shown is here the binding energy of run 47, the energetically most favored representative of cluster rank 3.



Interactions

	Attractive Charge		Pi-Sulfur
	Conventional Hydrogen Bond		Pi-Pi T-shaped
	Pi-Cation		Pi-Alkyl
	Pi-Sigma		

Supplemental Figure 33: Molecular docking of fenoterol into mOCT1 from AlphaFold DB using AutoDock 4.2. Shown is here the best ranked binding pose of fenoterol in mOCT1 out of 17 conformations in cluster rank 7 regarding the binding energy with its interacting amino residues in 2D. Following interactions are color-coded: Conventional H-bonds – green bold lines, van der Waals forces – thin green lines, Pi-Alkyl – pink, Donor-Donor – red, Pi-Pi Stacked – purple, Carbon Hydrogen bond; Pi-Donor Hydrogen Bond – mint green, Pi-Sulfur – yellow, Pi-Cation – orange. Heteroatoms are color-coded as well: red – oxygen, blue – nitrogen, yellow – sulfur.

```

MODEL          9
USER           Run = 9
USER           Cluster Rank = 7
USER           Number of conformations in this cluster = 17
USER
USER           RMSD from reference structure           = 4.781 A
USER
USER           Estimated Free Energy of Binding        = -5.88 kcal/mol [(1)+(2)+(3)-(4)]
USER           Estimated Inhibition Constant, Ki      = 48.88 uM (micromolar) [Temperature = 298.15 K]
USER
USER           (1) Final Intermolecular Energy        = -8.86 kcal/mol
USER               vdW + Hbond + desolv Energy        = -8.68 kcal/mol
USER               Electrostatic Energy                = -0.18 kcal/mol
USER           (2) Final Total Internal Energy        = -1.98 kcal/mol
USER           (3) Torsional Free Energy              = +2.98 kcal/mol
USER           (4) Unbound System's Energy [(2)]     = -1.98 kcal/mol
  
```

Supplemental Figure 34: Molecular docking of fenoterol into mOCT1 using AutoDock 4.2. Shown is here the binding energy of run 9, the energetically most favored representative of cluster rank 7.

Score	Expect	Method	Identities	Positives	Gaps
909 bits(2350)	0.0	Compositional matrix adjust.	432/556(78%)	490/556(88%)	2/556(0%)
Query 1	MPTVDDILEQVGESGWFQKQAFLLCLLSAAFAPICVGVFLGFTPDHHCQSPGVAELSQ	60			
Sbjct 1	MPTVDD+LE VGE GWFQKQAFLLCLLSAAFAPICVGVFLGFTPDHHC+SPGVAELSQ	60			
Query 61	RCGWSPAEEELNYTPGLGPAGEA-FLGQCRRYEVDWNQSAALSCVDPLASLATNRSHLPLG	119			
Sbjct 61	RCGWSPAEEELNYTPGLG AGEA FL QC +YEVDWNQS L CVDPL+SLA NRSHLPL	120			
Query 120	PCQDGWVYDTPGSSIVTEFNLVCAWSKLDLDFQSCNLNAGFLFGSLGVGYFADRFGRKLCL	179			
Sbjct 121	PC+ GWVYDTPGSSIVTEFNLVC D+WK+DLFQSC+N GF GSL VGY ADRFGRKLCL	180			
Query 180	LGTVLVNAVSGVLMFAFSPNYMSMLLFRLLQGLVSKGNWMAGYTLITEFVSGSRRTVAIM	239			
Sbjct 181	L T LV ++SGVL A +P+Y SMLLFRLLQG+VSKG+W++GYTLITEFVSG RRT AI+	240			
Query 240	YQMAFTVGLVALTGLAYALPHWRWLQAVSLPTFLFLYYWCVPEsprwllsQKRNTAI	299			
Sbjct 241	YQ+AFVGLV L G+AYA+P WRWLQAVSLPTFLFLYYW VPESPRWLLSQR T+A+	300			
Query 300	KIMDHIAQKNGKLPADLKMLSLEEDVTEKLSPSFADLFRTPRLRKRFTILMYLWFTDSV	359			
Sbjct 301	+IM+ IAQKN K+PPADLKM+ LEED +E+ SPSFADLFRTP LRK T ILMYLF+ +V	360			
Query 360	LYQGLIILHMGATSGNLYLDFLYSALVEIPGAFIALITIDRVGRIYPMAMSNLLAGAACL	419			
Sbjct 361	LYQGLI+H+GAT NLYLDF YS+LVE P AFI L+TIDR+GRIY+P+A SNL+AGAACL+	420			
Query 420	MIFISPDHLHWNIIIMCVGRMGITIAIQMICLVNAELYPTFVRNLGVMVCSLDCDIGGII	479			
Sbjct 421	MIFI +LHWN+ + C+GRMG TI +QM+CLVNAELYPTF+RNLG+MVCS+LCD+GGI	480			
Query 480	TPFIVFRLREVWQALPLILFAVLGLLAAGVTLVLLPETKGVLPETMKDAENLG-RKAKPK	538			
Sbjct 481	TPF+VFRL EVWQALPLILF VLGL A VTLVLLPETKGVLPET+++AENLG RK+K K	540			
Query 539	ENTIYLVQVQTSVPSGT 554				
Sbjct 541	ENTIYL+VQT + T 556				

Supplemental Figure 35: Protein alignment of human OCT1 (Query) and mouse OCT1 (Sbjct) using the *blastp* (protein-protein BLAST) algorithm of the basic local alignment search tool (BLAST[®], available at <https://blast.ncbi.nlm.nih.gov/Blast.cgi?PAGE=Proteins>).

Score	Expect	Method	Identities	Positives	Gaps
908 bits(2347)	0.0	Compositional matrix adjust.	433/556(78%)	488/556(87%)	2/556(0%)
Query 1		MPTVDDILEQVGESGWFQKQAFLLCLLSAAFAPICVGIVFLGFTPDHHCQSPGVAELSQ			60
Sbjct 1		MPTVDD+LEQVGE GWFQKQAFLLCLLSAAFAPICVGIVFLGFTPDHHCQSPGVAELSQ			60
Query 61		RCGWSPAEEELNYTVPGLGPAGEA-FLGQCRRYEVDWNQSAALSCVDPLASLATNRSHLPLG			119
Sbjct 61		RCGWS AEELNYTVPGLGP+ EA FL QC RYEVDWNQS L CVDPL+SL NRS LPLG			120
Query 120		PCQDQGWVYDTPGSSIVTEFNLVCAADSWKLDLDFQSCNLNAGFLFGSLGVGYFADRFGRKLCL			179
Sbjct 121		PC+ GWVYDTPGSSIVTEFNLVC D+WK+DLFQSC+N GF GSL VGY ADRFGRKLCL			180
Query 180		LGTVLVNAVSGVLMFAFSPNYMSMLLFRLLQGLVSKGNWMAGYTLITEFVSGSGRRTVAIM			239
Sbjct 181		L T LV +VSGVL A +P+Y SMLLFRLLQG+VSKG+W++GYTLITEFVSGS RRT AI+			240
Query 240		YQMAFTVGLVALTGLAYALPHWRWLQAVSLPTFLFLLYYWCVPESPRWLLSQKRNTAEI			299
Sbjct 241		YQMAFTVGLV L G+AYA+P WRWLQAVSLPTFLFLLYY VPESPRWLLSQKR T A+			300
Query 300		KIMDHIAQKNGKLPADLKMLSLEEDVTEKLSPSFADLFRTPRLRKRTEFILMYLWFTDSV			359
Sbjct 301		+IM+ IAQKNGK+PPADLKML LEED +EK SPSFADLFRTP LRK T ILMYLWF+ +V			360
Query 360		LYQGLILHMGATSGNLYLDFLYSALVEIPGAFIALITIDRVGRIYPMAMSNLLAGAACL			419
Sbjct 361		LYQGLI+H+GAT NLYLDF YS+LVE P AFI L+TIDR+GRIYP+A SNL+ GAACL+			420
Query 420		MIFISPDHLHWNIIIMCVGRMGITIAIQMICLVNAELYPTFVRNLGVMVCSLDCDIGGII			479
Sbjct 421		MIFI +LHWN+ + C+GRMG TI +QM+CLVNAELYPTF+RNLG+MVCS+LCD+GGI			480
Query 480		TPFIVFRLREVWQALPLILFAVLGLLAAGVTLTLLPETKGVLPETMKDAENLG-RKAKPK			538
Sbjct 481		TPF+VFRL EVWQALPLILF VLGL A +TLLLPETKGVLPET+++AENLG RK+K K			540
Query 539		ENTIYLKVQTSSEPSGT 554			
Sbjct 541		ENTIYL+VQT + S T 556			

Supplemental Figure 36: Protein alignment of human OCT1 (Query) and rat OCT1 (Sbjct) using the blastp (protein-protein BLAST) algorithm of the basic local alignment search tool (BLAST[®], available at <https://blast.ncbi.nlm.nih.gov/Blast.cgi?PAGE=Proteins>).

5.2 List of figures

- Figure 1: Structural classification of membrane proteins in a simplified way. The phospholipid bilayer is composed of an amphiphilic structure, having a hydrophilic polar head and a hydrophobic tail consisting of two fatty acid chains. Adapted from [] 5
- Figure 2: Schematic representation of integral membrane proteins. 1-3 depicts three types of integral polytopic proteins. 4-7 represents four types of integral monotopic membrane protein. The orange circle shows the hydrophilic polar head and the attached fatty acyl tails represent the hydrophobic core. Adapted from [] 6
- Figure 3: The diverse functions of membrane proteins. Adapted from [] 13
- Figure 4: *Chemical structure of substrates transported by OCT1. 1) Tetraethylammonium (TEA⁺), prototypic cation. 2) 1-methyl-4-phenylpyridinium (MPP⁺), prototypic cation. 3) Thiamine, endogenous compound involved in biosynthetic pathway and neurotransmission. 4) Choline, endogenous compound involved in biosynthetic pathway and neurotransmission. 5) Quinine, anti-malarial drug to treat *Plasmodium falciparum*. 6) Lamivudine, antiretroviral drug used for the treatment of HIV-1 infection. 7) Metformin, anti-diabetic drug used to lower blood sugar in those with type 2 diabetes. 8) Imatinib, anti-cancer drug used for chronic myelogenous leukemia (CML) and acute lymphocytic leukemia (ALL).* .48
- Figure 5: *Predicted membrane topology of human OCTs (hOCT1, hOCT2, hOCT3, hOCTN1, hOCTN2).* Adapted from [] 50
- Figure 6: View of the modeled outward-open (upper panel) and inward-open (lower panel) binding cleft of rOCT1, with labeled amino acids (Trp218, Arg440, and Asp475) located in the inner parts. Adapted from [] 51
- Figure 7: Protein alignment of human, mouse, and rat OCT1 using the multiple sequence alignment tool Clustal Omega. [] Transmembrane helices (TMH) 1 to 12 are shown in boxes. 63
- Figure 8: *The role of TMH1 in transport kinetics comparing fenoterol and trospium of human and mouse OCT1 with its crucial amino acid differences. A) OCT1-mediated uptake of fenoterol with substituting effect at codon 36 – C36Y in human and Y36C in mouse OCT1. B) Shown are the absolute K_M values for fenoterol of the data shown in A. C) OCT1-mediated uptake of trospium with substituting effect at codon 32 – F32L in human and L32F in mouse OCT1. D) Shown are the absolute K_M values for trospium of the data shown in C. Adapted from [89]* 65
- Figure 9: Molecular docking of fenoterol into hOCT1 by AutoDock Vina. Shown is here the best binding pose of fenoterol (orange) in hOCT1 (green) regarding the binding affinity out of ten conformations. Polar interactions are shown by yellow dashed lines. The distance of amino acids in close proximity are shown in black dashed lines with its respective value in white. Pi-Pi interactions are displayed by orange dashed lines. Heteroatoms are color-coded as well: red – oxygen, blue – nitrogen, yellow – sulfur. ... 67
- Figure 10: Molecular docking of fenoterol into hOCT1 by AutoDock Vina. Shown is here the second best binding pose of fenoterol (orange) in hOCT1 (green) regarding the binding affinity out of ten conformations. Polar interactions are shown by yellow dashed lines. The distance of amino acids in close proximity are shown by black dashed lines with its respective value in white. Pi-Pi interactions are displayed by orange dashed lines. Heteroatoms are color-coded as well: red – oxygen, blue – nitrogen, yellow – sulfur. 68
- Figure 11: Molecular docking of fenoterol into hOCT1 by AutoDock Vina. Shown is here the third best binding pose of fenoterol (orange) in hOCT1 (green) regarding the binding affinity out of ten conformations. Polar interactions are shown by yellow dashed lines. The distance of amino acids in close proximity are shown by black dashed lines with its respective value in white. Pi-Pi interactions are displayed by orange dashed lines. Heteroatoms are color-coded as well: red – oxygen, blue – nitrogen, yellow – sulfur. 69
- Figure 12: Molecular docking of fenoterol into mOCT1 by AutoDock Vina. Shown is here the best binding pose of fenoterol (green) in mOCT1 (purple) regarding the binding affinity out of ten conformations. Polar interactions are shown by yellow dashed lines. The distance of amino acids in close proximity are shown by black dashed lines with its respective value in white. Pi-Pi interactions are displayed by cyan dashed lines. Heteroatoms are color-coded as well: red – oxygen, blue – nitrogen, yellow – sulfur. 70
- Figure 13: Molecular docking of fenoterol into mOCT1 by AutoDock Vina. Shown is here the second best binding pose of fenoterol (green) in mOCT1 (purple) regarding the binding affinity out of ten

conformations. Polar interactions are shown by yellow dashed lines. The distance of amino acids in close proximity are shown by black dashed lines with its respective value in white. Pi-Pi interactions are displayed by cyan dashed lines. Heteroatoms are color-coded as well: red – oxygen, blue – nitrogen, yellow – sulfur.	71
Figure 14: Molecular docking of fenoterol into mOCT1 by AutoDock Vina. Shown is here the third best binding pose of fenoterol (green) in mOCT1 (purple) regarding the binding affinity out of ten conformations. Polar interactions are shown by yellow dashed lines. The distance of amino acids in close proximity are shown by black dashed lines with its respective value in white. Pi-Pi interactions are displayed by cyan dashed lines. Heteroatoms are color-coded as well: red – oxygen, blue – nitrogen, yellow – sulfur.	72
Figure 15: Molecular docking of trospium into hOCT1 by AutoDock Vina. Shown is here the best binding pose of trospium (orange) in hOCT1 (green) regarding the binding affinity out of ten conformations. Polar interactions are shown by yellow dashed lines. The distance of amino acids in close proximity are shown by black dashed lines with its respective value in white. Pi-Pi interactions are displayed by orange dashed lines. Heteroatoms are color-coded as well: red – oxygen, blue – nitrogen, yellow – sulfur. ...	74
Figure 16: Molecular docking of trospium into hOCT1 by AutoDock Vina. Shown is here the second best binding pose of trospium (orange) in hOCT1 (green) regarding the binding affinity out of ten conformations. Polar interactions are shown by yellow dashed lines. The distance of amino acids in close proximity are shown by black dashed lines with its respective value in white. Pi-Pi interactions are displayed by orange dashed lines. Heteroatoms are color-coded as well: red – oxygen, blue – nitrogen, yellow – sulfur.	75
Figure 17: Molecular docking of trospium into hOCT1 by AutoDock Vina. Shown is here the third best binding pose of trospium (orange) in hOCT1 (green) regarding the binding affinity out of ten conformations. Polar interactions are shown by yellow dashed lines. The distance of amino acids in close proximity are shown by black dashed lines with its respective value in white. Pi-Pi interactions are displayed by orange dashed lines. Heteroatoms are color-coded as well: red – oxygen, blue – nitrogen, yellow – sulfur.	76
Figure 18: Molecular docking of trospium into mOCT1 by AutoDock Vina. Shown is here the best binding pose of trospium (green) in mOCT1 (purple) regarding the binding affinity out of ten conformations. Polar interactions are shown by yellow dashed lines. The distance of amino acids in close proximity are shown by black dashed lines with its respective value in white. Pi-Pi interactions are displayed by orange dashed lines. Heteroatoms are color-coded as well: red – oxygen, blue – nitrogen, yellow – sulfur. ...	78
Figure 19: Molecular docking of trospium into mOCT1 by AutoDock Vina. Shown is here the second best binding pose of trospium (green) in mOCT1 (purple) regarding the binding affinity out of ten conformations. Polar interactions are shown by yellow dashed lines. The distance of amino acids in close proximity are shown by black dashed lines with its respective value in white. Pi-Pi interactions are displayed by orange dashed lines. Heteroatoms are color-coded as well: red – oxygen, blue – nitrogen, yellow – sulfur.	79
Figure 20: Molecular docking of trospium into mOCT1 by AutoDock Vina. Shown is here the best binding pose of trospium (green) in mOCT1 (purple) regarding the binding affinity out of ten conformations. Polar interactions are shown by yellow dashed lines. The distance of amino acids in close proximity are shown by black dashed lines with its respective value in white. Pi-Pi interactions are displayed by orange dashed lines. Heteroatoms are color-coded as well: red – oxygen, blue – nitrogen, yellow – sulfur. ...	80
Figure 21: New orientation (rotamer) of Asp474 in hOCT1. The old side chain of Asp474 (blue) has been rotated more towards the active side. The new rotamer is represented in grey. The visible disks indicate pairwise overlap of van der Waals radii. Small green disks are shown when atoms are almost in contact or slightly overlapping. Large red discs indicate significant van der Waals overlap. The yellow dashed lines represent polar interactions with its distance.	83
Figure 22: New orientation (rotamer) of Lys214 in hOCT1. The old side chain of Lys214 (blue) has been rotated more towards the active side. The new rotamer is represented in grey. The visible disks indicate pairwise overlap of van der Waals radii. Small green disks are shown when atoms are almost in contact or slightly overlapping. Large red discs indicate significant van der Waals overlap. The yellow dashed lines represent polar interactions with its distance.	83

Figure 23: New orientation (rotamer) of Asp475 in mOCT1. The old side chain of Asp475 (salmon) has been rotated more towards the active side. The new rotamer is represented in grey. The visible disks indicate pairwise overlap of van der Waals radii. Small green disks are shown when atoms are almost in contact or slightly overlapping. Large red discs indicate significant van der Waals overlap. The yellow dashed lines represent polar interactions with its distance.84

Figure 24: New orientation (rotamer) of Lys215 in mOCT1. The old side chain of Lys215 (salmon) has been rotated more towards the active side. The new rotamer is represented in grey. The visible disks indicate pairwise overlap of van der Waals radii. Small green disks are shown when atoms are almost in contact or slightly overlapping. Large red discs indicate significant van der Waals overlap. The yellow dashed lines represent polar interactions with its distance.84

Figure 25: Molecular docking of fenoterol into hOCT1 by AutoDock Vina. Shown is here the fifth best binding pose of fenoterol (orange) in hOCT1 (green) with the new orientations of Asp474 and Lys214 regarding the binding affinity out of ten conformations. Polar interactions are shown by yellow dashed lines. The distance of amino acids in close proximity are shown by black dashed lines with its respective value in white. Pi-Pi interactions are displayed by orange dashed lines. Heteroatoms are color-coded as well: red – oxygen, blue – nitrogen, yellow – sulfur.85

Figure 26: Molecular docking of fenoterol into hOCT1 by AutoDock Vina. Shown is here the best ranked binding pose of fenoterol (orange) in hOCT1 (green) with the new orientations of Asp474 and Lys214 regarding the binding affinity out of ten conformations. Polar interactions are shown by yellow dashed lines. The distance of amino acids in close proximity are shown by black dashed lines with its respective value in white. Pi-Pi interactions are displayed by orange dashed lines. Heteroatoms are color-coded as well: red – oxygen, blue – nitrogen, yellow – sulfur.86

Figure 27: Molecular docking of fenoterol into hOCT1 by AutoDock Vina. Shown is here the second best ranked binding pose of fenoterol (orange) in hOCT1 (green) with the new orientations of Asp474 and Lys214 regarding the binding affinity out of ten conformations. Polar interactions are shown by yellow dashed lines. The distance of amino acids in close proximity are shown by black dashed lines with its respective value in white. Pi-Pi interactions are displayed by orange dashed lines. Heteroatoms are color-coded as well: red – oxygen, blue – nitrogen, yellow – sulfur.87

Figure 28: Molecular docking of fenoterol into mOCT1 by AutoDock Vina. Shown is here the best ranked binding pose of fenoterol (green) in mOCT1 (purple) with the new orientations of Asp475 and Lys215 regarding the binding affinity out of ten conformations. Polar interactions are shown by yellow dashed lines. The distance of amino acids in close proximity are shown by black dashed lines with its respective value in white. Pi-Pi interactions are displayed by orange dashed lines. Heteroatoms are color-coded as well: red – oxygen, blue – nitrogen, yellow – sulfur.89

Figure 29: Molecular docking of fenoterol into mOCT1 by AutoDock Vina. Shown is here the second best ranked binding pose of fenoterol (green) in mOCT1 (purple) with the new orientations of Asp475 and Lys215 regarding the binding affinity out of ten conformations. Polar interactions are shown by yellow dashed lines. The distance of amino acids in close proximity are shown by black dashed lines with its respective value in white. Pi-Pi interactions are displayed by orange dashed lines. Heteroatoms are color-coded as well: red – oxygen, blue – nitrogen, yellow – sulfur.90

Figure 30: Molecular docking of fenoterol into mOCT1 by AutoDock Vina. Shown is here the fourth best ranked binding pose of fenoterol (green) in mOCT1 (purple) with the new orientations of Asp475 and Lys215 regarding the binding affinity out of ten conformations. Polar interactions are shown by yellow dashed lines. The distance of amino acids in close proximity are shown by black dashed lines with its respective value in white. Pi-Pi interactions are displayed by orange dashed lines. Heteroatoms are color-coded as well: red – oxygen, blue – nitrogen, yellow – sulfur.91

Figure 31: Molecular docking of trospium into hOCT1 by AutoDock Vina. Shown is here the best ranked binding pose of trospium (orange) in hOCT1 (green) with the new orientations of Asp474 and Lys214 regarding the binding affinity out of ten conformations. Polar interactions are shown by yellow dashed lines. The distance of amino acids in close proximity are shown by black dashed lines with its respective value in white. Pi-Pi interactions are displayed by orange dashed lines. Heteroatoms are color-coded as well: red – oxygen, blue – nitrogen, yellow – sulfur.93

Figure 32: Molecular docking of trospium into hOCT1 by AutoDock Vina. Shown is here the second best ranked binding pose of trospium (orange) in hOCT1 (green) with the new orientations of Asp474 and

Lys214 regarding the binding affinity out of ten conformations. Polar interactions are shown by yellow dashed lines. The distance of amino acids in close proximity are shown by black dashed lines with its respective value in white. Pi-Pi interactions are displayed by orange dashed lines. Heteroatoms are color-coded as well: red – oxygen, blue – nitrogen, yellow – sulfur.94

Figure 33: Molecular docking of trospium into hOCT1 by AutoDock Vina. Shown is here the third best ranked binding pose of trospium (orange) in hOCT1 (green) with the new orientations of Asp474 and Lys214 regarding the binding affinity out of ten conformations. Polar interactions are shown by yellow dashed lines. The distance of amino acids in close proximity are shown by black dashed lines with its respective value in white. Pi-Pi interactions are displayed by orange dashed lines. Heteroatoms are color-coded as well: red – oxygen, blue – nitrogen, yellow – sulfur.95

Figure 34: Molecular docking of trospium into mOCT1 by AutoDock Vina. Shown is here the best ranked binding pose of trospium (green) in mOCT1 (purple) with the new orientations of Asp475 and Lys215 regarding the binding affinity out of ten conformations. Polar interactions are shown by yellow dashed lines. The distance of amino acids in close proximity are shown by black dashed lines with its respective value in white. Pi-Pi interactions are displayed by orange dashed lines. Heteroatoms are color-coded as well: red – oxygen, blue – nitrogen, yellow – sulfur.98

Figure 35: Molecular docking of trospium into mOCT1 by AutoDock Vina. Shown is here the second best ranked binding pose of trospium (green) in mOCT1 (purple) with the new orientations of Asp475 and Lys215 regarding the binding affinity out of ten conformations. Polar interactions are shown by yellow dashed lines. The distance of amino acids in close proximity are shown by black dashed lines with its respective value in white. Pi-Pi interactions are displayed by orange dashed lines. Heteroatoms are color-coded as well: red – oxygen, blue – nitrogen, yellow – sulfur.99

Figure 36: Molecular docking of trospium into mOCT1 by AutoDock Vina. Shown is here the third best ranked binding pose of trospium (green) in mOCT1 (purple) with the new orientations of Asp475 and Lys215 regarding the binding affinity out of ten conformations. Polar interactions are shown by yellow dashed lines. The distance of amino acids in close proximity are shown by black dashed lines with its respective value in white. Pi-Pi interactions are displayed by orange dashed lines. Heteroatoms are color-coded as well: red – oxygen, blue – nitrogen, yellow – sulfur. 100

Figure 37: A) AlphaFold 3D structure prediction of hOCT1 (UniProt ID: O15245). AlphaFold produces a per-residue confidence score (pLDDT) between 0 and 100. Regions below 50 pLDDT may be unstructured in isolation. Model confidence is color-coded: Very high (pLDDT > 90) – dark blue; Confident (90 > pLDDT > 70) – light blue; Low (70 > pLDDT > 50) – yellow; Very low (pLDDT < 50) – orange. B) hOCT1 protein structures of AlphaFold (green) and our own generated homology model (blue) were aligned using PyMol. 102

Figure 38: Detailed insight into the alignment of the hOCT1 protein structure from AlphaFold DB (UniProt ID: O15245) with our homology model using PyMol. A) Difference in the orientation of Asp474 from the AlphaFold DB model (green) and our native homology model (light blue). B) Difference in the orientation of Asp474 from the AlphaFold model (green) and our homology model with new rotamers (light blue). 103

Figure 39: Molecular docking of fenoterol into hOCT1 from AlphaFold DB using AutoDock Vina. Shown is here the best ranked binding pose of fenoterol (orange) in hOCT1 (green) regarding the binding affinity out of 20 conformations. Polar interactions are shown by yellow dashed lines. The distance of amino acids in close proximity are shown by black dashed lines with its respective value in grey. Pi-Pi interactions are displayed by orange dashed lines. Heteroatoms are color-coded as well: red – oxygen, blue – nitrogen, yellow – sulfur. 105

Figure 40: Molecular docking of fenoterol into hOCT1 from AlphaFold DB using AutoDock Vina. Shown is here the second best ranked binding pose of fenoterol (orange) in hOCT1 (green) regarding the binding affinity out of 20 conformations. Polar interactions are shown by yellow dashed lines. The distance of amino acids in close proximity are shown by black dashed lines with its respective value in grey. Pi-Pi interactions are displayed by orange dashed lines. Heteroatoms are color-coded as well: red – oxygen, blue – nitrogen, yellow – sulfur. 106

Figure 41: Molecular docking of fenoterol into hOCT1 from AlphaFold DB using AutoDock Vina. Shown is here the fifteenth best ranked binding pose of fenoterol (orange) in hOCT1 (green) regarding the binding affinity out of 20 conformations. Polar interactions are shown by yellow dashed lines. The

distance of amino acids in close proximity are shown by black dashed lines with its respective value in grey. Pi-Pi interactions are displayed by orange dashed lines. Heteroatoms are color-coded as well: red – oxygen, blue – nitrogen, yellow – sulfur. 107

Figure 42: Molecular docking of trospium into hOCT1 from AlphaFold DB using AutoDock Vina. Shown are here the three best ranked binding poses of trospium (salmon) in hOCT1 (green) regarding the binding affinity out of 20 conformations. Polar interactions are shown by yellow dashed lines. The distance of amino acids in close proximity are shown by black dashed lines with its respective value in grey. Pi-Pi interactions are displayed by orange dashed lines. Heteroatoms are color-coded as well: red – oxygen, blue – nitrogen, yellow – sulfur. 108

Figure 43: Overview of the three best ranked conformations during flexible docking of fenoterol (grey) in hOCT1 using AutoDock Vina. Following amino residues (orange) orientation are shown: Phe32, Cys36, Phe159, Lys214, Phe244, Asp474. The protein structure is hidden, seen are only the amino acids and the ligand, which are overlaid. 110

Figure 44: Flexible docking of fenoterol into hOCT1 from AlphaFold DB using AutoDock Vina. Shown is here the best ranked binding pose of fenoterol (orange) in hOCT1 out of 20 conformations regarding the binding affinity with its interacting amino residues (grey) in 3D. Following interactions are color-coded: Conventional H-bonds – green bold lines, van der Waals forces – thin green lines, Pi-Alkyl – pink, Donor-Donor – red, Pi-Pi Stacked – purple, Pi-Donor; Pi-Sulfur – mint green, Pi-Sulfur – yellow, Pi-Cation – orange. Heteroatoms are color-coded as well: red – oxygen, blue – nitrogen, yellow – sulfur. 112

Figure 45: Flexible docking of fenoterol into hOCT1 from AlphaFold DB using AutoDock Vina. Shown is here the second best ranked binding pose of fenoterol (orange) in hOCT1 out of 20 conformations regarding the binding affinity with its interacting amino residues (grey). Following interactions are color-coded: Conventional H-bonds – green bold lines, van der Waals forces – thin green lines, Pi-Alkyl – pink, Donor-Donor – red, Pi-Pi Stacked – purple, Pi-Donor; Pi-Sulfur – mint green, Pi-Sulfur – yellow, Pi-Cation – orange. Heteroatoms are color-coded as well: red – oxygen, blue – nitrogen, yellow – sulfur. 113

Figure 46: Flexible docking of fenoterol into hOCT1 from AlphaFold DB using AutoDock Vina. Shown is here the third best ranked binding pose of fenoterol (orange) in hOCT1 out of 20 conformations regarding the binding affinity with its interacting amino residues (grey). Following interactions are color-coded: Conventional H-bonds – green bold lines, van der Waals forces – thin green lines, Pi-Alkyl – pink, Donor-Donor – red, Pi-Pi Stacked – purple, Pi-Donor; Pi-Sulfur – mint green, Pi-Sulfur – yellow, Pi-Cation – orange. Heteroatoms are color-coded as well: red – oxygen, blue – nitrogen, yellow – sulfur. 114

Figure 47: Flexible docking of fenoterol into mOCT1 from AlphaFold DB using AutoDock Vina. Shown is here the best ranked binding pose of fenoterol (blue) in hOCT1 out of 20 conformations regarding the binding affinity with its interacting amino residues (grey). Following interactions are color-coded: Conventional H-bonds – green bold lines, van der Waals forces – thin green lines, Pi-Alkyl – pink, Donor-Donor – red, Pi-Pi Stacked – purple, Pi-Donor; Pi-Sulfur – mint green, Pi-Sulfur – yellow, Pi-Cation – orange. Heteroatoms are color-coded as well: red – oxygen, blue – nitrogen, yellow – sulfur. 116

Figure 48: Flexible docking of fenoterol into mOCT1 from AlphaFold DB using AutoDock Vina. Shown is here the second best ranked binding pose of fenoterol (blue) in hOCT1 out of 20 conformations regarding the binding affinity with its interacting amino residues (grey). Following interactions are color-coded: Conventional H-bonds – green bold lines, van der Waals forces – thin green lines, Pi-Alkyl – pink, Donor-Donor – red, Pi-Pi Stacked – purple, Pi-Donor; Pi-Sulfur – mint green, Pi-Sulfur – yellow, Pi-Cation – orange. Heteroatoms are color-coded as well: red – oxygen, blue – nitrogen, yellow – sulfur. 117

Figure 49: Flexible docking of fenoterol into mOCT1 from AlphaFold DB using AutoDock Vina. Shown is here the third best ranked binding pose of fenoterol (blue) in hOCT1 out of 20 conformations regarding the binding affinity with its interacting amino residues (grey). Following interactions are color-coded: Conventional H-bonds – green bold lines, van der Waals forces – thin green lines, Pi-Alkyl – pink, Donor-Donor – red, Pi-Pi Stacked – purple, Pi-Donor; Pi-Sulfur – mint green, Pi-Sulfur – yellow, Pi-Cation – orange. Heteroatoms are color-coded as well: red – oxygen, blue – nitrogen, yellow – sulfur. 118

Figure 50: Overview of the three best ranked conformations during flexible docking of fenoterol (grey) in mOCT1 (green) using AutoDock Vina. Following amino residues orientation are shown: Phe32,

Cys36, Phe159, Lys214, Phe244, Asp474. The protein structure is hidden, seen are only the amino acids and the ligand, which are overlaid.	120
Figure 51: New orientation (rotamer) of Asp474 in hOCT1. The old side chain of Asp474 (blue) has been rotated more towards the active side. The new rotamer is represented in grey. The visible disks indicate pairwise overlap of van der Waals radii. Small green disks are shown when atoms are almost in contact or slightly overlapping. Large red discs indicate significant van der Waals overlap. The yellow dashed lines represent polar interactions with its distance.	121
Figure 52: Molecular docking of fenoterol into hOCT1 from AlphaFold DB by AutoDock Vina. Shown is here the best ranked binding pose of fenoterol (salmon) in hOCT1 (green) with the new orientation of Asp474 regarding the binding affinity out of twenty conformations. Polar interactions are shown by yellow dashed lines. The distance of amino acids in close proximity are shown by black dashed lines with its respective value in white. Pi-Pi interactions are displayed by orange dashed lines. Heteroatoms are color-coded as well: red – oxygen, blue – nitrogen, yellow – sulfur.	122
Figure 53: Molecular docking of fenoterol into hOCT1 from AlphaFold DB by AutoDock Vina. Shown is here the second best ranked binding pose of fenoterol (salmon) in hOCT1 (green) with the new orientation of Asp474 regarding the binding affinity out of twenty conformations. Polar interactions are shown by yellow dashed lines. The distance of amino acids in close proximity are shown by black dashed lines with its respective value in white. Pi-Pi interactions are displayed by orange dashed lines. Heteroatoms are color-coded as well: red – oxygen, blue – nitrogen, yellow – sulfur.	123
Figure 54: Molecular docking of fenoterol into hOCT1 from AlphaFold DB by AutoDock Vina. Shown is here the second best ranked binding pose of fenoterol (salmon) in hOCT1 (green) with the new orientation of Asp474 regarding the binding affinity out of twenty conformations. Polar interactions are shown by yellow dashed lines. The distance of amino acids in close proximity are shown by black dashed lines with its respective value in white. Pi-Pi interactions are displayed by orange dashed lines. Heteroatoms are color-coded as well: red – oxygen, blue – nitrogen, yellow – sulfur.	124
Figure 55: Molecular docking of trospium into hOCT1 from AlphaFold DB by AutoDock Vina. Shown is here the best ranked binding pose of trospium (orange) in hOCT1's interacting amino acids (gray) with the new orientation of Asp474 regarding the binding affinity out of twenty conformations. Following interactions are color-coded: Conventional H-bonds – green bold lines, van der Waals forces – thin green lines, Pi-Alkyl – pink, Donor-Donor – red, Pi-Pi Stacked – purple, Carbon Hydrogen bond; Pi-Donor Hydrogen Bond – mint green, Pi-Sulfur – yellow, Pi-Cation – orange. Heteroatoms are color-coded as well: red – oxygen, blue – nitrogen, yellow – sulfur.	127
Figure 56: Molecular docking of trospium into hOCT1 from AlphaFold DB by AutoDock Vina. Shown is here the second best ranked binding pose of trospium (orange) in hOCT1's interacting amino acids (gray) with the new orientation of Asp474 regarding the binding affinity out of twenty conformations. Following interactions are color-coded: Conventional H-bonds – green bold lines, van der Waals forces – thin green lines, Pi-Alkyl – pink, Donor-Donor – red, Pi-Pi Stacked – purple, Carbon Hydrogen bond; Pi-Donor Hydrogen Bond – mint green, Pi-Sulfur – yellow, Pi-Cation – orange. Heteroatoms are color-coded as well: red – oxygen, blue – nitrogen, yellow – sulfur.	128
Figure 57: Molecular docking of trospium into hOCT1 from AlphaFold DB by AutoDock Vina. Shown is here the third best ranked binding pose of trospium (orange) in hOCT1's interacting amino acids (gray) with the new orientation of Asp474 regarding the binding affinity out of twenty conformations. Following interactions are color-coded: Conventional H-bonds – green bold lines, van der Waals forces – thin green lines, Pi-Alkyl – pink, Donor-Donor – red, Pi-Pi Stacked – purple, Carbon Hydrogen bond; Pi-Donor Hydrogen Bond – mint green, Pi-Sulfur – yellow, Pi-Cation – orange. Heteroatoms are color-coded as well: red – oxygen, blue – nitrogen, yellow – sulfur.	129
Figure 58: Molecular docking of fenoterol into hOCT1 from AlphaFold DB by AutoDock 4.2. Shown is here the third best ranked binding pose of fenoterol (purple) in hOCT1 out of 14 conformations from the cluster rank 4 with its interacting amino acids (gray) regarding the binding energy. Following interactions are color-coded: Conventional H-bonds – green bold lines, van der Waals forces – thin green lines, Pi-Alkyl – pink, Donor-Donor – red, Pi-Pi Stacked – purple, Carbon Hydrogen bond; Pi-Donor Hydrogen Bond – mint green, Pi-Sulfur – yellow, Pi-Cation – orange. Heteroatoms are color-coded as well: red – oxygen, blue – nitrogen, yellow – sulfur.	132

Figure 59: Molecular docking of fenoterol into hOCT1 from AlphaFold DB by AutoDock 4.2. Shown is here the best ranked binding pose of fenoterol (purple) in hOCT1 from cluster rank 1 with its interacting amino acids (gray) regarding the binding energy. Following interactions are color-coded: Conventional H-bonds – green bold lines, van der Waals forces – thin green lines, Pi-Alkyl – pink, Donor-Donor – red, Pi-Pi Stacked – purple, Carbon Hydrogen bond; Pi-Donor Hydrogen Bond – mint green, Pi-Sulfur – yellow, Pi-Cation – orange. Heteroatoms are color-coded as well: red – oxygen, blue – nitrogen, yellow – sulfur. 133

Figure 60: Molecular docking of fenoterol into hOCT1 from AlphaFold DB by AutoDock 4.2. Shown is here the best ranked binding pose of fenoterol (purple) in hOCT1 from cluster rank 2 with its interacting amino acids (gray) regarding the binding energy. Following interactions are color-coded: Conventional H-bonds – green bold lines, van der Waals forces – thin green lines, Pi-Alkyl – pink, Donor-Donor – red, Pi-Pi Stacked – purple, Carbon Hydrogen bond; Pi-Donor Hydrogen Bond – mint green, Pi-Sulfur – yellow, Pi-Cation – orange. Heteroatoms are color-coded as well: red – oxygen, blue – nitrogen, yellow – sulfur. 134

Figure 61: Molecular docking of fenoterol into hOCT1 from AlphaFold DB by AutoDock 4.2. Shown is here the best ranked binding pose of fenoterol (purple) in hOCT1 from cluster rank 1 with its interacting amino acids (gray) regarding the binding energy. Following interactions are color-coded: Conventional H-bonds – green bold lines, van der Waals forces – thin green lines, Pi-Alkyl – pink, Donor-Donor – red, Pi-Pi Stacked – purple, Carbon Hydrogen bond; Pi-Donor Hydrogen Bond – mint green, Pi-Sulfur – yellow, Pi-Cation – orange. Heteroatoms are color-coded as well: red – oxygen, blue – nitrogen, yellow – sulfur. 135

Figure 62: Molecular docking of tropium into hOCT1 from AlphaFold DB by AutoDock 4.2. Shown is here the best ranked binding pose of tropium (orange) in hOCT1 from cluster rank 1 with its interacting amino acids (gray) regarding the binding energy. Following interactions are color-coded: Conventional H-bonds – green bold lines, van der Waals forces – thin green lines, Pi-Alkyl – pink, Donor-Donor – red, Pi-Pi Stacked – purple, Carbon Hydrogen bond; Pi-Donor Hydrogen Bond – mint green, Pi-Sulfur – yellow, Pi-Cation – orange. Heteroatoms are color-coded as well: red – oxygen, blue – nitrogen, yellow – sulfur. 137

Figure 63: Molecular docking of tropium into hOCT1 from AlphaFold DB by AutoDock 4.2. Shown is here the best ranked binding pose of tropium (orange) in hOCT1 from cluster rank 2 with its interacting amino acids (gray) regarding the binding energy. Following interactions are color-coded: Conventional H-bonds – green bold lines, van der Waals forces – thin green lines, Pi-Alkyl – pink, Donor-Donor – red, Pi-Pi Stacked – purple, Carbon Hydrogen bond; Pi-Donor Hydrogen Bond – mint green, Pi-Sulfur – yellow, Pi-Cation – orange. Heteroatoms are color-coded as well: red – oxygen, blue – nitrogen, yellow – sulfur. 138

Figure 64: Molecular docking of tropium into hOCT1 from AlphaFold DB by AutoDock 4.2. Shown is here the best ranked binding pose of tropium (orange) in hOCT1 from cluster rank 3 with its interacting amino acids (gray) regarding the binding energy. Following interactions are color-coded: Conventional H-bonds – green bold lines, van der Waals forces – thin green lines, Pi-Alkyl – pink, Donor-Donor – red, Pi-Pi Stacked – purple, Carbon Hydrogen bond; Pi-Donor Hydrogen Bond – mint green, Pi-Sulfur – yellow, Pi-Cation – orange. Heteroatoms are color-coded as well: red – oxygen, blue – nitrogen, yellow – sulfur. 139

Figure 65: Molecular docking of tropium into hOCT1 from AlphaFold DB by AutoDock 4.2. Shown is here the best ranked binding pose of tropium (orange) in hOCT1 from cluster rank 4 with its interacting amino acids (gray) regarding the binding energy. Following interactions are color-coded: Conventional H-bonds – green bold lines, van der Waals forces – thin green lines, Pi-Alkyl – pink, Donor-Donor – red, Pi-Pi Stacked – purple, Carbon Hydrogen bond; Pi-Donor Hydrogen Bond – mint green, Pi-Sulfur – yellow, Pi-Cation – orange. Heteroatoms are color-coded as well: red – oxygen, blue – nitrogen, yellow – sulfur. 140

Figure 66: Molecular docking of fenoterol into mOCT1 from AlphaFold DB by AutoDock 4.2. Shown is here the best ranked binding pose of fenoterol (purple) in mOCT1 from cluster rank 1 with its interacting amino acids (gray) regarding the binding energy. Following interactions are color-coded: Conventional H-bonds – green bold lines, van der Waals forces – thin green lines, Pi-Alkyl – pink, Donor-Donor – red, Pi-Pi Stacked – purple, Carbon Hydrogen bond; Pi-Donor Hydrogen Bond – mint green, Pi-Sulfur –

yellow, Pi-Cation – orange. Heteroatoms are color-coded as well: red – oxygen, blue – nitrogen, yellow – sulfur.	143
Figure 67: Molecular docking of fenoterol into mOCT1 from AlphaFold DB by AutoDock 4.2. Shown is here the best ranked binding pose of fenoterol (purple) in mOCT1 from cluster rank 2 with its interacting amino acids (gray) regarding the binding energy. Following interactions are color-coded: Conventional H-bonds – green bold lines, van der Waals forces – thin green lines, Pi-Alkyl – pink, Donor-Donor – red, Pi-Pi Stacked – purple, Carbon Hydrogen bond; Pi-Donor Hydrogen Bond – mint green, Pi-Sulfur – yellow, Pi-Cation – orange. Heteroatoms are color-coded as well: red – oxygen, blue – nitrogen, yellow – sulfur.	144
Figure 68: Molecular docking of fenoterol into mOCT1 from AlphaFold DB by AutoDock 4.2. Shown is here the best ranked binding pose of fenoterol (purple) in mOCT1 from cluster rank 3 with its interacting amino acids (gray) regarding the binding energy. Following interactions are color-coded: Conventional H-bonds – green bold lines, van der Waals forces – thin green lines, Pi-Alkyl – pink, Donor-Donor – red, Pi-Pi Stacked – purple, Carbon Hydrogen bond; Pi-Donor Hydrogen Bond – mint green, Pi-Sulfur – yellow, Pi-Cation – orange. Heteroatoms are color-coded as well: red – oxygen, blue – nitrogen, yellow – sulfur.	145
Figure 69: Molecular docking of fenoterol into mOCT1 from AlphaFold DB by AutoDock 4.2. Shown is here the best ranked binding pose of fenoterol (purple) in mOCT1 from cluster rank 7 with its interacting amino acids (gray) regarding the binding energy. Following interactions are color-coded: Conventional H-bonds – green bold lines, van der Waals forces – thin green lines, Pi-Alkyl – pink, Donor-Donor – red, Pi-Pi Stacked – purple, Carbon Hydrogen bond; Pi-Donor Hydrogen Bond – mint green, Pi-Sulfur – yellow, Pi-Cation – orange. Heteroatoms are color-coded as well: red – oxygen, blue – nitrogen, yellow – sulfur.	146
Figure 70: Molecular docking of trospium into mOCT1 from AlphaFold DB by AutoDock 4.2. Shown is here the best ranked binding pose of trospium (orange) in mOCT1 from cluster rank 1 with its interacting amino acids (gray) regarding the binding energy. Following interactions are color-coded: Conventional H-bonds – green bold lines, van der Waals forces – thin green lines, Pi-Alkyl – pink, Donor-Donor – red, Pi-Pi Stacked – purple, Carbon Hydrogen bond; Pi-Donor Hydrogen Bond – mint green, Pi-Sulfur – yellow, Pi-Cation – orange. Heteroatoms are color-coded as well: red – oxygen, blue – nitrogen, yellow – sulfur.	149
Figure 71: Molecular docking of trospium into mOCT1 from AlphaFold DB by AutoDock 4.2. Shown is here the best ranked binding pose of trospium (orange) in mOCT1 from cluster rank 2 with its interacting amino acids (gray) regarding the binding energy. Following interactions are color-coded: Conventional H-bonds – green bold lines, van der Waals forces – thin green lines, Pi-Alkyl – pink, Donor-Donor – red, Pi-Pi Stacked – purple, Carbon Hydrogen bond; Pi-Donor Hydrogen Bond – mint green, Pi-Sulfur – yellow, Pi-Cation – orange. Heteroatoms are color-coded as well: red – oxygen, blue – nitrogen, yellow – sulfur.	150
Figure 72: Molecular docking of trospium into mOCT1 from AlphaFold DB by AutoDock 4.2. Shown is here the best ranked binding pose of trospium (orange) in mOCT1 from cluster rank 3 with its interacting amino acids (gray) regarding the binding energy. Following interactions are color-coded: Conventional H-bonds – green bold lines, van der Waals forces – thin green lines, Pi-Alkyl – pink, Donor-Donor – red, Pi-Pi Stacked – purple, Carbon Hydrogen bond; Pi-Donor Hydrogen Bond – mint green, Pi-Sulfur – yellow, Pi-Cation – orange. Heteroatoms are color-coded as well: red – oxygen, blue – nitrogen, yellow – sulfur.	151
Figure 73: Molecular docking of trospium into mOCT1 from AlphaFold DB by AutoDock 4.2. Shown is here the best ranked binding pose of trospium (orange) in mOCT1 from cluster rank 4 with its interacting amino acids (gray) regarding the binding energy. Following interactions are color-coded: Conventional H-bonds – green bold lines, van der Waals forces – thin green lines, Pi-Alkyl – pink, Donor-Donor – red, Pi-Pi Stacked – purple, Carbon Hydrogen bond; Pi-Donor Hydrogen Bond – mint green, Pi-Sulfur – yellow, Pi-Cation – orange. Heteroatoms are color-coded as well: red – oxygen, blue – nitrogen, yellow – sulfur.	152

5.3 List of Schemes

Scheme 1: Overview of common lipid-anchored proteins in the plasma membrane. Protein p60-vSrc and Protein p21-ras are in the cytosolic side, facing the interior of the cell. Thy-1 protein is in the exoplasmic face, facing the outside of the cell. Adapted from [1].	8
Scheme 2: The different types of membrane proteins and their related functions. Transporters (left) carry ions or molecules in or out of the cell across the membrane, regulating the intracellular composition. Receptors (middle) regulate cell signaling by transmitting a chemical signal from the extracellular environment into the cell. Enzymes (right) serve as catalysts, enabling a biochemical reaction by decreasing the activation energy. Adapted from [2].	9
Scheme 3: Posttranslational modification pathways in MP expression systems. Schematic overview of most frequent PTMs and their impact on structure and function of MPs. Adapted from [3].	17
Scheme 4: Electron microscopy studies can be performed on various material such as ternary complexes observed as single particles or crystals. Adapted from [4].	23
Scheme 5: The outline of SBVS and LBVS approaches. Adapted from [5].	26
Scheme 6: Workflow of the structure-based drug design (SBDD) process. Adapted from [6].	29
Scheme 7: Steps of homology modeling. Adapted from [7].	33
Scheme 8: The evaluation of the force field in AutoDock 4. Adapted from [8].	41
Scheme 9: Methodology comparison of AutoDock 4 and AutoDock Vina. Adapted from [9].	45
Scheme 10: Illustration of the ligand transport cycle through conformation changes by the organic cation transporter 1.	49
Scheme 11: Location of OCTs in A) hepatocytes (liver), B) small intestinal enterocytes, C) in brain, D) bronchial epithelial cell (lung), and E) tubular cells (kidney). Adapted from [10].	54

5.4 Supplementary Figures

Supplemental Figure 1: Protonation states of fenoterol. Calculation results of microspheres distribution according to its pH.	163
Supplemental Figure 2: Flexible docking of fenoterol into hOCT1 from AlphaFold DB using AutoDock Vina. Shown is here the best ranked binding pose of fenoterol (green) in hOCT1 out of 20 conformations regarding the binding affinity with its interacting amino residues (grey) in 2D. Following interactions are color-coded: Conventional H-bonds – green, Pi-Alkyl – pink, Donor-Donor – red, Pi-Pi Stacked – purple, Pi-Donor; Pi-Sulfur – mint green, Pi-Sulfur – yellow, Pi-Cation – orange. Heteroatoms are color-coded as well: red – oxygen, blue – nitrogen, yellow – sulfur.	164
Supplemental Figure 3: Flexible docking of fenoterol into hOCT1 from AlphaFold DB using AutoDock Vina. Shown is here the second best ranked binding pose of fenoterol in hOCT1 out of 20 conformations regarding the binding affinity with its interacting amino residues in 2D. Following interactions are color-coded: Conventional H-bonds – green, Pi-Alkyl – pink, Donor-Donor – red, Pi-Pi Stacked – purple, Pi-Donor; Pi-Sulfur – mint green, Pi-Sulfur – yellow, Pi-Cation – orange. Heteroatoms are color-coded as well: red – oxygen, blue – nitrogen, yellow – sulfur.	164
Supplemental Figure 4: Flexible docking of fenoterol into hOCT1 from AlphaFold DB using AutoDock Vina. Shown is here the third best ranked binding pose of fenoterol in hOCT1 out of 20 conformations regarding the binding affinity with its interacting amino residues in 2D. Following interactions are color-coded: Conventional H-bonds – green, Pi-Alkyl – pink, Donor-Donor – red, Pi-Pi Stacked – purple, Pi-Donor; Pi-Sulfur – mint green, Pi-Sulfur – yellow, Pi-Cation – orange. Heteroatoms are color-coded as well: red – oxygen, blue – nitrogen, yellow – sulfur.	165
Supplemental Figure 5: Flexible docking of fenoterol into mOCT1 from AlphaFold DB using AutoDock Vina. Shown is here the best ranked binding pose of fenoterol in hOCT1 out of 20 conformations regarding the binding affinity with its interacting amino residues in 2D. Following interactions are color-coded: Conventional H-bonds – green, Pi-Alkyl – pink, Donor-Donor – red, Pi-Pi Stacked – purple, Pi-Donor; Pi-Sulfur – mint green, Pi-Sulfur – yellow, Pi-Cation – orange. Heteroatoms are color-coded as well: red – oxygen, blue – nitrogen, yellow – sulfur.	165
Supplemental Figure 6: Flexible docking of fenoterol into mOCT1 from AlphaFold DB using AutoDock Vina. Shown is here the second best ranked binding pose of fenoterol in hOCT1 out of 20 conformations regarding the binding affinity with its interacting amino residues in 2D. Following interactions are color-coded: Conventional H-bonds – green, Pi-Alkyl – pink, Donor-Donor – red, Pi-Pi Stacked – purple, Pi-Donor; Pi-Sulfur – mint green, Pi-Sulfur – yellow, Pi-Cation – orange. Heteroatoms are color-coded as well: red – oxygen, blue – nitrogen, yellow – sulfur.	166
Supplemental Figure 7: Flexible docking of fenoterol into mOCT1 from AlphaFold DB using AutoDock Vina. Shown is here the third best ranked binding pose of fenoterol in hOCT1 out of 20 conformations regarding the binding affinity with its interacting amino residues in 2D. Following interactions are color-coded: Conventional H-bonds – green, Pi-Alkyl – pink, Donor-Donor – red, Pi-Pi Stacked – purple, Pi-Donor; Pi-Sulfur – mint green, Pi-Sulfur – yellow, Pi-Cation – orange. Heteroatoms are color-coded as well: red – oxygen, blue – nitrogen, yellow – sulfur.	166
Supplemental Figure 8: Rotamer docking of trospium into hOCT1 from AlphaFold DB using AutoDock Vina. Shown is here the best ranked binding pose of trospium in hOCT1 out of 20 conformations regarding the binding affinity with its interacting amino residues in 2D. Following interactions are color-coded: Conventional H-bonds – green bold lines, van der Waals forces – thin green lines, Pi-Alkyl – pink, Donor-Donor – red, Pi-Pi Stacked – purple, Carbon Hydrogen bond; Pi-Donor Hydrogen Bond – mint green, Pi-Sulfur – yellow, Pi-Cation – orange. Heteroatoms are color-coded as well: red – oxygen, blue – nitrogen, yellow – sulfur.	167
Supplemental Figure 9: Rotamer docking of trospium into hOCT1 from AlphaFold DB using AutoDock Vina. Shown is here the second best ranked binding pose of trospium in hOCT1 out of 20 conformations regarding the binding affinity with its interacting amino residues in 2D. Following interactions are color-coded: Conventional H-bonds – green bold lines, van der Waals forces – thin green lines, Pi-Alkyl – pink, Donor-Donor – red, Pi-Pi Stacked – purple, Carbon Hydrogen bond; Pi-Donor Hydrogen Bond – mint green, Pi-Sulfur – yellow, Pi-Cation – orange. Heteroatoms are color-coded as well: red – oxygen, blue – nitrogen, yellow – sulfur.	167

Supplemental Figure 10: Rotamer docking of trospium into hOCT1 from AlphaFold DB using AutoDock Vina. Shown is here the second best ranked binding pose of trospium in hOCT1 out of 20 conformations regarding the binding affinity with its interacting amino residues in 2D. Following interactions are color-coded: Conventional H-bonds – green bold lines, van der Waals forces – thin green lines, Pi-Alkyl – pink, Donor-Donor – red, Pi-Pi Stacked – purple, Carbon Hydrogen bond; Pi-Donor Hydrogen Bond – mint green, Pi-Sulfur – yellow, Pi-Cation – orange. Heteroatoms are color-coded as well: red – oxygen, blue – nitrogen, yellow – sulfur.....	168
Supplemental Figure 11: Molecular docking of fenoterol into hOCT1 from AlphaFold DB using AutoDock 4.2. Shown is here the third best ranked binding pose of fenoterol in hOCT1 out of 14 conformations in cluster rank 4 regarding the binding energy with its interacting amino residues in 2D. Following interactions are color-coded: Conventional H-bonds – green bold lines, van der Waals forces – thin green lines, Pi-Alkyl – pink, Donor-Donor – red, Pi-Pi Stacked – purple, Carbon Hydrogen bond; Pi-Donor Hydrogen Bond – mint green, Pi-Sulfur – yellow, Pi-Cation – orange. Heteroatoms are color-coded as well: red – oxygen, blue – nitrogen, yellow – sulfur.....	169
Supplemental Figure 12: Molecular docking of fenoterol into hOCT1 using AutoDock 4.2. Shown is here the binding energy of run 80 of cluster rank 4.....	169
Supplemental Figure 13: Molecular docking of fenoterol into hOCT1 from AlphaFold DB using AutoDock 4.2. Shown is here the best ranked binding pose of fenoterol in hOCT1 out of 4 conformations in cluster rank 1 regarding the binding energy with its interacting amino residues in 2D. Following interactions are color-coded: Conventional H-bonds – green bold lines, van der Waals forces – thin green lines, Pi-Alkyl – pink, Donor-Donor – red, Pi-Pi Stacked – purple, Carbon Hydrogen bond; Pi-Donor Hydrogen Bond – mint green, Pi-Sulfur – yellow, Pi-Cation – orange. Heteroatoms are color-coded as well: red – oxygen, blue – nitrogen, yellow – sulfur.....	170
Supplemental Figure 14: Molecular docking of fenoterol into hOCT1 using AutoDock 4.2. Shown is here the binding energy of run 5, the energetically most favored representative of cluster rank 1.....	170
Supplemental Figure 15: Molecular docking of fenoterol into hOCT1 from AlphaFold DB using AutoDock 4.2. Shown is here the best ranked binding pose of fenoterol in hOCT1 out of 5 conformations in cluster rank 2 regarding the binding energy with its interacting amino residues in 2D. Following interactions are color-coded: Conventional H-bonds – green bold lines, van der Waals forces – thin green lines, Pi-Alkyl – pink, Donor-Donor – red, Pi-Pi Stacked – purple, Carbon Hydrogen bond; Pi-Donor Hydrogen Bond – mint green, Pi-Sulfur – yellow, Pi-Cation – orange. Heteroatoms are color-coded as well: red – oxygen, blue – nitrogen, yellow – sulfur.....	171
Supplemental Figure 16: Molecular docking of fenoterol into hOCT1 using AutoDock 4.2. Shown is here the binding energy of run 93, the energetically most favored representative of cluster rank 2.....	171
Supplemental Figure 17: Molecular docking of fenoterol into hOCT1 from AlphaFold DB using AutoDock 4.2. Shown is here the best ranked binding pose of fenoterol in hOCT1 out of 7 conformations in cluster rank 3 regarding the binding energy with its interacting amino residues in 2D. Following interactions are color-coded: Conventional H-bonds – green bold lines, van der Waals forces – thin green lines, Pi-Alkyl – pink, Donor-Donor – red, Pi-Pi Stacked – purple, Carbon Hydrogen bond; Pi-Donor Hydrogen Bond – mint green, Pi-Sulfur – yellow, Pi-Cation – orange. Heteroatoms are color-coded as well: red – oxygen, blue – nitrogen, yellow – sulfur.....	172
Supplemental Figure 18: Molecular docking of fenoterol into hOCT1 using AutoDock 4.2. Shown is here the binding energy of run 22, the energetically most favored representative of cluster rank 3.....	172
Supplemental Figure 19: Molecular docking of trospium into hOCT1 from AlphaFold DB using AutoDock 4.2. Shown is here the best ranked binding pose of trospium in hOCT1 out of 5 conformations in cluster rank 1 regarding the binding energy with its interacting amino residues in 2D. Following interactions are color-coded: Conventional H-bonds – green bold lines, van der Waals forces – thin green lines, Pi-Alkyl – pink, Donor-Donor – red, Pi-Pi Stacked – purple, Carbon Hydrogen bond; Pi-Donor Hydrogen Bond – mint green, Pi-Sulfur – yellow, Pi-Cation – orange. Heteroatoms are color-coded as well: red – oxygen, blue – nitrogen, yellow – sulfur.....	173
Supplemental Figure 20: Molecular docking of trospium into hOCT1 using AutoDock 4.2. Shown is here the binding energy of run 3, the energetically most favored representative of cluster rank 1.....	173
Supplemental Figure 21: Molecular docking of trospium into hOCT1 from AlphaFold DB using AutoDock 4.2. Shown is here the best ranked binding pose of trospium in hOCT1 out of 74 conformations in cluster	

rank 2 regarding the binding energy with its interacting amino residues in 2D. Following interactions are color-coded: Conventional H-bonds – green bold lines, van der Waals forces – thin green lines, Pi-Alkyl – pink, Donor-Donor – red, Pi-Pi Stacked – purple, Carbon Hydrogen bond; Pi-Donor Hydrogen Bond – mint green, Pi-Sulfur – yellow, Pi-Cation – orange. Heteroatoms are color-coded as well: red – oxygen, blue – nitrogen, yellow – sulfur..... 174

Supplemental Figure 22: Molecular docking of trospium into hOCT1 using AutoDock 4.2. Shown is here the binding energy of run 13, the energetically most favored representative of cluster rank 2. 174

Supplemental Figure 23: Molecular docking of trospium into hOCT1 from AlphaFold DB using AutoDock 4.2. Shown is here the best ranked binding pose of trospium in hOCT1 out of 16 conformations in cluster rank 3 regarding the binding energy with its interacting amino residues in 2D. Following interactions are color-coded: Conventional H-bonds – green bold lines, van der Waals forces – thin green lines, Pi-Alkyl – pink, Donor-Donor – red, Pi-Pi Stacked – purple, Carbon Hydrogen bond; Pi-Donor Hydrogen Bond – mint green, Pi-Sulfur – yellow, Pi-Cation – orange. Heteroatoms are color-coded as well: red – oxygen, blue – nitrogen, yellow – sulfur..... 175

Supplemental Figure 24: Molecular docking of trospium into hOCT1 using AutoDock 4.2. Shown is here the binding energy of run 39, the energetically most favored representative of cluster rank 3. 175

Supplemental Figure 25: Molecular docking of trospium into hOCT1 from AlphaFold DB using AutoDock 4.2. Shown is here the best ranked binding pose of trospium in hOCT1 in cluster rank 4 regarding the binding energy with its interacting amino residues in 2D. Following interactions are color-coded: Conventional H-bonds – green bold lines, van der Waals forces – thin green lines, Pi-Alkyl – pink, Donor-Donor – red, Pi-Pi Stacked – purple, Carbon Hydrogen bond; Pi-Donor Hydrogen Bond – mint green, Pi-Sulfur – yellow, Pi-Cation – orange. Heteroatoms are color-coded as well: red – oxygen, blue – nitrogen, yellow – sulfur. 176

Supplemental Figure 26: Molecular docking of trospium into hOCT1 using AutoDock 4.2. Shown is here the binding energy of run 86, the energetically most favored representative of cluster rank 4. 176

Supplemental Figure 27: Molecular docking of fenoterol into mOCT1 from AlphaFold DB using AutoDock 4.2. Shown is here the best ranked binding pose of fenoterol in mOCT1 out of 37 conformations in cluster rank 1 regarding the binding energy with its interacting amino residues in 2D. Following interactions are color-coded: Conventional H-bonds – green bold lines, van der Waals forces – thin green lines, Pi-Alkyl – pink, Donor-Donor – red, Pi-Pi Stacked – purple, Carbon Hydrogen bond; Pi-Donor Hydrogen Bond – mint green, Pi-Sulfur – yellow, Pi-Cation – orange. Heteroatoms are color-coded as well: red – oxygen, blue – nitrogen, yellow – sulfur. 177

Supplemental Figure 28: Molecular docking of fenoterol into mOCT1 using AutoDock 4.2. Shown is here the binding energy of run 88, the energetically most favored representative of cluster rank 1. 177

Supplemental Figure 29: Molecular docking of fenoterol into mOCT1 from AlphaFold DB using AutoDock 4.2. Shown is here the best ranked binding pose of fenoterol in mOCT1 out of 3 conformations in cluster rank 2 regarding the binding energy with its interacting amino residues in 2D. Following interactions are color-coded: Conventional H-bonds – green bold lines, van der Waals forces – thin green lines, Pi-Alkyl – pink, Donor-Donor – red, Pi-Pi Stacked – purple, Carbon Hydrogen bond; Pi-Donor Hydrogen Bond – mint green, Pi-Sulfur – yellow, Pi-Cation – orange. Heteroatoms are color-coded as well: red – oxygen, blue – nitrogen, yellow – sulfur..... 178

Supplemental Figure 30: Molecular docking of fenoterol into mOCT1 using AutoDock 4.2. Shown is here the binding energy of run 8, the energetically most favored representative of cluster rank 2. 178

Supplemental Figure 31: Molecular docking of fenoterol into mOCT1 from AlphaFold DB using AutoDock 4.2. Shown is here the best ranked binding pose of fenoterol in mOCT1 out of 3 conformations in cluster rank 3 regarding the binding energy with its interacting amino residues in 2D. Following interactions are color-coded: Conventional H-bonds – green bold lines, van der Waals forces – thin green lines, Pi-Alkyl – pink, Donor-Donor – red, Pi-Pi Stacked – purple, Carbon Hydrogen bond; Pi-Donor Hydrogen Bond – mint green, Pi-Sulfur – yellow, Pi-Cation – orange. Heteroatoms are color-coded as well: red – oxygen, blue – nitrogen, yellow – sulfur..... 179

Supplemental Figure 32: Molecular docking of fenoterol into mOCT1 using AutoDock 4.2. Shown is here the binding energy of run 47, the energetically most favored representative of cluster rank 3. 179

Supplemental Figure 33: Molecular docking of fenoterol into mOCT1 from AlphaFold DB using AutoDock 4.2. Shown is here the best ranked binding pose of fenoterol in mOCT1 out of 17 conformations in

cluster rank 7 regarding the binding energy with its interacting amino residues in 2D. Following interactions are color-coded: Conventional H-bonds – green bold lines, van der Waals forces – thin green lines, Pi-Alkyl – pink, Donor-Donor – red, Pi-Pi Stacked – purple, Carbon Hydrogen bond; Pi-Donor Hydrogen Bond – mint green, Pi-Sulfur – yellow, Pi-Cation – orange. Heteroatoms are color-coded as well: red – oxygen, blue – nitrogen, yellow – sulfur.	180
Supplemental Figure 34: Molecular docking of fenoterol into mOCT1 using AutoDock 4.2. Shown is here the binding energy of run 9, the energetically most favored representative of cluster rank 7.	180
Supplemental Figure 35: Protein alignment of human OCT1 (Query) and mouse OCT1 (Sbjct) using the blastp (protein-protein BLAST) algorithm of the basic local alignment search tool (BLAST [®] , available at https://blast.ncbi.nlm.nih.gov/Blast.cgi?PAGE=Proteins).	181
Supplemental Figure 36: Protein alignment of human OCT1 (Query) and rat OCT1 (Sbjct) using the blastp (protein-protein BLAST) algorithm of the basic local alignment search tool (BLAST [®] , available at https://blast.ncbi.nlm.nih.gov/Blast.cgi?PAGE=Proteins).	182

5.5 List of Tables

Table 1: The evolution of SLC22 transporters. Adapted from [1].....	47
Table 2: Expression of human organic cation transporter 1 (hOCT1) in tumors in different organs detected on mRNA and/or protein level. +, expression; d, decreased expression in tumor versus respective organ; s, similar expression in tumor and respective organ. Adapted from [1].....	55
Table 3: Binding affinities and RMSD values of fenoterol in hOCT1 analyzed by AutoDock Vina. Root mean square deviation (RMSD) values measuring the average between atoms of a position relative to the best fitting position, are calculated using only movable heavy atoms. Two variants of RMSD metrics are provided, rmsd l.b. (RMSD lower bound) and rmsd u.b. (RMSD upper bound). They differ in how the atoms are matched in the distance calculation; rmsd u.b. matches each atom in one conformation with itself in the other conformation, ignoring any symmetry; rmsd l.b. matches each atom in one conformation with the closest atom of the same element type in the other conformation.....	69
Table 4: Binding affinities and RMSD values of fenoterol in mOCT1 analyzed by AutoDock Vina. Root mean square deviation (RMSD) values measuring the average between atoms of a position relative to the best fitting position, are calculated using only movable heavy atoms. Two variants of RMSD metrics are provided, rmsd l.b. (RMSD lower bound) and rmsd u.b. (RMSD upper bound). They differ in how the atoms are matched in the distance calculation; rmsd u.b. matches each atom in one conformation with itself in the other conformation, ignoring any symmetry; rmsd l.b. matches each atom in one conformation with the closest atom of the same element type in the other conformation.....	73
Table 5: Binding affinities and RMSD values of trospium in hOCT1 analyzed by AutoDock Vina. Root mean square deviation (RMSD) values measuring the average between atoms of a position relative to the best fitting position, are calculated using only movable heavy atoms. Two variants of RMSD metrics are provided, rmsd l.b. (RMSD lower bound) and rmsd u.b. (RMSD upper bound). They differ in how the atoms are matched in the distance calculation; rmsd u.b. matches each atom in one conformation with itself in the other conformation, ignoring any symmetry; rmsd l.b. matches each atom in one conformation with the closest atom of the same element type in the other conformation.....	77
Table 6: Binding affinities and RMSD values of trospium in mOCT1 analyzed by AutoDock Vina. Root mean square deviation (RMSD) values measuring the average between atoms of a position relative to the best fitting position, are calculated using only movable heavy atoms. Two variants of RMSD metrics are provided, rmsd l.b. (RMSD lower bound) and rmsd u.b. (RMSD upper bound). They differ in how the atoms are matched in the distance calculation; rmsd u.b. matches each atom in one conformation with itself in the other conformation, ignoring any symmetry; rmsd l.b. matches each atom in one conformation with the closest atom of the same element type in the other conformation.....	81
Table 7: Binding affinities and RMSD values of fenoterol in hOCT1 with new rotamers analyzed by AutoDock Vina. Root mean square deviation (RMSD) values measuring the average between atoms of a position relative to the best fitting position, are calculated using only movable heavy atoms. Two variants of RMSD metrics are provided, rmsd l.b. (RMSD lower bound) and rmsd u.b. (RMSD upper bound). They differ in how the atoms are matched in the distance calculation; rmsd u.b. matches each atom in one conformation with itself in the other conformation, ignoring any symmetry; rmsd l.b. matches each atom in one conformation with the closest atom of the same element type in the other conformation.	88
Table 8: Binding affinities and RMSD values of fenoterol in mOCT1 with new rotamers analyzed by AutoDock Vina. Root mean square deviation (RMSD) values measuring the average between atoms of a position relative to the best fitting position, are calculated using only movable heavy atoms. Two variants of RMSD metrics are provided, rmsd l.b. (RMSD lower bound) and rmsd u.b. (RMSD upper bound). They differ in how the atoms are matched in the distance calculation; rmsd u.b. matches each atom in one conformation with itself in the other conformation, ignoring any symmetry; rmsd l.b. matches each atom in one conformation with the closest atom of the same element type in the other conformation.	92
Table 9: Binding affinities and RMSD values of trospium in hOCT1 with new rotamers analyzed by AutoDock Vina. Root mean square deviation (RMSD) values measuring the average between atoms of a position relative to the best fitting position, are calculated using only movable heavy atoms. Two variants of RMSD metrics are provided, rmsd l.b. (RMSD lower bound) and rmsd u.b. (RMSD upper	

bound). They differ in how the atoms are matched in the distance calculation; rmsd u.b. matches each atom in one conformation with itself in the other conformation, ignoring any symmetry; rmsd l.b. matches each atom in one conformation with the closest atom of the same element type in the other conformation. 96

Table 10: Binding affinities and RMSD values of trospium in mOCT1 with new rotamers analyzed by AutoDock Vina. Root mean square deviation (RMSD) values measuring the average between atoms of a position relative to the best fitting position, are calculated using only movable heavy atoms. Two variants of RMSD metrics are provided, rmsd l.b. (RMSD lower bound) and rmsd u.b. (RMSD upper bound). They differ in how the atoms are matched in the distance calculation; rmsd u.b. matches each atom in one conformation with itself in the other conformation, ignoring any symmetry; rmsd l.b. matches each atom in one conformation with the closest atom of the same element type in the other conformation. 101

Table 11: Structural alignment with PyMol. Our native homology model was aligned to the protein structure model of human OCT1 from AlphaFold DB (UniProt ID: O15245) using the “align” command in PyMol. The RMSD (Root Mean Square Deviation) of the aligned atoms after outlier rejection is reported. 103

Table 12: Binding affinities and RMSD values of fenoterol in hOCT1 from AlphaFold DB analyzed by AutoDock Vina. Root mean square deviation (RMSD) values measuring the average between atoms of a position relative to the best fitting position, are calculated using only movable heavy atoms. Two variants of RMSD metrics are provided, rmsd l.b. (RMSD lower bound) and rmsd u.b. (RMSD upper bound). They differ in how the atoms are matched in the distance calculation; rmsd u.b. matches each atom in one conformation with itself in the other conformation, ignoring any symmetry; rmsd l.b. matches each atom in one conformation with the closest atom of the same element type in the other conformation. 107

Table 13: Binding affinities and RMSD values of fenoterol in hOCT1 from AlphaFold DB analyzed by AutoDock Vina. Root mean square deviation (RMSD) values measuring the average between atoms of a position relative to the best fitting position, are calculated using only movable heavy atoms. Two variants of RMSD metrics are provided, rmsd l.b. (RMSD lower bound) and rmsd u.b. (RMSD upper bound). They differ in how the atoms are matched in the distance calculation; rmsd u.b. matches each atom in one conformation with itself in the other conformation, ignoring any symmetry; rmsd l.b. matches each atom in one conformation with the closest atom of the same element type in the other conformation. 109

Table 14: Binding affinities and RMSD values of fenoterol in hOCT1 from AlphaFold DB analyzed by flexible Docking using AutoDock Vina. Root mean square deviation (RMSD) values measuring the average between atoms of a position relative to the best fitting position, are calculated using only movable heavy atoms. Two variants of RMSD metrics are provided, rmsd l.b. (RMSD lower bound) and rmsd u.b. (RMSD upper bound). They differ in how the atoms are matched in the distance calculation; rmsd u.b. matches each atom in one conformation with itself in the other conformation, ignoring any symmetry; rmsd l.b. matches each atom in one conformation with the closest atom of the same element type in the other conformation. 115

Table 15: Binding affinities and RMSD values of fenoterol in hOCT1 from AlphaFold DB analyzed by flexible Docking using AutoDock Vina. Root mean square deviation (RMSD) values measuring the average between atoms of a position relative to the best fitting position, are calculated using only movable heavy atoms. Two variants of RMSD metrics are provided, rmsd l.b. (RMSD lower bound) and rmsd u.b. (RMSD upper bound). They differ in how the atoms are matched in the distance calculation; rmsd u.b. matches each atom in one conformation with itself in the other conformation, ignoring any symmetry; rmsd l.b. matches each atom in one conformation with the closest atom of the same element type in the other conformation. 119

Table 16: Binding affinities and RMSD values of fenoterol in hOCT1 from AlphaFold DB analyzed by flexible Docking using AutoDock Vina. Root mean square deviation (RMSD) values measuring the average between atoms of a position relative to the best fitting position, are calculated using only movable heavy atoms. Two variants of RMSD metrics are provided, rmsd l.b. (RMSD lower bound) and rmsd u.b. (RMSD upper bound). They differ in how the atoms are matched in the distance calculation; rmsd u.b. matches each atom in one conformation with itself in the other conformation, ignoring any

symmetry; rmsd l.b. matches each atom in one conformation with the closest atom of the same element type in the other conformation.....	125
Table 17: Binding affinities and RMSD values of trospium in hOCT1 from AlphaFold DB analyzed by rotamer Docking using AutoDock Vina. Root mean square deviation (RMSD) values measuring the average between atoms of a position relative to the best fitting position, are calculated using only movable heavy atoms. Two variants of RMSD metrics are provided, rmsd l.b. (RMSD lower bound) and rmsd u.b. (RMSD upper bound). They differ in how the atoms are matched in the distance calculation; rmsd u.b. matches each atom in one conformation with itself in the other conformation, ignoring any symmetry; rmsd l.b. matches each atom in one conformation with the closest atom of the same element type in the other conformation.....	130
Table 18: Cluster analysis of conformations after molecular docking of fenoterol into hOCT1 from AlphaFold DB using AutoDock 4.2. Shown is here the summary of pose clustering and binding energy from the docking log file (dlg).....	136
Table 19: Cluster analysis of conformations after molecular docking of trospium into hOCT1 from AlphaFold DB using AutoDock 4.2. Shown is here the summary of pose clustering and binding energy from the docking log file (dlg).....	141
Table 20: Cluster analysis of conformations after molecular docking of fenoterol into mOCT1 from AlphaFold DB using AutoDock 4.2. Shown is here the summary of pose clustering and binding energy from the docking log file (dlg).....	147
Table 21: Cluster analysis of conformations after molecular docking of trospium into mOCT1 from AlphaFold DB using AutoDock 4.2. Shown is here the summary of pose clustering and binding energy from the docking log file (dlg).....	153

6 References

- ¹ Tsukihara, Tomitake, and Soo Jae Lee. "Membrane proteins: structure and function." *Journal of Synchrotron Radiation* 6.4 (1999): 918-927.
- ² Almeida, Jose G., et al. "Membrane proteins structures: A review on computational modeling tools." *Biochimica et Biophysica Acta (BBA)-Biomembranes* 1859.10 (2017): 2021-2039.
- ³ <https://www.creative-biolabs.com/blog/index.php/membrane-protein-overview/>
- ⁴ Lodish H, Berk A, Zipursky SL, et al. *Molecular Cell Biology*. 4th edition. New York: W. H. Freeman; 2000. Section 3.4, Membrane Proteins.
- ⁵ Whited, A. M., and Alexander Johs. "The interactions of peripheral membrane proteins with biological membranes." *Chemistry and physics of lipids* 192 (2015): 51-59.
- ⁶ Nalivaeva, N. N., and A. J. Turner. "Lipid Anchors to Proteins." *Handbook of Neurochemistry and Molecular Neurobiology*.
- ⁷ https://user.uni-frankfurt.de/~dingerma/Podcast/CytologieWS10_6.pdf
- ⁸ <https://www.nature.com/scitable/topicpage/protein-function-14123348/>
- ⁹ Tan, Sandra, Hwee Tong Tan, and Maxey CM Chung. "Membrane proteins and membrane proteomics." *Proteomics* 8.19 (2008): 3924-3932.
- ¹⁰ Biologydictionary.net Editors. "Channel Protein." *Biology Dictionary*, Biologydictionary.net, 20 Jun. 2018, <https://biologydictionary.net/channel-protein/>.
- ¹¹ Cooper, G. M. (2010). *Transport of Small Molecules*. Retrieved from Nih.gov website: <https://www.ncbi.nlm.nih.gov/books/NBK9847/>
- ¹² Zoppi, Lois. "Role of Membrane Proteins in Physiology". News-Medical. 15 January 2022. <<https://www.news-medical.net/life-sciences/Role-of-Membrane-Proteins-in-Physiology.aspx>>.
- ¹³ <https://www.tocris.com/cell-biology/signal-transduction>
- ¹⁴ Zihni, Ceniz, et al. "Tight junctions: from simple barriers to multifunctional molecular gates." *Nature reviews Molecular cell biology* 17.9 (2016): 564-580.
- ¹⁵ <https://ib.bioninja.com.au/standard-level/topic-1-cell-biology/13-membrane-structure/membrane-proteins.html>
- ¹⁶ Dominguez, Roberto, and Kenneth C. Holmes. "Actin structure and function." *Annual re-view of biophysics* 40 (2011): 169-186.
- ¹⁷ Carpenter, Elisabeth P., et al. "Overcoming the challenges of membrane protein crystallography." *Current opinion in structural biology* 18.5 (2008): 581-586.
- ¹⁸ Junge, F., et al. "Large-scale production of functional membrane proteins." *Cellular and Molecular Life Sciences* 65.11 (2008): 1729-1755.
- ¹⁹ Lacapere, Jean-Jacques, et al. "Determining membrane protein structures: still a challenge!" *Trends in biochemical sciences* 32.6 (2007): 259-270.
- ²⁰ Hunte, Carola, and Hartmut Michel. "Crystallisation of membrane proteins mediated by antibody fragments." *Current opinion in structural biology* 12.4 (2002): 503-508.
- ²¹ Manjasetty, Babu A., et al. "Automated technologies and novel techniques to accelerate protein crystallography for structural genomics." *Proteomics* 8.4 (2008): 612-625.
- ²² Santos, Rita, et al. "A comprehensive map of molecular drug targets." *Nature reviews Drug discovery* 16.1 (2017): 19-34.

-
- ²³ Ferreira, Leonardo G., et al. "Molecular docking and structure-based drug design strategies." *Molecules* 20.7 (2015): 13384-13421.
- ²⁴ Lionta, Evanthia, et al. "Structure-based virtual screening for drug discovery: principles, applications and recent advances." *Current topics in medicinal chemistry* 14.16 (2014): 1923-1938.
- ²⁵ Batool, Maria, Bilal Ahmad, and Sangdun Choi. "A structure-based drug discovery paradigm." *International journal of molecular sciences* 20.11 (2019): 2783.
- ²⁶ Deleu, Magali, et al. "Complementary biophysical tools to investigate lipid specificity in the interaction between bioactive molecules and the plasma membrane: A review." *Biochimica et Biophysica Acta (BBA)-Biomembranes* 1838.12 (2014): 3171-3190.
- ²⁷ Muhammed, Muhammed Tilahun, and Esin Aki-Yalcin. "Homology modeling in drug discovery: Overview, current applications, and future perspectives." *Chemical biology & drug design* 93.1 (2019): 12-20.
- ²⁸ Monje-Galvan, Viviana, and Jeffery B. Klauda. "Peripheral membrane proteins: Tying the knot between experiment and computation." *Biochimica et Biophysica Acta (BBA)-Biomembranes* 1858.7 (2016): 1584-1593.
- ²⁹ Forli, Stefano, et al. "Computational protein–ligand docking and virtual drug screening with the AutoDock suite." *Nature protocols* 11.5 (2016): 905-919.
- ³⁰ Yuriev, Elizabeth, Mark Agostino, and Paul A. Ramsland. "Challenges and advances in computational docking: 2009 in review." *Journal of Molecular Recognition* 24.2 (2011): 149-164.
- ³¹ Fan, Hao, et al. "Molecular docking screens using comparative models of proteins." *Journal of chemical information and modeling* 49.11 (2009): 2512-2527.
- ³² Yuriev, Elizabeth, Mark Agostino, and Paul A. Ramsland. "Challenges and advances in computational docking: 2009 in review." *Journal of Molecular Recognition* 24.2 (2011): 149-164.
- ³³ Corbeil, Christopher R., Eric Therrien, and Nicolas Moitessier. "Modeling reality for optimal docking of small molecules to biological targets." *Current Computer-Aided Drug Design* 5.4 (2009): 241-263.
- ³⁴ Morris, Garrett M., et al. "AutoDock4 and AutoDockTools4: Automated docking with selective receptor flexibility." *Journal of computational chemistry* 30.16 (2009): 2785-2791.
- ³⁵ Bitencourt-Ferreira, Gabriela, Val Oliveira Pinto, and Walter Filgueira de Azevedo. "Docking with AutoDock4." *Docking Screens for Drug Discovery*. Humana, New York, NY, 2019. 125-148.
- ³⁶ Goodsell, David S., and Arthur J. Olson. "Automated docking of substrates to proteins by simulated annealing." *Proteins: Structure, Function, and Bioinformatics* 8.3 (1990): 195-202.
- ³⁷ Huey, Ruth, et al. "A semiempirical free energy force field with charge-based desolvation." *Journal of computational chemistry* 28.6 (2007): 1145-1152.
- ³⁸ Morris, Garrett M., et al. "Automated docking using a Lamarckian genetic algorithm and an empirical binding free energy function." *Journal of computational chemistry* 19.14 (1998): 1639-1662.
- ³⁹ Santos-Martins, Diogo, et al. "Accelerating AutoDock4 with GPUs and gradient-based local search." *Journal of Chemical Theory and Computation* 17.2 (2021): 1060-1073.
- ⁴⁰ Solis, Francisco J., and Roger J-B. Wets. "Minimization by Random Search Techniques." *Mathematics of Operations Research*, vol. 6, no. 1, INFORMS, 1981, pp. 19–30, <http://www.jstor.org/stable/3689263>.

-
- ⁴¹ Trott, Oleg, and Arthur J. Olson. "AutoDock Vina: improving the speed and accuracy of docking with a new scoring function, efficient optimization, and multithreading." *Journal of computational chemistry* 31.2 (2010): 455-461.
- ⁴² Chang, Max W., et al. "Virtual screening for HIV protease inhibitors: a comparison of AutoDock 4 and Vina." *PloS one* 5.8 (2010): e11955.
- ⁴³ Sahoo, Swagatika, et al. "Membrane transporters in a human genome-scale metabolic knowledge-base and their implications for disease." *Frontiers in physiology* 5 (2014): 91.
- ⁴⁴ Liang, Yu, Siqi Li, and Ligong Chen. "The physiological role of drug transporters." *Protein & cell* 6.5 (2015): 334-350.
- ⁴⁵ Koepsell, Hermann. "Organic cation transporters in health and disease." *Pharmacological reviews* 72.1 (2020): 253-319.
- ⁴⁶ Nigam, Sanjay K. "The SLC22 transporter family: a paradigm for the impact of drug transporters on metabolic pathways, signaling, and disease." *Annual review of pharmacology and toxicology* 58 (2018): 663-687.
- ⁴⁷ Koepsell H, Lips K, Volk C. 2007. Polyspecific organic cation transporters: structure, function, physiological roles, and biopharmaceutical implications. *Pharm Res.* 24(7): 1227–1251.
- ⁴⁸ Keller, Thorsten, et al. "Rat organic cation transporter 1 contains three binding sites for substrate 1-methyl-4-phenylpyridinium per monomer." *Molecular pharmacology* 95.2 (2019): 169-182.
- ⁴⁹ Minuesa, Gerard, et al. "Drug uptake transporters in antiretroviral therapy." *Pharmacology & therapeutics* 132.3 (2011): 268-279.
- ⁵⁰ Meyer, Marleen J., et al. "Opioids as substrates and inhibitors of the genetically highly variable organic cation transporter OCT1." *Journal of medicinal chemistry* 62.21 (2019): 9890-9905.
- ⁵¹ Chen R, Nelson JA. 2000. Role of organic cation transporters in the renal secretion of nucleosides. *Biochem Pharmacol.* 60(2):215–219.
- ⁵² van Montfoort JE, Muller M, Groothuis GM, Meijer DK, Koepsell H, Meier PJ. 2001. Comparison of "type I" and "type II" organic cation transport by organic cation transporters and organic anion-transporting polypeptides. *J Pharmacol Exp Ther.* 298(1):110–115.
- ⁵³ Wang DS, Kusuvara H, Kato Y, Jonker JW, Schinkel AH, Sugiyama Y. 2003. Involvement of organic cation transporter 1 in the lactic acidosis caused by metformin. *Mol Pharmacol.* 63(4):844–848.
- ⁵⁴ Ishiguro N, Saito A, Yokoyama K, Morikawa M, Igarashi T, Tamai I. 2005. Transport of the dopamine D2 agonist pramipexole by rat organic cation transporters OCT1 and OCT2 in kidney. *Drug Metab Dispos.* 33(4):495–499.
- ⁵⁵ Kimura N, Masuda S, Tanihara Y, Ueo H, Okuda M, Katsura T, Inui K. 2005. Metformin is a superior substrate for renal organic cation transporter OCT2 rather than hepatic OCT1. *Drug Metab Pharmacokin.* 20(5):379–386.
- ⁵⁶ Yonezawa A, Masuda S, Yokoo S, Katsura T, Inui K. 2006. Cisplatin and oxaliplatin, but not carboplatin and nedaplatin, are substrates for human organic cation transporters (SLC22A1-3 and multidrug and toxin extrusion family). *J Pharmacol Exp Ther.* 319(2):879–886.
- ⁵⁷ Zhang S, Lovejoy KS, Shima JE, Lagpacan LL, Shu Y, Lapuk A, Chen Y, Komori T, Gray JW, Chen X, et al. 2006. Organic cation transporters are determinants of oxaliplatin cytotoxicity. *Cancer Res.* 66(17):8847–8857.

-
- ⁵⁸ Giannoudis A, Davies A, Lucas CM, Harris RJ, Pirmohamed M, Clark RE. 2008. Effective dasatinib uptake may occur without human organic cation transporter 1 (hOCT1): implications for the treatment of imatinib-resistant chronic myeloid leukemia. *Blood*. 112(8):3348–3354.
- ⁵⁹ Jung N, Lehmann C, Rubbert A, Knispel M, Hartmann P, van Lunzen J, Stellbrink HJ, Fa-etkenheuer G, Taubert D. 2008. Relevance of the organic cation transporters 1 and 2 for antiretroviral drug therapy in human immunodeficiency virus infection. *Drug Metab Dispos*. 36(8):1616–1623.
- ⁶⁰ Sogame Y, Kitamura A, Yabuki M, Komuro S. 2009. A comparison of uptake of metformin and phenformin mediated by hOCT1 in human hepatocytes. *Biopharm Drug Dispos*. 30(8):476–484.
- ⁶¹ Herraez E, Lozano E, Macias RI, Vaquero J, Bujanda L, Banales JM, Marin JJ, Briz O. 2013. Expression of SLC22A1 variants may affect the response of hepatocellular carcinoma and cholangiocarcinoma to sorafenib. *Hepatology*. 58(3): 1065–1073.
- ⁶² Andreev E, Brosseau N, Carmona E, Mes-Masson AM, Ramotar D. 2016. The human organic cation transporter OCT1 mediates high affinity uptake of the anticancer drug daunorubicin. *Sci Rep*. 6(1):20508.
- ⁶³ Deutsch B, Neumeister C, Schwantes U, Fromm MF, König J. 2019. Interplay of the organic cation transporters OCT1 and OCT2 with the apically localized export protein MATE1 for the polarized transport of trospium. *Mol Pharm*. 16(2):510–517.
- ⁶⁴ Nies, Anne T., et al. "Expression of organic cation transporters OCT1 (SLC22A1) and OCT3 (SLC22A3) is affected by genetic factors and cholestasis in human liver." *Hepatology* 50.4 (2009): 1227-1240.
- ⁶⁵ Giacomini KM, Huang S-M, Tweedie DJ, Benet LZ, Brouwer KLR, Chu X, Dahlin A, Evers R, Fischer V, Hillgren KM, et al. 2010. Membrane transporters in drug development. *Nat Rev Drug Discov*. 9(3):215–236.
- ⁶⁶ Nigam SK. 2015. What do drug transporters really do? *Nat Rev Drug Discov*. 14(1):29–44.
- ⁶⁷ Giacomini KM, Galetin A, Huang SM. 2018. The international transporter consortium: summarizing advances in the role of transporters in drug development. *Clin Pharmacol Ther*. 104(5):766–771.
- ⁶⁸ Zamek-Gliszczynski MJ, Taub ME, Chothe PP, Chu X, Giacomini KM, Kim RB, Ray AS, Stocker SL, Unadkat JD, Wittwer MB, et al. 2018. Transporters in drug development: 2018 ITC recommendations for transporters of emerging clinical importance. *Clin Pharmacol Ther*. 104(5): 890–899.
- ⁶⁹ Brosseau, Nicolas, and Dindial Ramotar. "The human organic cation transporter OCT1 and its role as a target for drug responses." *Drug metabolism reviews* 51.4 (2019): 389-407.
- ⁷⁰ Egenberger, Brigitte, et al. "A substrate binding hinge domain is critical for transport-related structural changes of organic cation transporter 1." *Journal of Biological Chemistry* 287.37 (2012): 31561-31573.
- ⁷¹ Gorboulev, Valentin, et al. "Selectivity of the polyspecific cation transporter rOCT1 is changed by mutation of aspartate 475 to glutamate." *Molecular pharmacology* 56.6 (1999): 1254-1261.
- ⁷² Meyer, M. J., Tuerkova, A., Römer, S., Wenzel, C., Seitz, T., Gaedcke, J., ... & Tzvetkov, M. V. (2020). Differences in Metformin and Thiamine Uptake between Human and Mouse Organic Cation Transporter 1: Structural Determinants and Potential Consequences for Intrahepatic Concentrations. *Drug Metabolism and Disposition*, 48(12), 1380-1392.

-
- ⁷³ Boxberger, Kelli H., Bruno Hagenbuch, and Jed N. Lampe. "Ligand-dependent modulation of hOCT1 transport reveals discrete ligand binding sites within the substrate translocation channel." *Biochemical pharmacology* 156 (2018): 371-384.
- ⁷⁴ Dakal, Tikam Chand, Rajender Kumar, and Dindial Ramotar. "Structural modeling of human organic cation transporters." *Computational biology and chemistry* 68 (2017): 153-163.
- ⁷⁵ Nies, Anne T., et al. "Expression of organic cation transporters OCT1 (SLC22A1) and OCT3 (SLC22A3) is affected by genetic factors and cholestasis in human liver." *Hepatology* 50.4 (2009): 1227-1240.
- ⁷⁶ Kato, Yukio, et al. "Organic cation/carnitine transporter OCTN2 (Slc22a5) is responsible for carnitine transport across apical membranes of small intestinal epithelial cells in mouse." *Molecular pharmacology* 70.3 (2006): 829-837.
- ⁷⁷ Tzvetkov, Mladen Vassilev, et al. "The effects of genetic polymorphisms in the organic cation transporters OCT1, OCT2, and OCT3 on the renal clearance of metformin." *Clinical Pharmacology & Therapeutics* 86.3 (2009): 299-306.
- ⁷⁸ Lips, Katrin Susanne, et al. "Polyspecific cation transporters mediate luminal release of acetylcholine from bronchial epithelium." *American journal of respiratory cell and molecular biology* 33.1 (2005): 79-88.
- ⁷⁹ Horvath, Gabor, et al. "Epithelial organic cation transporters ensure pH-dependent drug absorption in the airway." *American journal of respiratory cell and molecular biology* 36.1 (2007): 53-60.
- ⁸⁰ Berg, Tove, et al. "Expression of MATE1, P-gp, OCTN1 and OCTN2, in epithelial and immune cells in the lung of COPD and healthy individuals." *Respiratory research* 19.1 (2018): 1-13.
- ⁸¹ Heise, Michael, et al. "Downregulation of organic cation transporters OCT1 (SLC22A1) and OCT3 (SLC22A3) in human hepatocellular carcinoma and their prognostic significance." *BMC cancer* 12.1 (2012): 1-10.
- ⁸² Schaeffeler, Elke, et al. "DNA methylation is associated with downregulation of the organic cation transporter OCT1 (SLC22A1) in human hepatocellular carcinoma." *Genome medicine* 3.12 (2011): 1-12.
- ⁸³ Al-Abdulla, Ruba, et al. "Epigenetic events involved in organic cation transporter 1-dependent impaired response of hepatocellular carcinoma to sorafenib." *British journal of pharmacology* 176.6 (2019): 787-800.
- ⁸⁴ Matthaai J, Seitz T, Jensen O, Tann A, Prukop T, Tadjerpisheh S, Brockmoller J, Tzvetkov MV. 2019. OCT1 deficiency affects hepatocellular concentrations and pharmacokinetics of cycloguanil, the active metabolite of the antimalarial drug proguanil. *Clin Pharmacol Ther.* 105(1):190–200.
- ⁸⁵ Gupta S, Wulf G, Henjakovic M, Koepsell H, Burckhardt G, Hagos Y. 2012. Human organic cation transporter 1 is expressed in lymphoma cells and increases susceptibility to irinotecan and paclitaxel. *J Pharmacol Exp Ther.* 341(1): 16–23.
- ⁸⁶ Watkins DB, Hughes TP, White DL. 2015. OCT1 and imatinib transport in CML: is it clinically relevant? *Leukemia.* 29(10): 1960–1969.
- ⁸⁷ Jumper, John, et al. "Highly accurate protein structure prediction with AlphaFold." *Nature* 596.7873 (2021): 583-589.

-
- ⁸⁸ Varadi, Mihaly, et al. "AlphaFold Protein Structure Database: Massively expanding the structural coverage of protein-sequence space with high-accuracy models." *Nucleic acids research* 50.D1 (2022): D439-D444.
- ⁸⁹ Meyer, Marleen J., et al. "Amino acids in transmembrane helix 1 confer major functional differences between human and mouse orthologs of the polyspecific membrane transporter OCT1." *Journal of Biological Chemistry* (2022): 101974.
- ⁹⁰ Sievers, Fabian, et al. "Fast, scalable generation of high-quality protein multiple sequence alignments using Clustal Omega." *Molecular systems biology* 7.1 (2011): 539.
- ⁹¹ Gründemann, Dirk, et al. "Drug excretion mediated by a new prototype of polyspecific transporter." *Nature* 372.6506 (1994): 549-552.
- ⁹² Gorboulev, Valentin, et al. "Cloning and characterization of two human polyspecific organic cation transporters." *DNA and cell biology* 16.7 (1997): 871-881.
- ⁹³ Haberkorn, Bastian, Martin F. Fromm, and Jörg König. "Transport of Drugs and Endogenous Compounds Mediated by Human OCT1: Studies in Single-and Double-Transfected Cell Models." *Frontiers in Pharmacology* 12 (2021).
- ⁹⁴ Gorboulev, Valentin, et al. "Subtype-specific affinity for corticosterone of rat organic cation transporters rOCT1 and rOCT2 depends on three amino acids within the substrate binding region." *Molecular pharmacology* 67.5 (2005): 1612-1619.
- ⁹⁵ Popp, Christian, et al. "Amino acids critical for substrate affinity of rat organic cation transporter 1 line the substrate binding region in a model derived from the tertiary structure of lactose permease." *Molecular pharmacology* 67.5 (2005): 1600-1611.
- ⁹⁶ Meyer, Marleen J., and Mladen V. Tzvetkov. "OCT1 Polyspecificity—Friend or Foe?." *Frontiers in Pharmacology* 12 (2021).
- ⁹⁷ Gallivan, Justin P., and Dennis A. Dougherty. "Cation- π interactions in structural biology." *Proceedings of the National Academy of Sciences* 96.17 (1999): 9459-9464.
- ⁹⁸ Volk, Christopher, et al. "Five amino acids in the innermost cavity of the substrate binding cleft of organic cation transporter 1 interact with extracellular and intracellular corticosterone." *Molecular pharmacology* 76.2 (2009): 275-289.
- ⁹⁹ Koepsell, Hermann. "Substrate recognition and translocation by polyspecific organic cation transporters." (2011): 95-101.
- ¹⁰⁰ Gorboulev, Valentin, et al. "Assay conditions influence affinities of rat organic cation transporter 1: analysis of mutagenesis in the modeled outward-facing cleft by measuring effects of substrates and inhibitors on initial uptake." *Molecular Pharmacology* 93.4 (2018): 402-415.
- ¹⁰¹ Chen, Tao, Meixiu Li, and Jingquan Liu. " π - π stacking interaction: a nondestructive and facile means in material engineering for bioapplications." *Crystal Growth & Design* 18.5 (2018): 2765-2783.
- ¹⁰² Gómez-Tamayo, José C., et al. "Analysis of the interactions of sulfur-containing amino acids in membrane proteins." *Protein Science* 25.8 (2016): 1517-1524.
- ¹⁰³ Valley, Christopher C., et al. "The methionine-aromatic motif plays a unique role in stabilizing protein structure." *Journal of Biological Chemistry* 287.42 (2012): 34979-34991.
- ¹⁰⁴ Chen, Eugene C., et al. "Discovery of competitive and noncompetitive ligands of the organic cation transporter 1 (OCT1; SLC22A1)." *Journal of medicinal chemistry* 60.7 (2017): 2685-2696.

¹⁰⁵ Lexa, Katrina W, and Heather A Carlson. "Protein flexibility in docking and surface mapping." *Quarterly reviews of biophysics* vol. 45,3 (2012): 301-43. doi:10.1017/S0033583512000066

¹⁰⁶ Gebauer, Lukas, et al. "Molecular basis for stereoselective transport of fenoterol by the organic cation transporters 1 and 2." *Biochemical pharmacology* 197 (2022): 114871.